Spatiotemporal Characterization and Analysis of Drought in Mainland Southeast Asia

Unlocking the Potential of Long Earth Observation Time Series

Dissertation zur Erlangung der Doktorwürde der
Philosophischen Fakultät der
Julius-Maximilians-Universität Würzburg

vorgelegt von

Ha Van Tuyen

aus München

May 2025

Julius-Maximilians-
UNIVERSITÄT
WÜRZBURG

Cover image:
The cover image shows the MODIS-based drought condition in part of mainland Southeast Asia acquired in 2023. The darkred and orange colors show drier conditions, while dark-green exhibits wetter conditions. The line feature represents river network in the region.

Funding:
This thesis is published and printed with the support of the German Academic Exchange Service.

Eingereicht am: 20.05.2025

Von: Ha Van Tuyen
Ort: Lehrstuhl für Fernerkundung der Julius-Maximilians-Universität Würzburg, in Kooperation mit dem Deutschen Fernerkundungsdatenzentrum (DFD) des Deutschen Zentrums für Luft- und Raumfahrt (DLR)

Erstbetreuerin: Prof. Dr. Claudia Künzer, Universität Würzburg
Zweitbetreuer: Prof. Dr. Heiko Paeth, Universität Würzburg
Drittsbetreuer: Prof. Dr. Tobias Ullmann, Universität Würzburg

This dissertation was prepared at the department “Land Surface Dynamics” of the German Remote Sensing Data Center (DFD), Earth Observation Center (EOC), German Aerospace Center (DLR), Oberpfaffenhofen, Germany.

"When the well's dry,
we know the worth of water."

— Benjamin Franklin

English Summary

Drought is a complex and reoccurring hazard event. It ranks among the costliest natural climate-related disasters and manifests in various forms, posing significant challenges in mapping its characteristics and assessing its widespread impacts. Mainland Southeast Asia (MSEA), a major region of tropical agriculture and vegetation ecosystems, has become increasingly susceptible to drought hazards. As global warming continues, the frequency and severity of droughts in this region are projected to intensify, presenting risks to food security, biodiversity, and local economies. Despite the urgency of addressing these challenges, the limited availability of publicly accessible, long-term ground-based climate data in the study region hampers the development of an accurate and consistent region-wide drought monitoring system. This data gap makes tracking, predicting, and mitigating drought impacts more challenging. In this context, satellite-based data offers a great alternative. Satellite-based measurements can provide frequent and consistent records of land surface variables at a high spatial resolution over large and remote areas. Many satellite sensors, such as the Moderate Resolution Imaging Spectrometer (MODIS), enable the detection and monitoring of long historical drought conditions, overcoming the limitations of ground-based systems. This dissertation aims to harmonize long-term satellite observations for monitoring and assessing drought conditions at regional and local scales. Specifically, this thesis first provided a detailed and comprehensive review of satellite-based drought remote sensing. Subsequently, a monitoring framework for mapping vegetation-based drought characteristics was developed, facilitating more automatic and consistent observations. The research then examined the responses of vegetation-based drought to multi-temporal climate and soil drought conditions, uncovering critical relationships between these variables. Finally, this thesis conducted a local scale assessment of agricultural drought vulnerability in a drought-prone region.

A detailed review of 102 satellite-based drought studies within the region revealed a significant increase in drought articles over the study period (2000-2021), especially over the last eight years. Vietnam and Thailand had the largest number of drought articles, accounting for nearly 40%. Most studies focused on monitoring drought conditions using a single vegetation-based or precipitation-based drought indicator ($\sim$ 53%). Agricultural and vege-

tative droughts received the most attention, but long-term drought studies and deep-learning methods were still limited. Notably, no studies have offered spatial details of drought characteristics derived from optical sensors. Also, little research has been conducted to investigate the responses of vegetation to multitemporal climate-soil drought conditions and assess drought vulnerability.

Given these research gaps, this analysis generated a gap-free monthly vegetation time series derived from the MODIS data. A developed framework of mapping vegetation-based drought characteristics enabled the automatic identification of the severe drought years and their characteristics from 2000 to 2021. Apart from drought characteristics, the seasonal trends of vegetation-based drought were identified using the Mann-Kendall test and Theil-Sen slope estimator. The findings of this analysis indicated several severe drought years in the study region, namely 2000, 2004-2005, 2010, 2016, and 2019-2020. Higher drought duration and frequency were primarily detected in Central Myanmar, Cambodia, eastern Thailand, and the Lower Mekong Delta. Central Myanmar witnessed the highest drought occurrence rate ($\sim 60\%$), while other countries experienced nearly 40%, except for Laos. Thailand and Vietnam experienced nearly 15 prolonged drought events over the last two decades. This analysis also indicated that the longest drought events have primarily been detected in Cambodia and Laos, where increased dry trends have been observed. Land use types and elevation significantly influence drought conditions derived from vegetation-based data, underscoring the complex interactions between environmental factors and drought severity.

Subsequently, vegetation-based drought conditions were examined with multitemporal climate-soil drought indices, representing short-term, median-term, and long-term drought conditions. This analysis revealed a significant positive relationship between vegetation-based drought and climate-soil drought indices. Stronger drought responses were observed in lower elevation zones, especially in rainfed cropland, mixed forests, and deciduous forests. In contrast, evergreen forest and irrigated crop vegetation responded less to drought indices, especially in high-elevation zones. Short-term drought disturbances accounted for nearly 93% of the observed variations in the natural and undisturbed vegetation ecosystems among the twelve climate-soil drought indices. In addition, this study assessed agricultural drought vulnerability in the drought-prone region of Vietnamese Central Highlands by integrating time series vegetation-climate-soil drought indices with socioeconomic data. The analysis followed the vulnerability framework established by the Intergovernmental Panel on Climate Change (IPCC), focusing on three key components: exposure, sensitivity, and adaptive capacity. The findings revealed that exposure, largely driven by soil moisture deficits, accounted for nearly 65% of the agricultural drought vulnerability. The highest lev-

els of vulnerability were concentrated in the central areas of Dak Lak and Gia Lai provinces, where drought exposure and sensitivity were elevated. In contrast, Lam Dong province exhibited lower drought vulnerability despite high exposure, thanks to its lower sensitivity and stronger adaptive capacity, highlighting the critical role of socioeconomic resilience in mitigating drought impacts.

Vietnamese Summary

Hạn hán là một sự kiện nguy hiểm phức tạp và tái diễn. Nó được xếp vào loại thảm họa thiên tai tự nhiên tổn thất cao nhất và biểu hiện dưới nhiều hình thức khác nhau, đặt ra những thách thức đáng kể trong việc lập bản đồ các đặc điểm của nó và đánh giá tác động rộng rãi của nó. Đông Nam Á lục địa (MSEA), một khu vực quan trọng về hệ sinh thái nông nghiệp và thảm thực vật nhiệt đới, ngày càng dễ bị ảnh hưởng bởi các mối nguy hiểm do hạn hán. Khi tình trạng nóng lên toàn cầu tiếp diễn, tần suất và mức độ nghiêm trọng của hạn hán ở khu vực này được dự báo sẽ gia tăng, gây ra rủi ro cho an ninh lương thực, đa dạng sinh học và nền kinh tế địa phương. Mặc dù việc giải quyết những thách thức này rất cấp bách, nhưng việc dữ liệu khí hậu mặt đất dài hạn có thể truy cập công khai tại khu vực nghiên cứu còn hạn chế đã cản trở việc phát triển một hệ thống giám sát hạn hán chính xác và nhất quán trên toàn khu vực. Những hạn chế về dữ liệu khiến việc theo dõi, dự đoán và giảm thiểu tác động của hạn hán trở nên khó khăn hơn. Trong bối cảnh này, dữ liệu vệ tinh là một giải pháp thay thế tiềm năng. Các phép đo dựa trên vệ tinh có thể cung cấp thông tin thường xuyên và nhất quán về các thông số bề mặt đất ở độ phân giải không gian cao trên các khu vực rộng lớn và không thể tiếp cận được. Nhiều cảm biến vệ tinh, chẳng hạn như Máy quang phổ hình ảnh độ phân giải trung bình (MODIS), cho phép phát hiện và giám sát các điều kiện hạn hán trong lịch sử lâu dài, khắc phục những hạn chế của các hệ thống trên mặt đất. Luận án này nhằm mục đích sử dụng các quan sát vệ tinh dài hạn để giám sát và đánh giá các điều kiện hạn hán ở quy mô khu vực và địa phương. Cụ thể, luận án này đầu tiên cung cấp một đánh giá chi tiết và toàn diện về các nghiên cứu về hán dựa sử dụng công nghệ vệ tinh. Sau đó, một khuôn khổ giám sát để lập bản đồ các đặc điểm hạn hán dựa trên thảm thực vật đã được phát triển, tạo điều kiện cho các quan sát tự động và nhất quán hơn. Sau đó, nghiên cứu đã kiểm tra các phản ứng của hạn hán dựa trên thảm thực vật đối với các điều kiện hạn hán dựa trên độ ẩm đất và khí hậu đa thời gian, khám phá ra mối quan hệ quan trọng giữa các biến này. Cuối cùng, luận án này đã tiến hành đánh giá hạn hán nông nghiệp.

Một đánh giá chi tiết 102 nghiên cứu về hạn hán dựa trên vệ tinh trong khu vực Đông Nam Á đã chỉ ra rằng có sự gia tăng đáng kể các bài báo khoa học về hạn hán trong giai đoạn nghiên cứu (2000-2021), đặc biệt là trong tám năm qua. Việt Nam và Thái Lan có số lượng bài báo về hạn hán lớn nhất, chiếm gần 40%. Hầu hết các nghiên cứu tập trung vào việc theo dõi tình trạng hạn hán bằng cách sử dụng một chỉ số hạn hán dựa trên thảm thực vật hoặc dựa trên lượng mưa (~53%). Hạn hán nông nghiệp và hạn hán thực vật nhận được nhiều sự quan tâm nhất, nhưng

các nghiên cứu hạn hán dài hạn và phương pháp học sâu vẫn còn hạn chế. Đáng chú ý là không có nghiên cứu nào cung cấp thông tin chi tiết về không gian của các đặc điểm hạn hán thu được từ các cảm biến quang học. Ngoài ra, rất ít nghiên cứu được tiến hành để tìm hiểu phản ứng của thảm thực vật đối với các điều kiện hạn hán khí hậu và độ ẩm đất đa thời gian và đánh giá mức độ dễ bị hạn hán.

Với những khoảng trống nghiên cứu, phân tích này đã tạo ra một bộ dự liệu chuỗi thời gian thực vật hàng tháng từ dữ liệu MODIS. Một khuôn khổ phát triển để lập bản đồ các đặc điểm hạn hán dựa trên thảm thực vật cho phép tự động xác định những năm hạn hán nghiêm trọng và các đặc điểm của chúng từ năm 2000 đến năm 2021. Ngoài các đặc điểm hạn hán, xu hướng theo mùa của hạn hán dựa trên thảm thực vật đã được xác định bằng cách sử dụng kiểm định Mann-Kendall và ước lượng độ dốc Theil-Sen. Những phát hiện của phân tích này chỉ ra một số năm hạn hán nghiêm trọng trong khu vực nghiên cứu, cụ thể là năm 2000, 2004-2005, 2010, 2016 và 2019-2020. Thời gian và tần suất hạn hán cao hơn chủ yếu được phát hiện ở khu vực trung tâm Myanmar, Campuchia, khu vực phía Đông Thái Lan và Hạ lưu đồng bằng sông Cửu Long. Miền Trung Myanmar chứng kiến tỷ lệ xảy ra hạn hán cao nhất (~60%), trong khi các quốc gia khác trải qua gần 40%, ngoại trừ Lào. Thái Lan và Việt Nam đã trải qua gần 15 đợt hạn hán kéo dài trong hai thập kỷ qua. Các phân tích gần đây chỉ ra rằng các đợt hạn hán dài nhất chủ yếu được phát hiện ở Campuchia và Lào, nơi đã quan sát thấy xu hướng khô hạn gia tăng. Các loại hình sử dụng đất và độ cao ảnh hưởng đáng kể đến tình trạng hạn hán thu được từ dữ liệu dựa trên thảm thực vật, cho thấy sự tương tác phức tạp giữa các yếu tố môi trường và mức độ nghiêm trọng của hạn hán.

Các điều kiện hạn hán dựa trên thảm thực vật đã được kiểm tra bằng các chỉ số hạn hán khí hậu và độ ẩm đất đa thời gian, đại diện cho các điều kiện hạn hán ngắn hạn, trung hạn và dài hạn. Phân tích này cho thấy mối quan hệ tích cực đáng kể giữa hạn hán dựa trên thảm thực vật và các chỉ số hạn hán khí hậu-đất. Phản ứng hạn hán mạnh hơn đã được quan sát thấy ở các vùng có độ cao thấp hơn, đặc biệt là ở đất trồng trọt phụ thuộc vào nước mưa, rừng hỗn giao và rừng rụng lá. Ngược lại, rừng thường xanh và cây trồng được tưới tiêu ít phản ứng hơn với các chỉ số hạn hán, đặc biệt là ở các vùng có độ cao lớn. Hạn ngắn hạn có thể giải thích gần 93% các biến động quan sát được trong các hệ sinh thái thảm thực vật tự nhiên và không bị xáo trộn trong số mười hai chỉ số hạn hán khí hậu-đất. Ngoài ra, nghiên cứu này đánh giá mức độ dễ bị hạn hán trong nông nghiệp ở vùng dễ bị hạn hán của Tây Nguyên Việt Nam bằng cách tích hợp các chỉ số hạn hán thực vật-khí hậu-đất theo chuỗi thời gian với dữ liệu kinh tế xã hội. Phân tích sử dụng khuôn khổ dễ bị tổn thương do Ủy ban liên chính phủ về biến đổi khí hậu (IPCC) thiết lập, tập trung vào ba yếu tố chính: mức độ phơi nhiễm, độ nhạy và khả năng thích ứng.

Các phát hiện cho thấy mức độ phơi nhiễm, chủ yếu là do thiếu hụt độ ẩm đất, đóng góp gần 65% mức độ dễ bị hạn hán trong nông nghiệp. Mức độ dễ bị tổn thương cao nhất tập trung ở các vùng trung tâm của tỉnh Đắk Lắk và Gia Lai, nơi có mức độ phơi nhiễm và độ nhạy cảm với hạn hán cao. Ngược lại, tỉnh Lâm Đồng có mức độ dễ bị tổn thương do hạn hán thấp hơn mặc dù mức độ phơi nhiễm cao, nhờ độ nhạy cảm thấp hơn và khả năng thích ứng mạnh hơn, nhấn mạnh vai trò quan trọng của khả năng phục hồi kinh tế xã hội trong việc giảm thiểu tác động của hạn hán.

Acknowledgement

I would like to extend my deepest gratitude to those who have supported me throughout my PhD journey at the Department of Land Surface Dynamics (LAX), German Remote Sensing Data Center (DFD), German Aerospace Center (DLR). Their supportive encouragement, guidance, and belief in me have been instrumental in bringing this dissertation to success. Without their support, this work would not have been possible.

First and foremost, I would like to express my sincere thanks to my main supervisor, Prof. Dr. Claudia Kuenzer, for her unwavering support and guidance throughout my PhD journey over the past three years. I remember our first meeting, where she outlined a comprehensive vision of the PhD process and how best to navigate it. Her insightful approach provided me with a clear and structured path, especially in the early stages of my research. During the PhD, I always received her thoughtful feedback and encouragement, which consistently pushed me to progress and refine my work.

I would like to thank my co-supervisors, Prof. Dr. Heiko Paeth and Dr. Tobias Ullmann at the University of Würzburg, for their support and significant contributions to my research work. Their insights and constructive feedback were crucial in enhancing my dissertation. I also thank Dr. Christina Schäfer for her support during my enrolment process at the University of Wuerzburg.

Moving to Germany and joining DLR was a major transition for me, and I am grateful to my co-team leader, Juliane Huth, for her great help in making my start smooth and productive and during my PhD study at Coast and River Basin Team, LAX. I also sincerely thank Dr. Felix Bachofer, my co-team leader, for his guidance and continuous support during my time at DLR.

To all my colleagues at LAX for the great team atmosphere and their kind support and feedback. I would like to give special thanks to my team members and fellow PhD students: Soner Uereyen, Thorsten Hoeser, Sophie Reinermann, Jonas Koehler, Philipp Reiners, Patrick Sogno, Patrick Kacic, Kjirsten Coleman, Niklas Daniel, Samuel Fridolin, Robin Spanier, Marco Wegler, Samip Shrestha, Karina Raquel, and Martina Wenzl. I am also

grateful for the opportunities the LAX PhD group provided to engage in after-work activities, helping me navigate and balance my daily life in Germany.

I would like to extend my heartfelt thanks to my former landlord in Gilching, Frau Sigl, for her incredible support during my early days in Germany. She offered tremendous help, from assisting with my VISA paperwork to occasionally caring for my daughter when I had to be at the office. Her kindness and generosity made a significant difference during a challenging time. I am also sincerely grateful to my friend, Nguyen Van Huy, for his ongoing support in addressing my technical questions during the PhD period. A special thanks also goes to my friends, Ban Thi My and Luong Han, for her support with study resources and interesting academic discussions. I also give special thanks to Prof. Phan Van Tan at Hanoi National University of Science for his generous support and data sharing.

My journey would not have been possible without the unwavering love and support from my family. Thank you to my parents and entire family for trusting me and constantly encouraging me to pursue my goals. My heartfelt thanks go to my wife, Huong, and my daughter, Linh, who accompanied me to Germany and stood by my side every step of the way. Their constant encouragement, shared joy, and comfort in times of difficulty made all the difference; I am very grateful for that.

Table of Contents

List of Figures

List of Tables

Abbreviations and Acronyms

ADVI	Agricultural Drought Vulnerability Index
AVHRR	Advanced Very High-Resolution Radiometer
CCI	Climate Change Initiative
CHIRPS	Climate Hazards Group Infrared Precipitation with Station
DEM	Digital Elevation Model
DLR	German Aerospace Center
EA	Agricultural Drought Vulnerability Index
ECMWF	European Center for Medium-Range Weather Forecasts
ERA5	ECMWF Reanalysis 5th Generation
ENSO	El Niño-Southern Oscillation
ESA	European Space Agency
EO	Earth Observation
FAO	Food and Agriculture Organization
GEE	Google Earth Engine
GDP	Gross Domestic Product
GRACE	Gravity Recovery and Climate Experiment
GPP	Gross Primary Product
IDW	Inverse Distance Weighting
IPCC	Intergovernmental Panel on Climate Change
LAI	Leaf Area Index
LST	Land Surface Temperature
MERIS	Medium Resolution Imaging Spectrometer
MK	Mann-Kendall
MODIS	Moderate Resolution Imaging Spectroradiometer
NASA	National Aeronautics and Space Administration
NDVI	Normalized Difference Vegetation Index
NPP	Net Primary Product
NOAA	National Oceanic and Atmospheric Administration
NIR	Near Infrared

MVC	Median Value Composite
PCA	Principal Component Analysis
PET	Potential Evapotranspiration
RF	Random Forest
SAVI	Soil-adjusted Vegetation Index
SHAP	SHapley Additive exPlanations
SRTM	Shuttle Radar Topography Mission
SMAP	Soil Moisture Active Passive
SPI	Standardized Precipitation Index
SPEI	Standardized Precipitation Evapotranspiration Index
SPOT	Satellite Pour l'Observation de la Terre
SWDI	Soil Water Deficit Index
TCI	Temperature Condition Index
TRMM	Tropical Rainfall Measuring Mission
FPAR	Fraction of Photosynthetically Active Radiation
UN	United Nations
VCI	Vegetation Condition Index
VND	Vietnamese Dong
WDPA	World Database on Protected Areas
WGS	World Geodetic System
WMO	World Meteorological Organization

Chapter 1

Introduction

1.1 Drought hazards

Drought is a multifaceted and widespread phenomenon that occurs in most climatic zones and ranks among the costliest of all climate-related hazards. A distinctive feature of drought is its slow onset, often occurring over an extended period before its impact becomes visibly apparent. Given these characteristics, different definitions of drought have been proposed over the past decades. These definitions are often considered within specific disciplines and categorized according to different types of drought under both conceptual and operational frameworks (Wilhite and Glantz, 1985). Conceptually, drought is a prolonged precipitation deficit in a specific region. Although this conceptual definition offers a general understanding of drought, it has limited practical applications in addressing the complexities of drought studies. By contrast, operational definitions seek to translate the concept of drought into measurable characteristics, such as onset, termination, duration, frequency, intensity, and severity. In practice, the operational definition has been widely used to quantify drought characteristics over a given period of historical time. These definitions enable researchers and practitioners to examine drought conditions systematically. Drought characteristics can be derived from historical or projected time series (e.g., daily, monthly, and annual data).

Also, drought can be defined based on specific disciplines and is often classified into different types (Wilhite and Glantz, 1985). Generally, drought is categorized into four types: meteorological, agricultural, hydrological, and socioeconomic droughts (Wilhite and Glantz, 1985; Mishra and Singh, 2010). Meteorological drought is probably the most well-known type, occurring when there is a prolonged period of below-reference precipitation over a specific region and timeframe (Mishra and Singh, 2010; Dalezios et al., 2017). Other drought types typically originate from meteorological drought with different lagged

timescales. A short-term lack of precipitation (e.g., 1-3 months) can deplete the soil moisture, triggering agricultural drought (Wilhite and Glantz, 1985; Zhu et al., 2021). A deficit in soil moisture below a pre-defined point can affect vegetation ecosystems and cause a reduction in crop production or even crop failure. By contrast, a long-term shortage of precipitation can significantly lower the water surface and groundwater levels, resulting in hydrological drought (Wilhite and Glantz, 1985; Huang et al., 2017). Socioeconomic drought occurs when the water demand exceeds the available supply, significantly impacting human health, livelihoods, and economic activities (Zhu et al., 2021; Wilhite and Glantz, 1985). More recent research has introduced a new category known as ecological drought, and this type refers to water shortages within natural ecosystems that exceed the needs of plants and animals, disrupting ecosystem functions and biodiversity (Jiang et al., 2021; Sadiqi et al., 2022; Crausbay et al., 2020). Each type of drought may exhibit distinct characteristics and impacts, yet they are interconnected, and all stem from a precipitation deficit. Figure 1.1 presents a comprehensive overview of the various types of droughts, along with their specific triggers and associated impacts.

1.2 Impacts of drought

Drought is ranked the costliest among natural climate-related hazards worldwide and poses significant risks to human health, the environment, and economic stability. Agriculture is the first and most direct sector impacted by drought hazards. It accounted for nearly 80% of all direct consequences on agricultural production during drought (Esfahanian et al., 2017; Ha et al., 2022). Markova et al. (2018) reported that the Food and Agriculture Organization (FAO) estimated that droughts account for 18% of total crop damage in the least-developed countries and low-and middle-income countries. Also, the recent report by the United Nations Office for Disaster Risk Reduction revealed that drought hazards cause annual agricultural losses of nearly USD 6.4 billion in the United States, while this figure in Europe reached USD 9 billion (Erian et al., 2021). Africa also has faced significant challenges due to increasing drought frequency and intensity in recent years. In some regions of Africa, drought has exacerbated food crises, poverty, and social instability. For example, Anderson et al. (2021) reported that nearly 40–60% of the pastoralist population across sub-Saharan Africa experienced food insecurity crises due to drought hazards and political conflicts between 2009 and 2019. In Asia, drought has become more frequent and impacted larger areas of economic losses. Shi et al. (2020) examined drought and flood disasters in China from 1984 to 2010 and reported that drought affected about 3.8 million people and cost nearly USD 300 million per decade. In Central Asia, drought is among the biggest concerns, and recent studies revealed significant damage to vegetation due to drought in

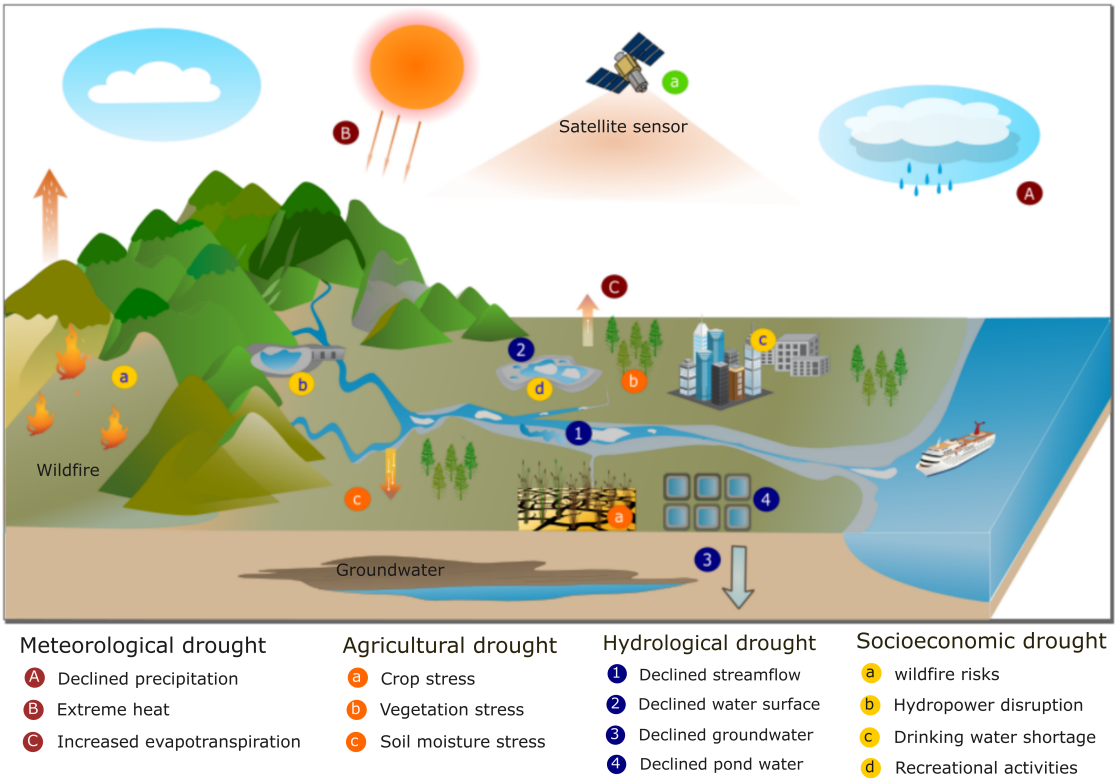

Figure 1.1: A simplified overview of main drought types and their connections. Meteorological drought is associated with decreased precipitation, increased temperatures, and evapotranspiration. Hydrological drought can be observed from decreased streamflow, groundwater, and water surface (e.g., ponds and lakes). Agricultural drought is primarily associated with decreased soil moisture, reduced crop production, and stressed vegetation ecosystems. Socioeconomic drought is primarily linked to water shortages for human and economic activities. These drought conditions can be detected and monitored by satellite sensors. This figure is adapted from a study by Ha et al. (2022).

this region (Yuan et al., 2022b; Liu et al., 2023; Guo et al., 2018b). In South Asia, drought frequently affects agriculture, and reported that drought can cause nearly 40% of annual rice production losses (Li et al., 2015). As drought is projected to increase in frequency and severity, economic losses due to drought are expected to increase, especially in dryland and less developed countries (Miyan, 2015; Price et al., 2022; Elkouk et al., 2022).

In Mainland Southeast Asia (MSEA), agriculture and fishery are among the most important sectors, supporting nearly 57% of its population across five different countries (Brown et al., 2008; ERCD-FAO, 2017). Rice is the main crop and plays a key role in local and national economies across the region. Industrial crops are also largely grown in Vietnam, Cambodia, and Thailand; for example, Vietnam is the second-largest coffee exporter worldwide (Fridell, 2014). However, this region has been increasingly vulnerable to drought and flood hazards in recent years. For example, the recent drought events in 2019 and 2020 caused an estimated loss of USD 840 million in Thailand. In Vietnam, Byrareddy et al.

Table 1.1: A collection of reported drought years and their associated impacts across the MSEA countries from 1960 to 2023. This dataset was sourced from the EM-DAT International Disaster Database.

Country	Drought Years	Associated Consequences	Deaths	People Affected	Homeless	Cost (x10^3 USD)	Events
Laos	1977, 1987, 1988, 1991, 1999, 2019	-	0	4,250,000	0	90	6
Myanmar	1979, 1981, 2018	-	0	9,050,000	20,000	240,054	3
Cambodia	1987, 1994, 2001, 2002, 2005, 2016	-	0	9,050,000	0	240,054	6
Vietnam	1987, 1997, 1999, 2002, 2005, 2015, 2019	Food shortage, Water shortage	0	8,545,558	0	8,763,728	8
Thailand	1991, 1993, 1999, 2002, 2005, 2008, 2010, 2011, 2012, 2014, 2015, 2016, 2019	Pollution	77	42,982,602	0	4,364,113	15
Total			**102**	**64,886,748**	**20,000**	**13,410,955**	**38**

(2021) reported that coffee production could be reduced by 6.7% during the drought years. In Cambodia, the drought event in 2016 affected nearly 32% of rice growing areas (Son and Thanh, 2022)). Notably, Venkatappa et al. (2021) used drought indicators and estimated that drought damaged about 9.2 million hectares of cropland between 1980 and 2019, while nearly 20.6 million tons of crop production was lost from 2015 to 2019. In addition, vegetation ecosystems in the region experienced significant changes due to drought. For instance, drought has exacerbated the forest loss across the study region in addition to human disturbances (Zhang et al., 2014; Chen et al., 2023). Apart from the estimated damage, the International Disaster Database provides reports of historical drought hazards worldwide from 1950 to the present. Table 1.1 provides a detailed description of drought years and their impacts on the MSEA region over the past seven decades. While the dataset may not capture every drought event in the region, it provides valuable insights into the severity and scale of the impacts observed during these periods. It is important to note that the quality of the recently collected data has significantly improved.

As seen in Table 1.1, the MSEA region has experienced several severe drought events and significant losses over the past five decades. Thailand had the highest number of drought events, with 13 events, whereas Myanmar had only three reported events. Generally, each country suffered from 6 to 8 drought events during this period. Notably, nearly 98% of economic losses due to drought came from Thailand and Vietnam. Vietnam was ranked the largest economic loss due to drought, accounting for about 65% of the total loss in the MSEA region. Over the past five decades, drought-related hazards have cost Vietnam an

estimated USD 8.7 billion, while Thailand incurred losses of around USD 4.4 billion. In contrast, Laos experienced the lowest financial impact from drought, with costs amounting to just USD 2 million. Also, drought has affected nearly 65 million people across five countries. For example, Thailand suffered from 15 drought events, affecting about 43 million people. Vietnam and Cambodia also had a large number of people affected by droughts, around 8.5 and 9 million people, respectively. Notably, Thailand had 77 reported deaths due to drought, and Myanmar had 25 deaths, whereas other countries primarily suffered from economic losses. Drought events in Myanmar caused 20 thousand people to become homeless. Food crises, water shortage, and pollution were common issues observed in the region as the aftershocks of drought.

1.3 Drought monitoring and management

Drought has traditionally been monitored and assessed using in-situ climate and soil moisture time series data, primarily through the measurements of historical precipitation and temperature. From these datasets, different indices are then developed and proposed, such as the most widely used Standardized Precipitation Index (SPI) (McKee et al., 1993), Standardized Precipitation Evapotranspiration Index (SPEI) (Vicente-Serrano et al., 2010), Palmer Drought Severity Index (PDSI) (Alley, 1984), and Soil Moisture Drought Index (SMDI) (Sohrabi et al., 2015). These indices provide valuable insights into different aspects of drought, such as meteorological, agricultural, and hydrological conditions based on in-situ climate or soil moisture measurements. While this method is considered one of the most reliable for capturing detailed and accurate drought information (Wilhite and Glantz, 1985), it is costly, labor-intensive, and challenging in data-sparse regions, including the MSEA countries. For instance, AghaKouchak et al. (2015) reported that many agricultural areas worldwide suffered from insufficient ground-based climate observations to capture the spatiotemporal variability of drought variables. Another challenge with ground-based meteorological drought monitoring is the lack of data standardization and consistency across regions. In the MSEA region, for example, there is no standardized framework or common platform for sharing meteorological station data. As a result, countries in the region collect and manage ground-based climate data differently, leading to variations in data quality, length of records, and measurement protocols. These discrepancies make it difficult to develop a holistic and accurate regional drought monitoring system. Consequently, most drought studies in the region have been limited to localized monitoring efforts. Moreover, climate-based indices cannot directly measure the impact of drought on vegetation ecosystems.

In recent years, remote sensing time series data has become a valuable alternative for monitoring and characterizing drought conditions. Earth observation data have been widely used to assess their impact on vegetation ecosystems, agriculture, and water resources. Drought information can be retrieved from different remote-sensing platforms, including thermal, multispectral, and microwave remote-sensing sensors. Among these, multispectral remote sensing received more attention due to its robustness and high sensitivity to drought-induced changes in vegetation health, soil moisture, and land surface conditions (Ha et al., 2022; AghaKouchak et al., 2015; West et al., 2019; Jiao et al., 2021). Numerous drought indices have been proposed to monitor drought conditions based on multispectral remote sensing data, including the Normalized Difference Vegetation Index (NDVI) (Tarpley et al., 1984), Vegetation Condition Index (VCI) (Liu and Kogan, 1996), Temperature Condition Index (TCI) (Kogan, 1995a), Vegetation Health Index (VHI) (Kogan et al., 2004), and Normalized Difference Drought Index (MNDDI) (Gu et al., 2007). Among these indices, NDVI has been the most widely used for drought monitoring due to its simplicity and broad applicability. However, it has some limitations due to its sensitivity to atmospheric disturbances and soil moisture saturation (Bajgiran et al., 2008). To address these limitations, other vegetation drought-based indices have been developed. Notably, VCI was introduced to overcome these shortcomings and recommended by the World Meteorological Organization (WMO) for global and regional drought monitoring (Svoboda et al., 2016).

With the unprecedented time series data and open-access policies, satellite-based data offers near-real-time, high spatial, and temporal observations of drought conditions over large areas. The monitoring and characterization of droughts have recently shifted from in-situ data to earth observation measurements. In the MSEA region, although in-situ drought monitoring remained widely used, the shift from station-based to satellite-based monitoring has become increasingly dominant in recent years. Our recent review study revealed that there has been a significant increase in satellite-based drought studies in the region over the last seven years (Ha et al., 2022). In the Lower Mekong Basin, the Mekong River Commission already established a drought forecasting and early warning system in 2018 (https://servirglobal.net/). This system employs four main drought indices: the combined drought index, the 1-month SPI, the soil moisture deficit index, and the standardized runoff index. This effort highlighted the importance of remote sensing data in monitoring and managing regional droughts. Several sensors such as Landsat, Sentinel-2, Moderate Resolution Imaging Spectroradiometer (MODIS), and Advanced Very High Resolution Radiometer (AVHR) have been widely used for monitoring drought hazards. MODIS has been widely used among these sensors due to its long-term observations and high spatiotemporal resolution (daily frequency). Despite its long-standing satellite and high spatial resolution, Landsat suffers from lower temporal resolution and frequent cloud cover in tropical areas

(Li et al., 2018a). Sentinel-2 is a promising sensor for monitoring drought with high spatiotemporal resolution, but it has a short data history and has only been available since 2015. AVHR has been observed on the earth since 1980, but it has a coarse resolution ($\sim$ 8 km), making it less suitable for regional drought monitoring. Given its balance of daily temporal coverage and moderate spatial resolution, MODIS remains one of the most effective sensors for drought monitoring, offering valuable insights for both short-term assessments and long-term trend analysis.

1.4 Rationale of the thesis

1.4.1 Research background

The MSEA is a major global crop-growing region and biodiversity hotspot. However, the ongoing global warming and intensified human activities have heightened its vulnerability to drought, posing significant threats to agriculture and ecosystems. This region has been and continues to experience significant climate variability, including increased temperatures and declined precipitation (Amnuaylojaroen and Chanvichit, 2019; Li et al., 2022b; Son et al., 2012; Ha et al., 2023; Phan-Van et al., 2022; Supharatid et al., 2022). Rainfed cropland dominates agricultural production across MSEA countries (Ha et al., 2023), making them particularly susceptible to shifts in rainfall patterns. Despite the growing vulnerability to drought and its widespread impacts, there has been little effort to provide consistent and region-wide monitoring and characterization of drought using earth observation time series. Thus, this dissertation aims to provide a detailed review and development framework of vegetation-based drought characteristics and their responses to multi-temporal climate and soil conditions. Also, it proposed a temporal harmonization approach to assess agricultural drought vulnerability by integrating remote sensing with socioeconomic time series data. This dissertation aims to provide a more holistic understanding of drought characteristics and vulnerability, delivering science-based insights for more robust drought mitigation and planning strategies.

1.4.2 Research objectives

The main objective of this doctoral dissertation is to provide (1) a detailed and comprehensive review of satellite-based drought remote sensing, (2) a spatiotemporal analysis of vegetation-based drought characteristics, (3) responses of vegetation-based drought to multi-temporal climate and soil drought conditions, and (4) assessment of agricultural drought vulnerability. The detailed research objectives are:

Objective 1: The first objective surveys the literature review and explores the efforts of satellite-based drought studies in Southeast Asia. Key areas of review include the spatiotemporal patterns of drought studies, the use of sensors and platforms, drought indices, and thematic drought applications. The primary goal of this review is to provide an overview of drought studies and identify research gaps from existing drought studies using EO data in the study region.

Objective 2: The second and primary objective covers the development and implementation framework for (1) generating a gap-free vegetation-based dataset and (2) monitoring and mapping drought characteristics using vegetation-based time series in the MSEA region. Vegetation-based drought conditions and their trends will be explored across different land cover types during dry and rainy seasons.

Objective 3: The third objective explores the responses of vegetation-based drought to multi-temporal climate and soil moisture factors, considering land cover types and elevation characteristics. This analysis aims to uncover how different ecosystems and terrains react to drought conditions over time. Also, an explainable machine learning method is developed to identify the drivers of vegetation-based drought related to climate and soil factors in natural and undisturbed areas.

Objective 4: The final objective of this dissertation is to assess agricultural drought vulnerability in a drought-prone region of the Vietnamese Central Highlands. This analysis aims to develop a robust understanding of agricultural drought vulnerability in the region by harmonizing temporal remote sensing and socioeconomic data.

Several research questions are formulated and investigated to address the respective objectives of this dissertation. The first group of questions concerns the existing literature review:

Research questions 1:

- What progress has been made in monitoring drought within the study region?
- How many satellite-based drought studies have been conducted, and what are their spatiotemporal patterns?
- What types of sensors, data sources, methods, indices, and thematic applications have been employed to monitor and detect drought conditions, and how have these studies cross-validated their output drought products to ensure accuracy and reliability?
- Which research gaps exist, and how can potential remote sensing and methods address these gaps?

The second group of questions addresses the implementation framework of automatic monitoring and characterization of vegetation-based drought conditions.

Research questions 2:

- What are the potentials and challenges of using satellite-based vegetation time series for monitoring and characterizing drought conditions?
- How can a drought event based on satellite-based vegetation be described using Run theory?
- What are spatiotemporal patterns of drought and their characteristics across the MSEA region from 2000 to 2022?
- Which specific years experienced severe drought, and how did drought conditions impact different land cover types during the dry and rainy seasons?
- How accurately do vegetation-based drought indicators perform compared to traditional climate-based indices?

The next set of questions focuses on vegetation-based drought responses to multitemporal climate and soil drought indices and the key driving factors influencing these responses in natural and undisturbed ecosystems.

Research questions 3:

- To what extent do climate and soil-based drought indicators influence vegetation-based conditions in the MSEA region, and how do these relationships vary across different land cover types and elevations?
- What are the main drivers of vegetation-based drought conditions in natural and undisturbed ecosystems in the MSEA region?

The final group of questions focuses on agricultural drought vulnerability in a drought-prone region of the Vietnamese Central Highlands. Specifically, this section addresses the following questions.

Research questions 4:

- What is the vulnerability framework outlined by the Intergovernmental Panel on Climate Change (IPCC), and how is it applied in the context of agricultural drought?
- Which variables are most appropriate for assessing agricultural drought vulnerability, and how should they be assigned to each vulnerability component (exposure, sensitivity, and adaptive capacity)?

- What methods are used to harmonize temporal remote sensing data with socioeconomic time series for a detailed drought vulnerability assessment?
- To what extent does each variable contribute to the respective components of agricultural drought vulnerability?
- What are the spatial patterns of agricultural drought vulnerability, and where are the identified drought hotspots in the region?

1.5 Dissertation outlines

This dissertation has seven main chapters, each designed to answer the corresponding questions of the objectives. The first chapter introduces drought concepts and types and describes how they are identified, managed, and monitored using remote sensing and ground-based observations (Chapter 1). The second chapter provides an overview of the study area, focusing on its climatic, geographic, and agricultural characteristics (Chapter 2). The third chapter presents a detailed review of recent progress in EO-based drought monitoring and characterization, identifying methodologies and research gaps from existing literature (Chapter 3). The next chapter developed a monitoring framework for mapping drought characteristics and seasonal trends using vegetation-based time series data (Chapter 4). The responses of vegetation-based drought to multitemporal climate-soil drought indices are presented in Chapter 5. After characterizing and assessing drought conditions across the MSEA region, Chapter 6 offers an agricultural drought vulnerability assessment in the drought-prone Vietnamese Central Highlands before presenting a conclusion and potential outlooks in Chapter 7.

Chapter 2

Study area

2.1 Geographical location and topography

Mainland Southeast Asia (MSEA), a subcontinent of Asia located in Southeast Asia, consists of five different countries: Cambodia, Laos, Myanmar, Thailand, and Vietnam (Figure 2.1). This region covers an area of nearly 2 million km^2, covering a wide range of topographic features, and has become a major global producer of agriculture. Geographically, the MSEA is bordered by China to the north, while its southern and eastern boundaries extend to the Gulf of Thailand and the East Sea, respectively. One of the most significant features in this region is the various characteristics of landforms, land cover types, water surface, and dense network of river systems (e.g., Mekong River). These geographical features enable various agricultural practices and growing vegetation ecosystems, especially along the Mekong River.

The MSEA mountains are characterized by high elevations (usually above 1000 m) and are primarily located in the northern and western parts of the region (Figure 2.1-a). The eastern extensions of the Himalayas contribute to the rugged terrain in the north of Myanmar, forming high mountains and deep valleys. Truong Son Range, running along the border between Laos and Vietnam, and the Tenasserim Hills are other significant mountainous areas. These highlands are crucial for biodiversity ecosystems and play a vital role in regulating climate and hydrology, acting as watersheds for the major rivers.

In contrast, the central and southern parts of the region feature expansive lowland plains and fertile river deltas. The Central Plains of Thailand and the Lower Vietnamese Mekong Delta are among the most productive agricultural areas, known as the "Rice Bowls" of Asia, due to their high rice productivity. Water surface frequently occurred in the Lower Vietnamese Mekong Delta, Red River Delta, and Lower Thailand (Figure 2.1-b). These low-lying areas are characterized by fertile alluvial soils deposited by river flooding, making

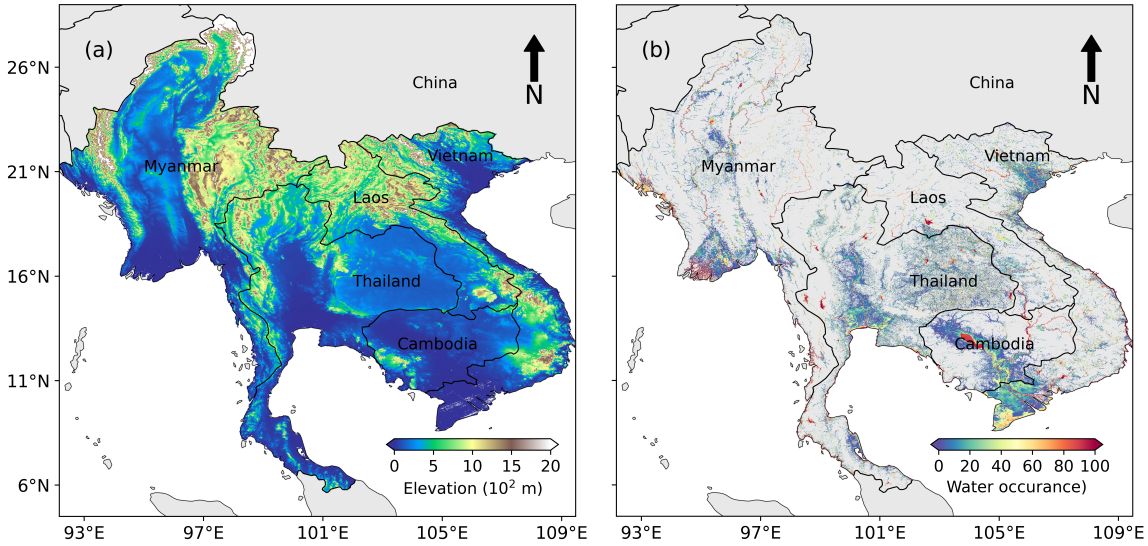

Figure 2.1: The topographic map of the study area highlights elevation gradients and water surface occurrence in Mainland Southeast Asia. The water surface occurrence produced from Landsat data (Pekel et al., 2016), while the elevation was obtained from NASA/CGIAR.

them ideal for intensive agriculture. The Tonle Sap Lake in Cambodia, the largest freshwater lake in the region, is another notable feature. In the south and east, the long coastlines along the Gulf of Thailand and the East Sea serve as critical hubs for marine biodiversity, fisheries, tourism, and economic development (e.g., marine transport and shipping industry).

2.2 Climatology and hydrology

The MSEA region lies in the tropics and experiences significant variations in precipitation and temperatures. Higher precipitation rates are primarily observed in the central coast of Vietnam and parts of Myanmar, whereas Thailand and central Myanmar experience lower precipitation rates (Figure 2.2-a). For example, Thailand has recorded the least precipitation, approximately 140 mm per month, over the past 20 years, while the central coast of Vietnam witnessed the highest precipitation rate, above 250 mm per month. Higher temperatures are reported in Thailand, Cambodia, Central Myanmar, and the Lower Vietnamese Mekong Delta (Figure 2.2). Recent studies projected an increase (decline) in temperature (precipitation) over the region in the upcoming decades (Supharatid et al., 2022; Almazroui et al., 2020; Tangang et al., 2020). Consequently, drought conditions are expected to worsen, impacting agricultural production and ecosystems.

Regarding seasonality, the MSEA region experiences a predominantly tropical and subtropical monsoon climate characterized by two wet and dry seasons. The region receives significant rainfall during the rainy season due to the southwest monsoon season from May to October (Mandapaka et al., 2017). This pattern can be observed in Figure 2.2c. In con-

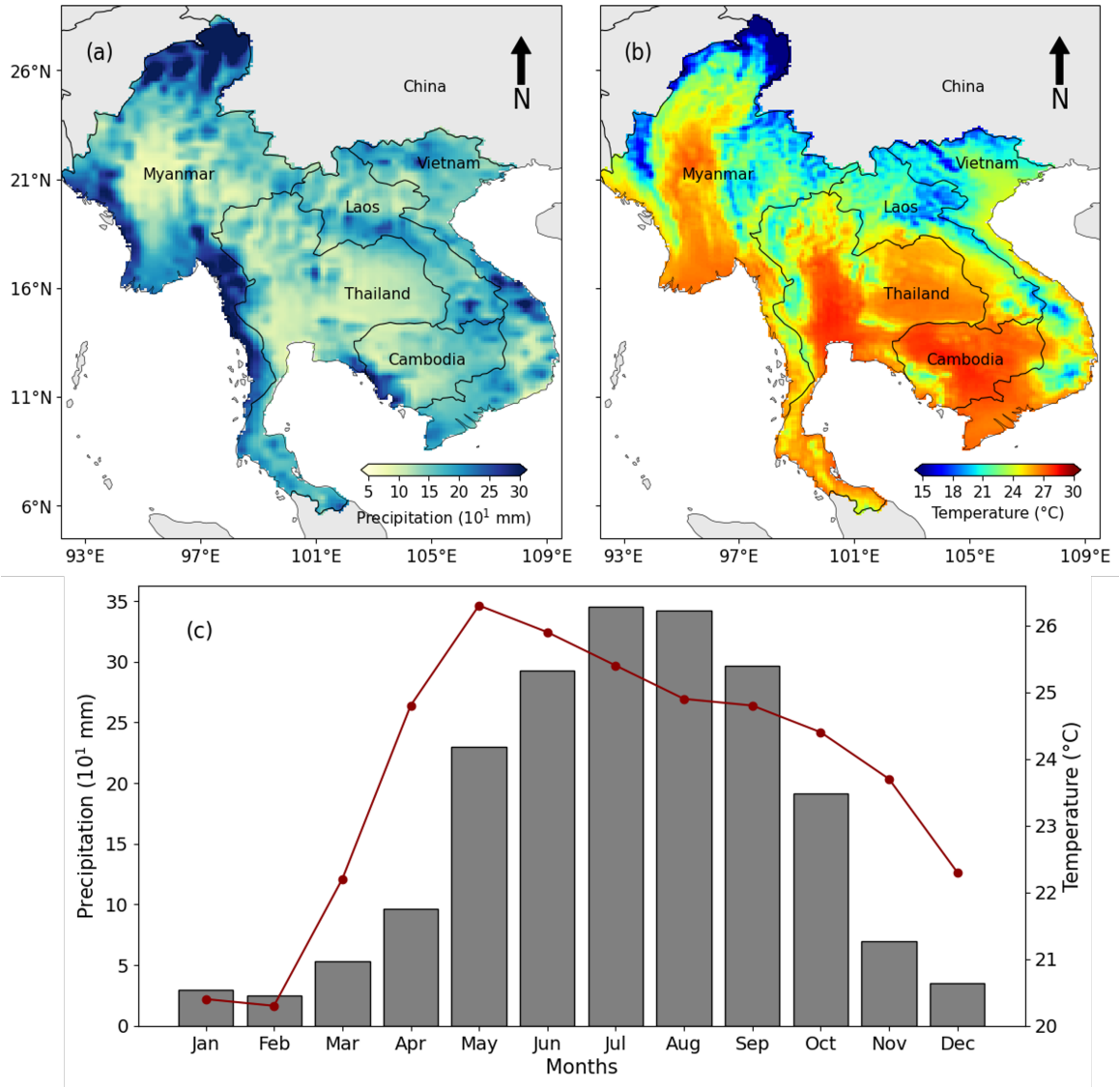

Figure 2.2: Spatial distribution of precipitation (a) and temperature (b) in Mainland Southeast Asia from 2000 to 2022. Monthly precipitation and temperature plots (c) are presented in bar and line graphs, respectively.

trast, the northeast monsoon from November to April brings drier conditions, influencing seasonal river flows and posing challenges for water management and agriculture. During this period, there is limited precipitation across the region. The highest (lowest) temperatures are observed in May and June (January and February). Overall, regions with higher temperatures tend to coincide with areas of lower precipitation, making them more vulnerable to drought conditions.

The MSEA countries exhibit variations in their climatic patterns and hydrological dynamics during both dry and rainy seasons (Figure 2.2). Cambodia, for instance, relies heavily on the seasonal floods of the Mekong River to sustain the Tonle Sap Lake, and this source of water is essential for its productive inland fisheries and agricultural production. Laos depends on the Mekong River and its tributaries for hydropower and agriculture. Myanmar

faces diverse climatic zones, from tropical to temperate, impacting water availability and agricultural productivity. Thailand manages its water resources through the Chao Phraya River Basin and faces water challenges during the dry season. Vietnam's Red River and Mekong Delta are critical for agriculture but increasingly susceptible to drought and salinity intrusion. Overall, the Mekong River plays a significant role in shaping the lives and economies of the MSEA countries. Still, this region has been increasingly vulnerable to drought hazards due to human-induced activities and climate change (Shrestha et al., 2016).

2.3 Land cover

The MSEA region features a wide range of land cover and land use types (Figure 2.3). Over the past two decades, significant changes in land cover and land use have occurred, driven by different factors such as economic development, urbanization, agricultural expansion, and deforestation. Here, the European Space Agency Climate Change Initiative (ESA CCI) land cover products were used to examine land cover types in the study region and their temporal characteristics (CCI, 2017). Overall, forests and agricultural lands dominate the land use in the region, collectively accounting for nearly 85% of the total land use. For example, cropland, rainfed and irrigated, accounted for nearly 38% of the landmass, while forests cover nearly 42% of the study region. Forests are diverse, from evergreen forests to deciduous forests, and this type is mainly observed in higher elevated mountains in Laos, northern Myanmar, and northern and central Vietnam. Conversely, agricultural land is primarily located in Central Myanmar, Thailand, and the Lower Mekong Basin. Rice, the region's main crop, is largely grown in Thailand and the Lower Vietnamese Mekong Delta. These two countries are also the largest rice exporters worldwide, accounting for nearly 25% of global rice exports (Yuan et al., 2022a).

The distribution of land cover and land use types varies significantly among the countries based on the ESA CCI land cover dataset (Figure 2.4). In Thailand, nearly 60% of the landmass is dedicated to agricultural practices, with forests covering approximately 25%. Vietnam, on the other hand, comprises about 39% cropland and 37% forestland. By contrast, Laos is primarily covered by forests ($\sim$ 57%) and shrublands ($\sim$ 28%), whereas cropland accounts for only 14%. Forests are similarly dominant in Myanmar, covering approximately 52% of its land area, and in Cambodia, where this land cover occupies about 46% of the country's territory. Shrublands are also dominant in some countries, such as Vietnam ($\sim$ 20%) and Myanmar ($\sim$ 18%). The other land uses (e.g., urban and water surface) account for less than 5% of the landmass in each of these countries.

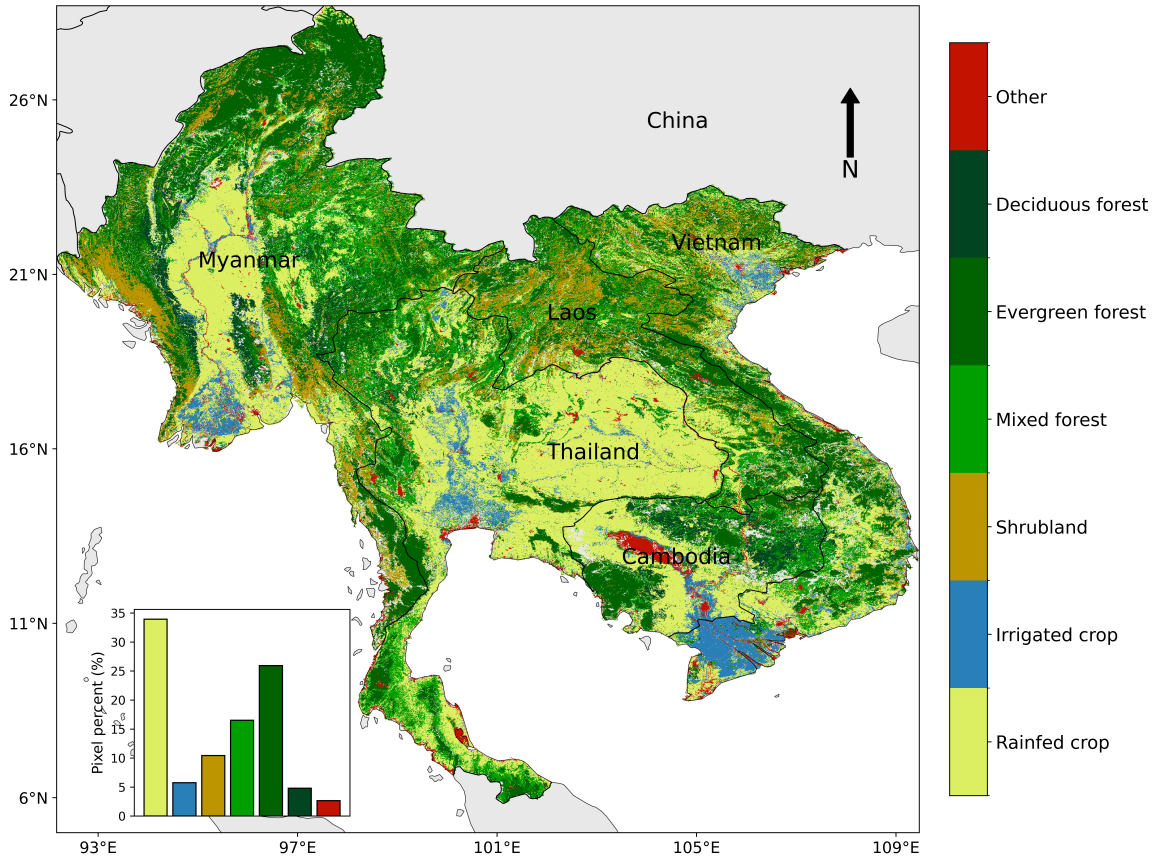

Figure 2.3: Spatial patterns of main land use and land cover types obtained from ESA CCI land cover products across the MSEA region. The inset plot in the map indicates the percentage of land cover types. Only stable pixels of land cover from 2000 to 2020 are examined.

Over the past 20 years, rapid urbanization and socio-economic development have significantly transformed land cover and land use across the region. However, the extent and nature of these changes have varied between countries. Generally, deforestation has been a major issue, driven by logging, agricultural expansion, and infrastructure development. Cambodia and Myanmar have experienced some of the highest deforestation rates (Hansen et al., 2013), while Vietnam and Thailand have implemented notable reforestation programs. For example, Cambodia suffered from nearly 50 thousand km^2 of forest loss from 1998 to 2018, while this figure for Myanmar was about 30 thousand km^2 over the same period (Namkhan et al., 2021). Agricultural expansion has seen increased intensification and diversification, with significant growth in cash crops such as rubber, coffee, and cassava. Urban growth has transformed land use patterns, often at the expense of cropland and forests. Vietnam and Cambodia witnessed annual urban growth ($\sim$ 14% per year) from 1992 to 2018 (Zhao et al., 2020). Recent studies projected land use change continues in the study region, and this transformation is expected to exacerbate the drought condition

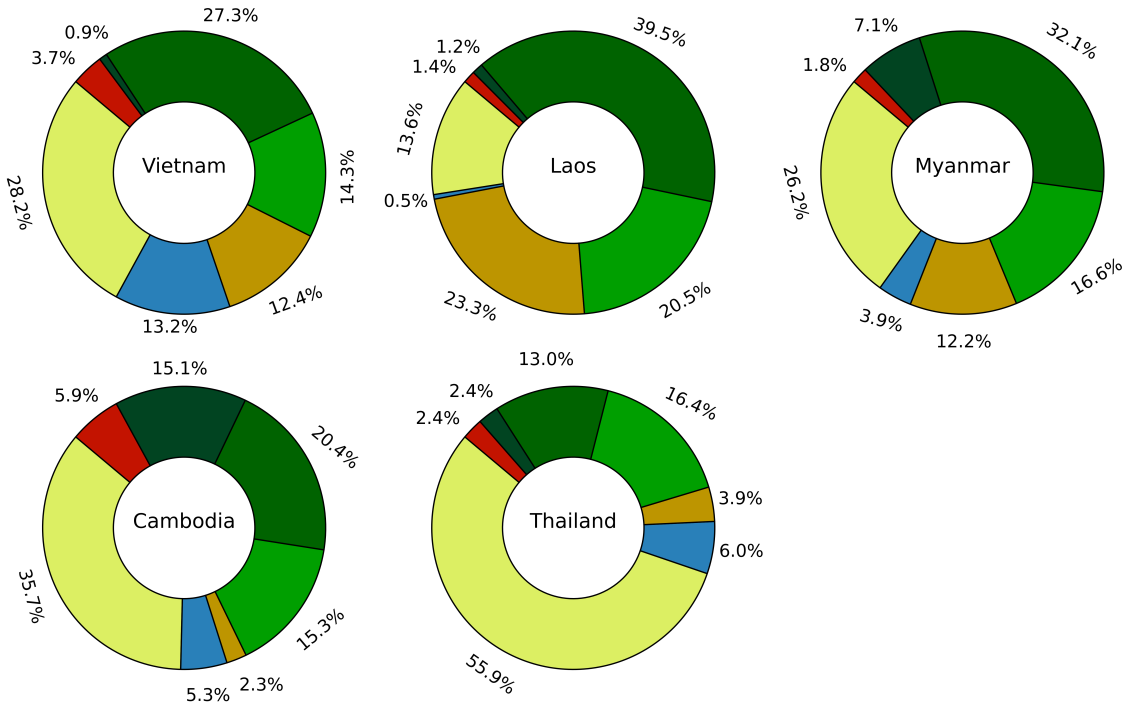

Figure 2.4: Percentage of land cover types by the MSEA countries derived from ESA CCI land cover products. Only stable pixels of land cover from 2000 to 2020 are examined.

and has major implications for biodiversity, water resources, and agricultural production (Chuah et al., 2018; van Vliet, 2019).

2.4 Socioeconomic context

The MSEA region is home to nearly 260 million population, accounting for about 3.1% of the global population. This region has experienced significant socio-economic transformations and urbanization over the past two decades. Despite these transformations, agriculture remains the predominant sector, employing a large portion of the population. For instance, nearly 70% of Myanmar's population is employed in agriculture, while in Vietnam, this figure is about 43%. Over the past 20 years, the region has seen a significant increase in GDP per capita and a marked decline in the poverty rate. In Thailand, the poverty rate has dramatically reduced from nearly 15% in 2000 to only 5.4% in 2020, and the country now boasts the highest GDP per capita in the study region, averaging around US$20,000 (Bank, 2023). Similarly, Vietnam has achieved notable economic milestones, with its current poverty rate reduced to approximately 5.7% and a GDP per capita of around US$4,500 (VGSD, 2023). Other countries still experienced high poverty rates, such as Laos ($\sim$ 24%) and Myanmar ($\sim$ 49%).

Among the countries in the region, Thailand has achieved significant economic transformation, advancing from a middle-income to an upper-middle-income country. The economy is diverse, with strong manufacturing, tourism, and agricultural sectors contributing to its growth. Forest conservation efforts in Thailand's northern and western highlands have mitigated some deforestation, while urban expansion, notably in Bangkok and surrounding areas, has reshaped land use patterns. Agriculture has diversified with increased cultivation of plantation crops alongside traditional rice farming. Likewise, Vietnam with the population of approximately 100 million has emerged as a rising economy with annual economic growth averaging 6–7% (VGSD, 2023). This growth is largely driven by a shift from a centrally planned to a market-oriented economy, alongside significant advancements in industrial production, services, and agriculture.

Cambodia, Laos, and Myanmar have also seen notable economic changes over the past decades. For instance, Cambodia has achieved outstanding economic growth, boasting one of the fastest-growing economies in the region from 1995 to 2019, with an impressive average annual growth rate of 7.6% (Bank, 2024). However, the COVID-19 pandemic severely impacted its economy from 2020 to 2022. This country began to show signs of recovery in 2023, achieving a growth rate of 5.4%. Despite their economic gains, this rapid development has come with significant environmental costs, including deforestation driven by logging, agricultural expansion, and urbanization, despite efforts to protect forested areas. Laos is still one of the least developed countries, and its economy mainly depends on hydropower, mining, and agriculture. Myanmar has recently experienced socio-economic changes, influenced by political reforms, impacting its landscape through logging, agriculture, and urbanization.

Chapter 3

A review of satellite-based drought in mainland Southeast Asia*

This chapter provides a detailed review of drought monitoring and assessment using satellite-based observation data in Southeast Asia from 2000 to 2021. There has been a growing number of drought-related studies in the region. However, there has been no detailed analysis and review to report the current progress of satellite-based drought studies. Thus, this was the first review to explore different aspects of drought-related studies, including temporal and spatial distribution of publications and remote sensing characteristics in the study region. The findings of this chapter present the existing state-of-the-art methods and limitations of previous research and highlight research gaps and potentials.

Specifically, Section 3.1 gives a methodological overview of the analysis of 102 research articles focusing on EO-based drought studies. Section 3.2 presents the findings of our review, highlighting the spatiotemporal distribution of studies, thematic applications, satellite sensors, and other related topics. The chapter concludes with a discussion of the challenges and opportunities associated with using satellite time series data for drought monitoring and assessment in Southeast Asia, offering insights into the potential for future advancements in this field.

3.1 Review objectives and methods

Drought has traditionally been monitored using in-situ measurement data, but this approach has major limitations, such as high cost and intensive labor. Recent advancements in remote sensing technologies and growing open data policies have enabled climatologists, hydrologists, and remote sensing researchers to access a vast amount of time series satellite

*This chapter is based in parts on Ha et al. (2022).

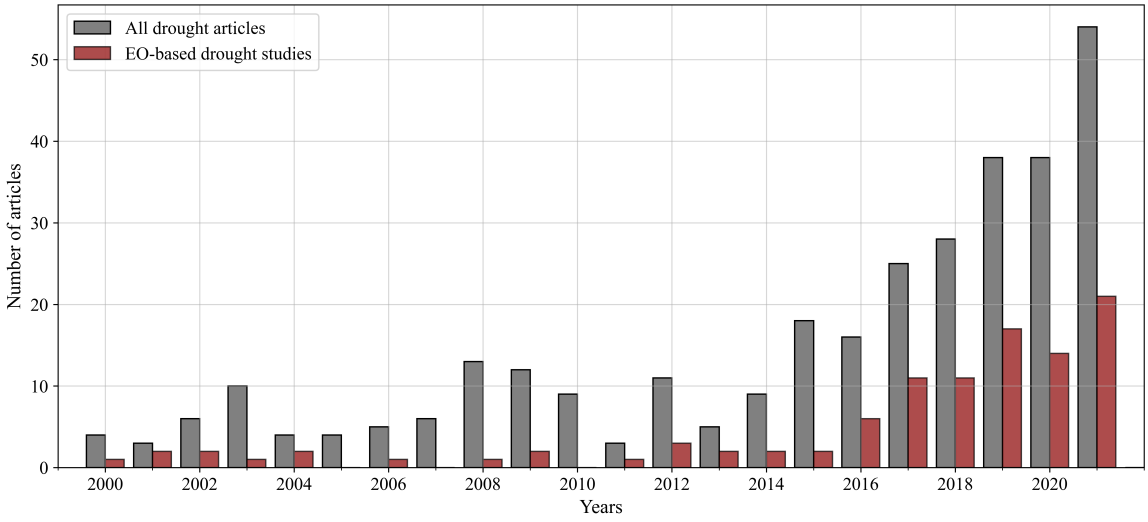

Figure 3.1: The number of annual drought studies in Southeast Asia from 2000 to 2021 using satellite-based earth observation and all other datasets sourced from Scopus database. Gray color indicates all drought–related research, while dark red represents satellite-based drought studies.

data for large-area drought monitoring and assessment. Consequently, these advancements have fueled a significant increase in scientific literature, and some research working groups have created extensive drought databases worldwide. For example, Vicente-Serrano et al. (2010) has recently produced a global dataset of multitemporal SPEI from 1901 to the present at 0.5 degrees.

While several reviews have been dedicated to surveying drought–related studies using earth observation data at global and regional scales (Damberg and AghaKouchak, 2014; Jiao et al., 2021; Barlow et al., 2016; Zhang and Zhou, 2015), there has been a lack of review studies focusing on Southeast Asia, where drought is frequently reported. For example, there has been a significant increase in drought studies using non-satellite and satellite-based approaches in Southeast Asia over the past 21 years (Figure 3.1). Therefore, this review summarizes recent progress in satellit-based drought studies, including spatial and temporal distribution, sensor characteristics, thematic applications, and drought indices. Also, this study discussed the potential of remote sensing measurements and its challenges regarding drought monitoring and assessment in Southeast Asia.

This chapter conducted a systematic literature search using the two primary academic platforms, Web of Science and Scopus. The preliminary investigation revealed a scarcity of relevant studies before 2000 in the Southeast Asian region, prompting to limit the search from January 2000 to December 2021. The review targeted peer-reviewed journal articles published in English, emphasizing EO-based methodologies for drought-related studies in Southeast Asia. The search expression included a variety of relevant terms, such as

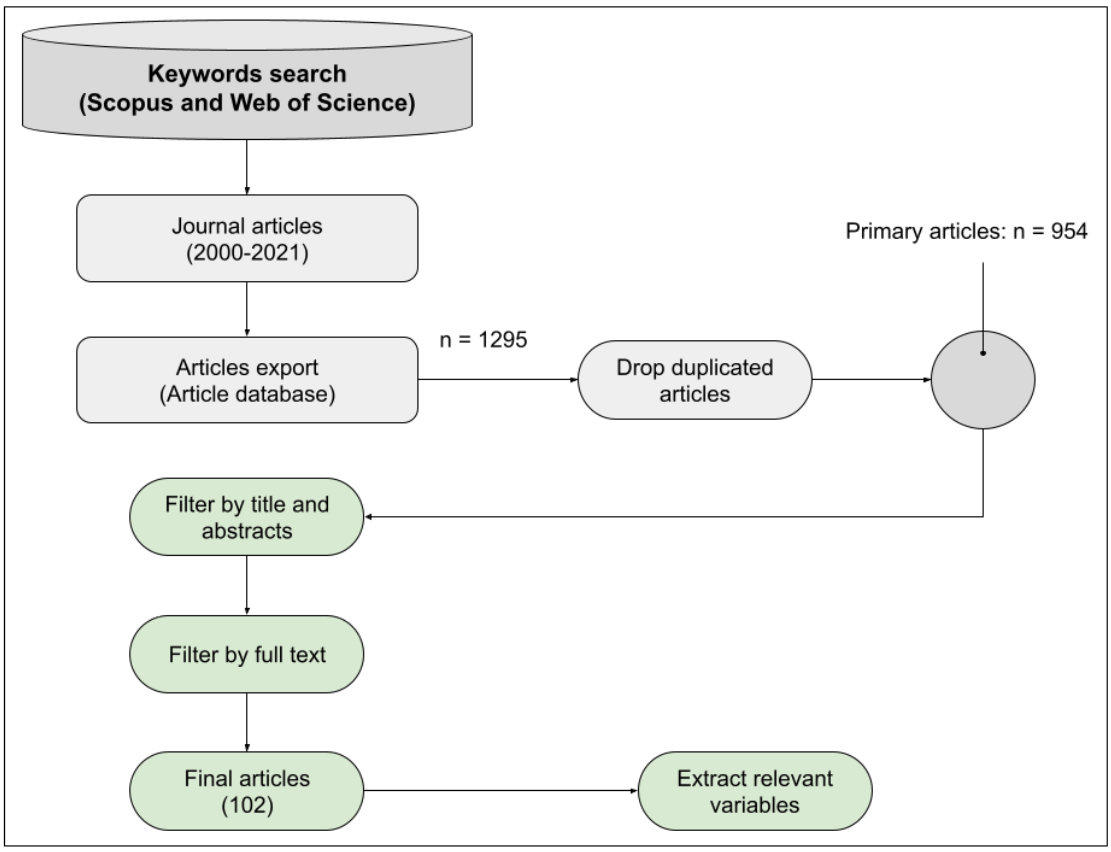

Figure 3.2: An overview framework of literature review from keyword search to analysis of drought studies in Southeast Asia. This diagram is adapted from a study by Ha et al. (2022).

"drought", "dry", "wildfire", and "remote sensing," alongside geographic terms related to Southeast Asia and the Mekong River Basin. The overall framework of the literature review undertaken in this study is presented in Figure 3.2.

The search query, structured as TS = ("drought*" OR "dry*" OR "wildfire") AND ("remote* sens*" OR "earth observation" OR "satellite*" OR MODIS OR Landsat OR Sentinel* OR SPOT OR AVHRR) AND ("Vietnam*" OR "Thailand" OR "Myanmar" OR "Lao*" OR "Cambodia*" OR "Malaysia*" OR "Singapore*" OR "Indonesia*" OR "Philippines" OR "Brunei" OR "Timor" OR "Mekong" OR "Southeast Asia*"), was used to search keywords in both databases. Here, the asterisk means included the rest of the word, such as Vietnam or Vietnamese. This search string began with drought and related terms/synonyms to broaden the search scope. Next, this topic combined Boolean operators to link remote sensing terms and geographic areas. This approach aimed to find as many drought-related studies in the region as possible to ensure a comprehensive literature database.

The search results returned 1,295 articles, many of which were duplicates. After removing duplicates, 954 articles remained. This study then manually reviewed titles and abstracts to exclude irrelevant studies, particularly those not utilizing satellite data or those

focused solely on non-satellite measurements. Articles were also screened to ensure they met our pre-defined criteria, focusing on satellite-based EO products and covering drought's meteorological, hydrological, agricultural, and ecological aspects. Finally, the final review included 102 articles covering various drought indicators and impacts, such as vegetation stress, surface water and groundwater variability, and drought-induced forest fires. This chapter included relevant drought-related studies utilizing satellite-based data published after 2021, where appropriate.

3.2 Results of the literature review

3.2.1 Annual number of drought studies

Southeast Asia is a major producer of agricultural products such as rice and coffee due to its tropical climate and soil fertility. However, the region has faced increasingly frequent droughts in recent decades, mainly driven by climate change and the El Niño-Southern Oscillation (ENSO) phenomenon. These challenges have imposed significant threats to food security, vegetation ecosystems, and water resources management in the region. As a result, there has been a growing interest in drought monitoring and assessment using remote sensing data from national governments and academic institutions. Figure 3.3 illustrated the annual increase in satellite-based articles focused on various drought monitoring methods and assessments over the past two decades.

After the El Niño event of 2015–2016, there has been a sharp increase in drought-related research in Southeast Asia (Figure 3.3). The number of published articles grew from under five in the first 15 years to nearly 25 in 2021. Before the ENSO events (2016), only a few studies were reported concerning agricultural and forest fire topics. In contrast, nearly 80% of drought studies have been published from 2018 to 2021. The highest number of drought publications was observed in 2021 (21 articles), followed by 2019 (19 articles). Regarding the drought types, agricultural drought was the most dominant from 2019 to 2021. This period also has witnessed an increase in hydrological and forest-related fire studies. For example, nearly 50% of hydrological studies were found during this period.

This peak in research output highlighted the growing concern and academic interest in understanding and mitigating drought impacts in the region, especially after significant drought events. The review also indicates that different drought types, agricultural, meteorological, hydrological, and socioeconomic, have been studied in Southeast Asia. However, agricultural drought has received the most attention, accounting for 57% of the total studies. This focus is likely due to the heavy reliance on agriculture for livelihoods and food security in the region, making it particularly vulnerable to drought conditions. Hydrological drought

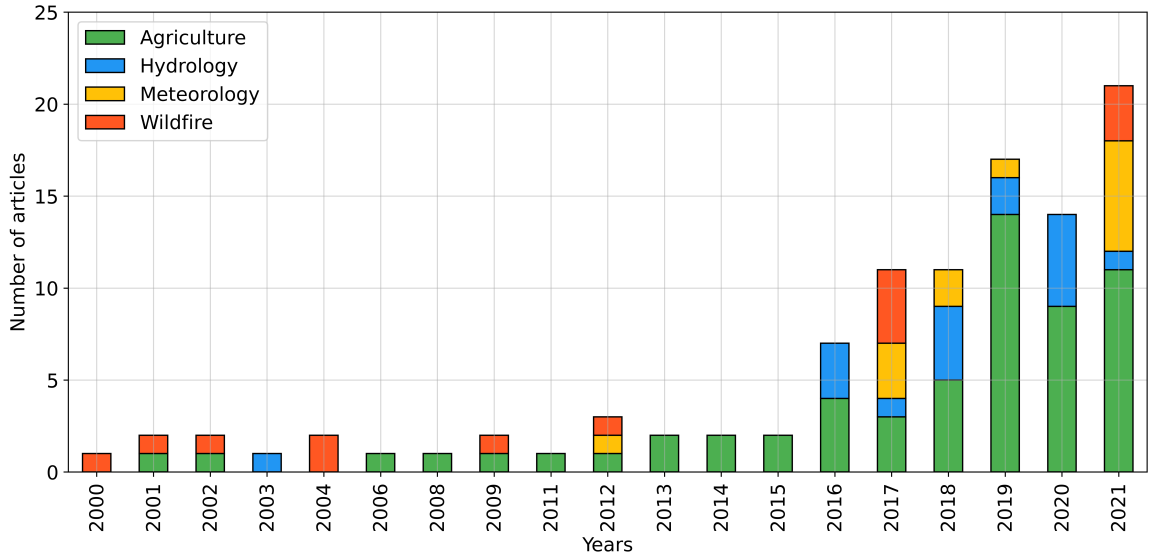

Figure 3.3: A stacked bar plot illustrated the increase in research publications on drought in Southeast Asia from 2000 to 2021. Among the different types of drought studies, agricultural drought received the most attention, while hydrological and forest-related droughts were the least frequently addressed.

was the second most examined type ($\sim$ 17%), reflecting the importance of understanding climate patterns and their implications for drought forecasting and management. Meteorological droughts and forest fires due to drought were less frequently studied, particularly in the first 15 years of the 21st century.

Drought studies in Southeast Asia have been disseminated across 60 journals. Notably, most of these studies appeared in non-remote sensing journals, and studies in Thailand have frequently been reported in local journals (Ha et al., 2022).

3.2.2 Spatial distribution of drought studies

Southeast Asian droughts have been observed and investigated across different spatial scales based on their specific characteristics and impacts, such as severity and duration. Drought hazards can occur at local, national, and regional scales. Thus, this review categorized the studies into two spatial scales: national and transnational studies. National drought studies focus on monitoring and assessing droughts within the administrative boundaries of a single country, such as at the district, provincial, or national level. On the other hand, transnational studies involve research conducted across two or more countries in the region, such as studies in Myanmar and Laos or the Lower Mekong Basin. The frequency of transnational drought studies is presented in Figure 3.4, while local studies are displayed as the total count of articles (Figure 3.5). Overall, a higher frequency of drought-related studies was found in Indonesia, Thailand, and Vietnam. These countries also had the highest number of drought studies across the region from 2000 to 2021.

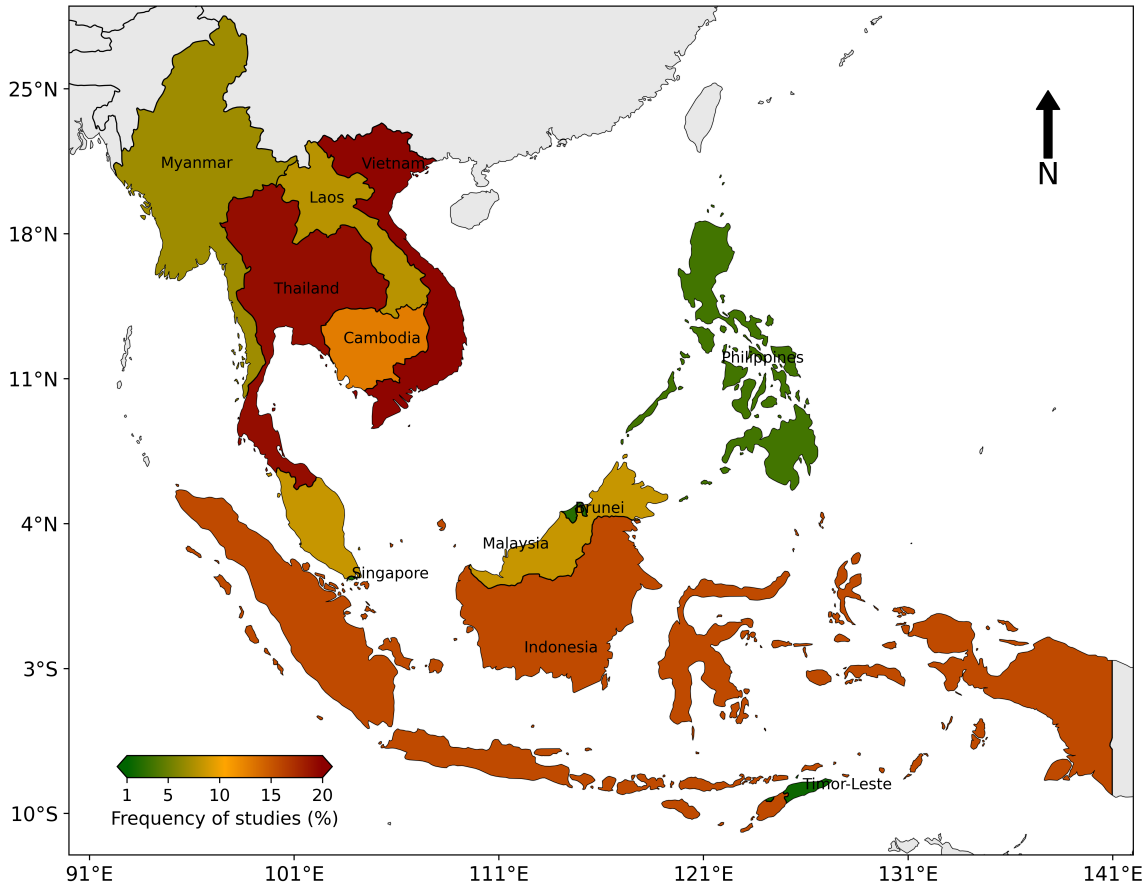

Figure 3.4: Spatial distribution of study frequency across Southeast Asia using satellite-based data from 2000 to 2023. Dark red indicates a higher frequency, while dark green presents a lower frequency of drought studies.

Figure 3.4 revealed that most drought-related studies in Southeast Asia were primarily concentrated in mainland regions. This region accounted for nearly 67% of the research. Notably, Thailand and Vietnam become the most studied countries, with 19% and 20%, respectively, underscoring their significance in drought research (e.g., drought monitoring and assessment). The higher frequency of studies in these countries reflects a notable concern for drought impacts and a robust scholarly interest in understanding and addressing the challenges posed by droughts in the region. Drought studies covered Indonesia with a frequency of approximately 16%, and it is ranked the third most studied country, followed by Cambodia at around 12%. Myanmar, Malaysia, and Laos had lower drought study frequency, from 6% to 8% of the studies. In contrast, other Southeast Asian countries were covered in less than 2% of the research over the past two decades. Notably, the Philippines and East Timor were among the least frequently studied, indicating a significant gap in research on drought impacts and management in these countries. This imbalance in research focus suggests that certain Southeast Asian countries may be underrepresented in the literature, potentially leading to a less comprehensive understanding of drought impacts across the entire region.

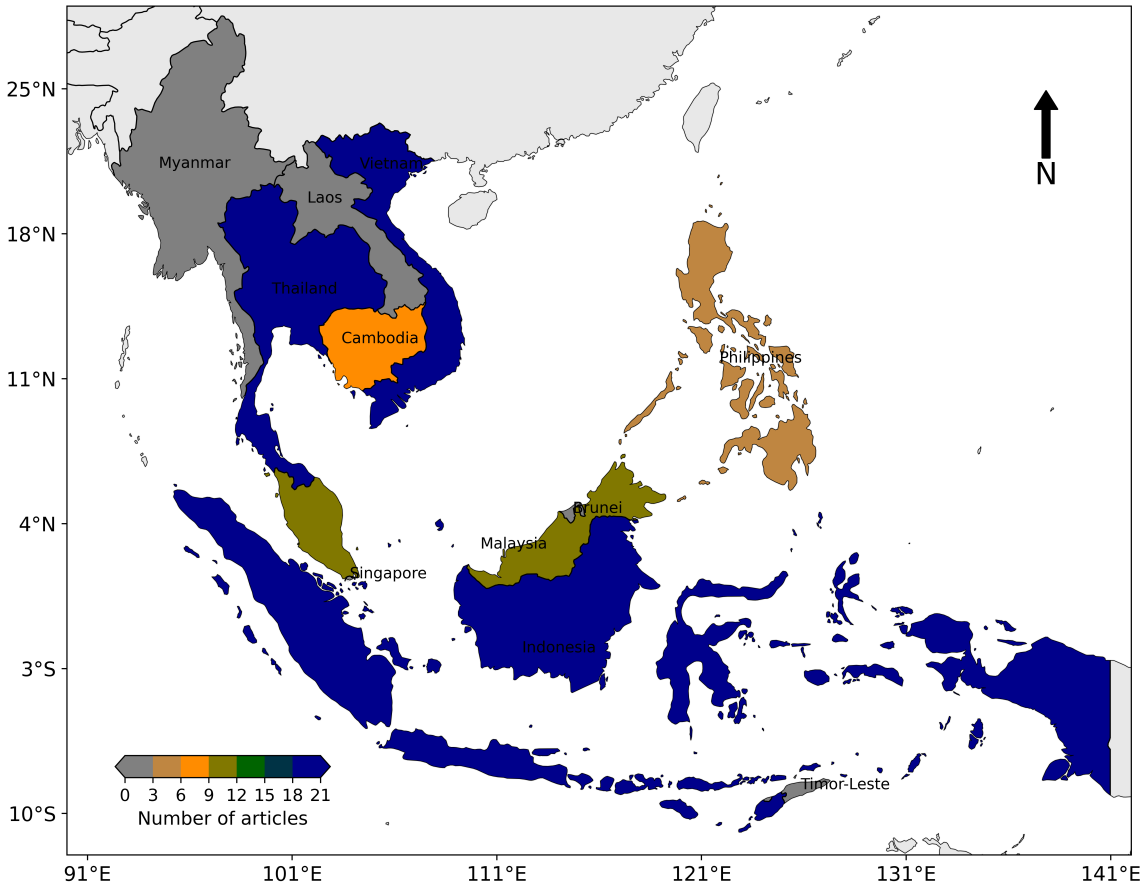

Figure 3.5: Spatial distribution of local and national EO-based drought studies across Southeast Asia from 2000 to 2021. The color bar indicates the number of articles corresponding to each country.

Regarding local and national drought studies, the analysis of drought studies revealed a significant research effort in some countries. Indonesia had the largest number of local and national drought studies, totaling 22 articles. Thailand ranked second with 21 studies, followed by Vietnam with 19 research articles. Malaysia contributed significantly, with around nine articles dedicated to drought research, while Cambodia had seven. These findings highlight a strong focus on these nations, likely due to their diverse climatic conditions and varying degrees of vulnerability to drought. In contrast, other countries in the region appear to be underrepresented in the literature. Notably, Myanmar and Laos have not featured any local or national drought studies using satellite-based observation data over the past decades. In addition, the remaining countries have contributed fewer than four articles each, indicating a significant gap in research coverage. This disparity suggests that regions with limited research might lack comprehensive insights into drought impacts and management, potentially hindering effective policy development and resource allocation in those areas.

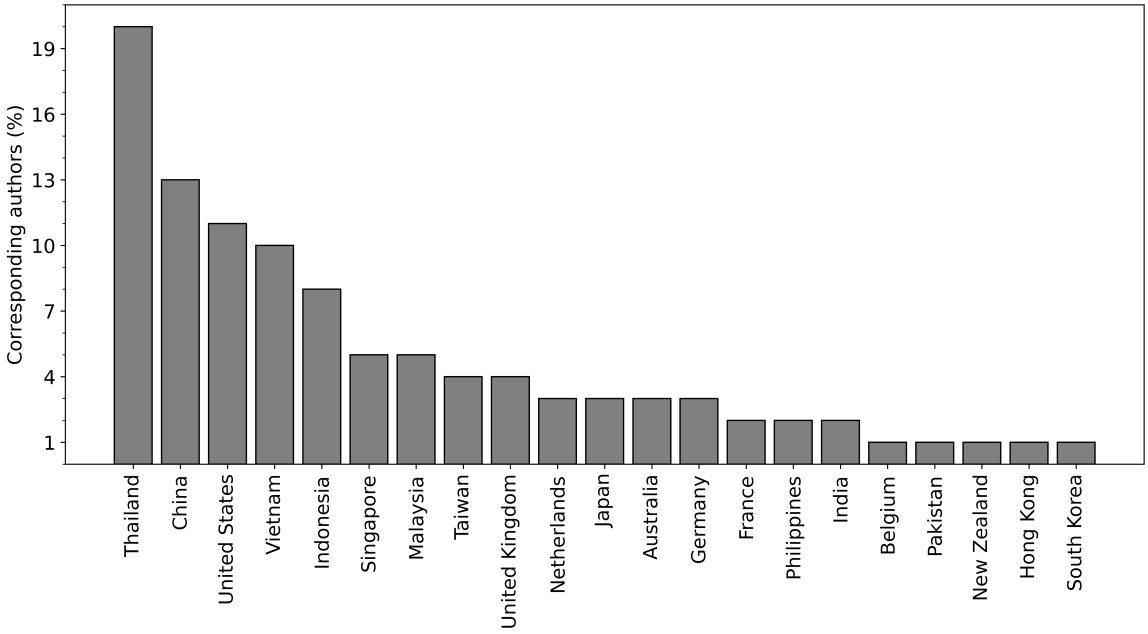

Figure 3.6: The percentage of corresponding authors associated with drought-related studies using EO data in Southeast Asia from 2000 to 2021.

The uneven distribution of drought studies is further highlighted by the significant role of international collaboration in drought research in Southeast Asian countries. Figure 3.6 displayed a significant presence of foreign institutions, as nearly 50% of corresponding authors come from outside the region. This indicates that while the research is geographically focused on Southeast Asia, a substantial portion of the academic leadership comes from other parts of the world. Specifically, nearly 75% of corresponding authors are based in Asia, underscoring the regional interest and expertise. In contrast, about 11% of the corresponding authors are from Europe, and 10% are from America, reflecting the global attention and interdisciplinary approach to studying drought impacts in Southeast Asia.

Within Southeast Asia, Thailand has been very active in drought monitoring and impact assessment (e.g., local scale studies), with approximately 20% of the corresponding authors coming from this country. Vietnam followed at around 11%, and Indonesia stood at 10%. The remaining Southeast Asian countries each contributed less than 5% of the corresponding authorship. These numbers suggest that while certain countries like Thailand and Vietnam are more prominently represented in leading drought research, many other nations in the study region are underrepresented in drought research and limited funding. This uneven distribution of corresponding authorship may have implications for the direction and focus of drought research in Southeast Asia, potentially affecting the development of locally relevant strategies and solutions.

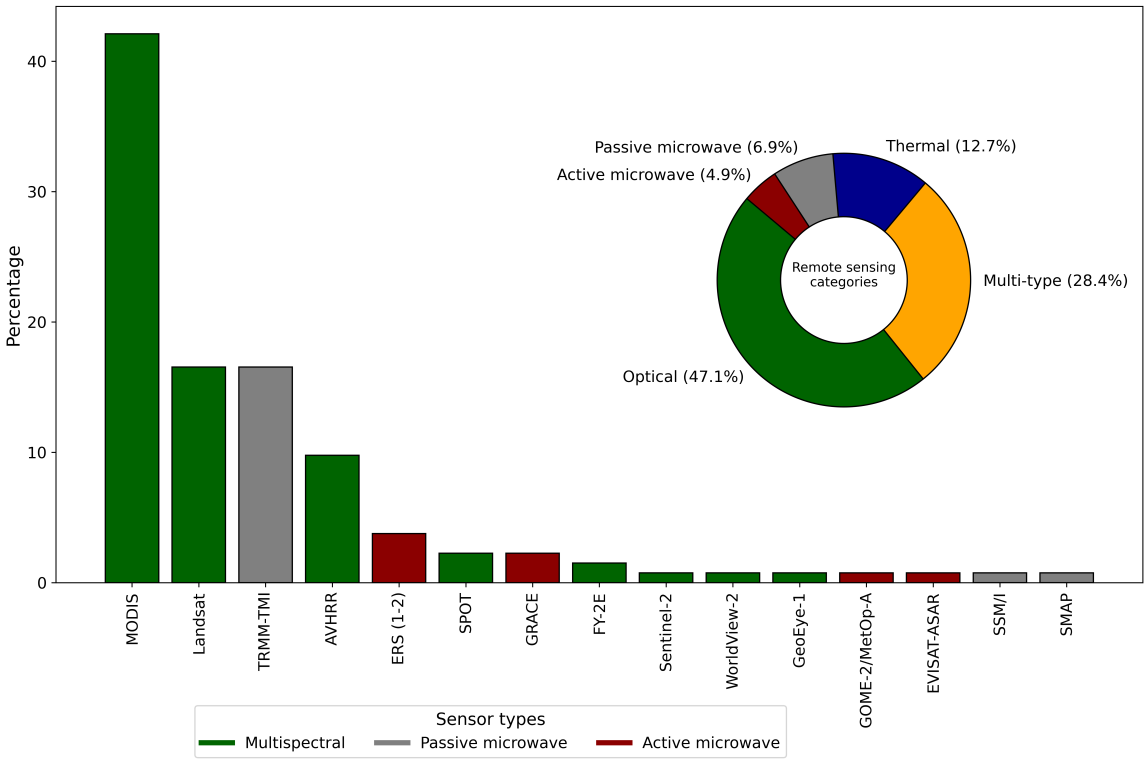

Figure 3.7: Percentage of satellite sensors and their categories used for drought monitoring and assessment over the past 21 years in Southeast Asia.

3.2.3 Satellite sensors of drought studies

In the last 21 years, numerous drought studies in Southeast Asia have employed a variety of satellite sensors, including active microwave, passive microwave, and optical satellites. For this review, remote sensing sensors were categorized into three primary types and further reclassified into five distinct remote sensing categories. Figure 3.7 illustrated the distribution of sensors and remote sensing categories used for drought mapping in Southeast Asia. In total, 15 satellite sensors were identified across these five categories.

Figure 3.7 indicated that multispectral sensors were the most used for drought monitoring and assessment in Southeast Asia ($\sim$ 75%). Passive microwave sensors are the next most frequently used, likely due to their ability to provide consistent data regardless of weather conditions or time of day. In contrast, active microwave sensors have seen the least use in the region, possibly due to their more complex data processing requirements and higher sensitivity to surface roughness, which may limit their applicability in drought studies.

Regarding the specific sensors, the MODIS sensor was the most frequently used, accounting for more than 40% of the studies (Figure 3.7). The TRMM and Landsat sensors were ranked second with about 16%. The AVHRR ranked third with nearly 10%. Other sensors have contributed under 5% over the past two decades (Figure 3.7). These remaining

sensors have limited applications in drought studies in the region. For example, the Sentinel-2 and SMAP sensors have rarely been applied to monitor drought conditions in Southeast Asia. In the tropics of Southeast Asia, cloud cover is a major limitation for drought monitoring using optical remote sensing sensors like Sentinel-2. In contrast, the complexity of SMAP passive remote sensing soil moisture poses a significant challenge in understanding and processing this data.

In addition, the pie chart in Figure 3.7 showed five major remote sensing categories used for drought monitoring and assessment in the study region. Overall, optical remote sensing received the greatest attention for monitoring and evaluating drought conditions, accounting for 47% of the data sources. In contrast, passive and active microwave satellite products were less used, representing less than 12% of the studies. The use of multi-sensor remote sensing has seen a rise in popularity in recent years, particularly for identifying drought-related phenomena, with around 29% of the publications in Southeast Asia incorporating this approach. Thermal remote sensing is another significant category, contributing to nearly 13% of drought studies in the region.

3.2.4 Satellite-based drought indices and validation

Drought hazards come in different forms and impact the environment and economy differently. Thus, several drought indices have been proposed to monitor and map various drought types. The SPI has been commonly used for meteorological drought, while the SWDI is more related to agricultural drought. Many drought indices have been used in Southeast Asia to monitor drought conditions. These indices are derived from various satellite sensors. This section considered 16 individual drought indices, categorizing them into eight predefined groups, including vegetation indices, precipitation indices, temperature indices, water indices, soil moisture indices, thermal indices, and others. Figure 3.8 illustrated different drought indices obtained from remote sensing data used for drought monitoring and assessment in Southeast Asia over the past 21 years. Overall, the majority of drought studies in Southeast Asia used vegetation-based and precipitation-based indices.

Drought studies in Southeast Asia have used diverse drought indices. Some studies have specified the name of drought indices, while others used anomaly indices or thematic remote sensing variables as drought indices. Nearly 17% of the studies employed "other" drought indices, such as evaporation indices and precipitation anomalies. Among the identified drought indices, the SPI was the most commonly used indicator, accounting for about 16% of the studies. The TAI index ranked third with 12%. Other indices, including NDVI, VHI, SMA, VCI, and TVDI, were used less frequently, ranging from 4% to 8% of the studies. The remaining indices were employed in fewer than 4% of the cases. For example, the

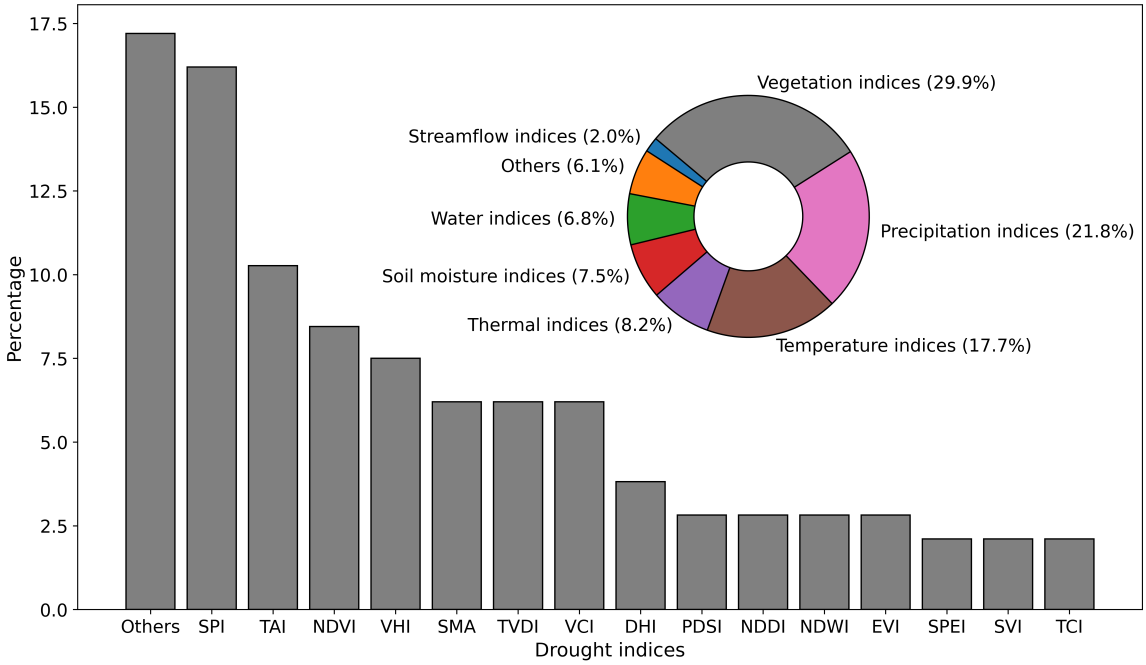

Figure 3.8: The percentage of individual indices and corresponding derived-input data used in drought studies across Southeast Asia from 2000 to 2021. SPI: Standardized Precipitation Index, NDVI: Normalized Difference Vegetation Index, TAI: Temperature Anomaly Index, VCI: Vegetation Condition Index, SMA: Soil Moisture Anomaly Index, VHI: Vegetation Health Index, TVDI: Temperature Vegetation Drought Index, DHI: Drought Hazard Index, EVI: Enhanced Vegetation Index, NDWI: Normalized Difference Water Index, NDDI: Normalized Difference Drought Index, PDSI: Palmer Drought Severity Index, TCI: Temperature Condition Index, SVI: Soil Vegetation Index, SPEI: Standardized Precipitation Evapotranspiration Index.

SPEI and TCI had less than 2.5% usage in the drought studies over the past 21 years in the study region.

Regarding drought indicator categories, the pie chart in Figure 3.8 displayed six different categories of drought indices used in Southeast Asia. The most commonly used category was vegetation-based, accounting for about 30% of the studies. The precipitation indicator group accounted for nearly 21%. In comparison, temperature-based indices ranked third, representing approximately 18% of the studies. The other indicator groups, including soil moisture and water indices, were used less frequently, each contributing to less than 10% of the studies. The streamflow-based index group was the least used, appearing in only 2% of the research, indicating a relatively limited focus on hydrological impacts in drought assessment across the region. In short, nearly 70% of drought indices used in the examined drought studies in Southeast Asia were derived from precipitation, vegetation, and temperature data. By contrast, the streamflow-based and water-based drought indices had fewer applications in the study region.

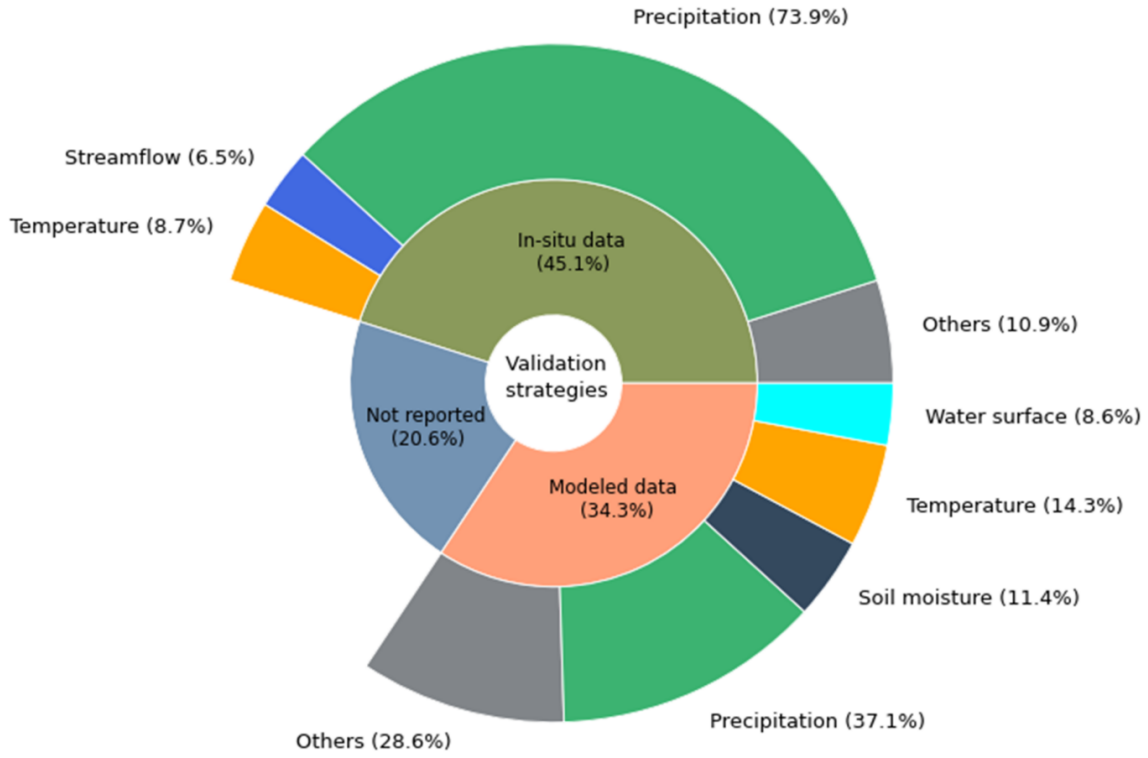

Figure 3.9: Types of validation data used for drought analysis in the region from 2000 to 2021. This figure is adapted from (Ha et al., 2022).

Regarding the cross-validation of drought indices, Figure 3.9 showed the percentage of validation strategies against the satellite-derived drought indices. Overall, nearly 80% of drought studies reported the accuracy assessment. Among the validation strategies, nearly 47% of the studies used in-situ climate measurements to cross-validate the drought products. Modeled data, including climate reanalysis data and satellite-based precipitation, reported 34%. Notably, nearly 21% of the studies did not report the accuracy assessment. Regardless of validation approaches, precipitation was the most commonly used data for cross-validating the drought conditions. Nearly 73% of the studies using in-situ data selected station-based precipitation for cross-validation. Likewise, precipitation from modeled data was frequently used for drought validation, accounting for 34%. Temperature and soil moisture from satellite-based observations or reanalysis data also gained popularity in drought validation. Together they accounted for nearly 26% of the studies using the modeled data (Figure 3.9). Other data, such as streamflow and water surface, were less frequently used in drought studies. For example, only 6.5% of the in-situ streamflow data was used to cross-validate drought conditions across Southeast Asia from 2000 to 2021.

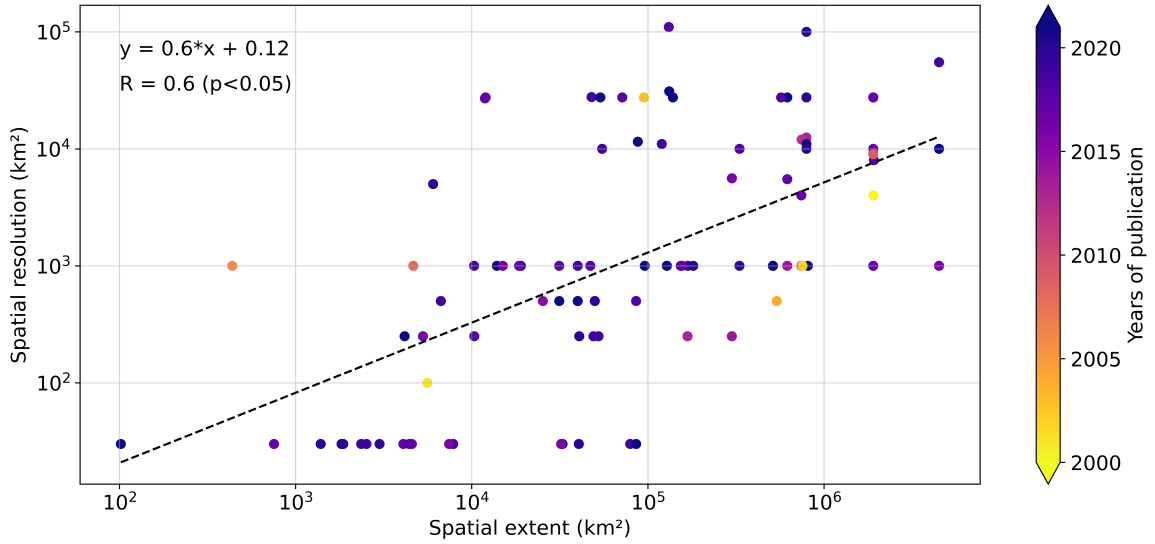

Figure 3.10: Correlation between spatial extent and spatial resolution reported in drought studies in Southeast Asia from 2000 to 2021. The color bar presents the years of publications.

3.2.5 Spatial resolution and data categories

Drought studies in Southeast Asia have been investigated with varying spatial extents and resolutions. Figure 3.10 showed the correlation between the spatial extent of a study area and its mapping resolution. The spatial extent of these studies ranges widely, from as small as 100 km^2 (local scale) to over 4 million km^2 (regional scale), with mapping resolutions varying from 30 m to approximately 110 km. Since droughts typically affect large regions, coarser resolutions are often preferred. The data suggests a positive trend between the map resolution and the spatial extent: as the study area increases in size, the spatial resolution of the produced map generally becomes coarser (Figure 3.10).

For spatial resolutions, the majority of drought studies in Southeast Asia employed relatively coarse spatial resolutions. It is observed that around 64% of the drought maps were generated with resolutions of 1 km or greater, while only 20% of the studies employed resolutions finer than 100 m. Although more recent research has begun to explore drought conditions at both low and high spatial resolutions, studies published before 2010 primarily used coarser resolutions. Notably, between 2018 and 2020, two studies examined drought at a very coarse resolution of approximately 111 km using data from the Gravity Recovery and Climate Experiment (GRACE), a collaborative mission between NASA and the German Aerospace Center (DLR). High spatial resolution data ($\leq$ 50 m) were primarily reported in local drought studies. No drought studies have covered over 1 million km^2 in Southeast Asia using high spatial resolution ($\leq$ 30 m) from 2000 to 2021.

Regarding spatial extent, over half of the studies were conducted across areas larger than 100,000 km^2. However, at regional and sub-regional scales, there were no studies that cov-

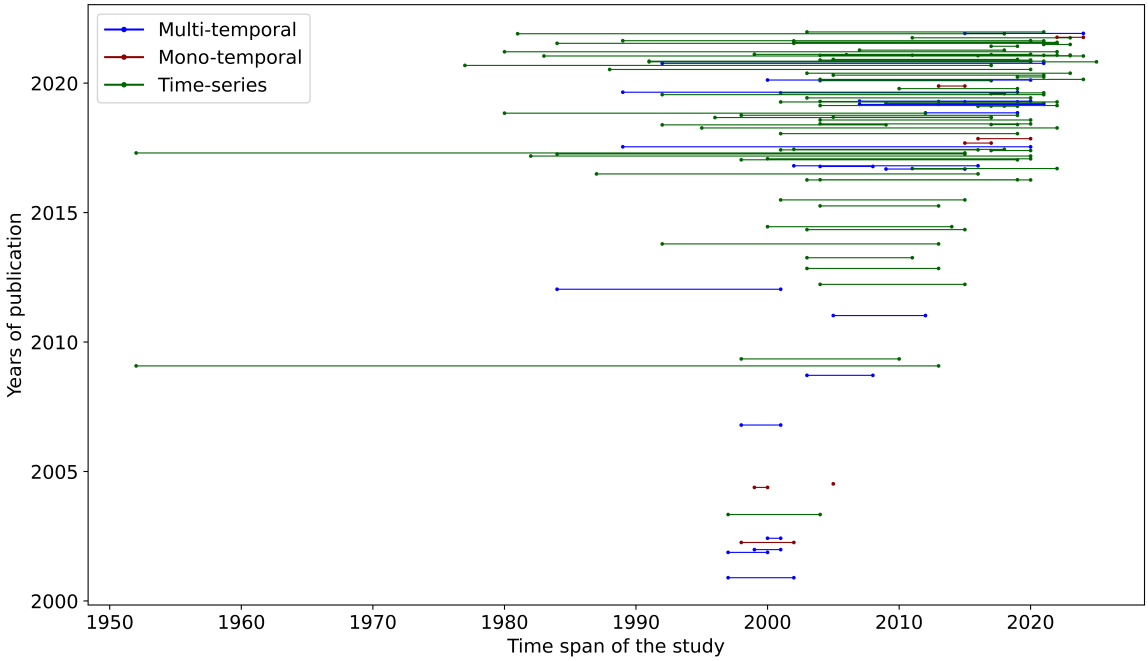

Figure 3.11: The duration of remote sensing data used in drought studies in Southeast Asia. The colors in the figure present three main types of temporal data. Time series indicates a continuous fixed period of data (e.g., monthly and annual), while multi-temporal data means data spans multiple periods. Mono-temporal data indicates data collected during a single period, representing a snapshot in time.

ered the entire region or mainland Southeast Asia with a resolution finer than 500 meters. Given that the area of most Southeast Asian countries ranges from 200,000 to 800,000 km^2, more than half of the drought studies were focused on local and national levels. Only three studies encompassed all Southeast Asian countries and four covered mainland Southeast Asian territory.

Regarding the duration of remote sensing data, Figure 3.11 presented the distribution of drought studies based on their duration. The majority of these studies in Southeast Asia used multi-temporal and time-series remote sensing data. For example, nearly 71% of the studies used time series data, while multi-temporal data accounted for 20%. In contrast, the single-date (mono-temporal) analyses were the least common, representing only 8.8% over the past two decades. There were only a few time-series drought studies before 2010, but this number has grown significantly in recent years. For instance, the last five years have seen a 10.7% increase in time-series drought publications. The year 2021 experienced the highest percentage of time series studies ($\sim$ 25%). Multi-temporal analyses were most frequently published in 2019, making up nearly 24% of the studies. In contrast, the use of mono-temporal analysis has decreased by 2.9% over the past five years. Despite a growing interest in time-series monitoring and assessment in the region, long-term studies (e.g., those extending beyond 30 years) remain relatively scarce. The analysis revealed that nearly

90% of drought studies utilized geospatial data covering periods of less than 30 years (Figure 3.11). On average, time-series studies spanned 18 years, while multi-temporal analyses had a mean duration of less than seven years. Notably, two studies explored drought conditions over periods exceeding 50 years.

3.2.6 Thematic application of drought studies

Drought is a complex phenomenon and can be quantified using different types of data and indices. This complexity results in many different types of droughts, each impacting the environment and economy differently. Each drought indicator can be used to assess different drought types, depending on the temporal lag or research objectives. For example, drought can be derived from precipitation, such as SPI, and this index is considered a meteorological drought if the SPI derives from a 3-month accumulative precipitation. However, the same index can be considered a hydrological drought if it is calculated over six months or nine months.

In recent years, satellite time series have been among the most commonly used sources for calculating drought indices. In Southeast Asia, there has been a rising interest in applying remote sensing to study droughts, resulting in a wide range of thematic applications. In this review, drought studies were categorized into four main applications: agriculture, hydrology, meteorology, and wildfire. These four applications were further divided into specific applications. For instance, agricultural applications included subcategories: vegetation stress, soil moisture, land use change, and crop stress. Several studies used vegetation indices to monitor drought effects on vegetation and forests, so these studies were grouped under vegetation stress. Hydrological applications included studies concerning streamflow, river, groundwater, and water surface variability. Figure 3.12 provided an overview of different drought applications and their subcategories in Southeast Asia from 2000 to 2021. Overall, most drought applications are dedicated to agriculture-related topics, accounting for nearly 58%. Hydrology is ranked second with nearly 16%, while wildfire and meteorology had lower rates of applications, at 14 and 12%, respectively. Among the agricultural applications, crop and vegetation stress received the most attention, accounting for nearly 43%. Fewer applications were contributed towards the soil moisture and land use droughts. Water surface applications associated with drought accounted for 12% of the studies. Other topics received less attention. For example, drought risk assessment witnessed only 2.8% of the studies, while streamflow and drought hotspot analysis accounted for 4.7% each.

Given the different drought applications in Southeast Asia, this study surveyed six thematic areas of drought application themes in detail. These themes included soil moisture and crop stress, vegetation stress, land use/land cover change due to drought, variations in

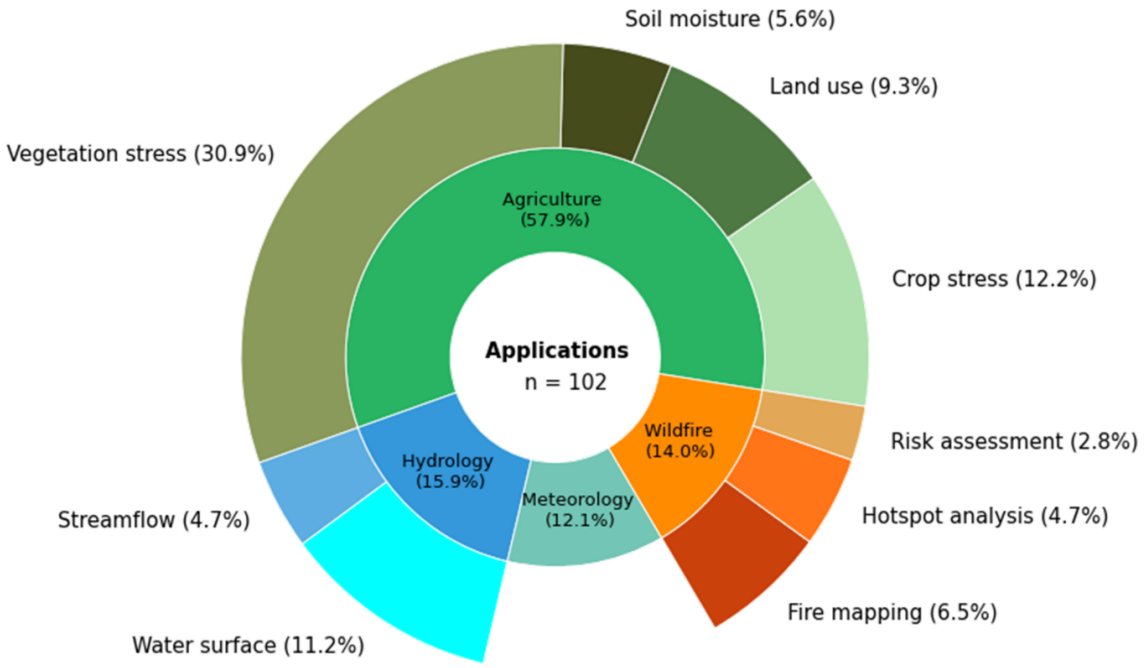

Figure 3.12: Distribution of thematic applications in drought studies across Southeast Asia. The figure presents drought applications across four major domains and nine subcategories, including crop stress, land use change, soil moisture, vegetation stress, streamflow and water surface variability, fire mapping, fire hotspot analysis, and fire risk assessment.

streamflow and water surfaces, forest fires linked to drought, and meteorological droughts. The following sections provided a detailed discussion of these thematic applications.

3.2.6.1 Vegetation-related applications

Vegetation growth is highly sensitive to drought hazards due to its dependence on water for essential processes, such as photosynthesis and nutrient uptake. Drought impacts can reduce vegetation growth and increase vulnerability to pests and diseases. In some cases, persistent drought conditions can damage the natural ecosystem (e.g., loss of biodiversity) and agricultural production. Southeast Asia is a major region of agriculture and biodiversity hotspot worldwide. For this reason, there has been a significant increase in drought studies dedicated to vegetation stress due to droughts over the past 20 years. Different aspects of drought-induced vegetation have been investigated. However, vegetation-based drought was the most investigated topic, accounting for nearly 31%. Thailand witnessed the largest number of vegetation drought applications (28%), while Vietnam ranked second with 14%. Indonesia and Malaysia together contributed to 23%. Other remaining countries had less than 5% of vegetation drought studies. Regarding the spatial extent of these studies, local and national vegetation drought studies were more frequently reported than regional applications. Nearly 90% of the studies were dedicated to local applications, while transnational studies received little attention.

Among the satellite-based indices, vegetation indices were the most commonly used index to derive vegetation drought information. These indices can be derived from multi-spectral sensors, such as Sentinel-2 and MODIS. Several vegetation indices have been used to monitor drought conditions in Southeast Asia. In Thailand, vegetation indices were the most used drought index for monitoring vegetation drought conditions, and these indices were mainly obtained from MODIS NDVI time series (Abhishek et al., 2021; Laosuwan et al., 2016; Rotjanakusol and Laosuwan, 2018; Thavorntam and Tantemsapya, 2013; Rotjanakusol and Laosuwan, 2019b; Uttaruk and Laosuwan, 2019; Sangpradid et al., 2021; Jomsrekrayom et al., 2021; Rotjanakusol and Laosuwan, 2019a; Thavorntam et al., 2015; Preedapirom et al., 2024; Jeefoo, 2023; Thavorntam et al., 2022). In contrast, Landsat-based vegetation drought monitoring has rarely been reported over the past two decades (Uttaruk and Laosuwan, 2017; Khampeera et al., 2018). In Vietnam, vegetation indices have been primarily employed for monitoring drought vulnerability (Tran et al., 2017), temperature-based drought (Dang et al., 2020) over a relatively short time frame (e.g., 5-10 years). Some recent studies investigated drought conditions using MODIS-based vegetation over the past two decades (Tran et al., 2023; Phan et al., 2020). In Indonesia, several drought studies used vegetation indices to monitor and assess local drought conditions (Rusdi et al., 2023; Mujiyo et al., 2023). Other countries reported less frequent vegetation drought studies over the study period.

In addition, several regional drought studies employed vegetation indices to report drought conditions in Southeast Asia. Qian et al. (2019) employed EVI and other indices to report the widespread decline of vegetation photosynthesis during the drought event in 2015-2016 across Southeast Asia. In the Lower Mekong Basin, Zhang et al. (2014) estimated the impact of drought on vegetation ecosystems, and they found that vegetation productivity can be reduced by up to 14% during drought years. Other studies also monitored forest changes during drought across the study region (Zhang et al., 2016; Perez and Comiso, 2014).

Most studies employed vegetation time series to monitor drought conditions at local and national levels using existing vegetation indices and drought classification systems. Little research has been done on drought machine learning, drought characterization, and method development. Xie and Fan (2021) tested different vegetation data reconstruction methods, such as Fourier-based harmonic analysis, Savitzky-Goly filter, and Whittaker smoother to derive drought information. They suggested that the reconstructed vegetation time series outperformed the unconstructed vegetation series in monitoring drought. Another study in Malaysia proposed a Southwest Monsoon drought classification system to assess natural and plantation vegetation (Mohd Razali et al., 2016). Some studies explored the potential

of microwave remote sensing and machine learning for monitoring drought in the region (Couturier et al., 2001; Prasetyo et al., 2021). Multi-sensor drought monitoring derived from vegetation indices has been reported in the studies by Arjasakusuma et al. (2018) and Zhang et al. (2016)).

In short, vegetation indices have been widely used to monitor vegetation-based drought conditions. Drought characteristics derived from vegetation indices have not been reported in Southeast Asia from 2000 to 2021. In addition, machine-learning applications and high spatial resolution have rarely been explored to monitor and characterize vegetation drought. Multi-sensor and microwave drought monitoring also need more attention since this topic has not yet been completely discovered in the region.

3.2.6.2 Soil moisture and crop stress applications

Soil moisture plays a key role in vegetation and crop growth, and if this impact persists prolonged, it can lead to crop failure. The deficiency of soil moisture can be considered an agricultural drought. In Southeast Asia, nearly 18% of the studies were dedicated to soil moisture drought and its impact on crops over the past 21 years. It is observed that drought studies in the region have extensively used vegetation indices as proxy soil moisture indicators for monitoring drought conditions. Soil moisture and crop-related drought conditions have been more frequently investigated in Thailand (Sa-Nguansilp et al., 2017; Raksapatcharawong et al., 2020; Sriwongsitanon et al., 2015; Raksapatcharawong and Veerakachen, 2019), in Vietnam (Luong et al., 2021), in Cambodia (Abhishek et al., 2021; Son and Thanh, 2022), and in the Lower Mekong Delta.

Satellite-based indices can be used to understand the spatial and temporal variability of soil moisture drought and their impact on agriculture. In Southeast Asia, vegetation-based indices have been widely used as proxy indicators for soil moisture drought. Several studies employed MODIS-based vegetation and temperature time series to detect agricultural drought and its impacts on cropland. Amalo et al. (2017) calculated the vegetation health index and detected nearly 2 thousand km^2 of extreme drought on agricultural land. In Cambodia, Son and Thanh (2022) estimated that nearly 31% of rice-growing areas suffered from severe drought conditions during the dry season in 2016. In Vietnam, Du et al. (2018) investigated agricultural drought in the Central Highlands and found that rice areas were more sensitive to precipitation, while forests had higher responses to the temperatures. Rice productivity in the Philippines has declined during the drought years (Parida et al., 2008), but rice yields in Cambodia annually increased without a clear relationship between drought parameters and rice yields (AghaKouchak et al., 2015). Other studies reported the impacts

of drought on crop patterns and production across Southeast Asian countries (Chen et al., 2011; Raksapatcharawong et al., 2020).

In addition to soil-vegetation-based indices, several studies employed vegetation-temperature-related indices as proxy soil moisture for drought monitoring, while other studies used composite indicators or simulated crop-drought productivity relationships (Chen et al., 2023; Perez et al., 2016; Son and Thanh, 2022; Shashikant et al., 2021). Overall, most soil moisture and crop-induced studies in Southeast Asia derived drought information from multispectral remote sensing observations. Soil moisture drought indices primarily included VHI, VCI, and soil moisture anomaly.

3.2.6.3 Drought-related to forest fires

Persistent drought conditions can increase the probability and frequency of wildfires, which can tremendously impact vegetation/forest ecosystems and the local economy. Southeast Asia lies in the tropics, where forests account for large areas of landmass. Over the past few decades, wildfires due to drought have frequently occurred and caused loss of biodiversity and natural forest ecosystems (Fuller et al., 2004; Vadrevu et al., 2019). In recent years, monitoring and mapping drought-induced wildfires received greater attention from the local universities and government institutions in the region. Nearly 14% of the studies were dedicated to forest-related fires due to drought, focusing on various aspects from wildfire risk assessment and forest fire mapping to hotspot analysis. However, drought-induced wildfire studies were focused primarily on Indonesia and Malaysia. For example, Indonesia ranked first with forest-related drought with about 70%, while Malaysia ranked second with 21%. The remaining countries received little research interest in drought-induced forest fires despite their frequent wildfires.

High temperatures are highly related to forest fires, and this property can be retrieved from thermal remote sensing. Hence, satellite-based thermal indices have been widely used to derive forest fire information due to drought. In Southeast Asia, a large number of drought-induced wildfires used thermal indices derived from MODIS and AVHRR sensors. During El Niño years, forests experienced more severe impacts, prompting an increase in studies during these periods (Gutman et al., 2000; Parameswaran et al., 2004; Noojipady et al., 2017; Siegert et al., 2001; Wooster et al., 2012,?). In Indonesia, forest fires were observed frequently in peatland and oil palms (Miettinen et al., 2017; Noojipady et al., 2017; Sloan et al., 2017; Lohberger et al., 2018). Drought-induced forest fires caused the loss of large-scale forest areas. For example, during the El Nino events in 1997 and 1998, nearly 3 million hectares of forests were lost on the island of Kalimantan, Indonesia (Fuller et al.,

2004). A recent study estimated nearly 107 thousand drought-induced forest fire hotspots during the drought event in 2015 across Indonesia and Malaysia (Miettinen et al., 2017).

Regarding the sensors of forest fire measurements, some studies employed a multi-sensor approach to detect forest fire events and hotspots (Noojipady et al., 2017; Parameswaran et al., 2004; Fanin and Van Der Werf, 2017). Overall, thermal anomaly indices and burnt products are frequently reported to be used to detect forest fire events, while other studies employed a burned mapping approach to identify the spatial extent of affected areas. For instance, Fanin and Van Der Werf (2017) estimated more than 4 million hectares of forest burnt during the drought event in 2015 with an accuracy of 84% using Sentinel-1 data. In short, drought-induced forest fire studies in the study region are mainly derived from multispectral remote sensing sensors (e.g., MODIS and Landsat), and thermal-based indices and burnt mapping are the frequently used methods for monitoring and detecting forest fire events.

3.2.6.4 Streamflow and water storage applications

Variations in surface water and streamflow can indicate hydrological drought. This process usually takes an extended period of time (e.g., six months or years) and has a significant impact on the environment and local economy. For example, lower lakes and rivers can directly affect agricultural production and hydropower plants. Although Southeast Asia lies in the tropics and experiences a good rainfall rate, this region also suffers from hydrological drought. Notably, a recent investigation revealed that the Lower Mekong Delta experienced a decline in water surface in some parts of the Lower Mekong Delta from 2001 to 2017 (Aires et al., 2020).

Given the importance of water resources, several studies were dedicated to surveying hydrology-related drought in Southeast Asia. It is observed that drought has caused significant variations in the surface water of the Tonle Sap Lake in Cambodia (Frappart et al., 2018; Tanaka et al., 2003). Specifically, Erban and Gorelick (2016) estimated that nearly 96% of rice crops in Cambodia remained uncultivated during the dry season because of the shortage of surface water. Optical remote sensing approaches have become more widely used in monitoring and estimating the dynamics of water surface, including rivers, lakes, and streamflow (Aires et al., 2020; Erban and Gorelick, 2016; Gu et al., 2021). In addition, recent studies have combined multispectral and microwave remote-sensing satellites for estimating surface water, for example, the use of MODIS, GRACE, ENVISAT, and TRMM (Frappart et al., 2018; Hidayat et al., 2017). In this regard, Pham-Duc et al. (2019) employed MODIS, GRACE, and ENVISAT sensors to monitor the monthly dynamics of surface and subsurface water in the Lower Mekong Delta and reported that maximum (min-

imum) surface waters were observed from July to August (March to April). Other studies cross-validated the satellite-based datasets for monitoring hydrological drought. In Vietnam, Le et al. (2020b) used in-situ measurements to cross-validate eight satellite-based precipitation datasets and found the CHIRPS potential for detecting hydrological drought. Correlation analysis was also used to analyze the relationship between surface water variation and droughts and the El Nino Southern Oscillation Index (ENSO) (Fok et al., 2018).

Despite some efforts, there is still limited research on subsurface water variability due to drought. Recent studies employed the GRACE dataset to monitor subsurface waters in the region (Pham-Duc et al., 2019; Jing et al., 2020). They reported a slight decline in water surface and subsurface water from 2003 to 2016, while the GRACE has potential for subsurface water monitoring. Also, little effort has been made to estimate hydrological drought using machine learning and deep learning. Future research should be prioritized to monitor and predict the hydrological drought given the increasing global climate crisis.

3.2.6.5 Drought-induced land use change

Land use changes and human activities can intensify drought conditions by degrading soil and vegetation. This degradation reduces crop productivity and results in higher costs for restoration and agricultural management. In Southeast Asia, increasing drought conditions can influence land use patterns and ecological ecosystems. For example, prolonged droughts have increased the frequency of forest fires across the region (Taylor et al., 1999). With the ongoing climate crisis, droughts can quicken the rate of land desertification and, therefore, threaten agricultural sectors.

Land-use-related drought studies received less attention in Southeast Asia during the study period. Only 9.5% of the studies during this period investigated the impacts of drought on land use patterns or related topics. Vietnam and Indonesia witnessed more studies on this topic (Tran et al., 2019b; Hien et al., 2019; Tran et al., 2019a; Phan et al., 2020; Tran et al., 2019c; Le et al., 2020a; Nita et al., 2020). For example, Hien et al. (2019) used climate and environmental data and estimated that nearly 35% of coastal parts of Binh Thuan province could experience desertification. This study also projected that the desertified area could reach nearly 140 thousand hectares by 2050. It is observed that MODIS and Landsat satellite sensors have been widely used to investigate land use-drought relationships in the region.

3.2.7 Meteorological drought

A lack of precipitation over a short period is usually considered a meteorological drought, which triggers other types of droughts. In Southeast Asia, meteorological drought studies mainly investigated precipitation-based drought and assessed their accuracy among different datasets. Most of these studies were conducted in Indonesia ($\sim$ 30%), and Thailand and Vietnam ranked second with 15% each. Other countries had a lower number of studies investigating meteorological drought. However, it is observed that nearly 70% of these studies were conducted in the MSEA region.

A wide range of precipitation datasets, both satellite-based and reanalysis products, have been created to support drought monitoring and characterization, and these datasets have different spatial and temporal resolutions and accuracy (Tian and Peters-Lidard, 2010; Sun et al., 2018). For this reason, some studies in the region cross-validated the accuracy of satellite-based precipitation for deriving drought information. Vu et al. (2018) used five different precipitation datasets to monitor drought, and they reported a higher accuracy obtained from Global Precipitation Climatology Center (GPCC) data. Other studies reported higher accuracy of drought information derived from the Tropical Rainfall Measuring Mission (TRMM) in Singapore and Malaysia (Tan et al., 2018, 2017). In Indonesia, Kuswanto and Naufal (2019) employed TRMM and Modern-Era Retrospective analysis for Research and Applications (MERRA-2) to estimate meteorological drought and found that the MERRA-2 had higher accuracy than its counterpart.

Regarding precipitation-based drought methods, the SPI was the most frequently used drought index to derive meteorological drought information in Southeast Asia, followed by the SPEI. Dimyati et al. (2024) derived the SPI from Climate Hazards Group InfraRed Precipitation with Station (CHIRPS) data and reported that meteorological drought occurred before the agricultural drought in Indonesia. One major limitation of using satellite-based precipitation data is coarse spatial resolution. For example, the CHIRPS has a spatial resolution of 5 km, while the spatial resolution of TRMM-based data is $\sim$ 28 km. This resolution may not be sufficient to monitor and characterize drought conditions at field scale. In short, there are still limited drought studies using satellite-based precipitation time series. The SPI and SPEI were two primary precipitation-based drought indices in the region. Despite their large-scale area and frequent observations, cross-validation and spatial enhancement should be focused on to ensure the quality and accuracy of the drought products.

3.3 Discussion and future directions

Southeast Asia witnessed a significant increase in satellite-based drought studies over the past 21 years. However, these studies were unevenly distributed among the countries. Nearly 70% of the studies were undertaken in four countries (Vietnam, Thailand, Indonesia, and Malaysia). This is likely due to frequent droughts and the availability of research funding in these countries. For example, Indonesia reported 22 mega-drought events, which affected nearly 8 million people from 1966 to 2021 (Ha et al., 2022). Likewise, Venkatappa et al. (2021) revealed that rainfed cropland in Thailand and Cambodia has been more vulnerable to drought than other countries. Despite the increase in drought studies, nearly 50% of the corresponding authors come from outside Southeast Asia. Notably, seven drought studies in Cambodia were not associated with Cambodian universities or institutions. This trend could be due to the lack of internal funding opportunities and technical expertise. Gerke and Evers (2006) reported a growing reliance on foreign institutions for science and research. Given the increasing climate crisis, strong collaboration is expected to boost drought research in the region.

Environmental satellites have been in orbit for nearly 50 years (Wulder et al., 2022), but only a handful of studies have investigated long-term drought conditions (e.g., $\geq$ 30 years) in Southeast Asia (Figure 3.11). Data quality, cloud cover, and technical expertise could be the main challenges in deriving long-term drought information in the region. Although the Landsat program opened its data archive from the 1970s to the present, early Landsat scenes had lower quality and less frequent observations of the land surface. In Southeast Asia, cloud cover significantly pollutes optical remote-sensing scenes (Li et al., 2018a). This limits the production of long-term drought products in the region. Furthermore, monitoring drought conditions over large-scale areas using long-term time series data requires high-performance computing platforms, which may be challenging in some countries.

Despite the growing number of drought-related publications, there has been a notable absence of studies focused on developing new drought indices in the region. All the studies employed existing drought indices derived from satellite-based time series or multi-temporal data to report drought conditions, such as drought severity. It is also observed that no studies have been reported to derive drought characteristics from optical remote sensing time series in the region. Some other studies reported drought characteristics at local and national scales based on non-satellite and reanalysis data (Le et al., 2019; Zhao et al., 2022; Khalil, 2020). In recent years, several studies reported flash drought, which lasts only a few weeks but profoundly impacts agriculture. In Southeast Asia, this drought has rarely been reported. Among various thematic applications, agriculture-related drought gained the most attention, likely due to extensive cropland in the region. Several studies were dedicated

to surveying vegetation-based drought, especially in Thailand, but little research has been done to assess the response of vegetation-based drought to other drought types in consideration of land cover types and elevation characteristics. Specific-crop drought impacts and assessments have rarely been undertaken across Southeast Asian countries. A lack of detailed crop type classification could be the main reason preventing the implementation of local and transnational studies on crop drought sensitivity assessment.

Cross-validation of remote sensing products serves as critical information in the decision-making process regarding drought mitigation and planning. Map uncertainties can give users the confidence to make timely, more accurate decisions. However, nearly 21% of the studies did not report drought mapping accuracy in Southeast Asia (Figure 3.9). Collecting in-situ measurements for cross-validation would be the main challenge in this region. It is observed that there has been no publicly available collection of station-based climate time series datasets in the region. In addition, there is no standard framework for cross-validating drought products in the region. Most studies used precipitation-based drought indices (e.g., SPEI and SPI) to cross-validate the derived drought products. For this reason, this study called for establishing a regional data-sharing platform of publicly accessible station-based climate data and a standard framework for drought cross-validation.

Agriculture is the main contributor to Southeast Asian economies, and this sector is probably the most affected by drought. Crops (e.g., rice) in this region require regular water, and crop fields are usually small and segmented. Hence, providing timely and detailed drought information requires high spatial and temporal resolutions. Despite the growing EO missions, acquiring weekly or monthly cloud-free drought time series from optical remote sensing is still challenging. A more advanced approach should be implemented to generate frequent and high spatial drought information. For example, the combined use of multi-satellite sensors and downscaling products would potentially overcome this limitation (Claverie et al., 2018; Hao et al., 2015; Jiao et al., 2021). Nguyen et al. (2020) integrated the harmonization of Landsat and Sentinel-2 collections to monitor the variability of cropland in the drought-prone regions of Vietnam and Lebanon. In addition, recent microwave EO missions can deliver daily and weekly climate and soil moisture measurements. Such datasets can offer critical insights into agricultural drought monitoring and assessment. Several studies recently explored such sensors, such as SMAP, to monitor agricultural drought in mainland Southeast Asian countries (Li et al., 2022b; Lakshmi et al., 2023; Le et al., 2022). The integration of multi-sensors together with a downscaling approach would provide new opportunities for monitoring and characterizing drought conditions at fine spatial and temporal resolutions.

3.4 Summary

This study presented a detailed analysis of 102 satellite-based drought studies in Southeast Asia available from the Web of Science and Scopus academic platforms from 2000 to 2021. The review covered various aspects of drought studies using earth observation data in the region, including geographical studies, satellite sensors, drought indices, and thematic drought applications. The number of satellite-based drought articles in the study region witnessed a significant increase over the study period, and Vietnam and Thailand had the largest drought articles, accounting for nearly 40%. Nearly half of the articles employed optical remote sensing, while microwave remote sensing was less frequently used, and the harmonization of Landsat and Sentinel data for drought monitoring remains unexplored. Most studies focused on monitoring drought conditions using single vegetation-based or precipitation-based drought indices. There have been no studies offering spatial details of drought characteristics derived from optical sensors. Also, the application of machine learning and deep learning in drought detection to improve early warning systems and mitigation planning has received little attention. Regarding the accuracy assessment, about 22% of articles did not report accuracy assessment information for drought mapping. While there has been a rise in time-series drought remote sensing, long-term measurements remain limited, highlighting the need for multi-sensor data fusion to create longer time-series observations. Also, there is a clear link between the spatial resolution of drought maps and the extent of study areas. More than half of the studies focused on local-scale drought monitoring, while nearly 64% of maps were produced at a resolution of 1 km or above. Thematic applications of drought studies also show a significant discrepancy, with agricultural and vegetative droughts being the most addressed (58%). Soil moisture and crop-specific drought monitoring remain underrepresented.

Chapter 4

*A monitoring framework of drought characteristics from vegetation data**

4.1 Input data

This chapter employed a wide array of datasets collected at different spatial resolutions for monitoring and mapping drought characteristics across the MSEA region from 2000 to 2021. The primary datasets include temporal MODIS, CHIRPS, and ESA CCI land cover products. The MODIS and CHIRPS data were composited in monthly time series from 2000 to 2021, while the annual land cover data were readily available from 2000 to 2020. Given their different spatial and temporal resolutions, these datasets are harmonized to ensure consistency. In this chapter, the MODIS 1 km spatial resolution was used as the primary data source, and other datasets were resampled to 1 km spatial resolution and converted to a geographic coordinate system. All of these data were accessed and partly processed through the Google Earth Engine (GEE) cloud computing platform (Gorelick et al., 2017). This section is organized into three parts to describe the MODIS satellites, land cover products, and climate data.

4.1.1 MODIS NDVI time series

MODIS is a key earth-observing instrument aboard the Terra and Aqua satellite sensors, covering 36 spectral bands (0.4 – 14.4 μm) of the electromagnetic spectrum. Both satellites have been designed in polar-orbiting and collected spectral information at different temporal frequencies, ranging from daily, eight days, to 16 days. The Terra satellite was launched by NASA in December 1999 and collected data in the morning local time at the equator, while the Aqua sensor was launched in May 2002 and collected data in the after-

*This chapter is based in parts on Ha et al. (2023).

noon. MODIS satellites collect the earth's information at three spatial resolutions: 250 m, 500 m, and 1 km.

Since its launch in 1999, MODIS satellites have become an essential source of data for monitoring and studying various aspects of environmental research, such as land cover change, droughts, and ecosystem assessment. In recognition of this importance, the MODIS Science Team has made great progress in producing different ready-analysis data products derived from MODIS instruments aboard Terra and Aqua satellites. The main products include radiation suite products (e.g., surface reflectance, surface temperature, and snow cover), vegetation products (e.g., vegetation indices, LAI/FPAR, and NPP/GPP), and land cover products (e.g., land cover change, forest fire, and vegetation cover conversion) (Didan et al., 2015). These products have been widely used to survey all types of environmental issues, from drought to global environmental change.

Among the MODIS-based derived products, the NDVI is one of the most used indices for monitoring regional and global ecosystems. There are multiple MODIS NDVI versions produced at spatial resolutions at 250 m, 500 m, and 1 km. This chapter used the latest MODIS NDVI version (6.1) from Terra and Aqua sensors to derive high spatiotemporal drought characteristics from 2000 to 2021. The NDVI version 6.1 collection is produced from georeferenced, radiometric, and atmospheric correction MODIS red and near-infrared reflectance at a 16-day frequency and 1 km spatial resolution. Each 16-day NDVI composite is selected from "highest quality" observations of a 16-day period using the maximum value composite method (Didan et al., 2015). The NDVI measures the proxy greenness of vegetation ecosystems and can be calculated from the normalized transformation of the near-infrared band to the red band. The specific calculation of the NDVI can be expressed as the following equation (Eq. 1).

$$NDVI = \frac{NIR - RED}{NIR + RED} \tag{1}$$

Where NDVI is the normalized difference vegetation index, the NIR represents near-infrared, while RED indicates the red band of the electromagnetic spectrum.

4.1.2 ESA CCI land cover

This study employed ESA CCI land cover and land use products from 2000 to 2020 at 300 m spatial resolution. This dataset is produced annually on a global scale by the ESA CCI program together with various scientific research institution partners. The MERIS satellite spectral composites are the main input data for producing the ESA CCI land cover

products in addition to other sensors (e.g., SPOT and PROBA-V). The combination of the state-of-the-art unsupervised and supervised classification (e.g., Random Forest) machine learning algorithms is used to generate consistent and continuous observations of the ESA CCI land surface types (Li et al., 2018b). These datasets are produced in epochs to ensure the stable and dynamic components of the global land cover surface (Bontemps et al., 2012). Each epoch represents five years (e.g., 1998-2002, 2003-2007, and 2008-2012). This approach ensures that every land cover pixel has multiple cross-verifications with several-year observations to minimize potential classification errors. The overall accuracy of the ESA CCI land cover products exceeded 75%, and the highest user accuracy values were reported in some specific land cover types, such as rainfed cropland, evergreen forests, and irrigated cropland (Bontemps et al., 2012).

The original ESA CCI land cover products were defined and classified into 37 land cover classes. However, this chapter reclassified the original classification scheme into six land cover types: rainfed cropland, irrigated cropland, shrubland, mixed forest, evergreen forest, deciduous forest, and other types (e.g., water bodies, bare land, and built-up areas). This section also resampled the original land cover data at 300m to 1 km spatial resolution based on the nearest neighbor method. The spatial map of land cover and its corresponding area in the MSEA region are presented in Chapter 2. Our stable land cover analysis indicated that the MSEA region suffered from only 6% of land cover change over the past two decades based on the ESA CCI land cover products 300 m spatial resolution. Also, recent studies revealed significant forest loss and land use transformation over the past ten years. For instance, Pauly et al. (2022) reported that the largest forest loss in Cambodia occurred from 2010 to 2014, while the early period witnessed stable land cover uses.

4.1.3 Precipitation and LST time series

Temperature and rainfall data were sourced from the MODIS LST and the Climate Hazards Group Infrared Precipitation with Station (CHIRPS) products to assess the drought observation results. The monthly LST data were extracted from the daytime MOD11A2 product (version 6.1) at 1 km spatial resolution spanning 2000 to 2021 using a mean value composite approach. This product has been significantly enhanced against the previous version in terms of calibrations, Terra infrared crosstalk adjustment, and polarization corrections (Wan et al., 2021a). Cloud-contaminated LST values were excluded to retain only clear-sky observations using the associated quality indicator band available in the MODIS LST products. Consequently, any missing data were linearly interpolated using the nearest neighbor measurements.

In addition, this chapter utilized the long-term CHIRPS pentad dataset, which offers near-global coverage at approximately 5 km spatial resolution from 1981 to the present. This dataset is generated using infrared cold cloud duration data from multiple satellites, such as TRMM and NOAA GridSat, and is further refined with station-based measurements (Funk et al., 2015). In the MSEA region, CHIRPS has been shown to outperform other satellite-based precipitation datasets (Dandridge et al., 2019). The CHIRPS data was composited into monthly time series from 2000 to 2021 and upscaled to a higher spatial resolution (1 km) using bilinear resampling.

4.2 Methodology

This section describes the detailed implementation framework of monitoring and characterizing vegetation-based drought using MODIS time series from 2000 to 2021. The overall workflow of the implementation approach is presented in Figure 4.1. The MODIS NDVI time series was first interpolated from 16-day time series data. Subsequently, the gap-free NDVI observations were composited into monthly measurements and reconstructed to remove any potential abrupt changes due to noise and outliers. This helps to maintain the reliable temporal curve of vegetation growth. Next, this analysis calculated the monthly VCI time series over the study period for drought analysis. Finally, different drought characteristics are investigated across the MSEA region, while the identification of severe drought years was proposed. Also, drought conditions were examined across various timescales, including monthly, seasonal, and annual periods. The final analysis cross-verified the reliability of VCI-based drought conditions against precipitation and temperature.

The organization of this section begins with the reconstruction of the NDVI time series (Section 4.2.1), followed by the computation of the VCI time series (Section 4.2.2). The next section is dedicated to spatial and temporal analysis of drought characteristics (Section 4.2.3), while Section 4.2.4. studied the spatial trends of the time series VCI-based drought over the past 20 years. The last section (Section 4.2.5) concerns the cross-verification to ensure the reliability of vegetation-based droughts.

4.2.1 Reconstruction of satellite-based vegetation time series

The continuous and consistent drought observations require gap-free and clear-sky measurements of remote sensing acquisitions. However, the MSEA region falls in the tropics and often suffers from cloud coverage. In this study, both sensors are employed to densify clear-sky time-series NDVI measurements. Figure 4.2 shows the spatial variations of cloud cover across the MSEA region from 2000 to 2021. Overall, large areas of the MSEA region

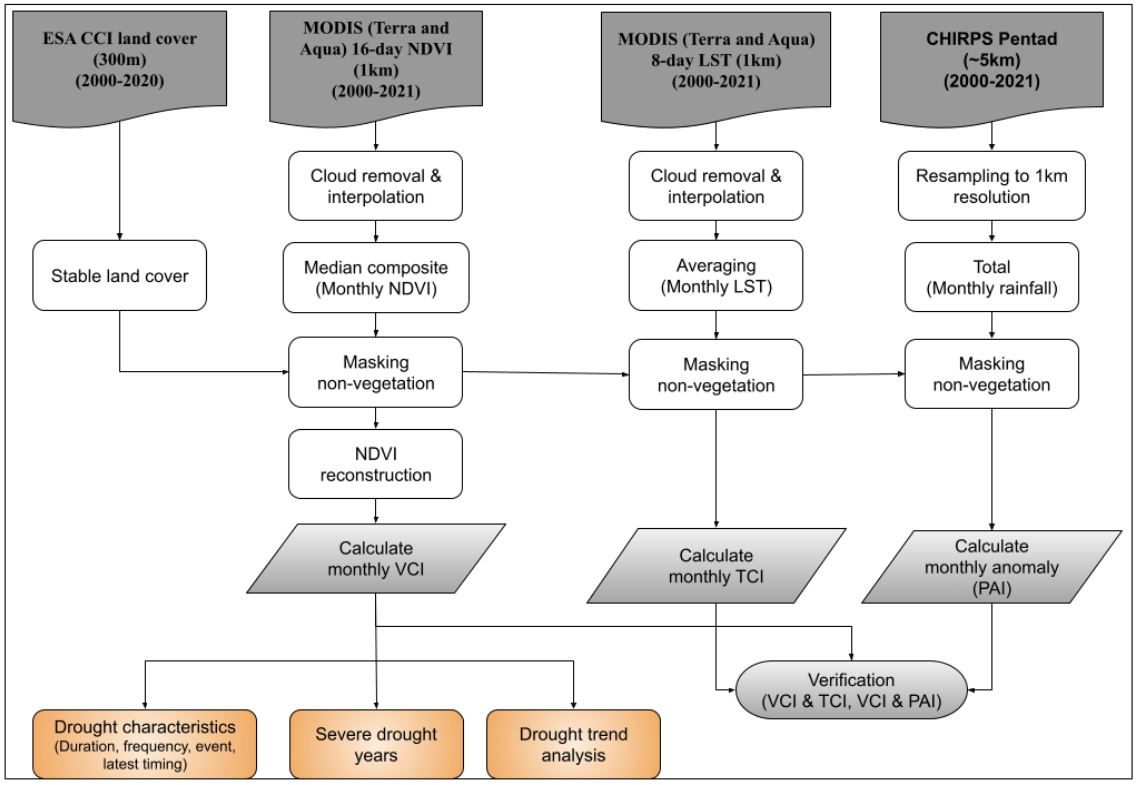

Figure 4.1: Overall workflow of drought monitoring and characterization from data pre-processing to cross-verification. This figure is adapted from a study by Ha et al. (2023).

suffered from frequent cloud contaminations. If a single sensor is used (Figure 4.2 a-b), cloud cover is observed more frequently in the Mekong Delta ($\sim$ 50%), northern Vietnam ($\sim$ 30%), and nearby Bangkok ($\sim$ 40%). The combination of both sensors demonstrated a significant increase in cloud-free observations (Figure 4.2-c). For example, the percentage of cloud cover dropped by nearly 10% in Thailand and Vietnam after the combination (Figure 4.2-d). Notably, the largest presence of cloud cover is detected from June to August, and this means there would be more significant data gaps during this period (Figure 4.2-d). These persistent clouds and shadows pose a major challenge to monitoring and assessing the optical remote sensing of drought measurements.

Many existing studies have used raw time-series remote sensing measurements or selected certain cloud-free images (e.g., Landsat and MODIS) to generate drought indices (Laosuwan et al., 2016; Tran et al., 2017; Rotjanakusol and Laosuwan, 2018). Although this method is simple and fast for delivering drought information, persistent clouds in the optical remote sensing data across the tropics impede the continuous and consistent derivation of accurate drought information. Reconstruction of time-series measurements is therefore essential to minimize noise, produce gap-free pixels, and enhance drought indices. In this study, the NDVI observations are linearly interpolated and composited in a monthly window and subsequently reconstructed using the Savitzky–Golay (SG) filter method.

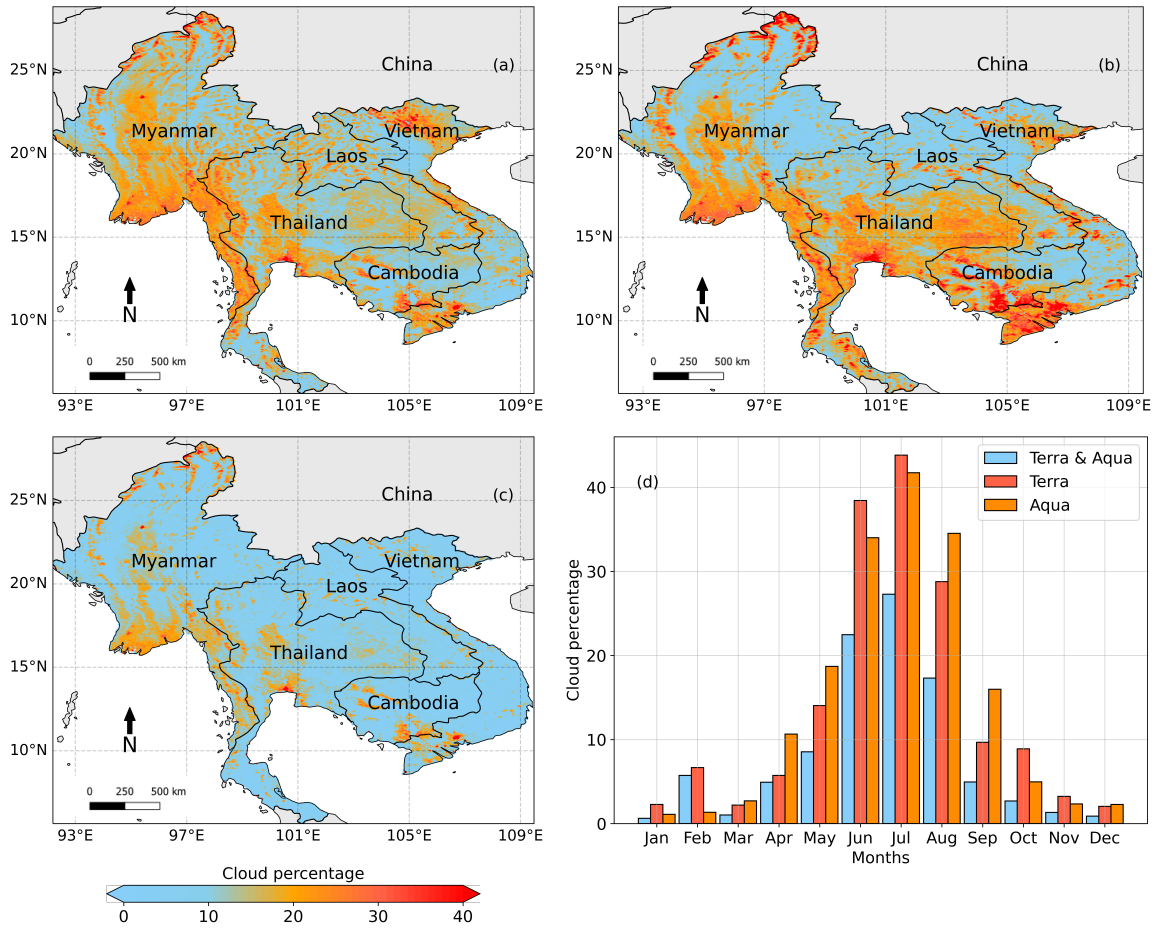

Figure 4.2: Spatial variability of cloud cover across the MSEA region observed from Terra sensor (a), Aqua sensor (b), and combined Terra and Aqua sensors (c). The bar plot displays the percentage of monthly cloud pixels over the study period (d).

A simple linear interpolation is applied for the NDVI time-series observations from 2000 to 2021. This method involves producing an estimated value for a missing measurement using the nearest preceding and succeeding NDVI observations (Chen et al., 2004). The basic equation of the linear interpolation can be expressed as follows (Eq. 2):

$$\hat{y} = y_1 + (y_2 - y_1)\frac{(t - t_1)}{(t_2 - t_1)} \tag{2}$$

Where $\hat{y}$ is the interpolated NDVI value at the time t, and y_1 and y_2 are the closest preceding and succeeding NDVI at the time t_1, t_2.

The NDVI data was subsequently composited in a monthly window using the median value composite method (MVC). It is noted that there are many temporal composite approaches with a fixed length, such as mean and maximum value composites, but the MVC was more stable and robust to outliers (Ruefenacht, 2016). A total of 263 monthly NDVI composite images are available over the study region from 2000 to 2021. Because of poten-

tial persistent clouds and the interpolation effects, the time-series NDVI observations may likely contain noise. Thus, this section further employed the SG filter for reconstructing the monthly NDVI measurements from 2000 to 2021. The SG filter is considered the most widely used method (Vaiphasa, 2006) because it can preserve the temporal curve of the NDVI data and produce better drought indices (Xie and Fan, 2021). The concept of the SG method is to fit a polynomial least-squares equation in a local moving window to reconstruct high-quality time-series measurements (Chen et al., 2004; Cao et al., 2018). This analysis selected two key parameters required for the SG method, including the local window size and the degree of polynomial orders. Finally, the parameters 2 and 5 for polynomial orders and window size were selected, respectively.

4.2.2 Vegetation drought index

The NDVI has been widely used to detect drought conditions, vegetation stress, and crop growth, but interpretive issues may arise when these results are extrapolated over heterogeneous land cover areas (Kogan, 1990; Bajgiran et al., 2008). This means the amount of vegetation can be attributed to differences in environmental conditions. In non-homogeneous areas, for example, the NDVI has higher values in the areas with abundant resources (e.g., more favorable climate and soil) compared to the areas with less productive environmental conditions (Kogan, 1990). These differences are mainly due to weather and ecosystem components. It is observed that the NDVI behaves differently under various climatic conditions, and the weather-induced NDVI variations are not easily detectable due to the weaker weather signal in the NDVI value compared to the ecological factors. Therefore, when the NDVI is used for monitoring weather impacts on vegetation, the weather component should be eliminated from the ecological component (Kogan, 1990; Bajgiran et al., 2008). Thus, the VCI was designed to enhance the weather-related components in the NDVI value (Kogan, 1990). The weather-induced NDVI envelope was linearly scaled from zero for minimum NDVI to 100 for maximum NDVI value for each grid cell and month. The entire procedure of the VCI is defined by the following expression (Eq. 3):

$$VCI_i = 100 * \frac{NDVI_i - NDVI_{\min}}{NDVI_{\max} - NDVI_{\min}} \tag{3}$$

While $NDVI_i$ is monthly NDVI, $NDVI_{\max}$ and $NDVI_{\min}$ are the maximum and minimum NDVI values, respectively, calculated for each grid pixel across the monthly period (12 months) using the entire NDVI record (2000-2021). In this study, VCI values are expressed as percentages, ranging from 0 to 100, to represent vegetation varying from extremely poor (indicative of drought) to optimal (non-drought) conditions. This chapter employed the

drought classifications proposed by Kogan (1995a) and Dutta et al. (2015), and the VCI values are reclassified into five levels of drought severity. A VCI between 50% and 100% indicates normal, non-drought conditions, while values between 30% and 50% signify mild drought. Moderate drought is defined by a VCI ranging from 20% to 30%, and values below 20% indicate severe drought, with those under 10% representing extreme drought conditions.

4.2.3 Spatiotemporal characteristics of drought

4.2.3.1 Identification of severe drought years

In this study, severe drought years were identified using the monthly VCI observations for a total of 21 years (2000-2021). A severe drought year is defined as the annual percentage of extreme value pixels (VCI $\leq$ 10) exceeding the long-term (21 years) average, while this section also considered the extreme VCI severity over the same period. The annual percentage of extreme pixels is identified by the following expression (Eq. 4):

$$SDY_i = \frac{\sum_1^j \left(\frac{VCI_{i,j}}{N}\right) \cdot 100\%}{M_i} \tag{4}$$

Where SDY_i and M_i are the percentage of extreme pixels and number of months at year i, respectively. The $VCI_{i,j}$ is the VCI value at month j in year i whereas N is the total valid pixels in the region.

In detail, this study computes the percentage of extreme VCI value pixels across years over the study period. These annual percentages are compared to the established baseline averages. If the percentage of extreme VCI pixels in any specific year exceeds or is equal to the baseline, that year is considered a severe drought year. It is assumed that other factors (e.g., human activities) can influence VCI values. However, these impacts are often more localized or gradual. Here, this approach relies on a long-term baseline. Therefore, any significant deviation above this baseline is a strong indicator of a climatic hazard event, making this approach a reliable tool for drought identification.

4.2.3.2 Characteristics of drought

The spatial characteristics of drought conditions are key to identifying the region of drought vulnerability. Several methods have been proposed to detect drought characteristics, such as Run theory and machine learning. The Run theory, originally introduced by Yevjevich et al. (1967), is among the most commonly used methods for characterizing

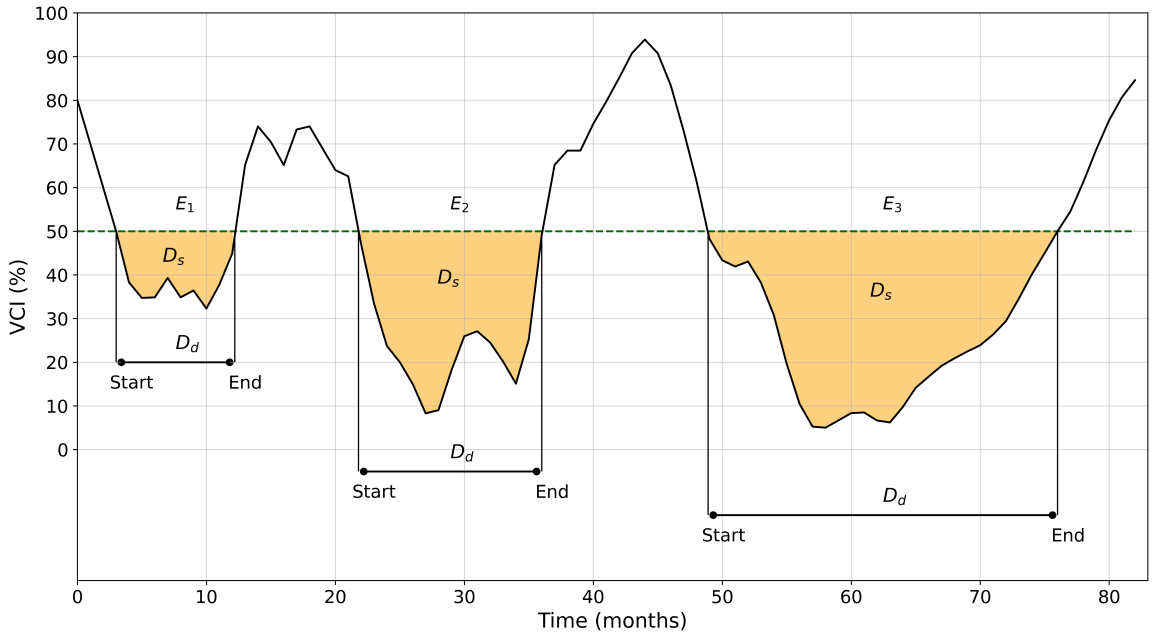

Figure 4.3: A schematic illustration of drought events and their characteristics using the VCI time series. Dd is the duration of a drought event, while Ds is the severity of drought conditions. The E1 means the drought event (E1 – E3). The dashed green line indicates the threshold for defining drought conditions. VCI values below 50% are considered drought, while those above 50% are considered non-drought. The "start" and "end" indicate the initiation and termination of a drought event, respectively.

drought events (Guo et al., 2018a; Raposo et al., 2023). This approach defines a drought event as a period of VCI values that falls below the pre-defined thresholds. Figure 4.3 shows the determination framework of drought events and their characteristics from satellite-based vegetation time series.

This study identified four main characteristics of drought in each grid cell from 2000 to 2021: number of drought events (E), latest drought year (T), drought frequency (F), and drought duration (D). These characteristics are frequently identified in meteorological drought studies (Guo et al., 2018a; Le et al., 2019). The number of drought events (E) reflects the drought conditions with a continuous consecutive VCI below a given threshold value for at least three months, while the drought duration (D) is the simple average length of drought months from 2000 to 2021. The drought year (T) represents the latest year with the maximum number of consecutive drought months, and the drought frequency (F) is the total number of drought events identified over the selected study period. In this study, a drought episode is defined as a continuous VCI value less than 50 because a persistent low-intensity drought condition can have a considerable effect on local agriculture, vegetation vigor, and the environment and can be helpful for an early warning system (Venturas et al., 2016; Guo et al., 2018a).

4.2.4 Analysis of time series drought trends

Numerous studies have employed parametric and non-parametric methods for detecting land surface trends from time-series remote sensing measurements (Mao et al., 2012; Branco et al., 2019; Xu et al., 2020; Damberg and AghaKouchak, 2014). The parametric methods are considered more statistically significant than non-parametric tests, but the data are assumed to be normally distributed, independent, and continuous (Liu et al., 2016; Wessels et al., 2012). In practice, time series vegetation observations are known for autocorrelation and non-normality (de Jong and de Bruin, 2012; Horion et al., 2014). Therefore, non-parametric methods are preferred to overcome these limitations.

In this study, the Mann-Kendall (MK) test combined with Sen's slope estimator is employed for detecting the significance of interannual drought trends over the two main growing seasons, summer (rainy) and winter (dry), from 2000 to 2021. This method was developed by Mann (1945) and Kendall (1948), and this approach became a widely used non-parametric test in climatology studies due to its robustness to non-normality and missing values (Guo et al., 2018a). The MK significance test identifies the strength and direction of a trend, whereas the magnitude of the slope is measured by means of Sen's slope method (Guo et al., 2018a). The detailed calculations of the MK test and Sen's slope methods have been well-documented in previous studies (Gajbhiye et al., 2016; Güçlü, 2018). In this chapter, the drought trends are detected at a significant level of $\alpha \leq 0.05$, where a positive (negative) slope indicates a significant increase (decrease) in drought conditions.

4.2.5 Cross-verification of drought conditions

The reliability of drought products plays a key role in drought monitoring and management at local and national levels. In practice, in-situ climatic factors are considered the most reliable for cross-validating drought conditions. However, in the MSEA region, collecting climate in-situ measurements is challenging, if not even possible. This study, therefore, cross-verified the VCI results using the monthly CHIRPS and MODIS LST products. The LST observations are transformed to the temperature condition index (TCI) based relative to the maximum and minimum temperatures, which reflects different vegetation responses to thermal canopy temperature (Kogan, 1995a).

Pearson correlation coefficient (R) and visual comparison were employed to examine the relationship between drought conditions and climatic factors. This study computed monthly correlation coefficients between the VCI and LST data for different land covers across the region at a significant level of $\alpha \leq 0.05$. The R-value ranges from -1 to 1, with a higher absolute R-value indicating a stronger correlation between drought and LST. The monthly

precipitation anomalies were temporally compared with the VCI results for different land covers from 2000 to 2021.

4.3 Results

4.3.1 Reliability of VCI-based drought conditions

Among the climatic factors, vegetation growth is highly sensitive to precipitation and temperature. Climate change can influence vegetation ecosystems' growth; in extreme cases, vegetation and crops can suffer from failure. A lack of rainfall causes surface moisture stress, while the high temperature generates thermal pressure for vegetation growth. Therefore, they can be reliable for cross-verifying the sensitivity of the VCI for drought monitoring. Figure 4.4 showed the temporal variability of correlation coefficients between the VCI and temperature from 2000 to 2021 across the MSEA region. In contrast, the visual comparison of the VCI and precipitation anomalies was presented in Figure 4.5 over the same period.

The monthly correlation coefficients (R) between the VCI and TCI were calculated to determine the relationship between VCI-based drought conditions and temperature under three main land cover types (cropland, forestland, and shrubland). Overall, a negative correlation existed between the VCI and TCI in the vegetative areas (Figure 4.4), but these correlation coefficients are characterized by the dry and rainy season variations in the study area. A negative correlation between the two datasets suggests that increased temperatures (drier conditions) are associated with the decline of the VCI (increased vegetation stress). This finding was aligned with the observation in the study of Son et al. (2012). Notably, higher absolute R values were mostly observed during the dry seasons, especially from January to March, while the wet seasons witnessed lower R values, between July and September. The temporal similarity of the R-value pattern was found across the land covers, but the cropland had higher absolute R-values in most cases (Figure 4.4).

The VCI results were also compared to the precipitation anomalies for the three main land cover types. Although there were discrepancies among the land cover types, the visual comparison indicated a good temporal agreement between the VCI and precipitation anomalies over the selected period (Figure 4.5). The closest agreement was observed in cropland, and the decline of VCI values was reflected in years of precipitation deficits (e.g., 2005, 2010, 2016, and 2019). In forest and shrub areas, the precipitation deficits were also followed by VCI variability, but this trend was temporally variable and not as strong as in cropland. For example, low precipitation in 2019 and 2020 can be considered a meteorological drought. However, these years were classified as non-drought, although the

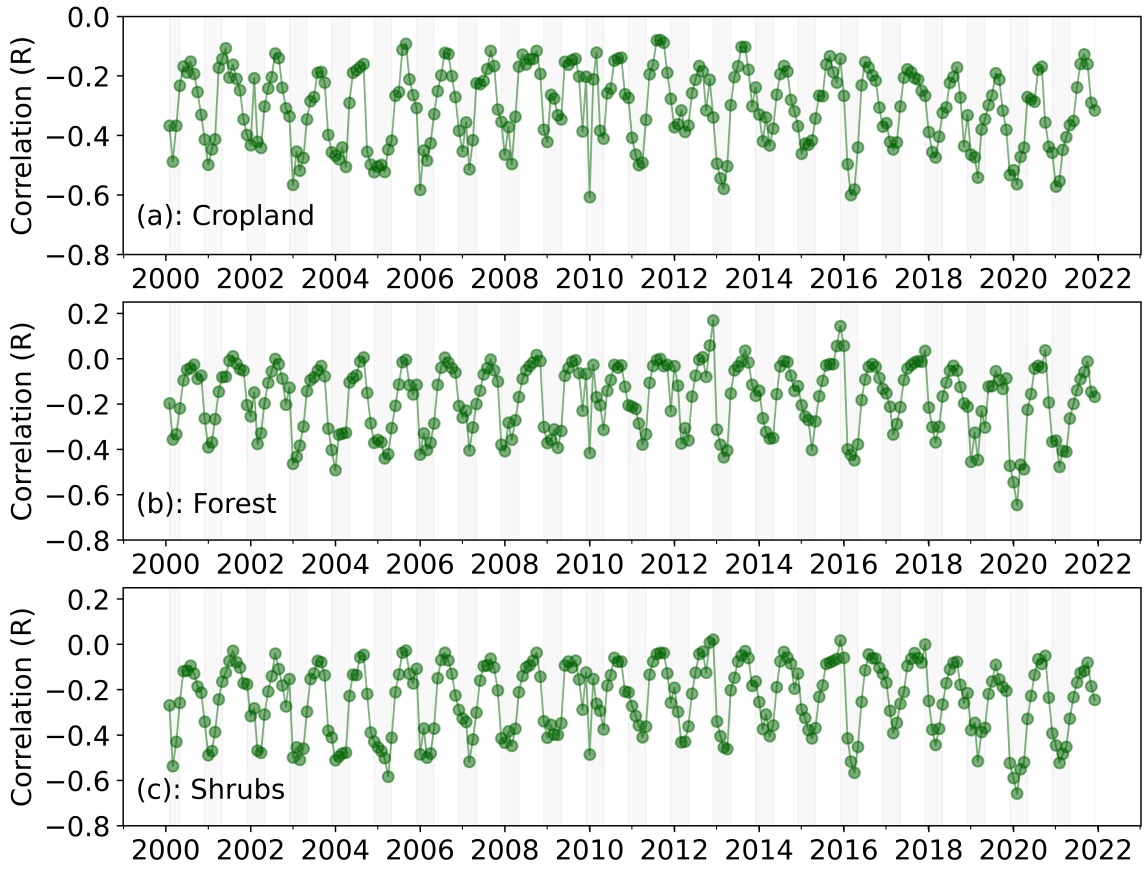

Figure 4.4: Correlation coefficients of monthly VCI and TCI across three main land cover types (a) cropland, (b) forests, and (c) shrublands over the MSEA region from 2000 to 2021.

forestland/shrubland VCI values decreased (Figure 4.5 b-c). These variations are likely attributed to the distinct sensitivity of forests and shrublands to drought conditions. Recent studies have demonstrated that in contrast to croplands and grasslands, forests and shrublands likely exhibit greater resilience and resistance to drought stress and other disturbances (Wei et al., 2022; Xu et al., 2018). Overall, the VCI values pattern is closely linked to the precipitation anomalies over the selected study period.

4.3.2 Spatial variability of monthly and annual VCI-based droughts

4.3.2.1 Long-term monthly drought conditions

Drought conditions exhibited significant spatial and temporal variability throughout the study period. Figure 4.6 displayed the spatial variability of the VCI-based drought conditions from January to December across the MSEA region from 2000 to 2021. On average, the monthly VCI values fluctuated between 55% and 62% across the region. The dry months witnessed lower VCI values (severe drought), while the rainy months experienced higher VCI values, indicating greener vegetation. For example, the analysis indicated that

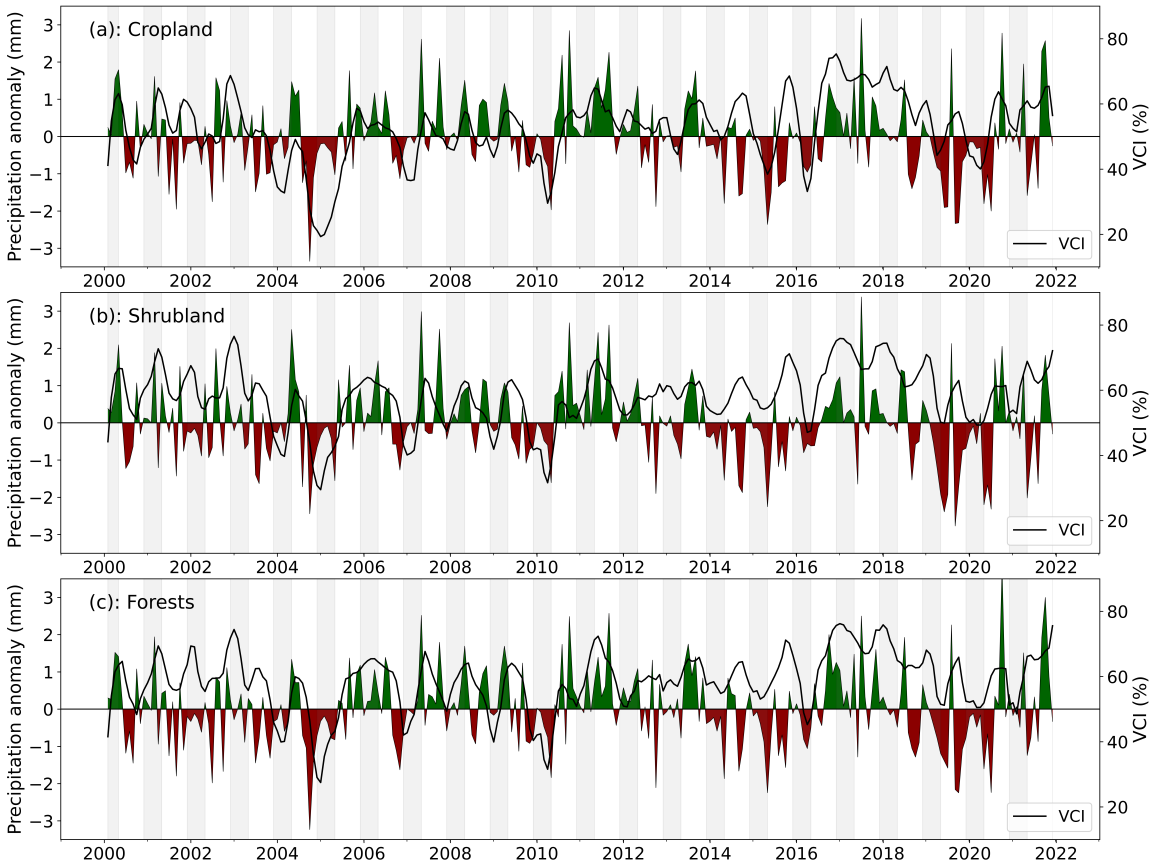

Figure 4.5: Temporal variations of the VCI and precipitation anomalies across three main land cover types (a) cropland, (b) forests, and (c) shrubland over the MSEA region from 2000 to 2021. The colors represent drought (dark red) and non-drought (green).

the lowest VCI values were found in February and March, while the largest VCI values were observed from July to October. Laos had the highest VCI values across the months (VCI = 61%), while Thailand and Vietnam experienced lower VCI values (VCI = 56%). Despite its temporal variability, Central Myanmar, parts of Cambodia, and Thailand experienced the lowest VCI values. These areas are likely more vulnerable to drought as vegetation experiences more stress and declines. Central Myanmar witnessed the lowest VCI values in April. It is estimated that nearly 40% of the country had VCI values below 50% this month. In comparison, Cambodia experienced the largest drought in February, accounting for nearly 55% of the country.

4.3.2.2 Drought conditions during the dry season

During the dry season, the VCI maps revealed distinct patterns and variability from 2000 to 2021. Lower VCI values were consistently observed across the study area (Figure 4.7). The lowest VCI values were observed in 2004, 2005, 2007, 2010, 2016, and 2020, and these years witnessed the VCI values below 50% across the study region. It is estimated that nearly 40% of the study area frequently experienced lower VCI values (VCI$\leq<$ 50%)

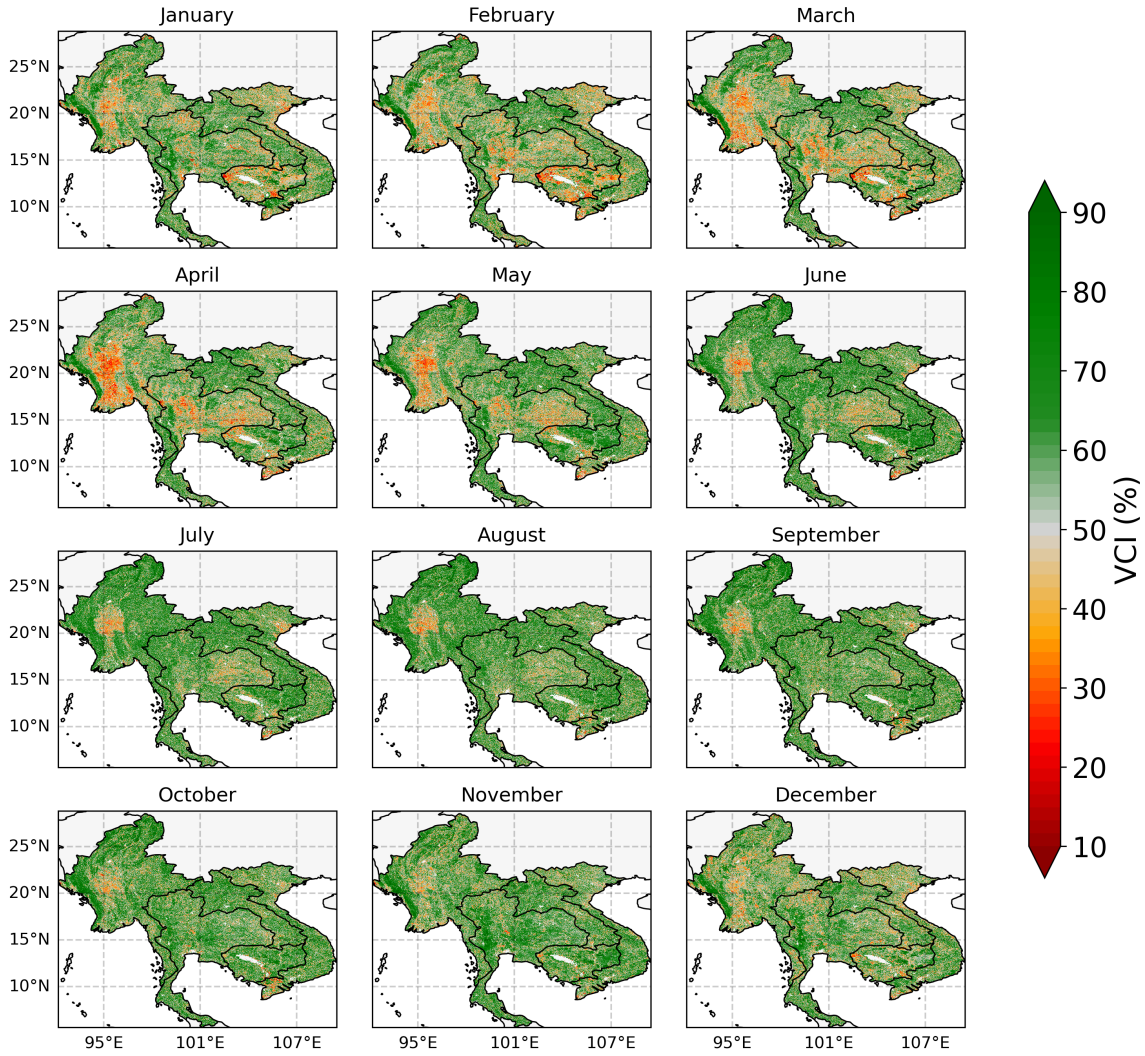

Figure 4.6: Spatial variability of monthly VCI-based droughts from 2000 to 2021 across the MSEA region.

during the dry season. Spatially, the lowest VCI values were observed in eastern Thailand and central Thailand in 2005 and 2010, respectively, while nearly entire Myanmar suffered from low VCI values in 2010. Northern Vietnam had low VCI values in 2004 and 2007 (Figure 4.7). Statistically, Thailand witnessed the lowest VCI values in 2005, with VCI = $\sim$ 20%, while 2017 had the highest VCI values (67%). Myanmar had the lowest VCI values in 2010, with VCI =$\sim$ 27%. Other remaining countries had the lowest VCI values in 2005, ranging from 28% to 30%. In contrast, some years witnessed high VCI values, such as in 2017 and 2018. Thailand and Myanmar had the highest VCI values in 2018 (VCI = 67%) and 2017 (VCI = 69%), respectively. In comparison, Cambodia had the highest VCI values in 2000 (VCI = 67%), while this number in Laos was found in 2023 (VCI = 68%).

Regarding the temporal drought and non-drought analysis, Figure 4.8 showed the temporal percentage of VCI-based drought and non-drought conditions across the MSEA region during the dry season from 2000 to 2021. Overall, the non-drought extent was often larger

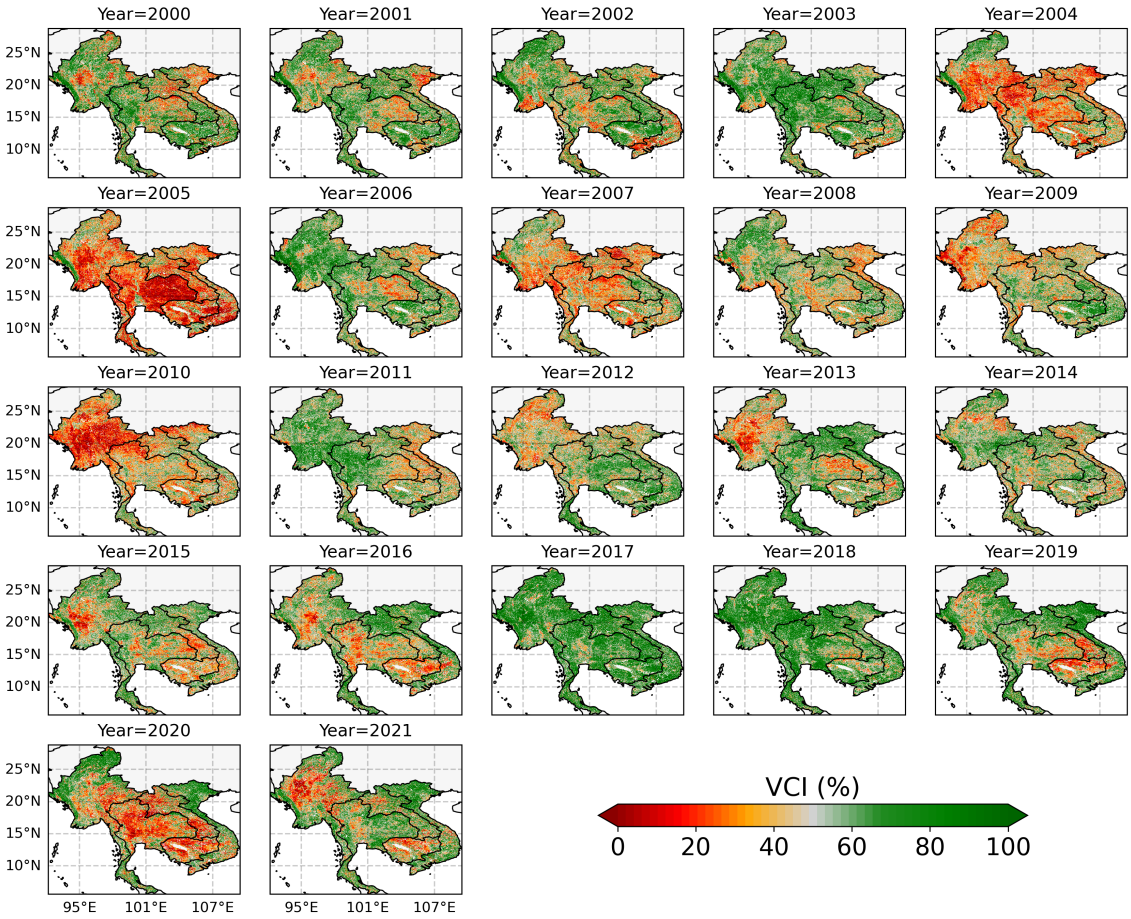

Figure 4.7: Spatial variability of VCI-based drought conditions during the dry season from 2000 to 2021 across the MSEA region.

than the drought extent. For example, nearly 60% of the study region experienced non-drought conditions (non-stress vegetation) from 2000 to 2003 (Figure 4.8), and this pattern was also seen from 2011 to 2021. More than 80% of the region was considered non-drought in 2017 and 2018. In some years, there was a larger extent of drought. The largest drought conditions were observed in 2005 ($\sim$ 82%) and 2010 ($\sim$ 72%), while the lowest was detected in 2017 ($\sim$ 12%) and 2018 ($\sim$ 16%). Droughts occurred in 30 to 50% of the region in other years; in some cases, drought affected less than 20%.

Apart from regional drought and non-drought analysis, Figure 4.9 displayed the proportion of drought extent across the examined countries over the study period. Thailand suffered from the largest drought extent in 2004, accounting for nearly 80% of the country. In 2007, nearly 76% of this country also suffered from drought (Figure 4.9). Laos suffered from the largest drought extent in 2010 and 2020, accounting for 64% and 67% of the country. Cambodia experienced the largest drought in recent years. In 2020, nearly 82% of the country suffered from drought conditions. The largest drought extent in Vietnam was found in 2004, with 74% of the country affected. In recent years, Vietnam suffered the low-

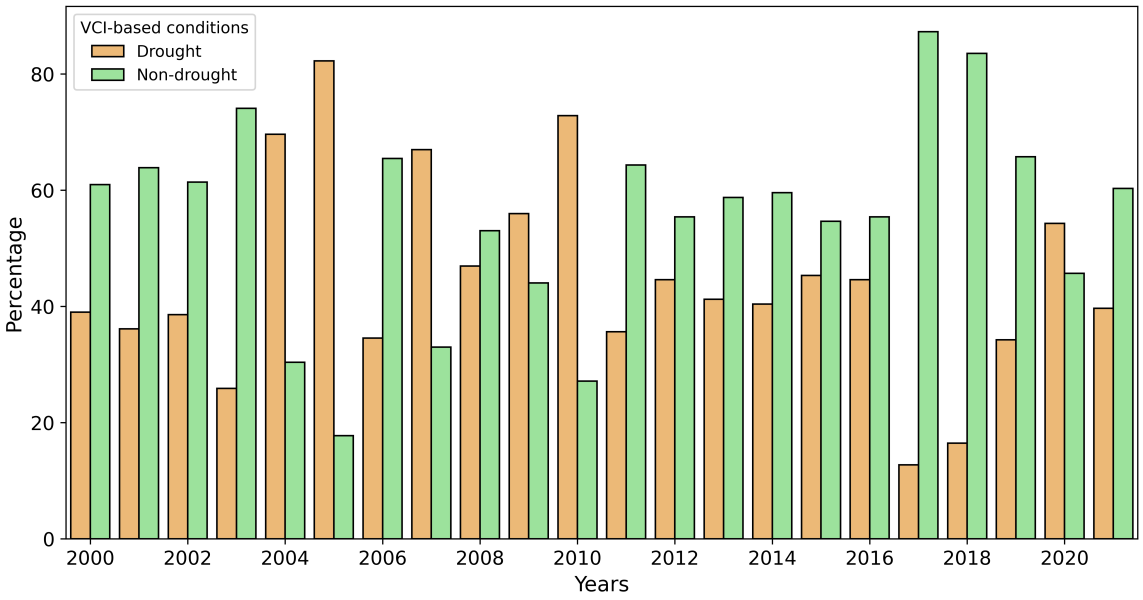

Figure 4.8: Temporal percentage of VCI-based drought and non-drought areas (in pixel unit) across the region during the dry season from 2000 to 2021. The drought conditions are defined as VCI values below 50%.

est drought proportion among the examined countries. By contrast, in the early 2000s, this country had the largest drought proportions. This observation contrasts Cambodia, where drought conditions occurred less in the early 2000s. For example, nearly 80% of the country had non-drought conditions during this period (Figure 4.10). Notably, Laos had high proportions of non-drought (healthier vegetation) across the study years. Likewise, Myanmar also experienced high proportions of non-drought conditions based on VCI values during the study period. In 2018, this country had the largest non-drought areas ($\sim$ 90%) among the examined countries. By contrast, this country's lowest proportion was observed during the dry seasons of 2009 and 2010. Also, it was hit hard in 2005; nearly 90% of the country was affected by drought.

4.3.2.3 Drought conditions during the rainy season

Figure 4.11 revealed spatial variability of VCI-based drought conditions from 2000 to 2021 despite the rainy season. The lowest VCI values were observed in 2004, 2005, and 2010, and these years witnessed VCI values below 50% across the study region. Spatially, the lowest VCI values were observed in eastern Thailand and central Myanmar, while Cambodia and Vietnamese Central Highlands suffered from lower VCI values in recent years. Generally, the countries' VCI values during the rainy season were higher than in the dry season. Thailand witnessed the lowest VCI values in 2004, with VCI = $\sim$ 41%, while 2021 had the highest VCI values (68%). During the rainy season, the lowest VCI values in Cambodia were nearly two times higher than in the dry season, at 51% in 2020. The highest VCI

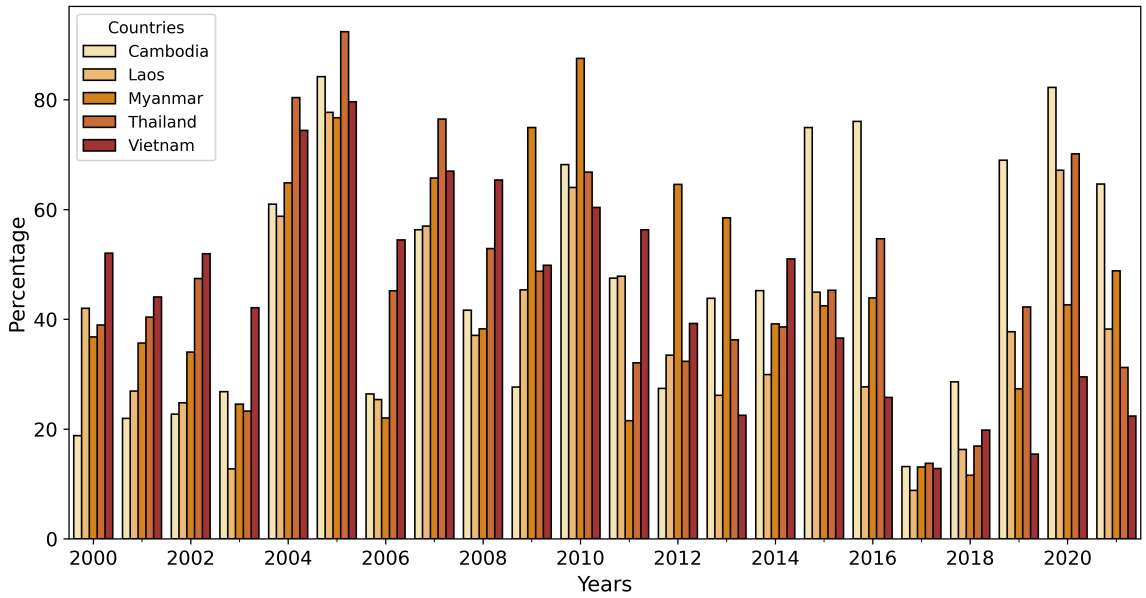

Figure 4.9: The percentage of annual drought conditions across the countries from 2000 to 2021 during the dry season. The drought condition is defined as VCI values below 50%.

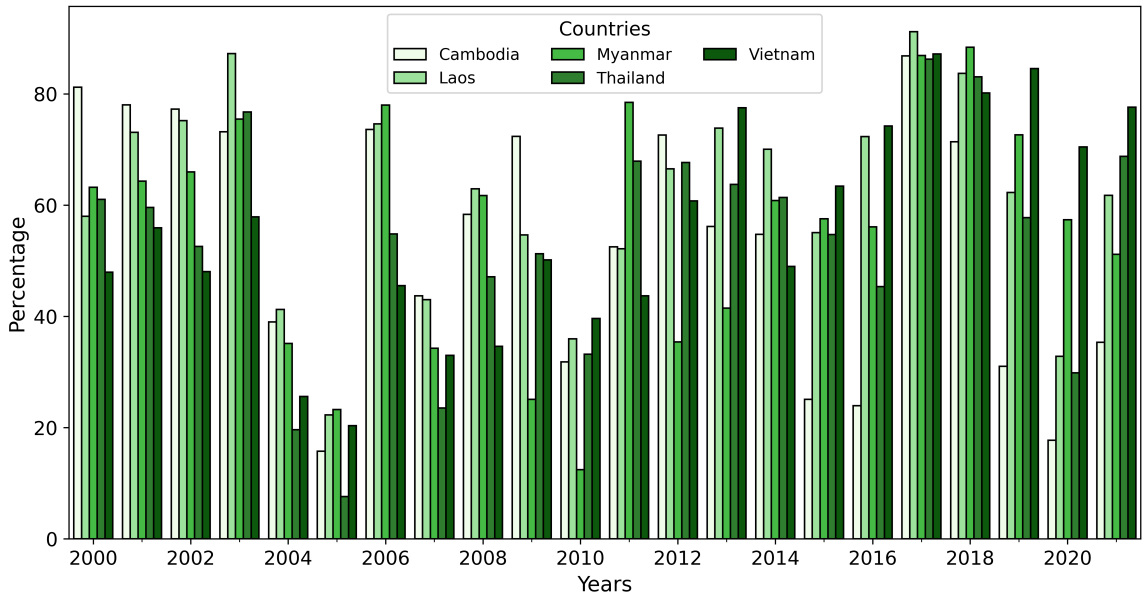

Figure 4.10: The percentage of annual VCI-based non-drought conditions across the countries from 2000 to 2021 during the dry season. The non-drought condition is defined as VCI values above or equal to 50%.

values were primarily found in 2017 and 2018 across the countries, but Laos and Myanmar had the largest VCI values in 2021 and 2011, respectively. On average, the region had a VCI value of 57%, and Laos had the highest VCI value ($\sim$ 59%) among the countries.

Figure 4.12 showed the temporal extent of VCI-based drought and non-drought conditions over the study period. Overall, higher non-drought extents were primarily observed across the region. Recent years witnessed a lower extent of drought, while there was an

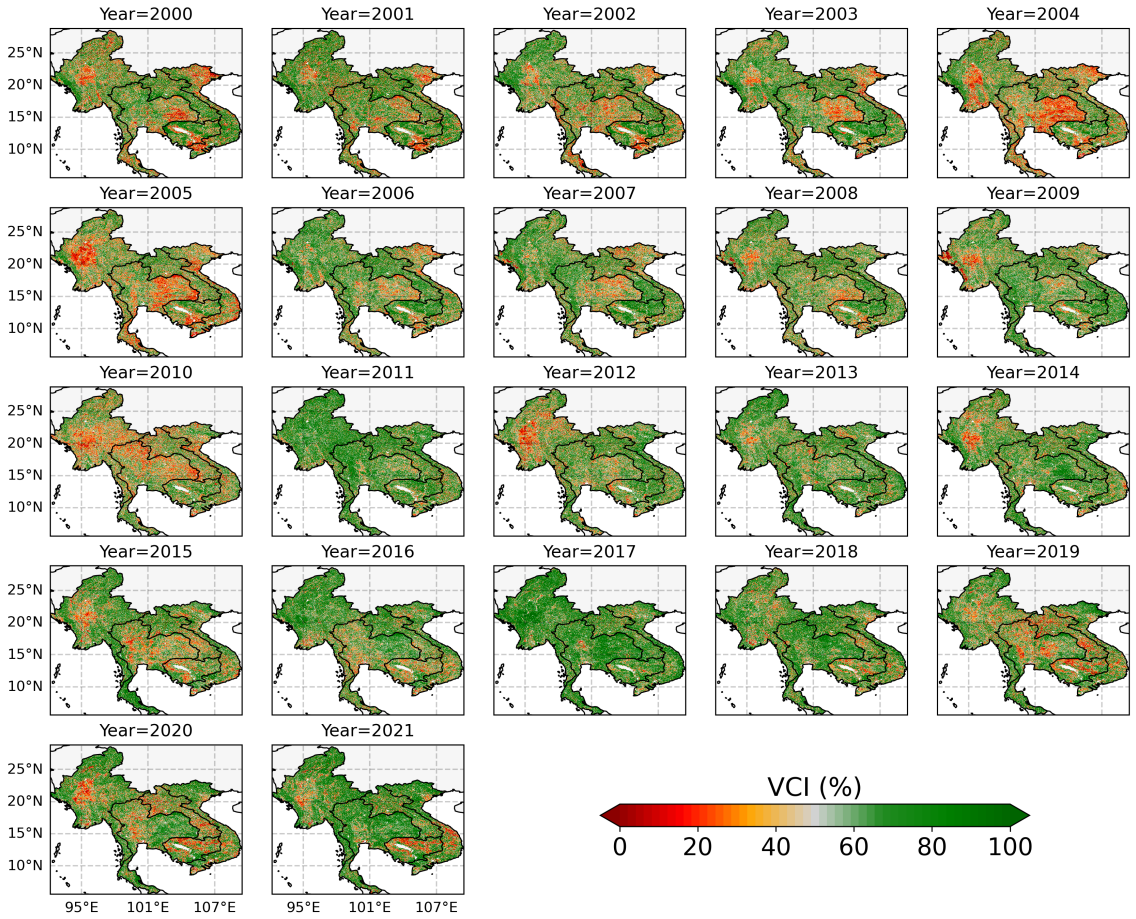

Figure 4.11: Spatial variability of VCI-based drought conditions during the rainy season from 2000 to 2021 across the MSEA region.

increase in the extent of non-drought conditions. The highest proportion of drought extent was detected in 2004, 2005, and 2010, accounting for nearly 50% of the region affected. Other years witnessed between 20% and 40% of the region affected by drought. The least affected years were observed in 2008 and 2011, affecting under 20% of the region.

Figure 4.13 displayed the proportion of drought extent across the examined countries during the rainy season. Like the dry season, Thailand suffered from the largest drought extent in 2004, accounting for nearly 66% of the country. In 2005, nearly 58% of this country also suffered from drought (Figure 4.13). Laos suffered from the largest drought extent in 2019 and 2020, accounting for 48% of the country. Cambodia experienced the largest drought in 2020, affecting 47% of the country. The largest drought extent in Vietnam was found in 2005, with 56% of the country affected. Myanmar had the largest drought extent during the rainy season in 2010, affecting 52% of the country. Cambodia and Laos suffered a larger drought proportion in recent years among the examined countries. During the rainy season in 2019 and 2020, nearly 50% of these countries suffered from drought conditions. By contrast, in the early 2000s, Vietnam and Thailand had the largest drought

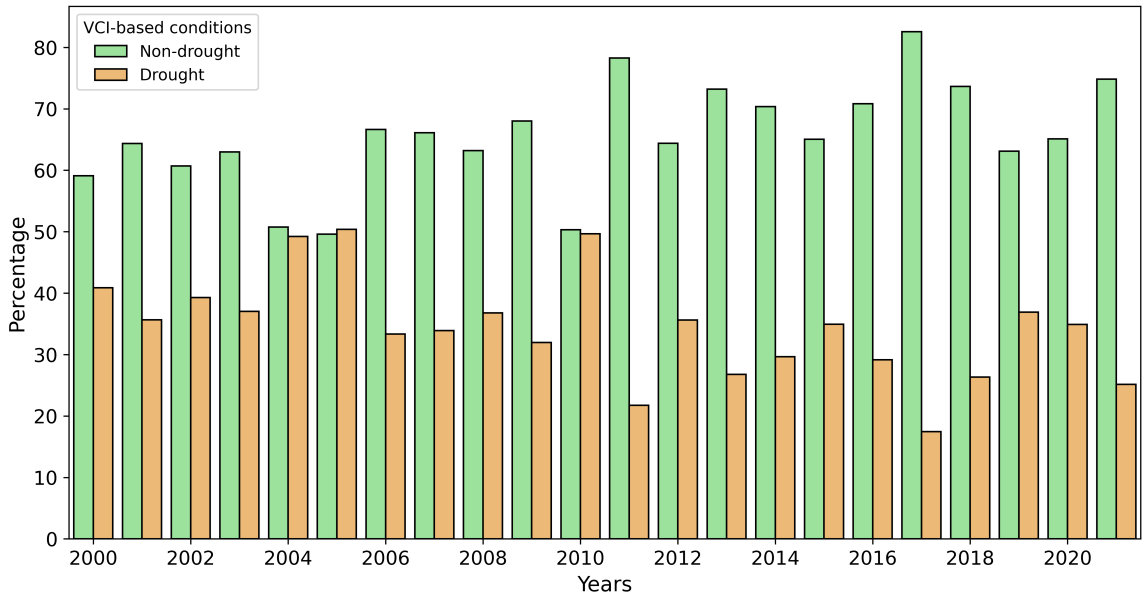

Figure 4.12: Temporal percentage of VCI-based drought and non-drought areas (in pixel unit) across the region during the rainy season from 2000 to 2021. The drought conditions are defined as VCI values below 50%.

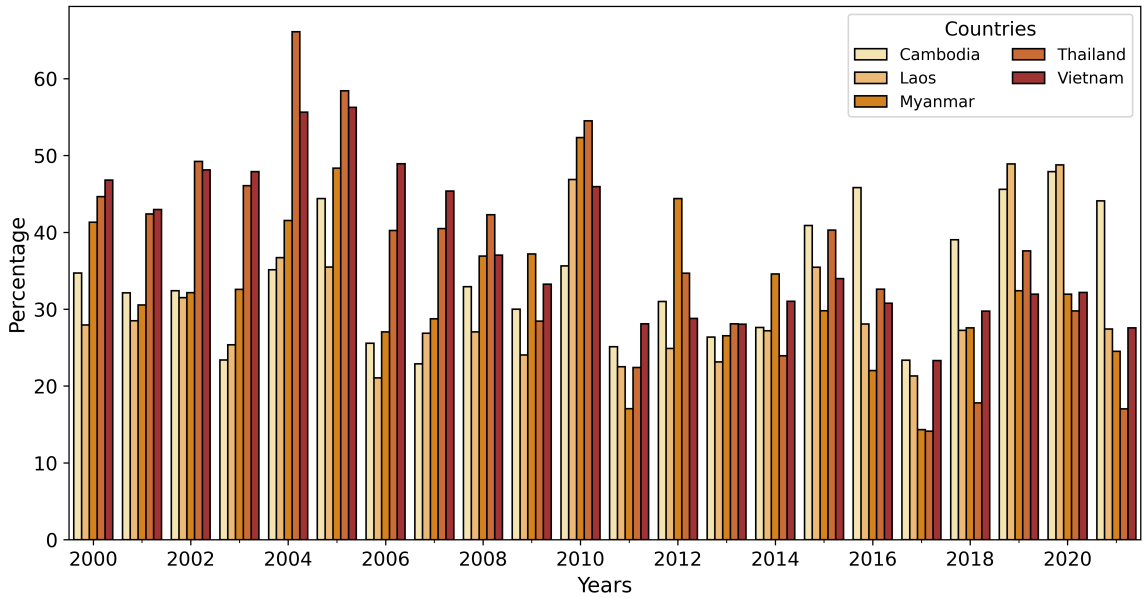

Figure 4.13: The percentage of annual VCI-based non-drought conditions across the countries from 2000 to 2021 during the rainy season. The non-drought condition is defined as VCI values above or equal to 50%.

proportions. For example, above 55% of these countries suffered drought in 2004 and 2005. These countries suffered significantly from drought in 2010, affecting more than 50% of their landmass. In 2012, Myanmar led the region, with nearly 47% of the country affected by drought. Generally, the proportion of drought based on VCI tended to get reduced despite its variability across the years.

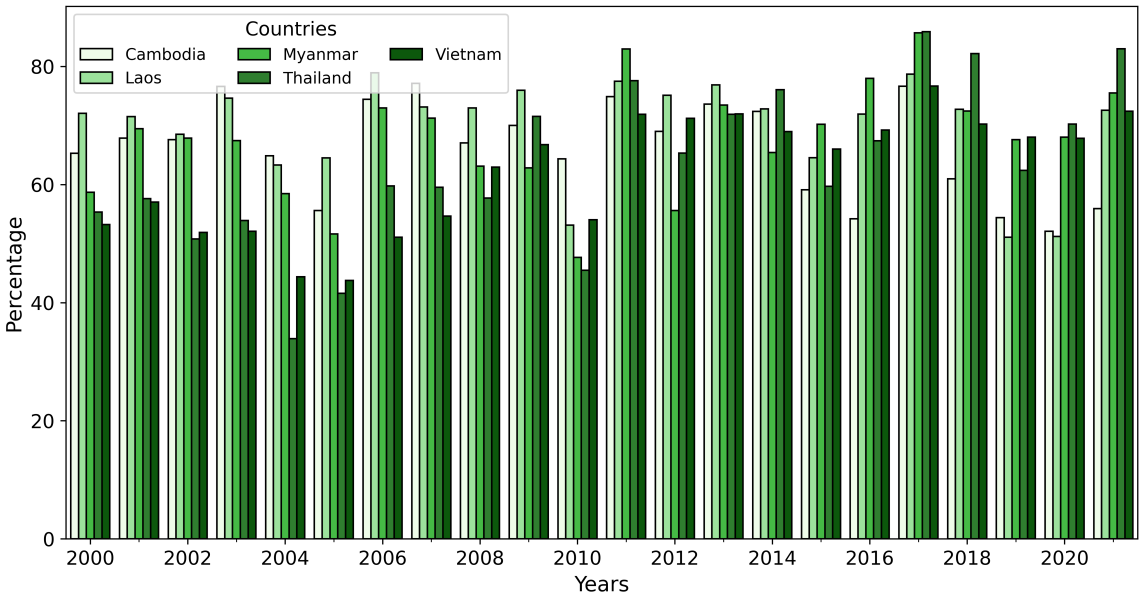

Figure 4.14: The percentage of annual VCI-based non-drought conditions across the countries from 2000 to 2021 during the rainy season. The non-drought condition is defined as VCI values above or equal to 50%.

Regarding the extent of non-drought, Figure 4.14 illustrated the annual percentage of non-drought during the rainy season from 2000 to 2021. Overall, larger proportions of non-drought (healthier vegetation) were observed across years and countries. Over the past ten years, a higher proportion of non-drought areas were detected. The highest proportion of non-drought was detected in 2018, above 75%. Before 2010, Cambodia and Laos had higher proportions of non-drought, indicating healthier vegetation during this period. However, this trend has reversed in recent years, when a lower non-drought extent was observed. This observation contrasts with Thailand and Vietnam. These countries have experienced less drought in recent years and have been covered by more than 70% of healthier vegetation (non-drought). Among the examined countries, Thailand had the largest proportion of non-drought in 2018 and 2021. Vietnam also experienced non-drought in 2013 and 2021. Approximately 72% of the country had VCI values above 50% these years. Similarly, in 2011, Myanmar had the largest non-drought extent, at 82%. Overall, drought conditions were less intensive during the rainy than during the dry season. Higher proportions of non-drought were primarily found in Thailand, Myanmar, and Vietnam over the past five years. By contrast, higher proportions of non-drought were detected in Cambodia and Laos in the early 2000s. Laos had the largest proportion of non-drought regardless of temporality, while Thailand had only 63%.

4.3.3 Temporal evolution of VCI-based drought by land cover types

Specific characteristics of different land cover types can influence the evolution and severity of drought conditions. Different vegetation types have different root systems and ability to access water. For example, rainfed crops may respond more to drought than irrigated crops. Figure 4.15 showed the monthly evolution of VCI-based drought conditions across six regional land cover types from 2000 to 2021. Overall, drought severity differs across land cover types, but the lowest VCI values were observed in 2005. Among the land cover types, rainfed cropland suffered from the most severe drought in 2005, with the VCI value reaching below 25%. Mixed forest and deciduous forests also experienced severe drought-induced stress during this period. Notably, the deciduous forests experienced drought-induced stress in recent years, such as 2019 and 2020. Among the forest types, evergreen forests suffered from the least drought. It can be seen that there was no indication of drought conditions in evergreen forests after 2010. In shrubland areas, droughts were visible in 2005 and 2010 (Figure 4.15), but other years were considered non-drought conditions. Regarding the VCI-based severity variations, irrigated cropland experienced fewer variations in drought severity across the study period, indicating stable growth and less drought influence. In contrast, other land cover types had higher fluctuations, indicating the stronger influence of drought. Despite the differences in severity, all land cover types followed similar temporal patterns, suggesting that while the intensity of drought impact varied, the timing of drought events was consistent across the landscape.

Drought conditions might vary significantly between countries due to differences in agricultural practices and human activities. In some countries, advanced irrigation systems and sustainable agricultural practices can mitigate the impacts of drought. In contrast, rainfed agriculture and unsustainable land use practices in other countries can exacerbate drought vulnerability. In Thailand, rainfed crops accounted for a large part of its agricultural sector and suffered from drought conditions. Generally, there was a temporal drought pattern across land cover types over time, but with different severity levels. In 2005, all land cover types experienced drought (Figure 4.16). Notably, deciduous forests had lower VCI values from 2004 to 2005, indicating continuous drought observations. In this regard, rainfed cropland also suffered from long-duration drought (Figure 4.16). Concerning wetter conditions, higher VCI values were observed in 2003, 2011, 2017, and 2018. These years can be considered wet years as the VCI values above 70% indicate wet conditions. Interestingly, irrigated cropland in 2016 suffered from greater drought than rainfed cropland (Figure 4.16). In 2020, deciduous forests indicated the most severe drought conditions. Evergreen forests have demonstrated resilience to drought over the years, and there has been no signal of drought in this forest in recent years (Figure 4.16).

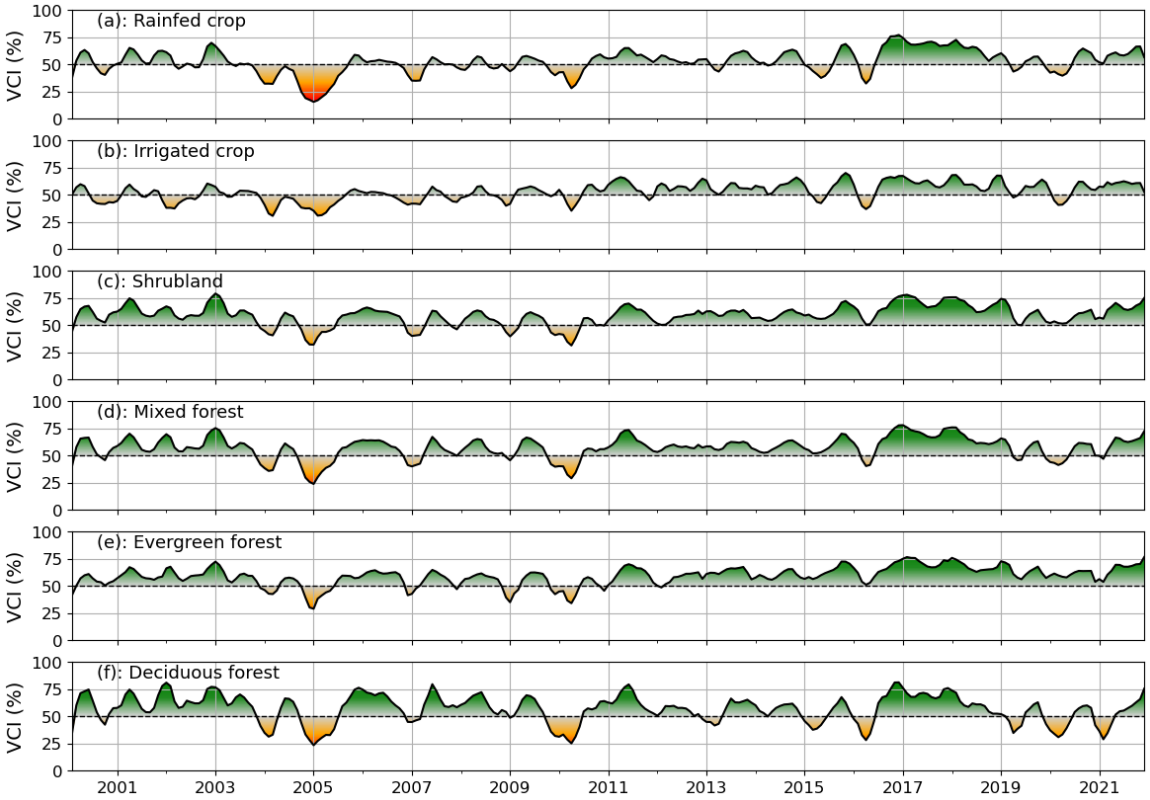

Figure 4.15: The temporal evolution of monthly VCI-based drought across the MSEA region for six main land cover types: (a) rainfed crop, (b) irrigated crop, (c) shrubland, (d) mixed forest, (e) evergreen forest, (f) deciduous forest. Dark red indicates drier conditions, while dark green presents wetter conditions.

In Cambodia, drought conditions were more severe than in other countries. There has been frequent drought in rainfed and irrigated cropland (Figure 4.17). For example, the irrigated crop VCI values were nearly below 50% from 2000 to 2010, indicating drought-induced conditions. By contrast, shrubland VCI values witnessed wetter conditions over the first 15 years, but in recent years, lower VCI values have been observed (Figure 4.17), indicating drier conditions. This condition was also found in mixed forests and deciduous forests. For example, deciduous forests had low VCI values (below 25%) in 2016, 2019, and 2020 (Figure 4.17), indicating severe drought conditions. Evergreen forests, however, indicated less drought. Overall, forests witnessed less drought in the first 15 years of the 21st century, but in recent years, they have experienced more severe drought conditions, especially in mixed and deciduous forests. In contrast, this condition was the opposite in rainfed and irrigated croplands. Despite frequent drought conditions, irrigated crops had lower VCI value variations (30-75%) over the study period (Figure 4.17).

In Laos, vegetation suffered from less frequent drought. Overall, vegetation suffered from drought-induced stress in 2005 and 2020 (Figure 4.18). These years witnessed continuous low VCI values extended over several months. Rainfed probably indicated the most se-

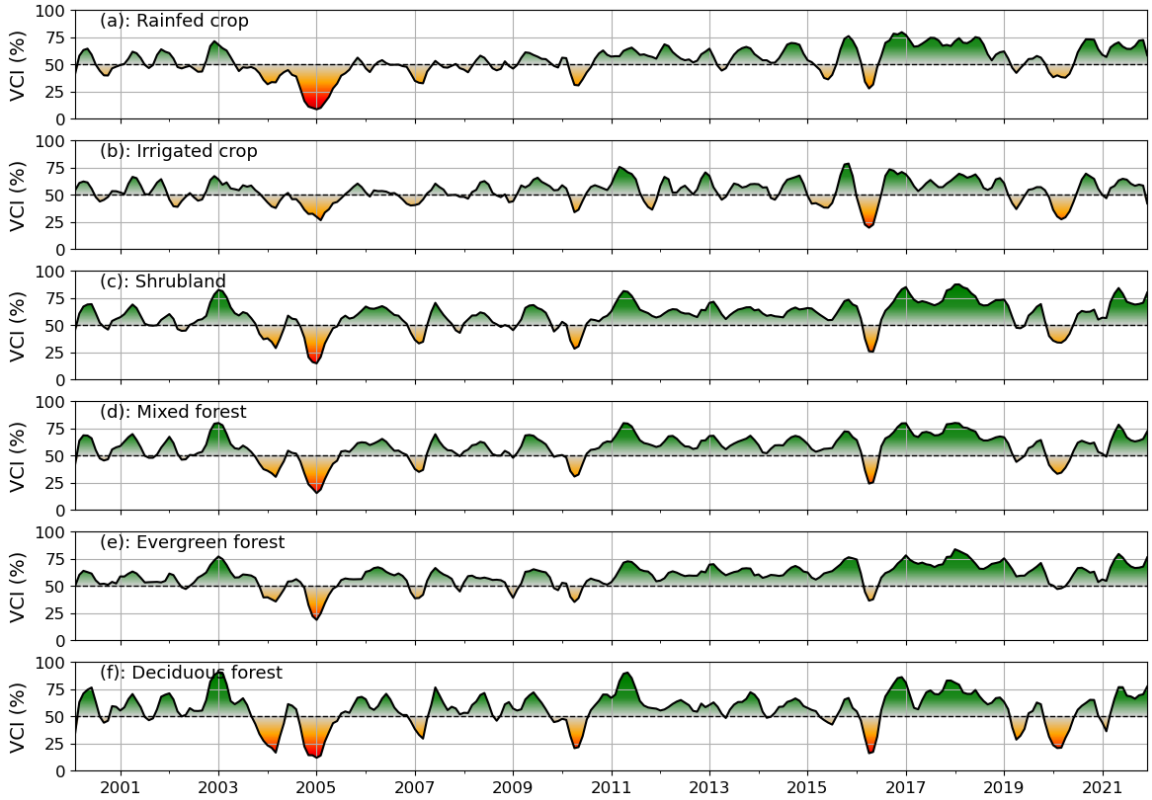

Figure 4.16: The temporal evolution of VCI-based drought in Thailand across six land cover types from 2000 to 2021: (a) rainfed crop, (b) irrigated crop, (c) shrubland, (d) mixed forest, (e) evergreen forest, and (f) deciduous forest. Dark red indicates drier conditions, while dark green presents wetter conditions.

vere drought in 2005 and 2020. This observation indicated that rainfed crops are extremely vulnerable to drought. Likewise, deciduous forests suffered from severe drought conditions during these years. Irrigated cropland experienced severe drought conditions in 2005 but less severe in recent years. Other land use types showed similar patterns of drought severity. Evergreen forest was the least affected by drought in recent years, indicating greater resilience to drought. The wettest conditions could be observed in 2017 across all land use types, where the VCI value stayed above 75%. Overall, shrubland indicated moderate and mild drought conditions, while severe drought conditions were primarily found in cropland. Forests generally indicated wetter conditions during the study period.

In Myanmar, drought conditions have shown a marked temporal pattern in specific years (Figure 4.19). Notably, the years 2005 and 2010 were recorded as the period of intense drought conditions. Both rainfed and irrigated crops experienced significantly low VCI values during these years. It is noted that all land use types witnessed severe and widespread drought conditions in 2010, with VCI values falling below 25% (Figure 4.19). For example, mixed and deciduous forests experienced VCI values below 25% for several months in 2010. It is observed that drought conditions have been less severe over the past decade.

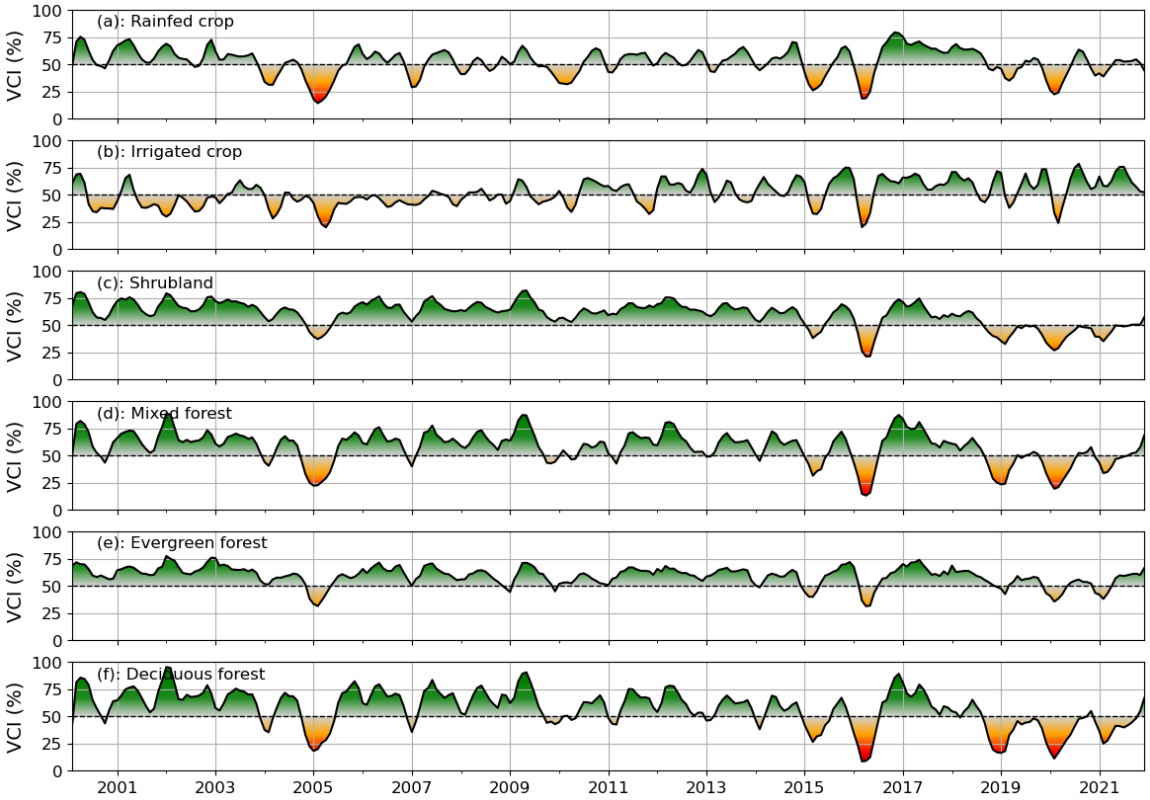

Figure 4.17: The temporal evolution of VCI-based drought in Cambodia across six land cover types from 2000 to 2021: (a) rainfed crop, (b) irrigated crop, (c) shrubland, (d) mixed forest, (e) evergreen forest, and (f) deciduous forest. Dark red indicates drier conditions, while dark green presents wetter conditions.

In contrast, drought conditions from 2000 to 2010 witnessed more severe conditions. In rainfed agriculture, the VCI values below 50% lasted nearly two years during 2004 and 2005 (Figure 4.19), indicating severe and widespread drought. Wet conditions were observed similarly in other countries but varied over time. The year 2017 witnessed very wet years; for example, deciduous forests experienced VIC values above 75%, indicating wet conditions. In recent years, slight drought conditions have been observed across the land cover types despite the decline in VCI. In short, all land use types indicated severe droughts in 2005 and 2010. Shrubland experienced the least drought conditions, possibly due to its resilience and ability to endure drought. Forests witnessed mild drought or non-drought in most cases in recent years (Figure 4.19).

In Vietnam, drought conditions have been less intense across the land cover types, especially over the past decade. Overall, drought conditions in Vietnam were more severe in the first ten years of the 21st century (Figure 4.20). In 2005, the VCI value witnessed the lowest across land cover types, while lower values were observed in 2004. Rainfed cropland experienced lower VCI values below 50% from 2004 to 2008. Likewise, irrigated cropland witnessed the longest drought stress over the study period, from 2000 to 2008, nearly eight

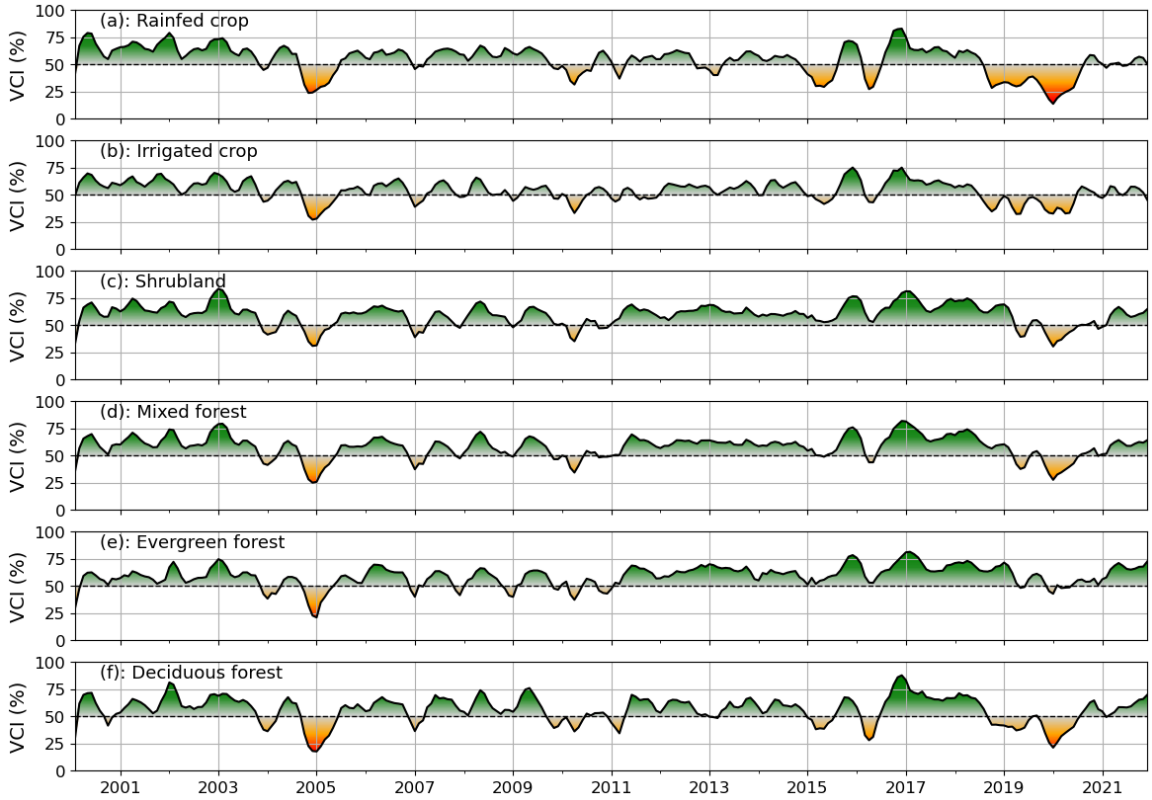

Figure 4.18: The temporal evolution of VCI-based drought in Laos across six land cover types from 2000 to 2021: (a) rainfed crop, (b) irrigated crop, (c) shrubland, (d) mixed forest, (e) evergreen forest, and (f) deciduous forest. Dark red indicates drier conditions, while dark green presents wetter conditions.

years. Looking at its severity classification, irrigated crops primarily experienced moderate or mild drought conditions during this period (Figure 4.20). These low VCI values indicated that rainfed and irrigated crops were more vulnerable to drought during these years. Forests shared similar patterns of drought conditions. Notably, deciduous forests have experienced moderate to mild drought in recent years. This forest also experienced relatively stable VCI values despite its normal conditions from 2010 to 2015. By contrast, the remaining forests witnessed wetter conditions during this period. The VCI value of evergreen and mixed forests stayed above 70% over the last seven years, indicating striving vegetation. This observation was also found in rainfed and irrigated areas. Over the past ten years, irrigated and rainfed crops have rarely been stressed due to drought (Figure 4.20).

4.3.4 Identified drought years

Severe drought years were identified from the percentage of extreme pixels (VCI $\leq$ 10) across the study region from 2000 to 2021. Figure 4.21 presented the annual distribution of extreme pixels and drought severity across the region throughout the study period. Overall, extreme pixels were variant across years, but the most severe drought years were identified

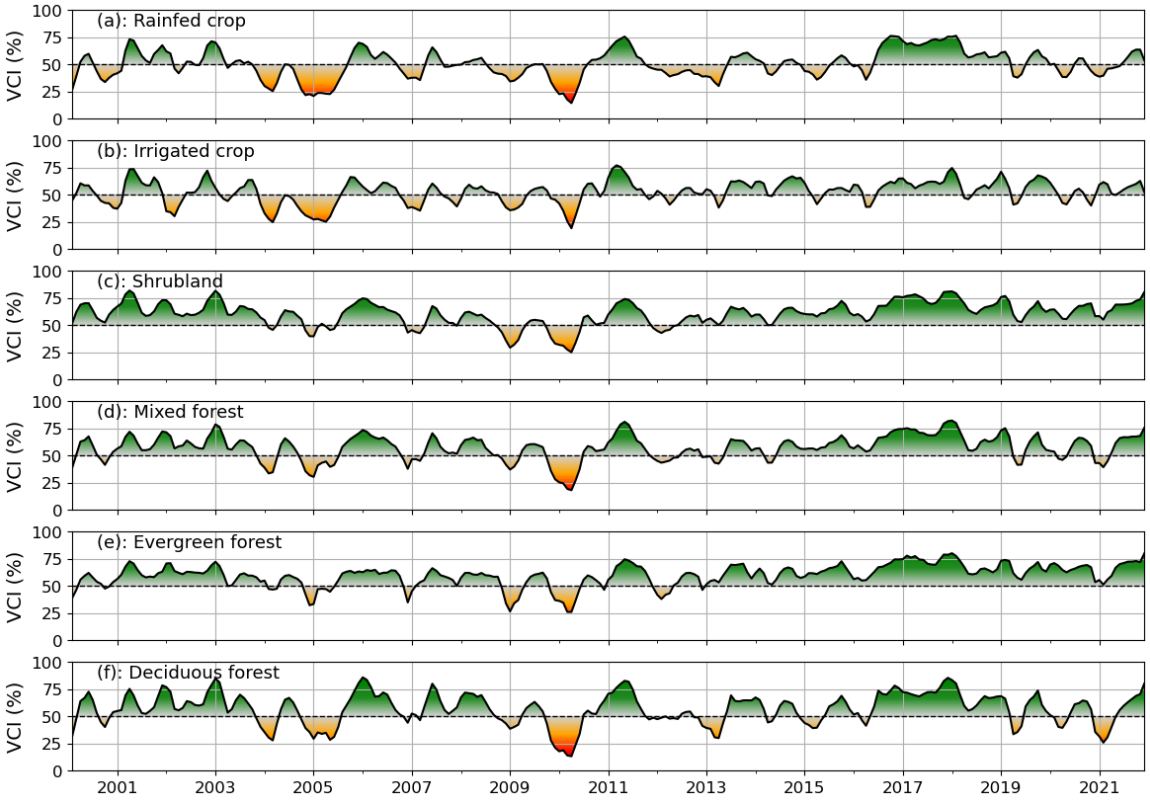

Figure 4.19: The temporal evolution of VCI-based drought in Myanmar across six land cover types from 2000 to 2021: (a) rainfed crop, (b) irrigated crop, (c) shrubland, (d) mixed forest, (e) evergreen forest, and (f) deciduous forest. Dark red indicates drier conditions, while dark green presents wetter conditions.

in 2000, 2004, 2005, 2010, 2016, 2019, and 2020, with a typically higher proportion of extreme VCI pixels. Among the drought years, 2004 and 2005 had the highest percentage of extreme VCI pixels, nearly 20%, whereas the extreme recorded VCI values reached the lowest point of about 2.3. Generally, the severe drought years were associated with extreme VCI values, indicating intense vegetation stress. However, this pattern did not consistently apply across all years. For example, extreme VCI severity was observed in 2001 and 2021, although there was a smaller proportion of extreme pixels. By contrast, these are the opposite of the drought years in 2016 and 2019. Since we considered drought conditions on an annual basis, a severe drought can occur with short durations (3-4 months) and then return to normal conditions. This behavior likely leads to higher VCI values overall.

The progression of severe droughts exhibited significant spatial and temporal variability, and they are primarily detected during the dry season. Figure 4.22 displayed the monthly maps of severe drought years and their spatiotemporal variability. The temporal analysis of severe drought years indicated that the most severe droughts were detected in the dry seasons of 2004 (January-April), 2005 (October 2004 - June 2005), 2010 (January-June), 2016 (March-May), and 2020 (January - May). Among these, the 2005 drought was the

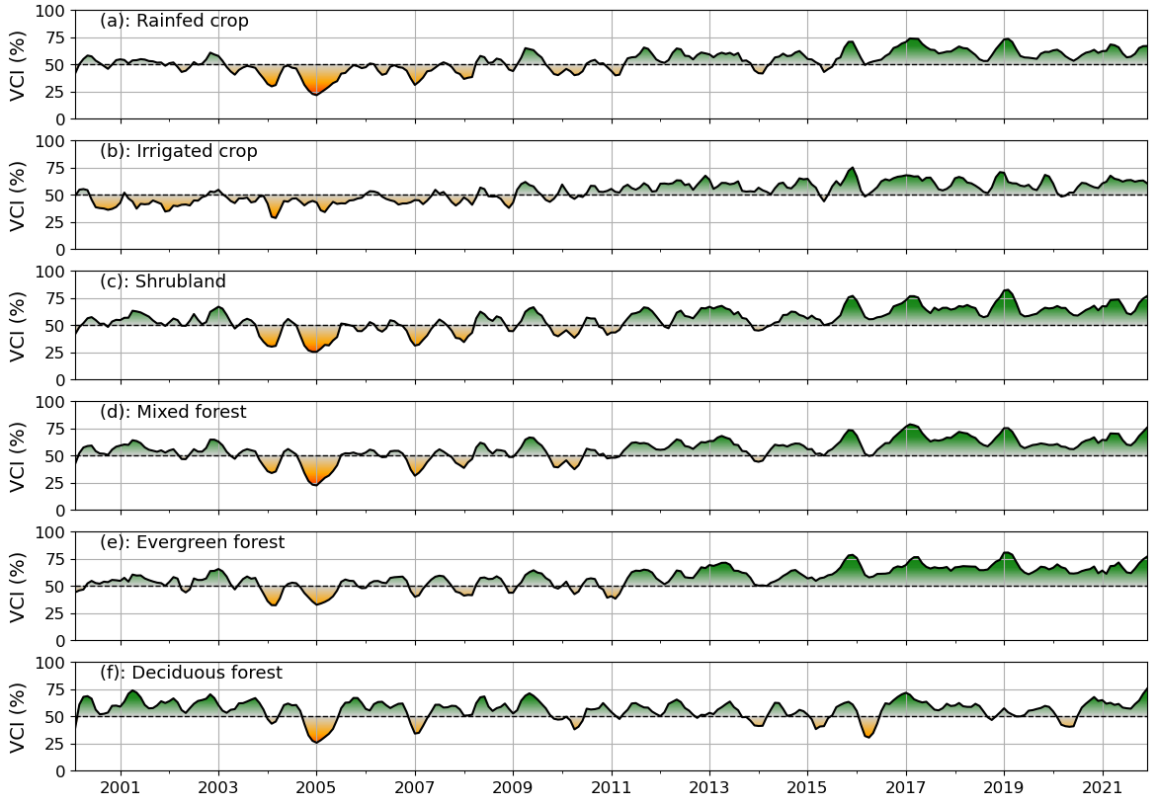

Figure 4.20: The temporal evolution of VCI-based drought in Vietnam across six land cover types from 2000 to 2021: (a) rainfed crop, (b) irrigated crop, (c) shrubland, (d) mixed forest, (e) evergreen forest, and (f) deciduous forest. Dark red indicates drier conditions, while dark green presents wetter conditions.

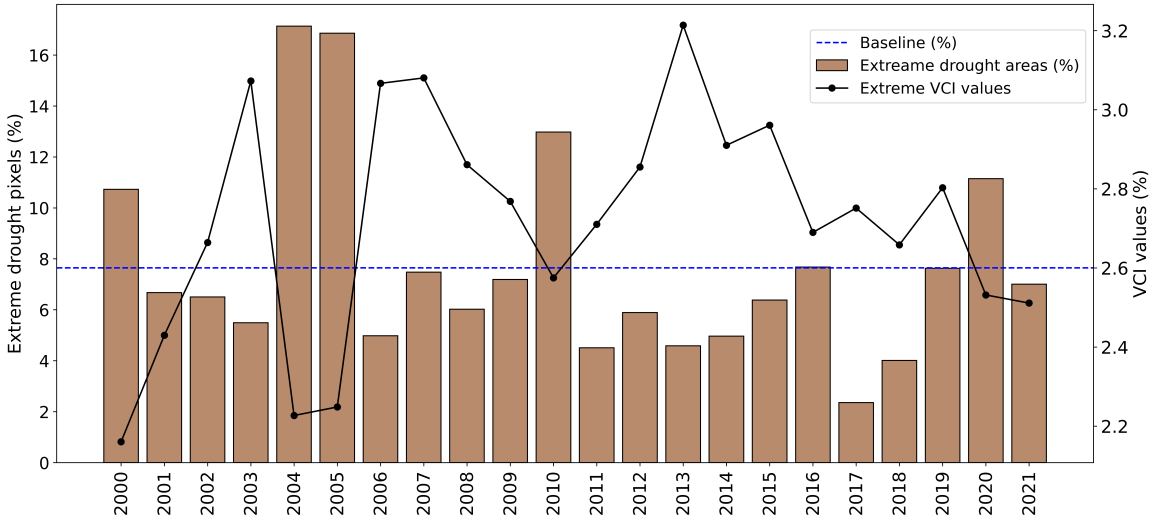

Figure 4.21: The annual percentage of extreme VCI pixels and its values across the MSEA region from 2000 to 2021. The bar plot indicates the annual percentage, while the line plot displays the mean values of the VCI below 10%.

longest, lasting nine months, with its peak from December 2004 to March 2005. Less severe droughts were found in 2000 and 2019, whereas the drought event in 2016 was severe, but it occurred short and returned to normal conditions by June. The wettest months during the

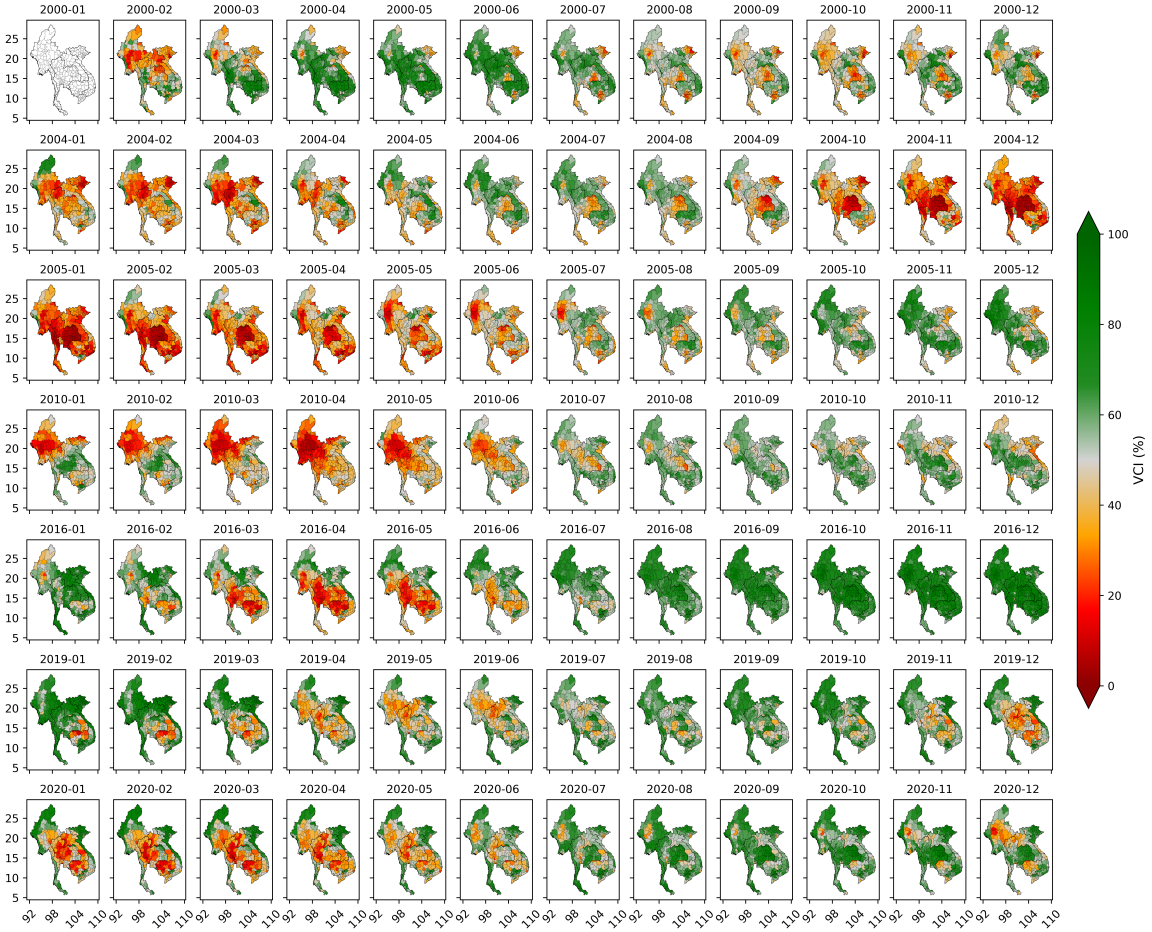

Figure 4.22: Spatial and temporal patterns of severe drought years across the MSEA region over the study period. The VCI values are averaged by province/districts across the region.

drought years were observed from August to December 2016, and this period experienced very high VCI values, indicating wetting conditions. Other months in 2000 (April-July) also experienced wet conditions, while other rainy months still suffered from moderate to mild drought. Moderate and severe droughts were spatially scattered over the study region but were most commonly identified in the plains of central Myanmar, Thailand, Cambodia, and the lower Vietnamese Mekong area. Regardless of the severity of the drought, the entire MSEA region suffered from drought during the dry season of 2004-2005. In 2010, a severe drought occurred in the northern region (e.g., Myanmar). By contrast, in 2016, the severe drought occurred mainly in the southern region, including Thailand and the lower Mekong Delta. In recent years, central Thailand and Cambodia have witnessed more severe droughts than other areas in the region.

In detail, severe drought conditions in 2000 were primarily observed in January and February, affecting the northern region (e.g., Myanmar, northern Laos, and Vietnam). However, this condition was scattered in specific areas from July to December, primarily affecting Central Myanmar, eastern Thailand, the Lower Vietnamese Mekong Delta, and north-

eastern Vietnam. In 2004, drought was very severe in the early months in southern Myanmar and northern Thailand. However, in the later months, eastern Thailand and Vietnamese Central highlands witnessed the most severe drought conditions. These areas became more intense in the early months of 2005. Thailand witnessed the most severe drought conditions from November 2004 to April 2005. In 2010, severe drought primarily occurred in Myanmar from January to March, but it was expanded to Thailand until July. In 2016, severe drought conditions started in March and lasted until May. Other months witnessed wet conditions. In January and February, drought conditions were specifically found in Cambodia and small parts of southern Thailand and central Myanmar. In 2019, Cambodia experienced severe drought conditions in January and February, and then it was gradually widespread towards Laos, Thailand, and Myanmar before return to normal conditions in August. In 2020, the region experienced more severe drought conditions than in 2019. Central Thailand and Cambodia witnessed the most severe drought in this year, while Myanmar and Vietnamese Central Highlands also got affected, but less intense during this period. Although no region-wide studies have identified severe drought years over the past years, several local studies reported droughts in Vietnam, Cambodia, and the Lower Mekong Delta. Vietnam, for example, suffered from the largest droughts in 2004-2005 (Tran et al., 2023) and 2005 and 2010 (Le et al., 2019). In the Lower Mekong Basin, severe drought years were reported in 2004-2005 (Son et al., 2012; Adamson, 2005), 2010 (Zhang et al., 2014), and 2015-2016 (Son and Thanh, 2022; Guo et al., 2017). An updated statistical analysis of in-situ drought events from the International Disaster Database revealed that the MSEA region suffered the largest drought events in 2005, 2010, 2015, 2016, and 2019 (Ha et al., 2022). Although this approach can identify severe drought years, it may not capture severe droughts with short durations, especially localized severe droughts. Also, a drought event can continuously occur from one year to another without interruption, and consequently, this approach may misidentify severe drought years. However, most of the drought events in the MSEA region last less than six months, so this is unlikely to be an issue. Severe drought years usually have significant impacts on agricultural production and the environment, and the identification of severe drought years can help understand the spatiotemporal structure of drought and its recurrence. Analysis of the drought years in the MSEA region revealed that severe drought typically occurs in the early dry seasons (November-December) and returns to normal conditions by the end of the dry season (April-May), with the severe drought cycle reoccurring every 4-5 years. This period corresponds to the ripening stage of rainfed rice crops (November-December) in Thailand, Cambodia, and Myanmar, whereas Vietnamese farmers begin the winter-spring rice cropping season. This information would be crucial for regional and local authorities to navigate water resource distribution and develop future drought mitigation risk plans.

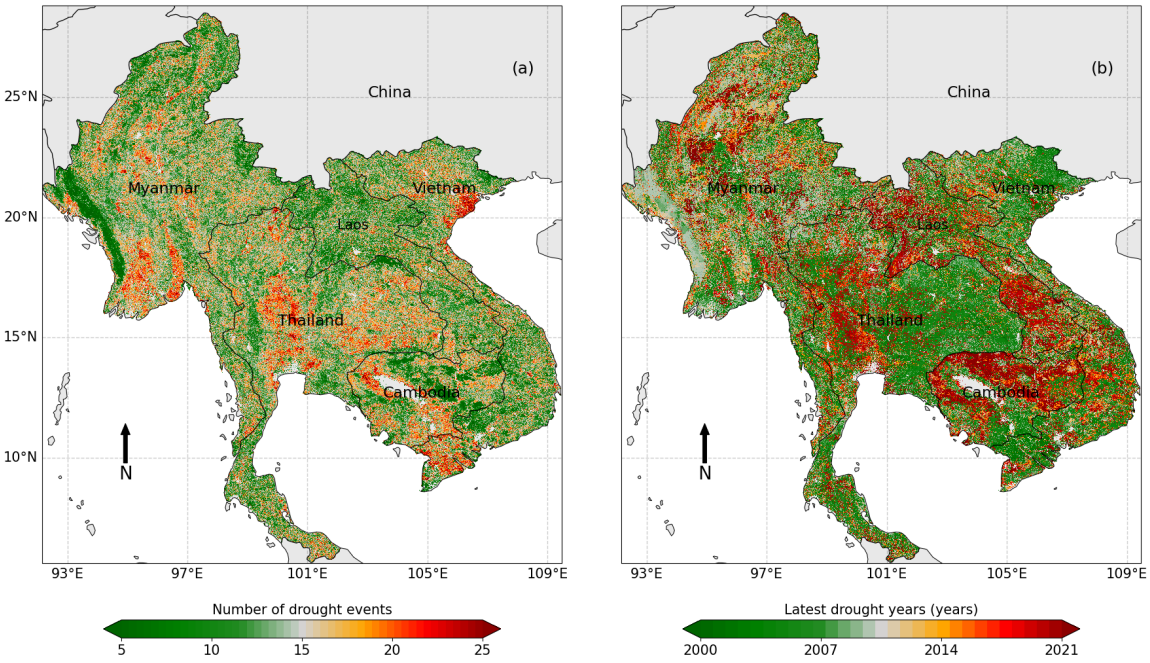

Figure 4.23: Spatial distribution of drought events and their latest occurrence across the MSEA region from 2000 to 2021.

4.3.5 Spatiotemporal drought characteristics

The long-term characteristics of drought are critical for understanding its spatiotemporal distribution. In this study, the spatial distribution of four drought characteristics during the 2000-2021 period is shown in Figure 4.23 and Figure 4.24. The number of prolonged drought events varied across the region, with up to 25 events observed in the lower Mekong Delta, central Thailand, and the Red River Delta (Figure 4.23-a). This result indicated typically longer periods of drought in these areas. The most recent drought recorded by the International Disaster Databases in the lower Vietnamese Mekong provinces lasted eight months (https://public.emdat.be), whereas Thailand suffered from nearly 17 months of drought in 2016. On average, the MSEA region suffered from 12-15 drought events over the selected study period. Thailand had the highest number of prolonged droughts, with 14.5 events, followed by Vietnam (about 14 events). Most severe drought spells occurred in 2005 and 2016 (e.g., in Thailand and Vietnam), covering nearly 20% of the MSEA region. In recent years, the lower Mekong Delta has suffered more prolonged drought events than other areas (Figure 4.23-b). The result indicated that nearly 35% of Cambodia experienced the longest droughts in 2020 and 2021, which is consistent with the severe decline in the Tonle Sap Lake (Lindsay et al., 2021).

Except for differences in the latest drought years, some common features exist between the drought duration and frequency. The mean duration was generally higher in central Myanmar and the Mekong Delta (Figure 4.24-a). Consequently, the drought frequency was

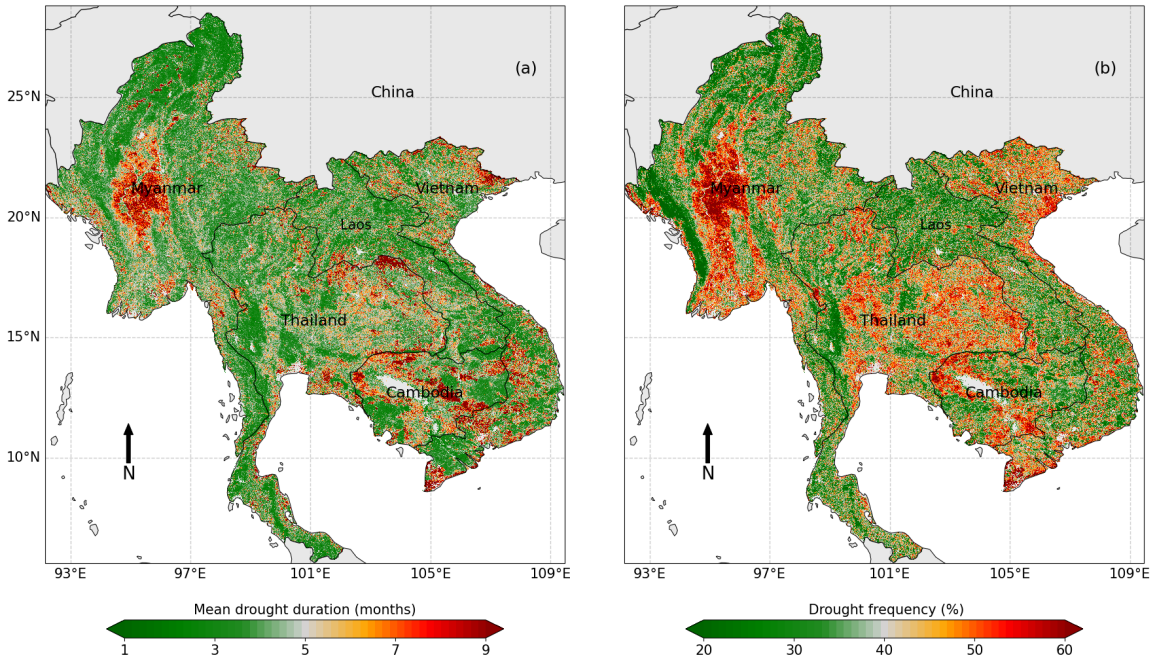

Figure 4.24: Spatial distribution of drought duration and frequency across the MSEA region from 2000 to 2021.

also larger than in other areas (Figure 4.24-b). Nearly 30% of the MSEA region generally suffered from more than five months of drought (longer than the dry season), and Cambodia had the highest mean drought duration with nearly six months. Vietnam ranked second with nearly 5.2 months, while Laos had the shortest duration with 4.3 months. In addition, the MSEA region was found to have a high drought frequency. On average, nearly 40% of droughts occurred in most countries, except for Laos, with 34%. Noticeably, the central region of Myanmar had the highest occurrence of drought ($\sim$ 60%), but with fewer prolonged drought events (Figure 4.23-a), implying shorter periods of drought in this area.

4.3.6 Time series trends of VCI-based drought

4.3.6.1 Spatial trends

Trend analyses were performed on the time-series VCI data from 2000 to 2021. Figure 4.25 showed the per-pixel trend analysis results during the dry and rainy growing seasons over the MSEA region. Green and red colors indicate decreasing and increasing drought conditions (or greening and browning vegetative trends), respectively, while gray colors represent non-significant trends or non-vegetative areas. Overall, decreasing drought conditions (increasing vegetation) predominated in northern Vietnam and eastern Thailand, whereas increasing drought conditions (browning vegetation) are apparent in Cambodia and southern Laos. Regionally, nearly 15% of the vegetative areas suffered from drought conditions, and the rest remained stable and resistant to drought hazards, with roughly 30%

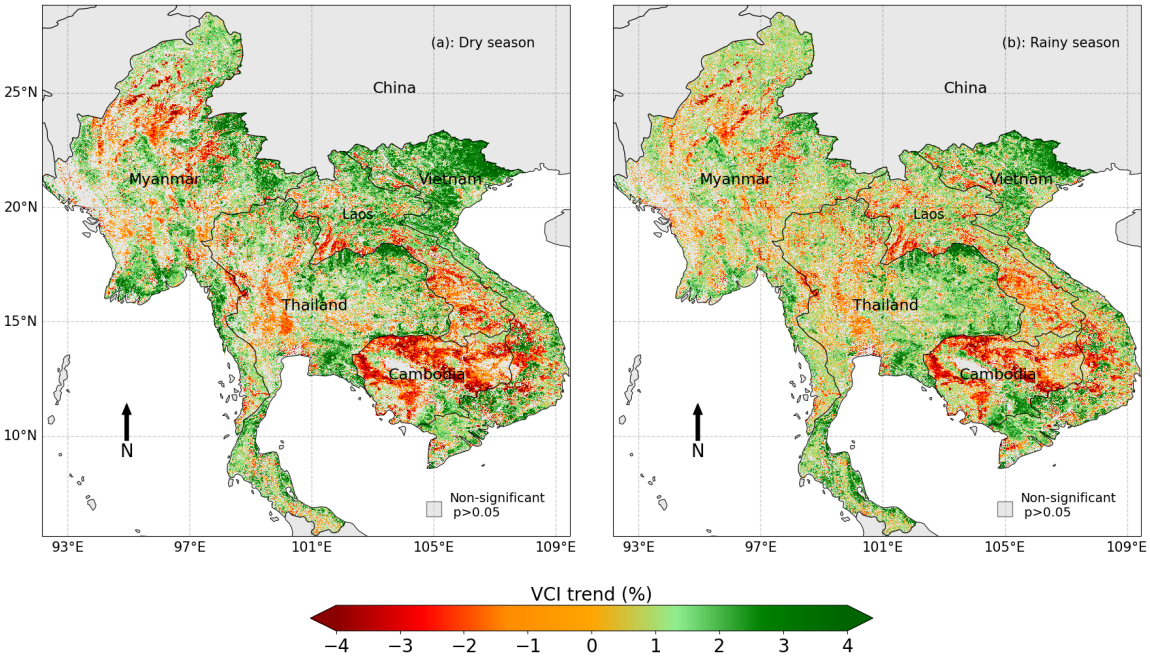

Figure 4.25: Spatial pattern of VCI-based drought trends during the dry season (a) and rainy season (b) from 2000 to 2021 across the MSEA region.

of the vegetation increasing over the study period. In the dry growing season, most of the forestland or shrubland witnessed a decreasing trend in drought (an increase in green forest). In comparison, cropland showed either no trend or a slight change (Fig. 4.25-a). By contrast, cropland experienced a decrease in the drought trend (increase in greenness) during the rainy season in eastern Thailand and the lower Mekong Delta. Laos and Myanmar remained relatively stable over the past 21 years (Fig. 4.25-b). Interestingly, the detected trend in northern Vietnam decreased from the dry to the rainy growing season.

Climate change and cropping practices likely explain differences in the spatial distribution of drought trends (vegetation stress). The increase in annual VCI is significant over northern Vietnam (VCI trend exceeds 4 $yr^{-}1$), where forests and shrubland dominate. In the past decade, forest restoration programs from the Vietnamese government have increased forest cover in addition to the rapid expansion of farm-based forest plantations (de Jong, 2010). In Cambodia, a large decline of the VCI (e.g., rate ≤ -3 $yr^{-}1$) was especially found surrounding the Tonle Sap Lake, where rainfed cropping systems are commonly practiced. Chen et al. (2021a) analyzed the multi-decadal variability of Tonle Sap Lake, and they revealed that the lake's water level has declined because of increasing climatic crises (e.g., precipitation deficits) and human activities (e.g., hydropower operations). The rainfed rice crop in eastern Thailand is primarily grown in the rainy season, whereas catastrophic flooding events usually occur in northern Vietnam. These could be the possibilities of the increasing (decreasing) VCI drought trends in Thailand (Vietnam).

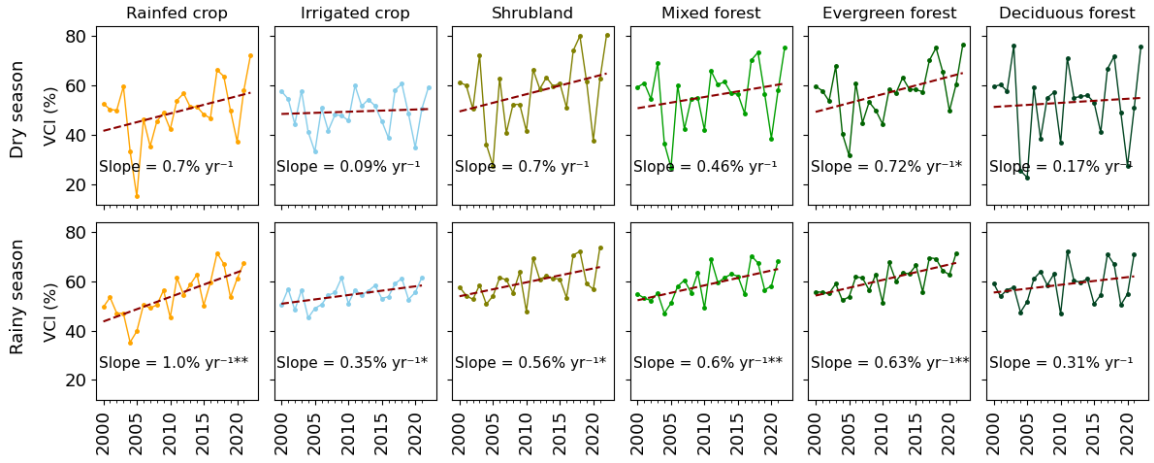

Figure 4.26: Temporal trends of VCI-based drought conditions in Thailand across six land cover types during the dry and rainy seasons from 2000 to 2021. Vertical columns represent land use types, while horizontal rows refer to the seasons. Statistically significant slopes are marked with two asterisks (**, p-value ≤ 0.01) and one asterisk (*, p-value ≤ 0.05).

4.3.6.2 Analysis of VCI trends across land cover types

Drought trends can vary among countries and land cover types. These variations can influence the increasing and decreasing vegetation over time, making it suitable to track drought trends. This section explored trends across different land cover types to examine the vegetation-induced drought from 2000 to 2021 during the dry and rainy seasons. In Thailand, all land cover types experienced an increase in VCI trends, indicating a decline in drought conditions during the dry and rainy seasons (Figure 4.26). Despite its increase, Thailand witnessed non-statistically significant trends during the dry season, except in evergreen forests. This means that the trends of VCI-based drought conditions across the vegetation types stayed relatively stable over the 21 years during the dry season. By contrast, the VCI-based drought during the rainy season experienced an increase over the study period, except in deciduous forests (Figure 4.26). Rainfed crops during the rainy season had the highest trend, at about 1% per year. Other vegetation types increased from 0.4 to 0.6% per year. This upward trend could be due to increased precipitation during the rainy season. Frequent rainfall can boost vegetation growth, leading to higher VCI values and reduced drought stress.

In Cambodia, vegetation-based drought experienced a declining trend across land cover types from 2000 to 2021 (Figure 4.27). Notably, irrigated crops witnessed an increase in VCI-based drought trend over the study period. Shrubland and deciduous forests witnessed the largest decline during the dry season. For example, shrubland had a decline rate of about 1.2% per year, indicating the upward trend of drought in the shrubland environment. Rainfed cropland and evergreen forests during the rainy season showed a non-statistically signif-

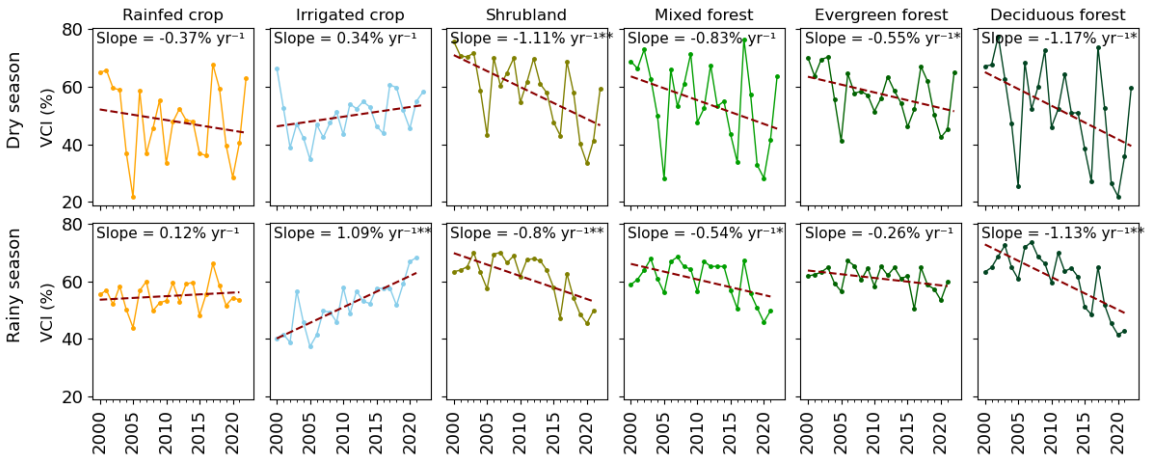

Figure 4.27: Temporal trends of VCI-based drought conditions in Cambodia across six land cover types during the dry and rainy seasons from 2000 to 2021. Vertical columns represent land use types, while horizontal rows refer to the seasons. Statistically significant slopes are marked with two asterisks (**, p-value ≤ 0.01) and one asterisk (*, p-value ≤ 0.05).

icant trend, while other vegetation types declined significantly. Only irrigated experienced a significant increase in VCI-based drought ($\sim$ 1% per year), indicating less vulnerability. Despite the rainy season, deciduous forests witnessed the largest rate of decline, at 1.1% per year. Forests in Cambodia often experience disturbance, and recent studies reported that Cambodia has been among the largest forest losers worldwide (Curtis et al., 2018; Hansen et al., 2013). Human disturbance and drought have exacerbated the decline of forests over the past 21 years.

In Laos, most land cover types witnessed relatively stable over the study period (Figure 4.28). During the dry season, the statistical test showed that the trend of VCI-based drought conditions was not statistically significant despite its upward trend. Cropland experienced a declining trend in VCI, while evergreen forests showed a significant increase trend. Rainfed and irrigated cropland experienced a declining VCI trend during the rainy season. This means these crops were vulnerable to drought, even during the rainy season. Another possibility is that irrigated systems were poorly functioning, while the precipitation rate might have declined over this country's study period. Other vegetation types stayed relatively the same.

In Myanmar, the VCI-based trend was relatively stable across land use types from 2000 to 2021. As can be seen from the line plot in Figure 4.29, despite its upward trend, the trend was not statistically significant. Evergreen forests experienced the highest trend during the dry season, while deciduous forests witnessed a slight decline. Likewise, VCI-based drought conditions during the rainy season experienced a non-statistically significant trend, except for evergreen forests. In this regard, evergreen forests increased by 0.52% per year.

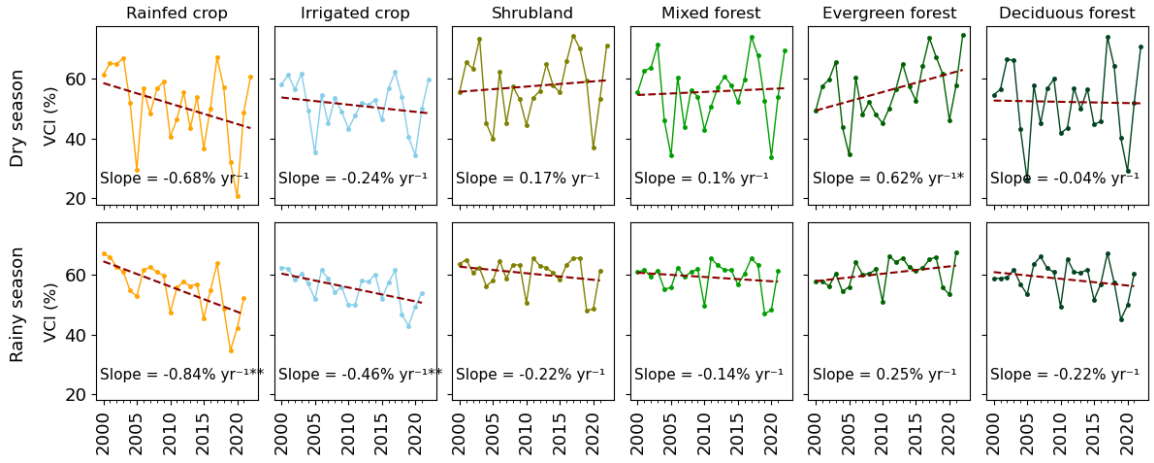

Figure 4.28: Temporal trends of VCI-based drought conditions in Laos across six land cover types during the dry and rainy seasons from 2000 to 2021. Vertical columns represent land use types, while horizontal rows refer to the seasons. Statistically significant slopes are marked with two asterisks (**, p-value ≤ 0.01) and one asterisk (*, p-value ≤ 0.05).

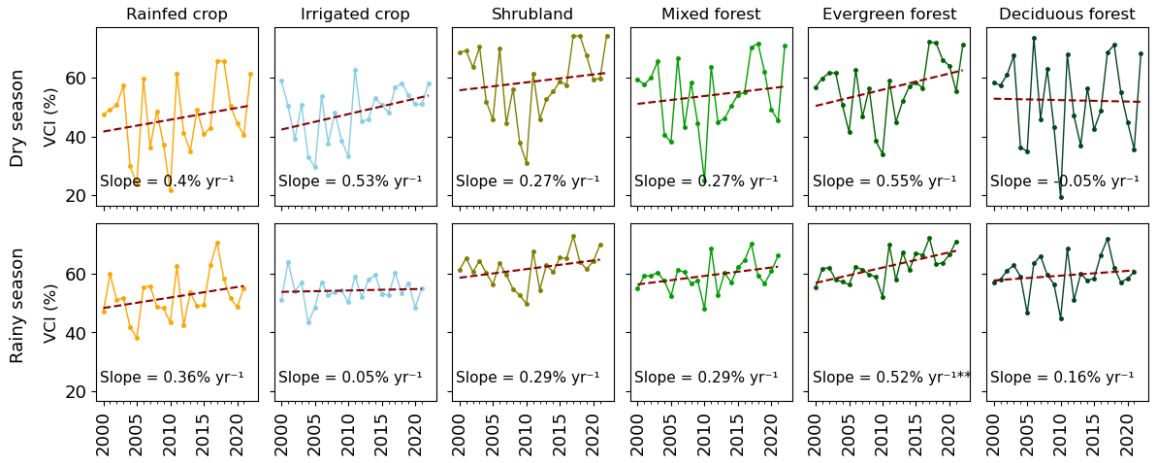

Figure 4.29: Temporal trends of VCI-based drought conditions in Myanmar across six land cover types during the dry and rainy seasons from 2000 to 2021. Vertical columns represent land use types, while horizontal rows refer to the seasons. Statistically significant slopes are marked with two asterisks (**, p-value ≤ 0.01) and one asterisk (*, p-value ≤ 0.05).

In Vietnam, there has been a significant increase in VCI-based drought across land cover types over the past 21 years (Figure 4.30). Despite the dry season, vegetation experienced upward trends. The largest increasing trend was observed in shrubland, at about 1.24% per year. Evergreen forests ranked second with above 1% per year. Despite its upward trend, deciduous forests indicated a non-statistically significant trend. Interestingly, the rainfed VCI-based trend was higher than the irrigated crop. This could be due to the recently improved irrigation system, which could be recorded in the ESA CCI land cover product. During the rainy season, most vegetation types witnessed an upward trend. Rainfed crops were less affected by drought and indicated an upward trend at 0.62% per year. Frequent

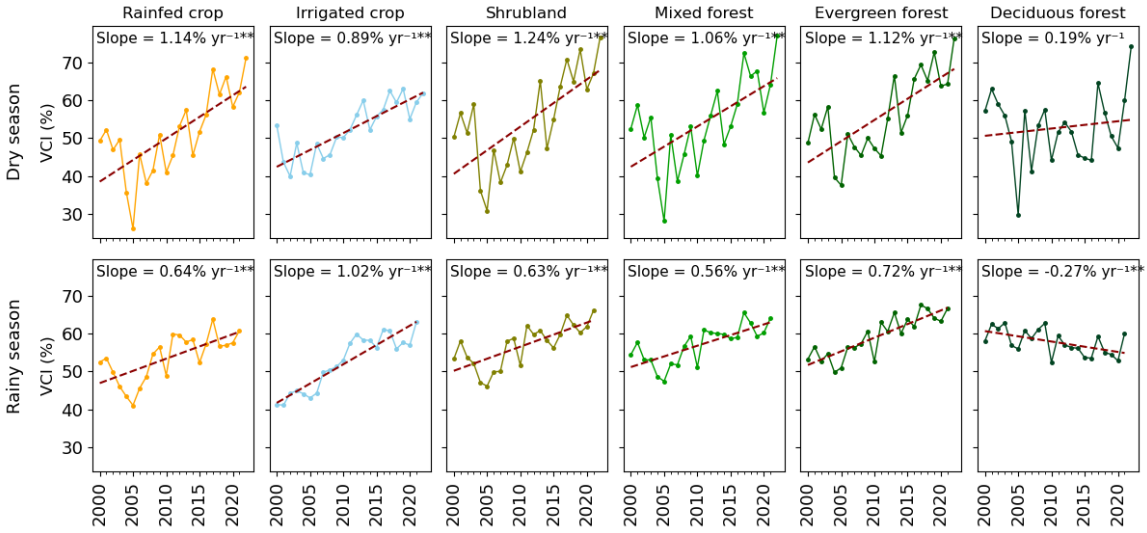

Figure 4.30: Temporal trends of VCI-based drought conditions in Vietnam across six land cover types during the dry and rainy seasons from 2000 to 2021. Vertical columns represent land use types, while horizontal rows refer to the seasons. Statistically significant slopes are marked with two asterisks (**, p-value ≤ 0.01) and one asterisk (*, p-value ≤ 0.05).

precipitation could be the main factor driving the increase in VCI values in rainfed crops. Irrigated crops witnessed the highest positive trend at 1.02% per year. Frequent precipitation and improved irrigation systems support large areas of Vietnamese agricultural land. Evergreen forests also experienced a high positive trend, indicating drought-reduced stress in this forest environment. In contrast, deciduous forests showed a negative trend, which means this forest frequently faced disturbance and drought hazards. A recent study reported that the Vietnamese Central Highlands experienced a large area of declining vegetation due to the expansion of industrial crops and intense drought conditions in recent years (Ha et al., 2024).

4.4 Discussion

4.4.1 Differences in drought characteristics among the countries

This study employed the VCI from MODIS time series observations from 2000 to 2021 across the MSEA region. Generally, drought monitoring derived from satellite-based vegetation time series provided plausible results. The identified severe drought years from the VCI-based drought conditions revealed a close agreement with previous studies and local reports. Despite its drought vulnerability and major agriculture, little research has examined drought conditions and their characteristics in the MSEA region. Li et al. (2022b) investigated meteorological and agricultural drought conditions in the MSEA region using soil moisture time series from 2015 to 2020, and they reported that the most severe

drought year occurred in 2016. Wang et al. (2022) derived SPI-based drought information from gridded precipitation data, and they found that the MSEA region suffered from multiple severe drought events in 2005, 2010-2012, 2015-2016, and 2019. Another recent study collected severe drought years from the International Disaster Database revealed drought events frequently reported in 2000, 2005, 2010, 2016, and 2019 across the MSEA countries (Ha et al., 2022). Apart from regional drought studies, several studies have monitored and characterized national and local drought conditions over the past decades. In Vietnam, Le et al. (2019) used in-situ climate observations to derive the Palmer drought severity index (PDSI) from 1980 to 2014; their findings indicated the latest severe drought events in 2000, 2005, and 2010. Likewise, other studies used precipitation-based drought indicators and revealed severe and extreme drought events in agreement with the findings of this chapter (Le et al., 2020a; Stojanovic et al., 2020). In other countries, Khadka et al. (2021) used in-situ precipitation-based drought indicators and identified the most intense drought conditions in 2004-2005 and 2015-2016 in northeastern Thailand from 1979 to 2017. Recent local studies also reported drought severity occurred in 2000, 2004-2005, 2010, 2016, and 2019-2020 based on both satellite-based and station-based climate time series data (Khalil, 2020,?; Lee and Dang, 2019; Sein et al., 2021).

Drought can be attributed to several factors, such as human and natural activities. In the MSEA region, drought has been primarily associated with El Niño events. This large-scale oceanic and atmospheric phenomenon can disrupt normal weather patterns. Phan-Van et al. (2022) examined the driving factors of drought in Southeast Asia, and their findings indicated that El Niño–Southern Oscillation (ENSO) strongly influenced drought conditions in this region. In addition, drought is strongly associated with the tropical Atlantic Sea surface temperatures and Indian Ocean dipole (Skliris et al., 2022; Räsänen et al., 2016; Power et al., 2020). Other factors, such as wildfires, biomass burning, and climate change, exacerbated drought conditions in this region (Wanders and Wada, 2015; Wooster et al., 2012; Field et al., 2009). Regarding VCI-based drought conditions, land use/land cover change and deforestation also strongly influence them. These activities can alter the vegetative cover, either positive or negative. For example, shifting agriculture can remove forests, leading to lower NDVI values and, thus, lower VCI values. By contrast, government forest replantation programs or large-scale agricultural activities can increase greener vegetation cover (De Jong, 2010), resulting in higher VCI values. Lower (higher) VCI values can misrepresent drought stress conditions in these cases. While these effects can distort the interpretation of VCI at the local level, they are less likely to significantly impact assessments at a larger scale, where the influence of such localized changes is minimized.

The temporal evolution of VCI-based drought conditions generally agreed with the temporal precipitation-based drought patterns. For example, Wang et al. (2022) used a precipitation-based drought system and reported that the precipitation anomalies reached the lowest in 2005, followed by 2010 and 2019 across the MSEA region. Likewise, Phan-Van et al. (2022) indicated the intense severity of drought conditions in 2005 and 2010 and the moderate drought conditions in 2016. Most local studies also reported the lowest precipitation anomalies or drought index values in 2005, 2010, and 2019-2020 (Le et al., 2019; Palanisamy et al., 2021; Khadka et al., 2024). Notably, some studies in Vietnam used precipitation-based indices and reported severe droughts in recent years, such as in 2016 and 2020 (Le et al., 2020a; Stojanovic et al., 2020). However, the VCI-based drought conditions in Vietnam (Figure 4.20) indicated nearly non-drought conditions over the past ten years. This discrepancy can be attributed to different aspects of drought that each method captures. A lack of rainfall can indicate drought, but this deficiency may not always translate into vegetation stress. The VCI-based drought indices reflect the health and greenness of vegetation, capturing the actual impact of drought on plant life. If resilient vegetation or effective water management practices are in place, the VCI may not show significant stress despite reduced rainfall. In Vietnam, the extensive irrigation systems and the government's proactive forest replantation programs in recent years have likely contributed to maintaining healthy vegetation cover (Byrareddy et al., 2021), even during periods of lower precipitation. These factors help buffer the impact of reduced rainfall, ensuring that vegetation remains robust and potentially leading to discrepancies between precipitation-based drought assessments and those derived from vegetation indices.

The spatial distribution of detected VCI-based drought characteristics (Figures 4.23 and 4.24) revealed distinct drought patterns across the MSEA region. More drought events were detected in the Lower Vietnamese and Cambodian Mekong Deltas, Central Thailand, Myanmar, and the Red River Delta. These areas also witnessed higher drought duration and frequency over the past 21 years. The combination of geographic, human, and climatic factors may potentially influence the drought characteristics in the MSEA. Central Myanmar lies in the Central Dry Zone and becomes vulnerable to drought due to its lower precipitation rate. In this area, rainfed crops are widely practiced and highly sensitive to drought conditions (Herridge et al., 2019; Tun et al., 2015). A lack of rainfall over an extended period can cause crop failure. Lower precipitation rates are also observed in Thailand and Cambodia (Figure 2.2), where rainfed cropland accounts for a large part of the agricultural sector (Figure 2.3). The Lower Mekong Deltas in Vietnam and Cambodia rely heavily on consistent river flows and seasonal flooding for agricultural activities. However, these regions have undergone significant changes due to their upstream infrastructure and water diversion projects. Recent studies reported that such interventions reduced the downstream

water flows during the dry seasons (Pokhrel et al., 2018; Le Huy et al., 2022), exacerbating drought conditions in these deltas. While seasonal flooding is crucial for agriculture, it can also damage crops, leading to lower VCI values. This reduction in VCI values can misrepresent drought conditions and lead to the misidentification of drought events. Notably, the longest drought events have occurred recently in Cambodia, southern Laos, and parts of Thailand (Figure 4.23-b). In contrast, eastern Thailand, northern Vietnam, and the Lower Mekong Basin (e.g., Cambodia and Vietnam) experienced the longest drought events in 2004 and 2005. These observations are aligned with previous studies (Li et al., 2022b; Räsänen et al., 2016). In Cambodia, recent studies have identified the most significant drought events during the dry seasons in 2016 and 2019-2020 (Li et al., 2022b; Son and Thanh, 2022; Venkatappa et al., 2021). In addition, Cambodia has experienced one of the highest rates of forest loss worldwide in recent years (Hansen et al., 2013; Zeng et al., 2018; Xiao et al., 2023), largely driven by the expansion of agriculture. Similarly, Laos has experienced significant forest disturbance, primarily due to deforestation and shifting agriculture practices (Chen et al., 2023; Xiao et al., 2023). The severe drought events and extensive forest loss have contributed to lower VCI values, exacerbating the severity of drought conditions in these countries. Consequently, these countries suffered from declining VCI trends, indicating increased drought conditions. The declining trends of VCI-based drought conditions in Cambodia and Laos have been seen in regional and global studies (Yin et al., 2024; Xu et al., 2020; Pan et al., 2018).

4.4.2 Potential and drawbacks of satellite-based vegetation drought monitoring and characterization

Drought is a complex and reoccurring natural hazard that can significantly impact agriculture, the economy, water resources, and the environment. Timely and regular monitoring and characterization of drought conditions is crucial to developing effective drought adaptation strategies and planning. Among various drought monitoring methods, deriving drought information from vegetation-based indices has become widespread due to their ability to reflect drought-induced vegetation conditions. Although changes in vegetation can be due to several factors, such as human activities, diseases, or natural hazards, vegetation-based drought can provide critical insights into drought-induced vegetation stress. For example, the VCI is a satellite-derived vegetation index that evaluates the vegetation health by comparing current observations with long-term historical data. This robust approach assesses the natural variability in vegetation, making it less susceptible to short-term fluctuations caused by non-drought factors.

One of the primary benefits of satellite-based vegetation drought indices is their ability to provide consistent and frequent observations of land surface over large areas. The VCI has been widely used to monitor drought conditions (Bajgiran et al., 2008; Quiring and Ganesh, 2010; Liu and Kogan, 1996; Kogan, 1990), but little research has investigated the possibility of drought characterization from this dataset. This study has developed a method to identify the severe drought years and found a threshold to characterize drought conditions. The findings of severe drought years and characteristics in this analysis agreed well with previous studies using climate data, demonstrating the effectiveness of the VCI-based indices for monitoring and characterizing drought conditions. In the MSEA region, collecting in-situ climate measurements is often challenging, if not impossible. Also, each country in the region has its own data standards, formatting, and processing methods, making it difficult to integrate and harmonize in-situ data from multiple sources. Therefore, developing novel approaches that leverage satellite-based vegetation indices for monitoring and characterizing droughts would enhance drought mitigation efforts and water resources management. Despite its advantages, satellite-based vegetation drought monitoring has some major limitations. Vegetation indices can be influenced by factors other than drought, such as human activities (e.g., deforestation, agriculture) and plant diseases, leading to misinterpretation of the data. In the Lower Vietnamese Mekong Delta, frequent water in the rice fields or seasonal flooding could damage crops and potentially misrepresent drought conditions. Cleared fields following crop harvests may give a false impression of drought, as the absence of vegetation could be mistaken for drought-induced stress rather than the result of normal agricultural practices. Also, cloud cover and atmospheric conditions can interfere with satellite readings, reducing the accuracy of the indices. Another drawback is that vegetation indices may not detect drought conditions until they significantly affect vegetation, potentially delaying early intervention. In this study, the greatest challenge could be the selection of vegetation-based drought indices and gap-free dense time series. Therefore, we have carefully reconstructed the time series of vegetation indices to maintain continuous and consistent land surface observations, contributing to the good performance of drought mappings.

4.5 Summary

The MSEA region is a major agricultural producer but has been increasingly vulnerable to drought conditions. This is the first detailed analysis of spatial and temporal drought characteristics and trends over the MSEA region using the monthly MODIS-based VCI drought indices from 2000 to 2021. An automatic approach was developed to identify the severe drought years and their characteristics. Four key characteristics of drought conditions in the

region have been detected, while the trend was calculated during the dry and rainy seasons. Spatiotemporal distribution of VCI-based drought conditions has been investigated at different scales and across land cover types. The key findings of this study can be summarized as follows:

Drought conditions exhibited significant temporal and spatial variability across the MSEA region. The dry season experienced more frequent and intense drought than the rainy season, especially from January to April. Despite some common patterns, each vegetation type experienced drought differently. Rainfed crops and deciduous forests suffered the most from drought conditions.

Among the countries, Vietnam has been less affected by drought detected by the VCI in recent years, while Cambodia has faced more drought events. Rainfed crops in Laos suffered from the longest drought conditions between 2019 and 2020. Several severe drought years were identified over the study period, including 2000, 2004, 2005, 2010, 2016, 2019, and 2020.

Higher drought duration and frequency were primarily detected in Central Myanmar, Cambodia, eastern Thailand, and the Lower Mekong Delta. Central Myanmar witnessed the highest drought occurrence rate (around 60%), while other countries experienced nearly 40%, except for Laos. Thailand and Vietnam experienced nearly 15 prolonged drought events over the last two decades. In recent years, the longest drought events were primarily detected in Cambodia and Laos, whereas eastern Thailand and northern Vietnam experienced the most significant drought in the early 2000s.

Northern Vietnam showed a wetting trend during the dry season, while eastern Thailand exhibited this trend predominantly during the rainy season. For example, cropland in Vietnam witnessed a wetting trend over the study period. In contrast, Cambodian croplands saw a significant increase in drying conditions, indicating their vulnerability to intense drought.

A strong correlation between VCI-based drought indicators and climatic factors was observed, with the highest correlation between temperature and VCI occurring during the dry season.

Chapter 5

*Responses of vegetation-based drought to climate and soil moisture**

5.1 Input data

This chapter employed several publicly available geospatial datasets, including MODIS time series, ERA5-Land reanalysis, land cover product, digital elevation model (DEM), soil properties, and the World Database on Protected Areas (WDPA). These datasets are collected in different spatial and temporal resolutions and can be accessed via the Google Earth Engine (GEE) platform. Standard preprocessing steps have been applied to enhance the consistent spatial and temporal observations and convert them to the geographic coordinates system. Each dataset is described in the following subsections and listed in Table 5.1.

5.1.1 MODIS time series

The MODIS data is widely regarded as the benchmark product for global and regional monitoring and assessment of land surface dynamics, especially within the satellite-based vegetation and land surface temperature (LST) time series. Over the past two decades, their applications have expanded across various topics, reflecting their growing importance in environmental monitoring and assessment research. Figure 5.1 showed the annual growth of articles that used MODIS data from 2000 to 2023 collected from Scopus platform. This study employed two common MODIS products, namely NDVI and LST datasets.

The MODIS NDVI data offer global, long-term, and continuous observations of land vegetation and productivity at multiple spatial resolutions (e.g., 250 m, 500 m, and 1 km) from 2000 to the present (Román et al., 2024; Roy et al., 2006). This study made use of a

*This chapter is based in parts on Ha et al. (2024).

Table 5.1: A list of satellite and reanalysis datasets was used in vegetation-drought responses. The data period indicates the timeframe during which the data was generated or last updated.

Datasets/sensors	Variables	Temporal resolution	Spatial resolution	Data period
MODIS	NDVI and LST	16/8-day	1 km	2000 - present
ERA5-Land	Precipitation, soil moisture, air temperature, net radiation, wind, humidity	Hourly	$\sim$ 10 km	1950 - present
Open soil data	Carbon organic, clay, and sand contents	-	250 m	2018
ESA CCI land cover	Land cover/land use	Yearly	300 m	2000 - 2020
SRTM DEM	Digital elevation model	-	90 m	2000
World Database Protected Areas (WDPA)	Terrestrial protected areas	-	-	2023

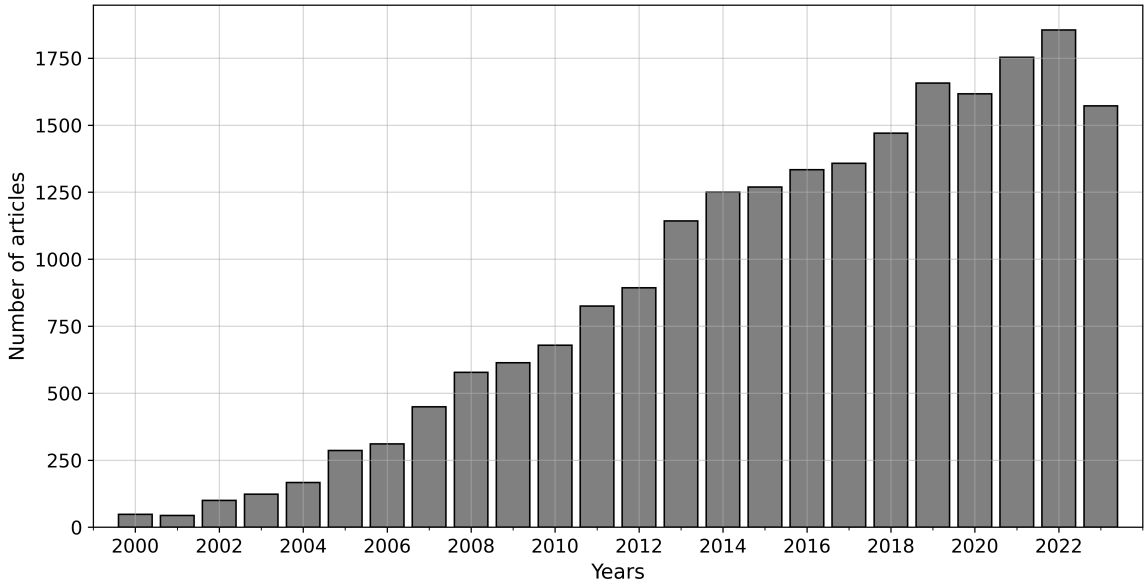

Figure 5.1: Annual number of studies using MODIS data from 2000 to 2023. Data were collected from Scopus database and keywords "MODIS" contains in the title, keywords, and abstract.

ready-analysis NDVI time series derived from Terra and Aqua sensors at 1 km spatial resolution. The NDVI values are calculated by the difference between the read and near-infrared light reflected by vegetation. Despite their daily observations, this study used a 16-day NDVI product (version 6.1) derived from geometrically and atmospherically corrected reflectance. The 16-day composites are generated from the best available observations within each 16-day window (Didan, 2021). This approach increased clear-sky measurements due to frequent clouds and shadows in the tropical region. If cloud-contaminated pixels were detected, an associated quality band (QA) was used to identify and remove cloudy pixels. After removing cloud-related pixels, a linear interpolation technique was applied to main-

tain the continuous presence of the NDVI data (Ha et al., 2023). Subsequently, the free-gap 16-day NDVI products were composited into monthly values using the median value composite (MVC) method. This study selected the MVC as it is robust to outliers to minimize the influence of abnormal data points. Despite the interpolation and monthly composites, the NDVI may still contain noise due to sensor limitations and atmospheric interference. The monthly NDVI values are then reconstructed to maintain the reliable curve of land vegetation growth using the Savitzky-Golay method (Ha et al., 2023). The final NDVI products covered the MSEA region from 2000 to 2022 and were converted to a geographic coordinate system.

LST data provides information about the earth's land surface temperatures. It is derived from the MODIS Terra and Aqua thermal infrared bands at 1 km spatial resolution. Although MODIS LST offers multiple versions, this study selected the latest MODIS LST 8-day 1 km resolution (version 6.1). This dataset is an analysis-ready product, corrected for atmospheric and geometric effects and surface emissivity (Wan et al., 2021b). Several global and regional studies have been conducted to cross-validate the MODIS LST data, and they found good agreements with the in-situ observations (Duan et al., 2019; Phan et al., 2019; Wan, 2008)). Due to the effects of clouds and shadows, this study employed the quality indicator band to mask out cloud-related pixels. Missing data were filled using linear interpolation based on the nearest clear-sky observations. Finally, monthly composites were generated in a geographic coordinate system at 1 km spatial resolution, spanning 2000 to 2022, using mean value composite.

5.1.2 Climate and soil data

Although several climatic and soil datasets are available, this study selected the ERA5-Land reanalysis product. This dataset is generated from the broader ERA5 reanalysis at 31 km spatial resolution by the European Centre for Medium-Range Weather Forecasts. The ERA5 integrates historical observations (e.g., in-situ and satellite data) with advanced numerical atmospheric-land simulation models to produce consistent and continuous measurements of global climate data (Muñoz-Sabater et al., 2021). The ERA5-Land is an enhanced version of ERA5 downscaled to a spatial resolution of 9 km. This study selected hourly ERA5-Land soil moisture and meteorological variables from 2000 to 2022. The climate variables included air temperature, precipitation, solar radiation, wind speed, and humidity. Several studies have demonstrated the usefulness of ERA5-Land in monitoring and assessing drought and climate conditions. Rahman et al. (2024) developed an integrated agricultural drought index using the ERA5-Land soil and meteorological variables, and their findings indicated that the index could effectively identify drought conditions in

Pakistan. Yilmaz (2023) cross-validated the ERA5-Land climate variables and found a high level of consistency with the station-based data. These applications and validation demonstrated the reliable accuracy of the ERA5-Land in monitoring and assessing climate and drought hazards.

5.1.3 Land cover product

This study employed ESA CCI land cover products from 2000 to 2020 at 300 m spatial resolution. This dataset offers an annual time series of global land cover maps using the advanced unsupervised and supervised machine learning algorithms (Li et al., 2018b). The main input data used to produce the ESA CCI land cover products are reflectance and vegetation indices derived from multiple satellites, primarily the MERIS (Medium Resolution Imaging Spectrometer) and the recent Sentinel-3 OLCI (Ocean and Land Colour Instrument) (Li et al., 2018b). These datasets are generated in epochs to ensure the stable and dynamic components of the global land cover surface (Bontemps et al., 2012). Each epoch represents five years (e.g., 1998-2002, 2003-2007, and 2008-2012). This approach ensures that every land cover pixel has multiple cross-verifications with several-year observations to minimize potential classification errors. The overall accuracy of the ESA CCI land cover products exceeded 75%, and the highest user accuracy values were reported in some specific land cover types, such as rainfed cropland, evergreen forests, and irrigated cropland (Bontemps et al., 2012). The original design of the ESA CCI land cover classification had 37 land cover types, but this chapter reclassified the original classification scheme into six land cover types: rainfed cropland, irrigated cropland, shrubland, mixed forest, evergreen forest, deciduous forest, and other types (e.g., water bodies, bare land, and built-up areas). Before the reclassification, this study selected only stable pixels, where land cover remained unchanged from 2000 to 2020. This approach ensured temporal consistency and enhanced the reliability of the analysis.

5.1.4 Auxiliary data

In support of this study, other geospatial datasets included elevation, protected areas, and soil property. The protected areas are sourced from the World Database on Protected Areas (WDPA), a dataset jointly generated by the UN Environment Program and the International Union for Conservation of Nature. This dataset contains a comprehensive and up-to-date source of information on global protected areas. In this chapter, the WDPA defined the protected areas where natural environments/ecosystems stayed undisturbed or less impacted by human activities. Although the WDPA contains different protected environments, such as national parks and marine protected areas, this study selected only terrestrial protected ar-

eas. There are 417 natural protected areas in the WDPA across the MSEA region at the time of writing this chapter. The protected areas within the MSEA region have varying shapes and sizes. The protected areas in Laos and Cambodia had the largest area, nearly 160 thousand and 115 thousand hectares, respectively. In contrast, Vietnam's protected areas had the smallest area, about 32 thousand hectares. The data for the protected areas are defined in the shapefile, and this vector data contains multi-part geometries with overlapping polygons. To simplify and avoid overlapping polygons, this study converted the multi-part geometries into single-part geometries and selected only polygons with at least 400 hectares (approximately 4 MODIS pixels).

Apart from the WDPA, this study collected Shuttle Radar Topography Mission (SRTM) elevation and soil properties. The SRTM elevation, generated at 90 m spatial resolution, provides detailed topographic information and covers nearly the entire global land surface (Berry et al., 2007). Topsoil properties, including clay, sand, and carbon organic contents, were also included to derive a soil-based drought indicator. These variables were generated from a collection of station-based soil properties using a robust ensemble random forest regression method and remote sensing data (Hengl, 2018). Despite their high spatial resolution, this study resampled all these datasets into 1 km spatial resolution to ensure consistency with the MODIS data.

5.2 Methodology

This section presents the workflow of method implementation to assess the response of vegetation to different drought indices during the dry season from 2000 to 2022 over the MSEA region. The responses of VCI-based drought to multi-temporal drought indices were explored in consideration of land cover types and elevation characteristics. The main steps included data pre-processing, derivation of vegetation condition and drought indices, and sensitivity analysis between vegetation-based drought and climate- and soil-based drought indices. Figure 5.2 displayed the overall framework of approach implementation.

5.2.1 Data preprocessing

This study prepared precipitation, soil moisture, and potential evapotranspiration (PET) time series data to derive climate-based drought indices. The ERA5-Land hourly data was first aggregated into daily observations. The PET data are essential for calculating the standardized precipitation evapotranspiration index (SPEI), but this product is unavailable in the ERA5-Land variables. This study used the FAO-56 Penman-Monteith method to estimate the PET from daily ERA5-Land variables, such as maximum temperature, mean

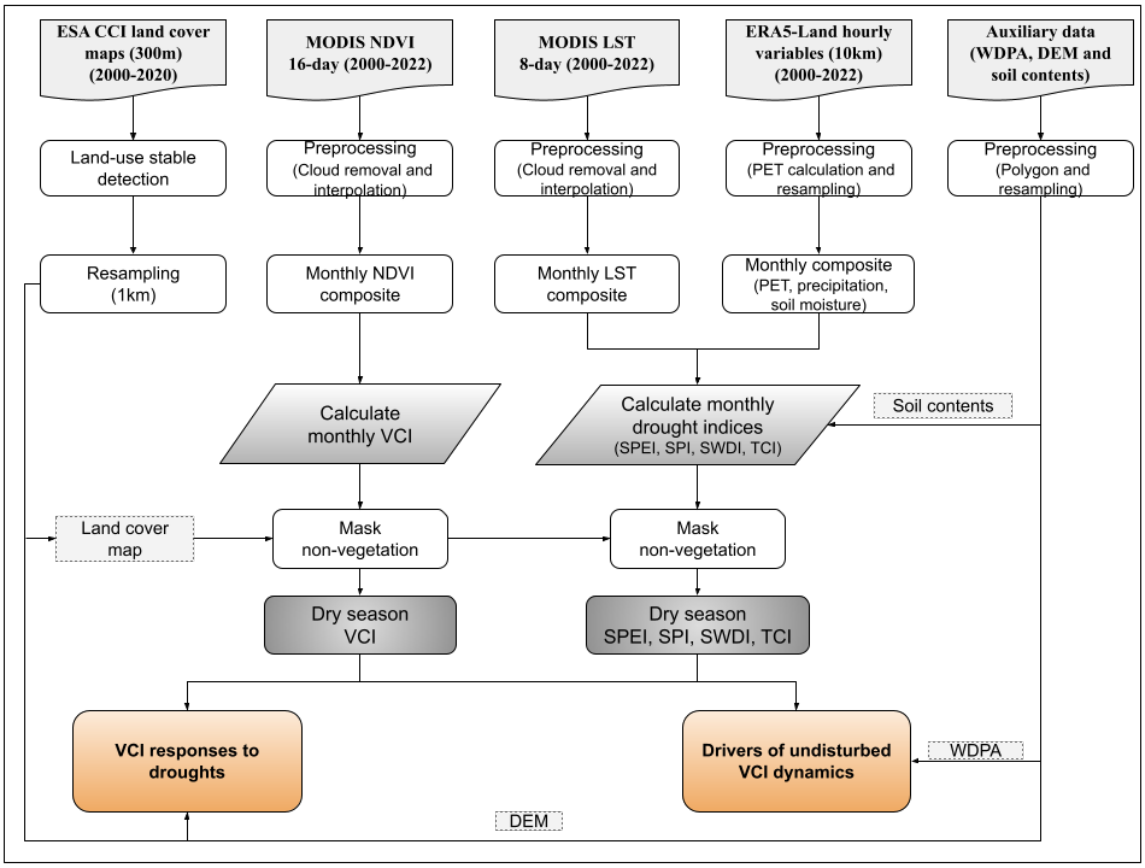

Figure 5.2: The overall framework of VCI-drought relationships over the MSEA region during the dry season from 2000 to 2022.

temperature, minimum temperature, relative humidity, wind speed, and solar radiation. The pyet Python package was used to estimate the PET, and its detailed documentation can be found in the study of Vremec et al. (2023). After deriving the PET time series data, we selected three ERA5-Land variables, namely PET, precipitation, and soil moisture, to aggregate them into a monthly time series from 2000 to 2022. The monthly data were resampled to a higher spatial resolution of 1 km to match the resolution of MODIS data.

5.2.2 Vegetation and drought indices

5.2.2.1 Vegetation condition index

The NDVI is among the most used indices for monitoring vegetation ecosystems and their sensitivity to climate and human activities (Fensholt et al., 2009; Li et al., 2013; Knauer et al., 2014). One of the major limitations of this indicator is that it mainly reflects vegetation greenness and may fail to detect subtle variations or signs of water stress, such as drought (Goward et al., 1991). Another limitation of the NDVI can be attributed to its seasonal and regional variability due to atmospheric and soil reflection effects. If the NDVI is transformed into the Vegetation Condition Index (VCI) by considering the long-term av-

erage and historical minimum and maximum values, the VCI can provide a more stable indicator of vegetation conditions (Kogan, 1990). The VCI is highly effective in detecting subtle changes in vegetation due to its strong sensitivity to both short- and long-term variations. The VCI normalizes the variations by comparing the current vegetation conditions to historical extremes, and this approach enables the detection of vegetation stress, a signal of drought conditions. Also, the VCI is presented as a percentage, with values ranging from 0% (indicating extremely poor vegetation) to 100% (representing healthy vegetation), making it easier to interpret (Kogan, 1995b; Liu and Kogan, 1996). The time-series VCI data is calculated per pixel using the following equation (Eq. 5):

$$VCI_i = 100 * \frac{NDVI_i - NDVI_{\min}}{NDVI_{\max} - NDVI_{\min}} \tag{5}$$

While $NDVI_i$ is monthly NDVI, $NDVI_{\max}$ and $NDVI_{\min}$ are the maximum and minimum NDVI values, respectively, calculated for each grid pixel across the monthly period (12 months) using the entire NDVI record (2000-2022).

5.2.2.2 Drought indices

Drought is among the most devastating natural disasters, manifesting in different forms and leading to different consequences (Ha et al., 2022; Venkatappa et al., 2021; Mishra and Singh, 2010). A wide range of drought indices has been developed to capture different drought conditions, such as meteorological, hydrological, and agricultural droughts. This section selected four key drought indices, namely the Standardized Precipitation Index (SPI), the Standardized Precipitation Evapotranspiration Index (SPEI), the Soil Water Deficit Index (SWDI), and the Temperature Condition Index (TCI). Each indicator represents short- and long-term drought conditions based on its selected temporal timescales (Mishra and Singh, 2010). For example, when the SPI and SPEI are calculated using the accumulation period of less than three months, it can be considered a meteorological drought (short-term drought). In contrast, longer timescales indicate hydrological drought, capturing more prolonged and persistent water deficits. On the other hand, the SWDI and TCI are widely used to detect short-term agricultural drought related to soil moisture and thermal temperatures. Drought indices in this section were calculated monthly from 2000 to 2022.

Among the drought indices, the SPI was probably the most widely used index for monitoring and assessing drought conditions, as proposed by McKee et al. (1993). This index is solely based on historical precipitation and can be calculated across multiple timescales to capture different types of drought conditions. The calculation process involved selecting a specific period and fitting a gamma distribution to the historical rainfall data (McKee et al.,

1993; Fang et al., 2019). The accumulative precipitation values are then transformed into a standard normal distribution with a mean of zero and a standard deviation of one. This study reviewed SPI literature and selected specific SPI timescales to assess their responses to vegetation-based drought. For example, short-term drought conditions can be effectively monitored by the SPI-1 (1 month) and SPI-3 (3 months), while median-term drought can be monitored by the SPI-6 (6 months) and SPI-9 (9 months). The longer-term drought can be detected by the SPI-12 (12 months). The SPI values typically range from negative to positive, whereas lower negative (positive) values indicate drier (wetter) conditions.

Despite its simplicity and widespread use, the SPI has certain limitations. It is solely based on historical rainfall data and does not account for other factors influencing droughts, such as temperature. To overcome this limitation, Vicente-Serrano et al. (2010) proposed an alternative drought index, the SPEI, which builds upon the SPI by integrating both historical precipitation and temperature data. This modification offers a more holistic approach to assessing drought conditions. Like the SPI, the SPEI can be calculated at multiple timescales, each representing different aspects of drought conditions. The calculation of SPEI involves determining the water balance (D) by calculating the difference between historical precipitation and the PET. As recommended by Vicente-Serrano et al. (2010), the water balance is calculated as the following equation (Eq. 6).

$$D_i = P_i - PET_i \tag{6}$$

Where D_i represents monthly water balance, and P_i and PET_i denote the precipitation and PET at month i, respectively. This study fitted a log-logistic probability distribution to the water balance data because it can handle both positive and negative values (Vicente-Serrano et al., 2010). Here the SPEI timescales are selected the same as observed in the SPI, representing different drought conditions.

In tropical and subtropical regions, thermal temperatures can significantly influence vegetation conditions. Higher temperatures can increase plant water demand and, in extreme cases, cause crop failure. This study considered the response of VCI-based drought to thermal temperatures. Here, the temperature condition index (TCI), a temperature-based drought index, is calculated from the LST time series (Kogan, 1995a). The MODIS LST data from 2000 to 2022 are linearly transformed into TCI and expressed in the following equation (Eq. 7).

$$TCI_i = 100 * \frac{LST_{\max} - LST_i}{LST_{\max} - LST_{\min}} \tag{7}$$

Where TCI and LST are the temperature condition index and land surface temperature at i^{th} month, respectively. The $LST_{\max}$ and $LST_{\min}$ are the maximum and minimum temperature values observed in a specific month (from January to December) during the selected study period (2000–2022). Higher TCI values indicate wetter conditions, whereas lower values denote drier conditions.

While the SPI, SPEI, and TCI offer essential insights into meteorological and hydrological aspects of drought, they may not directly reflect soil moisture agriculture. Recently, Mishra et al. (2017) has developed the SWDI using soil moisture time series data. Several studies have demonstrated the reliability of this index to monitor and characterize agricultural drought conditions. For example, Fang et al. (2021) used the SWDI based on a downscaled 1 km Soil Moisture Active Passive (SMAP) data from 2015 to 2019 to monitor drought conditions in Australia. Their findings indicated that the SMAP-based SWDI provided reliable accuracy with the in-situ drought observations. This study calculated the SWDI based on topsoil moisture and soil water properties using the following equation (Eq. 8).

$$SWDI_i = \frac{(\Theta - \Theta_{\text{FC}})}{\Theta_{\text{AFC}}} \tag{8}$$

Where Θ, Θ_{FC}, and Θ_{AFC} are soi moisture estimates, soil moisture at field capacity, and available water capacity, respectively. The Θ_{AFC} can be estimated from the soil moisture at field capacity Θ_{FC} and wilting point Θ_{WP} in the following equation (Eq. 9).

$$\Theta_{\text{AFC}} = \Theta_{\text{FC}} - \Theta_{\text{WP}} \tag{9}$$

The higher positive SWDI values indicate wetter conditions, while its negative values represent drought conditions. It is found that there has been a strong relationship between soil moisture (at field capacity and wilting point) and soil physical characteristics (e.g., clay, sand, and organic matter contents). This relationship can be expressed using the pedo-transfer functions (PTFs). Following the recommendation from previous studies (Fang et al., 2021; Mishra et al., 2017), this study used the modified PTFs version and expressed in the following equations (Eq. 10) and (Eq. 11).

$$\Theta_{WP} = \Theta'_{WP} + (\Theta'_{WP} * 0.14 - 0.02)$$
$$\Theta'_{WP} = 0.006 * OM + 0.487 * C - 0.024 * S + 0.005(S * OM) - 0.013 * (C * OM) + 0.068(S * C) + 0.031 \quad (10)$$

$$\Theta_{FC} = \Theta'_{FC} + (1.283(\Theta'_{FC})^2 - 0.374\Theta'_{FC} - 0.015)$$
$$\Theta'_{FC} = 0.011 * OM + 0.195 * C - 0.251 * S + 0.006(S * OM) - 0.027(C * OM) + 0.452(S * C) + 0.299 \quad (11)$$

While S, C, and OM represent the sand, carbon, and organic matter contents in percentage, Θ'_{FC} and Θ'_{WP} indicates the first solutions of Θ_{FC} and Θ_{WP}.

5.2.3 Analysis of vegetation-drought responses

5.2.3.1 Response of vegetation drought to climate and soil indices

The previous chapter primarily identified drought conditions during the dry seasons because the rainy season received higher precipitation and suffered from little drought. Hence, this chapter focused on the response of vegetation-based drought to climate-soil-based drought conditions from 2000 to 2022 during the dry season. The response of vegetation-based drought to climate and soil variables was explored using Spearman's rank statistical correlation analysis. This method was chosen due to its robustness in handling non-linear relationships and non-normally distributed data (Bisquert et al., 2017; Cao et al., 2022). The Spearman analysis evaluates the direction and strength of the monotonic relationships between the two variables (Tran et al., 2023), indicating how consistently one variable increases or decreases as the other changes. In this study, Spearman's correlation coefficients were identified per pixel at $p \leq 0.05$ significance level. Higher coefficients indicate a stronger relationship between the two variables. In this case, higher coefficients suggest that vegetation-based drought and climate-soil-based drought indices were closely related.

Before the calculation of the correlation, each drought indicator was converted into anomalies to mitigate the risk of spurious correlations (Udelhoven et al., 2009). For the multi-temporal drought indices such as SPI and SPEI, this study identified the maximum correlation coefficients across the selected timescales. By selecting the largest correlation coefficients, the study aimed to capture the most relevant timescale at which vegetation condition (VCI) is affected by drought. These maximum coefficients highlight the temporal

lag between precipitation deficits and vegetation response, as well as the degree to which VCI-based drought indicators are related to both climatic and soil moisture-driven drought conditions.

5.2.3.2 Drivers of vegetation drought in undisturbed environments

Natural and undisturbed environments play a key role in understanding how ecosystems respond to drought conditions. This study aimed to estimate the relative contributions of each drought index to the VCI variability during the dry season from 2000 to 2022. Our analysis selected protected areas where human activities are either absent or neglectable. Here, the protected areas primarily cover forest areas across the MSEA region.

While numerous studies have highlighted the influence of precipitation on vegetation variability (Fang et al., 2005; Guo et al., 2021; Zhang et al., 2013), raw climate data presents certain limitations. For example, precipitation may not provide short- and long-term information on drought conditions and fail to capture drought impacts on ecosystems. In contrast, drought indices offer more insights into multi-temporal drought information, such as meteorological and hydrological droughts. For instance, the SPEI is calculated at multiple timescales, and therefore, it can provide different aspects of drought conditions. Drought indices offer a more integrated assessment of drought impacts on vegetation ecosystems, as they consolidate several climatic factors into a single metric. In the case of the SPEI, this integration includes both temperature and precipitation, providing a more comprehensive tool for evaluating ecosystem responses to drought. This study employed all selected drought indices (SPI-1, SPI-3, SPI-6, SPI-9, SPI-12, SPEI-1, SPEI-3, SPEI-6, SPEI-9, SPEI-12, SWDI, TCI) for assessing the relative contributions of drought indices on VCI-based drought in natural and undisturbed protected areas.

Each drought type and indicator may have different levels of impact on vegetation-based drought. This study identified the relative contribution of climate and soil drought indices to vegetation-based drought using the explainable machine learning algorithm. We selected the Random Forest (RF) regression combined with the SHapley Additive exPlanations (SHAP) method to determine the overall and individual contributions of climate- and soil-based drought indices. The RF is a non-parametric ensemble learning regression that proved robust to non-linear patterns, outliers, and autocorrelation in time series data (Breiman, 2001; Gessner et al., 2015). Despite its outperformance, RF regression lacks the capability to estimate the individual contributions of specific observation data. This means that the RF can offer relative contributions, but it is difficult to determine the magnitude and direction of specific variables and data points. To address this issue, SHAP, a cooperative game theory, offers a more robust and interpretable method of feature contribution analysis.

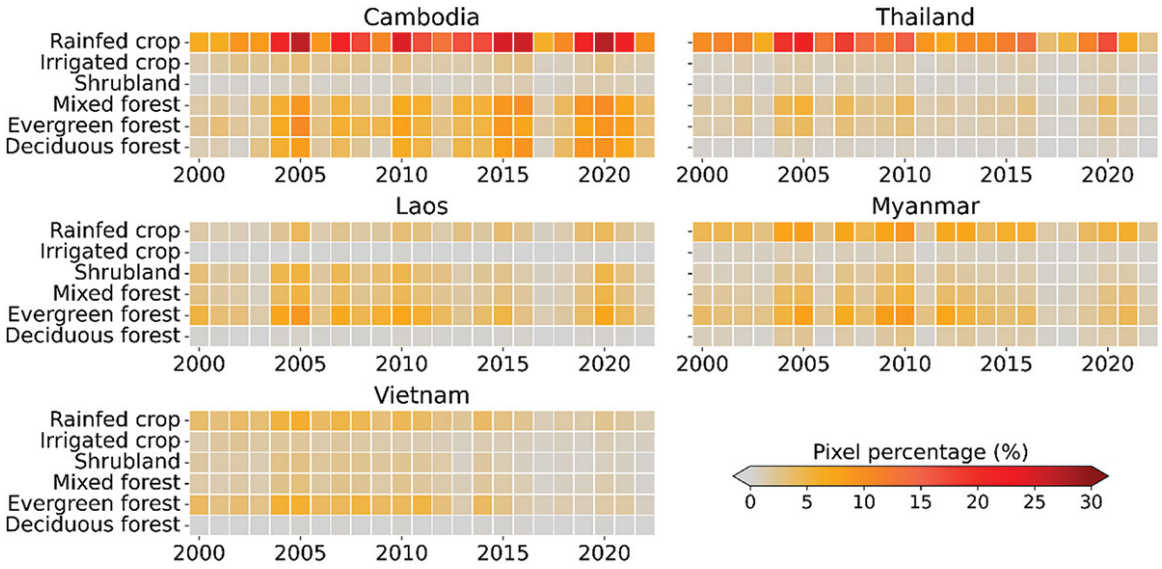

Figure 5.3: Temporal variability of VCI-based drought areas across land cover types and countries from 2000 to 2022.

The SHAP method computes Shapley values for each feature, reflecting their marginal contributions to individual predictions (Scott et al., 2017). The combination of RF regression and SHAP enhances model interpretability better to understand the influence of drought indices on VCI variability. This study trained the RF regression using time series drought indices to estimate the VCI variability during the dry season with 500 decision trees. Subsequently, the SHAP method was applied to the trained model, and the detailed contributions of drought indices were estimated. The SHAP values can be negative and positive, indicating directional impacts on the target variable.

5.3 Results

5.3.1 Vegetation drought by land cover types and elevations

Figure 5.3 showed the temporal evolution of VCI-based drought-affected areas across different land cover types in five MSEA countries from 2000 to 2022. Overall, the proportion of drought-affected areas in each country varied across land cover types and years. Rainfed cropland witnessed higher proportions of drought-affected areas across the countries.

The analysis revealed that rainfed cropland in Thailand and Cambodia has consistently experienced higher proportions of drought-affected areas (Figure 5.3). In Cambodia, drought conditions were especially severe. For example, nearly 35% of rainfed crops were impacted by drought in 2005 (Figure 5.3). Thailand also experienced significant droughts in its rainfed cropland, with approximately 25% affected in 2005 and 17% in 2020. In contrast,

rainfed cropland in Vietnam, Myanmar, and Laos displayed much lower drought-affected areas. For instance, Vietnam's rainfed cropland suffered from less than 5% of drought-affected areas across the studied years. Other countries had less than 10% of stressed rainfed crops due to drought. These findings were aligned with recent studies. Venkatappa et al. (2021) examined the drought impacts on cropland across the MSEA region, and they reported that Cambodia had the largest proportion of damaged rainfed cropland ($\sim$ 40%). Thailand was ranked second with nearly 30% of damaged rainfed cropland from 1980 to 2019, but Vietnam had less than 10% of damaged rainfed cropland during the same period (Venkatappa et al., 2021). These discrepancies in drought-affected areas across the MSEA countries can be attributed to a combination of climatic factors, resource availability, and farming practices. For instance, variations in precipitation and temperature significantly influence drought susceptibility in rainfed croplands. Vietnam typically receives higher precipitation and has lower temperatures during the dry seasons compared to Thailand and Cambodia. These favorable climatic conditions likely help mitigate the extent and severity of drought in Vietnam's rainfed croplands. In addition, Vietnam has substantially expanded its irrigation infrastructure into rainfed croplands over the past decade. However, the ESA CCI land cover product may not accurately detect rainfed croplands in Vietnam. For example, Kuenzer et al. (2018) assessed the accuracy of multiple global land cover products, and they reported that there has been a lack of agreement among the land cover products. As shown in the ESA CCI land cover product in Figure 2.3 (Chapter 2), nearly all croplands in the upper areas were defined as rainfed crops, while irrigated crops were primarily observed in rice-growing areas. These misclassification errors can influence the rainfed drought-affected areas.

Among the remaining vegetation types, evergreen and mixed forests suffered from larger proportions of drought-affected areas (Figure 5.3). In Cambodia, all forest types have frequently witnessed the largest proportions of drought-affected areas. For example, the largest proportion of drought-affected areas (10-15%) in Cambodian forests was primarily observed in 2005, 2010, 2016, and 2020. In other countries, evergreen forests had a higher proportion of drought-affected areas. Notably, Thailand and Vietnam had the lowest proportion of forest drought-affected areas in recent years. In Vietnam, the proportion of forest drought-affected areas has been less than 3% over the past seven years. Recent studies reported that Cambodian forests experienced declining trends due to forest disturbance, such as deforestation and drought (Hansen et al., 2013; Grogan et al., 2015). Likewise, Myanmar and Laos suffered from forest disturbance due to drought and shifting agriculture (Chen et al., 2023). It is also noted that deciduous forests had a lower proportion of drought-affected areas. This could be due to the forest's resilience and limited area proportion. In the MSEA region, deciduous forests accounted for the smallest proportion of forest types.

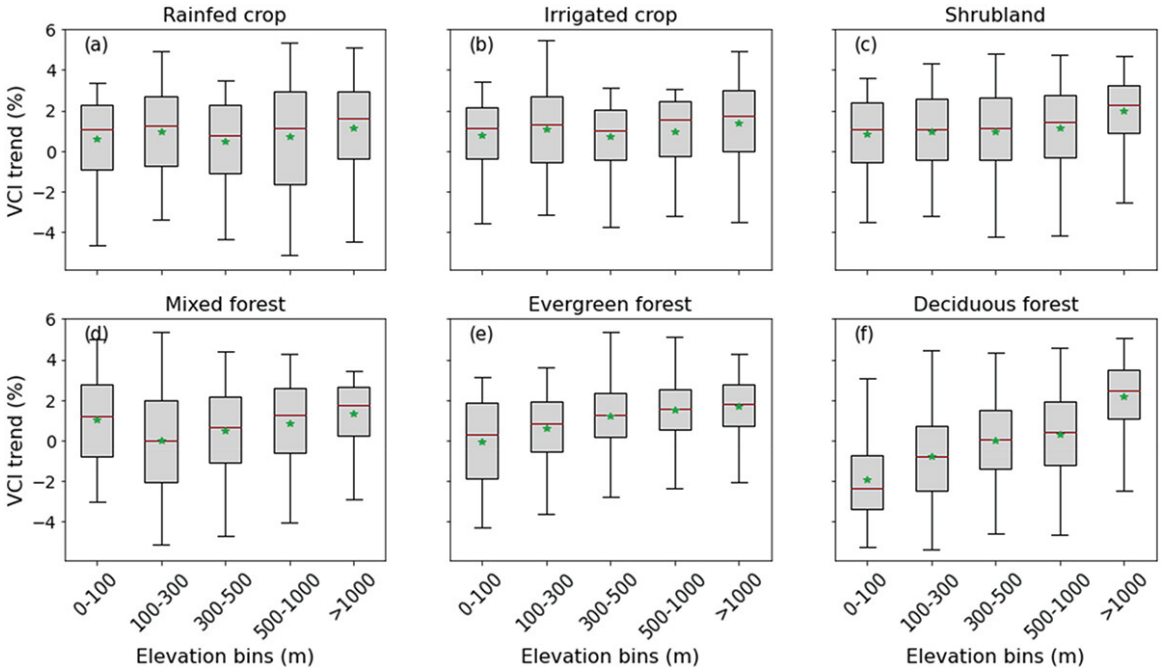

Figure 5.4: The trends of VCI-based condition across land cover and elevation characteristics in the MSEA region.

As shown in Figure 2.3 (Chapter 2), Cambodia and Myanmar had the largest area of deciduous forests, accounting for nearly 15% and 7%, respectively. Other remaining countries had less than 2% of deciduous forests.

Apart from the drought-affected areas, this analysis also investigated the VCI-based drought conditions across the elevation characteristics. Figure 5.4 displayed the VCI trends across land cover types and elevation zones. Overall, higher VCI trends were observed in higher elevation zones. Despite the positive trends, VCI trends for rainfed and irrigated crops stayed relatively stable across elevation zones. For example, the VCI of rainfed and irrigated crop trends experienced about 1.5% yearly. Similarly, shrubland witnessed positive VCI trends; the highest trend was above 1000 m elevation. Regardless of forest types, the VCI witnessed an increasing trend in higher elevations. The VCI trend of evergreen forests increased from 0.3% in 100 m to nearly 2% above 1000 m elevation. Notably, deciduous forests witnessed the largest increase in the VCI trends, from -2% (in 100 m) to approximately 2% (above 1000 m), respectively (Figure 5.4). The observed increasing VCI trends at higher elevations likely reflect the lower temperatures and higher moisture availability in these areas, and such conditions can facilitate vegetation growth during dry periods. At higher altitudes, forests can benefit from reduced evapotranspiration rates and enhanced water retention in the soil, enabling vegetation to maintain healthier conditions even in fluctuating environmental conditions. Cislaghi et al. (2019) examined the soil nutrients across elevation characteristics, and they reported that higher elevations are less vulnerable to soil erosion and land use intensity. These trends suggest that higher-elevation ecosystems

are becoming more resilient to drought stressors. Despite the largest trend, the deciduous forests experienced a negative trend across elevation zones, except for areas above 1000 m. Further analysis indicated that nearly 85% of deciduous forests in Cambodia below 100 m zone, experienced declining trends. In contrast, deciduous forests at higher elevations, above 500 m, were predominantly found in Myanmar ($\sim$ 73%) and Thailand ($\sim$ 17%) with positive trends. These trends align with the spatial distribution of the VCI trends, as shown in Figure 3.10 (Chapter 3). In lower elevations, forests may experience more human and natural disturbances, such as shifting agriculture, urbanization, and higher sensitivity to climatic stressors (e.g., extreme heat and drought). Recent studies also reported that tropical deciduous forests had a greater vulnerability to disturbances at lower elevations (Zoungrana et al., 2018; Jeganathan et al., 2014). Vegetation in these areas may be more susceptible to water deficits and higher temperatures, leading to poorer vegetation health than higher elevations. These results highlight the importance of considering both land cover and elevation when assessing vegetation resilience and drought impacts.

5.3.2 Spatial variability of climate and soil drought indices

In the MSEA region, there has been considerable variability in the extent and severity of drought across different drought indices from 2000 to 2022. Overall, climate-based drought indices provide clearer insights into temporal drought conditions, offering a more detailed understanding of drought fluctuations over time. In contrast, soil-based drought indices show similar patterns throughout the study period, indicating a more consistent response to drought across the region. Figure 5.5 showed the spatial and temporal patterns of drought conditions using the SPI-3 during the dry season from 2000 to 2022. It is noted that the most severe drought conditions were observed across multiple years due to precipitation deficits, such as in 2005, 2010, and 2020. For example, the SPI-3-based drought indicator revealed that nearly 85% of the study region suffered from drought. As shown in Figure 5.5, the Lower Mekong Basin experienced the most severe drought conditions in 2005. This area also frequently suffered from drought due to lack of precipitation. Notably, drought events in 2010 occurred mainly in Central and southern Myanmar. The recent drought event in 2020 covered a large extent, accounting for nearly 75% of the study area. Notably, the dry seasons in 2007 and 2013 also experienced severe drought conditions, and these patterns were primarily detected in Central Myanmar and northern Thailand. In comparison, the MSEA region experienced wetting conditions across multiple years, indicating the precipitation above the long-term average. For example, most of the countries in the region witnessed wetting conditions in 2022 (Figure 5.5).

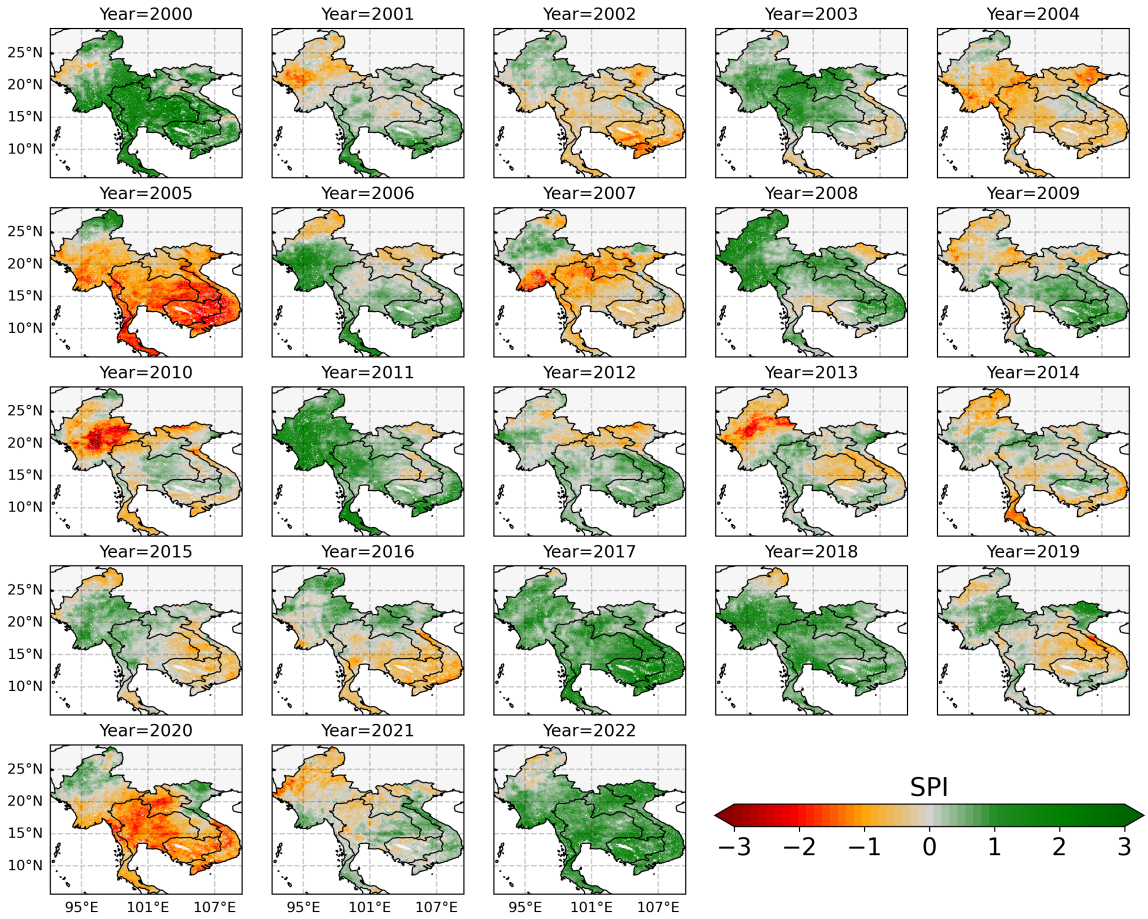

Figure 5.5: Spatial variability of short-term drought conditions based on the SPI-3 during the dry season from 2000 to 2022 over the MSEA region. Lower values (dark red) indicate drier conditions, while higher values (dark green) represent wetter conditions.

Figure 5.6 indicated the spatiotemporal dynamics of drought conditions using the SPEI-3 index from 2000 to 2022. Despite the similar spatial patterns observed with SPI-3, the study region experienced less severe drought overall (Figure 5.6). It is observed that drought conditions from SPEI-3 were closely aligned with the SPI-3 during both dry and wet years from 2000 to 2022. Slight disparities in the drought severity levels between the two indices can be attributed to the calculation method and input data. While the SPI is based solely on precipitation, the SPEI is calculated using precipitation and PET data. The lower SPEI-3 values suggest that while rainfall deficits (as measured by SPI-3) are similar, evapotranspiration may have mitigated the drought severity (Laimighofer and Laaha, 2022). This could indicate that lower temperatures or higher humidity levels could lead to reduced atmospheric water demand, thus reducing the impact of precipitation shortfalls. In some regions, the SPEI demonstrated its robustness in capturing drought conditions (Berhail and Katipoğlu, 2023; Vicente-Serrano et al., 2010), reflecting the balance between moisture inputs (precipitation) and losses (evapotranspiration).

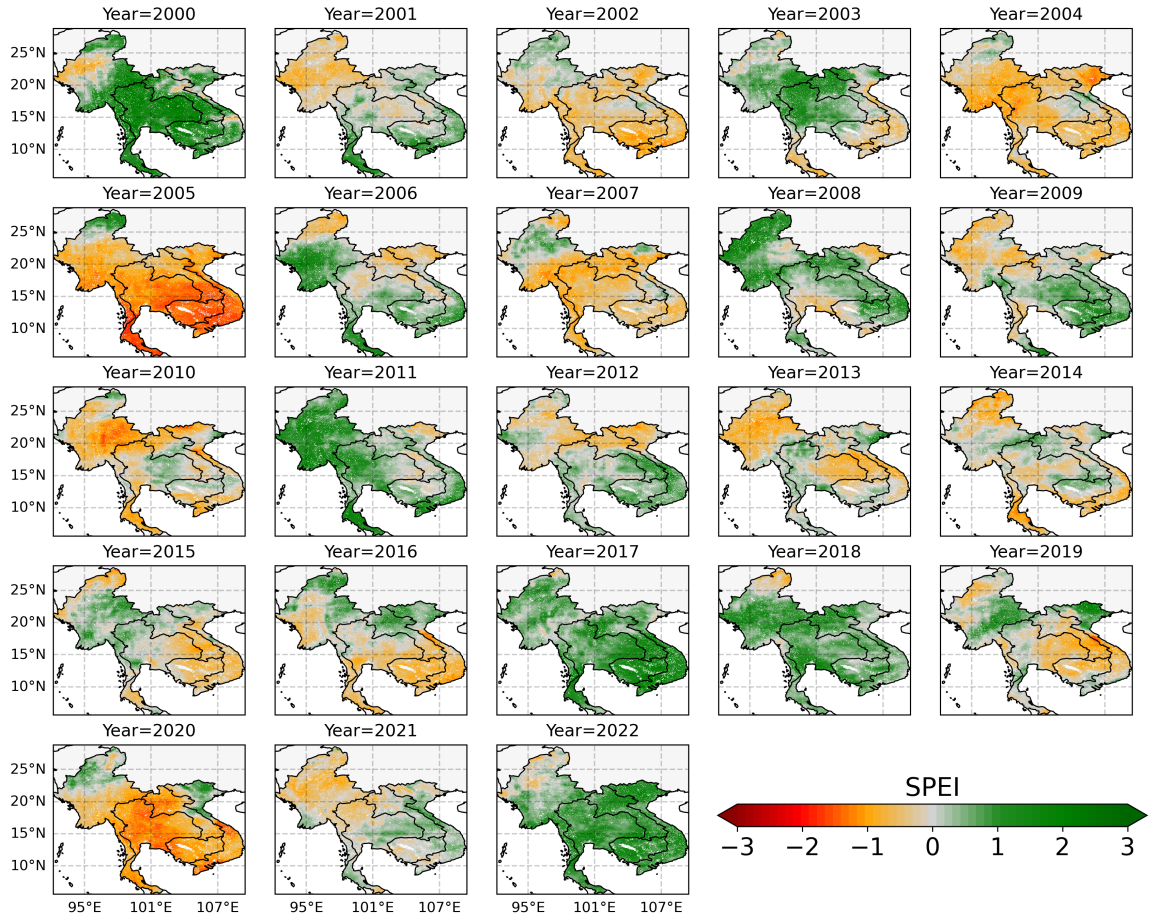

Figure 5.6: Spatial variability of short-term drought conditions based on the SPEI-3 during the dry season from 2000 to 2022 over the MSEA region. Lower values (dark red) indicate drier conditions, while higher values (dark green) represent wetter conditions.

Apart from the SPEI-3 and SPI-3 drought indices, Figure 5.7 presented the spatiotemporal patterns of temperature-based drought from 2000 to 2022. Generally, lower SPEI-3 and SPI-3 values correspond to lower TCI values, indicating drought conditions. Despite the severe drought conditions of the SPEI-3 and SPI-3 in 2005, the TCI this year revealed less intense drought conditions than in other years. The lowest TCI values (extreme droughts) were dominantly observed in 2010, 2013, 2016, 2019, and 2020. Although the SPEI-3 and SPI-3 revealed moderate drought conditions in 2013 and 2016, the study region experienced significantly low TCI values during these years, indicating extreme drought conditions. The year 2019 probably witnessed the hottest dry season, this pattern was largely observed in the Lower Mekong Delta, except for Myanmar. Lower TCI values in 2020 mainly occurred in Thailand and Laos, and other countries experienced less extreme heat. Interestingly, SPEI-3 and SPI-3 revealed relatively wet conditions in 2017, but the TCI revealed moderate drought by TCI. Lower TCI values suggest that even though the region experienced favorable precipitation, surface temperatures were elevated.

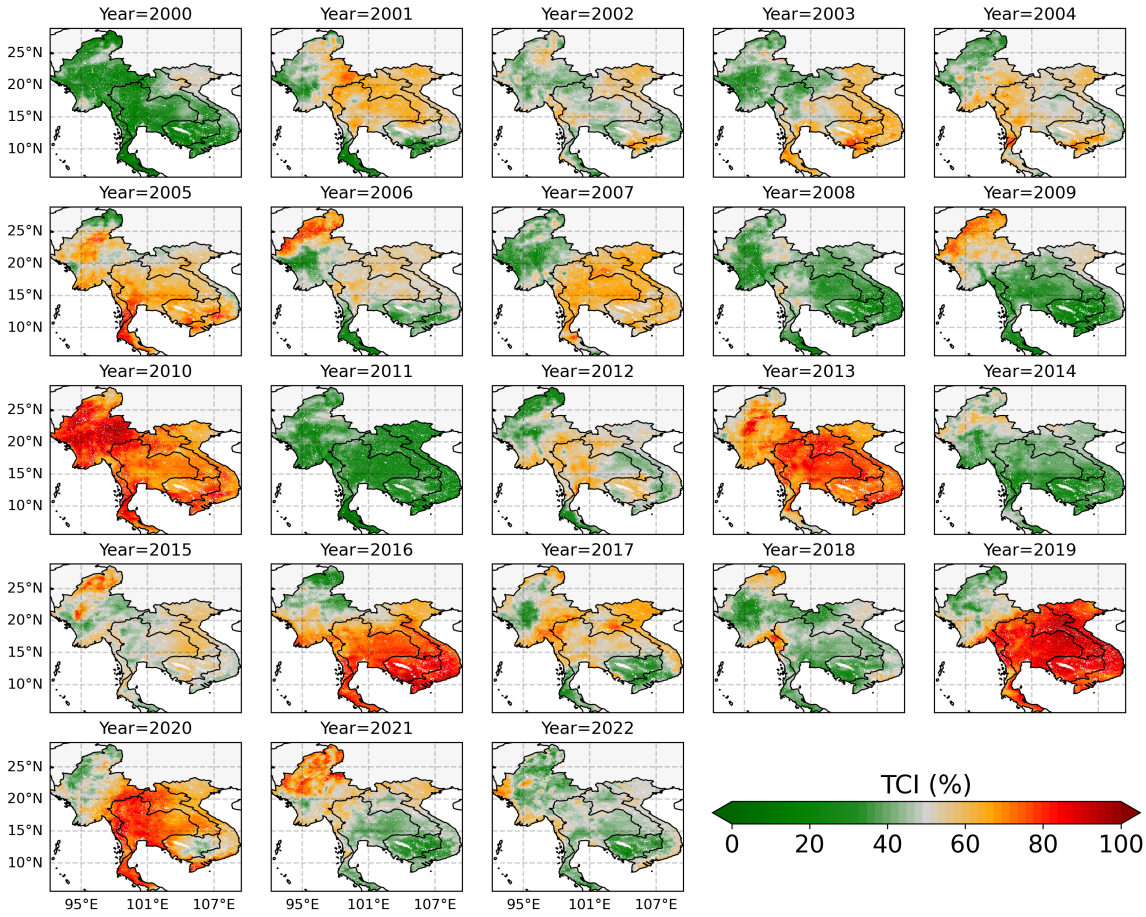

Figure 5.7: Spatial variability of short-term drought conditions based on the TCI during the dry season from 2000 to 2022 over the MSEA region. Lower values (dark green) indicate wetter conditions, while higher values (dark red) represent drier conditions.

In contrast to other drought indices, the SWDI revealed similar spatial patterns across the dry seasons from 2000 to 2022. Figure 5.8 illustrated the spatiotemporal variability of SWDI-based drought conditions. Clearly, lower SWDI values were primarily detected in the Lower Vietnamese Mekong Delta, southern Thailand, and southern Myanmar. Despite their spatial variability, the SWDI values maintained relatively similar temporal patterns across the study period (Figure 5.8). More severe soil moisture drought conditions were observed in 2004-2005, 2007, 2010, and 2020. Some specific areas witnessed soil moisture drought conditions across the study period. In the MSEA region, there have been no drought studies using the SWDI. However, a recent study reported that the SWDI usually agreed well with the SPEI and SPI (Guo et al., 2018b).

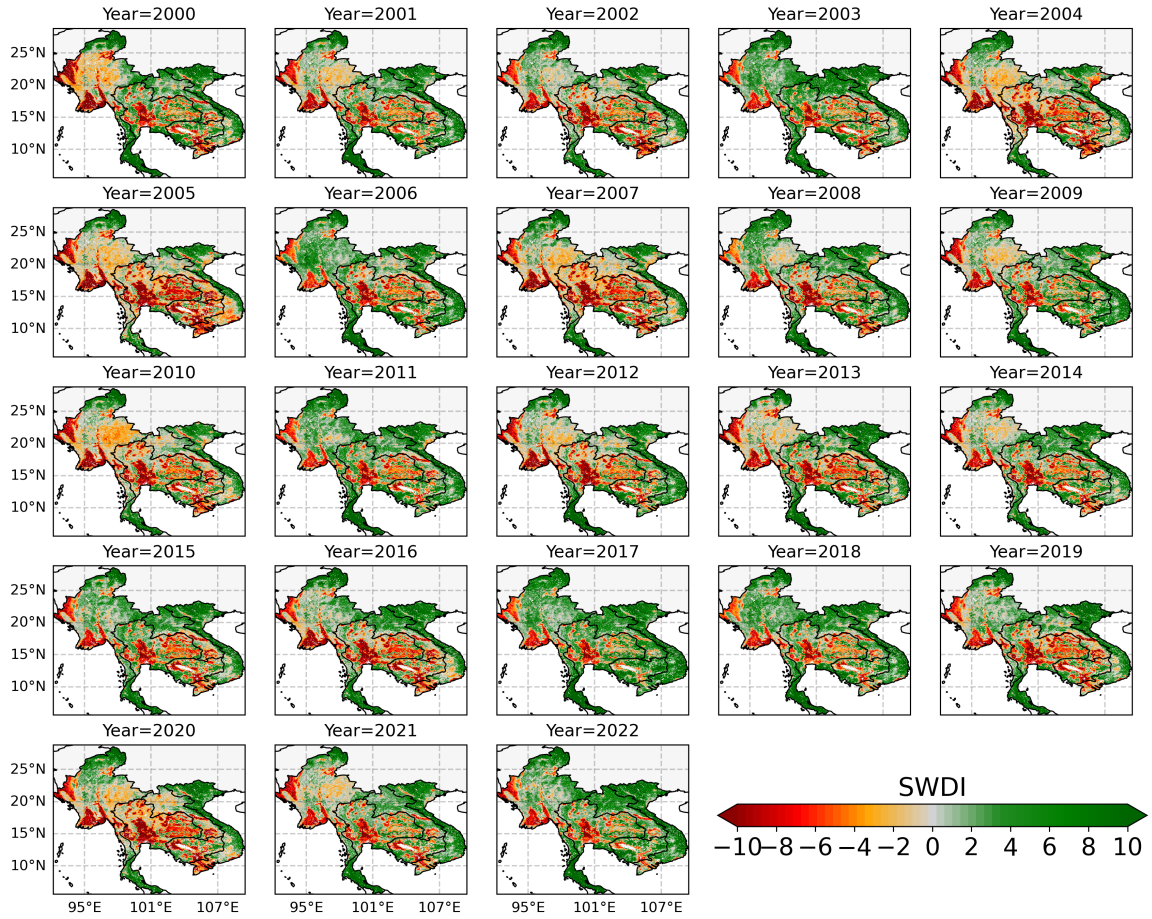

Figure 5.8: Spatial variability of short-term drought conditions based on the SWDI during the dry season from 2000 to 2022 over the MSEA region. Lower values (dark red) indicate drier conditions, while higher values (dark green) represent wetter conditions.

5.3.3 Responses of vegetation to drought indices

5.3.3.1 Spatial patterns of vegetation-drought responses

The VCI is a useful indicator for assessing drought and vegetation conditions. Thus, this section focused on the spatial distribution of VCI-drought relationships over the past two decades in the MSEA region. This study calculated per-pixel Spearman correlation coefficients between the VCI-SPEI and VCI-SPI at multiple time scales. In the case of multi-timescale SPEI and SPI indices, only maximum coefficients were presented in Figure 5.9. Generally, short-term drought indices (e.g., SPI-1, SPI-3, and SPI-6) had stronger relationships with the VCI. In the first three timescales, SPEI and SPI accounted for nearly 90% of the maximum coefficients. Notably, nearly 40% of the study area had the highest correlation coefficients between the SPI-3 and VCI. Likewise, this figure was similar for the SPEI-3. Long-term drought indices (SPI-9/SPEI-9 and SPI-12/SPEI-12) witnessed weaker relationships with the VCI, indicating a neglectable influence on vegetation. The TCI generally experienced the largest relationships with the VCI during the dry season among the climate

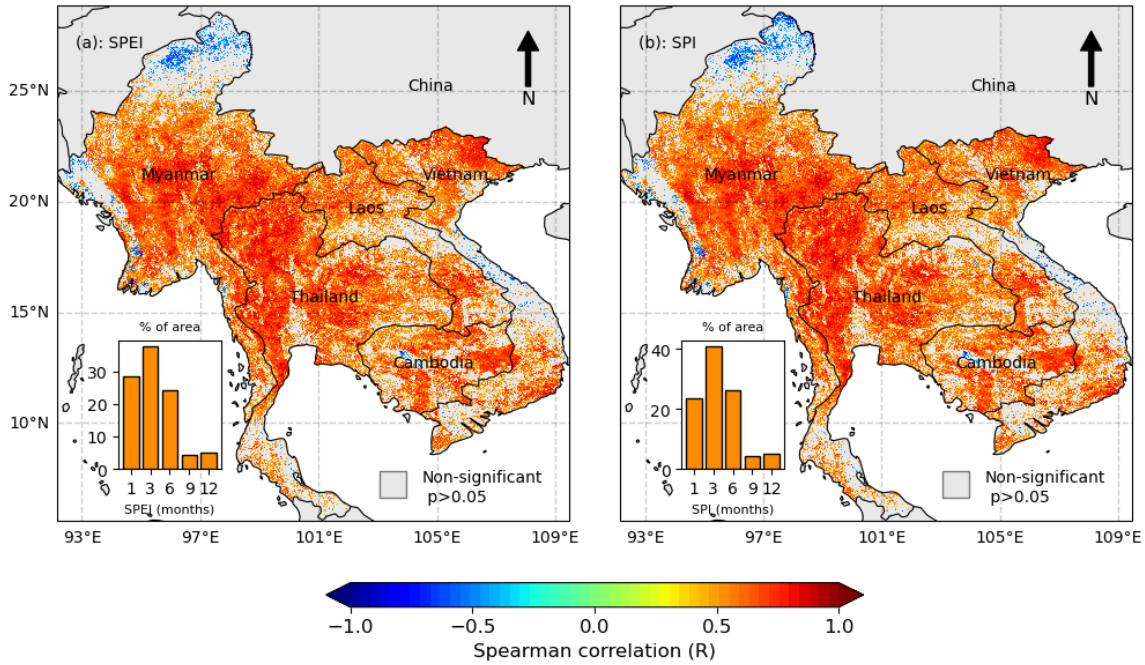

Figure 5.9: Spatial responses of VCI-SPEI (a) and VCI-SPI (b) across the MSEA region during the dry season from 2000 to 2022. The inset plot represents the percentage of maximum coefficients across selected timescales (1, 3, 6, 9, and 12 months). The dark blue represents negative coefficients, while the dark red indicates positive correlations at $p \leq 0.05$. The gray area indicated non-significant pixels or no data available.

and soil-based drought indices. The VCI responses to both SPEI and SPI exhibited similar spatial patterns regarding correlation coefficients (Figure 5.9). Negative correlation values were predominantly concentrated in high mountains in northern Myanmar, while the central coast of Vietnam and parts of central Laos showed non-statistically significant correlations. In contrast, other regions displayed strong positive correlation coefficients, indicating a robust relationship between VCI and the SPEI/SPI in those areas. Statistically, nearly 66% of the study area witnessed positively significant coefficients between the VCI and SPEI/SPI, while the proportion of non-significant coefficients accounted for about 32%. It is observed that northern Thailand and southern Myanmar witnessed the strongest positive correlations between the VCI and SPEI/SPI during the dry seasons, indicating the stronger sensitivity of the VCI to precipitation-based drought in these areas. On average, Thailand had the strongest VCI-SPEI responses, with R-value = 0.64, while Myanmar witnessed the smallest R-value = 0.54. The VCI-SPEI/SPI responses in other countries ranged from 0.54 to 0.59.

Apart from precipitation-based drought indices, the VCI also experienced strong responses to the soil and temperatures. Figure 5.10 showed the spatial responses between the VCI and SWDI/TCI during the dry seasons. Despite stronger overall responses, the VCI-TCI/SWDI data exhibited similar spatial patterns. For instance, approximately 56% of the study area showed positive correlations between the VCI and SWDI, with R-values

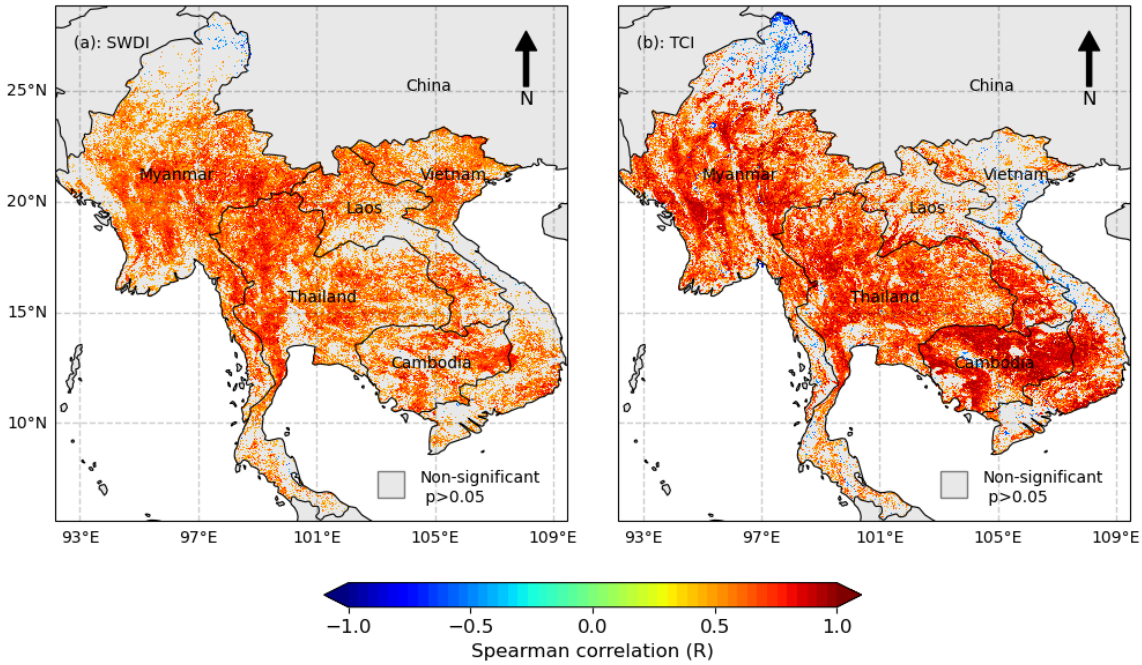

Figure 5.10: Spatial responses of VCI-SWDI (a) and VCI-TCI (b) across the MSEA region during the dry season from 2000 to 2022. The dark blue represents negative coefficients, while the dark red indicates positive correlations at $p \leq 0.05$.

around 0.6. Notably, large regions along the central coast of Vietnam and northern Myanmar displayed non-significant relationships, aligning with the patterns observed for the SPEI and SPI indices. Among the drought indices, the VCI had the highest correlation with the TCI, indicating a strong influence of temperatures on the VCI. The highest correlation coefficients were primarily observed in Cambodia, while non-significant R values were detected in central and northern Vietnam (Figure 5.10). Some areas of the Lower Vietnamese Mekong Delta and northern Laos also experienced non-significant responses. Notably, Cambodia had the largest area of the VCI-TCI positive response ($\sim$ 80%), and Thailand ranked second with nearly 70%. Myanmar ranked third with 60%. Vietnam had a modest proportion of the country with positive coefficients (R-value = 0.35), accounting for 35%.

Despite certain spatial variations, there was a strong positive correlation between the VCI and drought indices. This suggests that changes in VCI values, whether increasing or decreasing, are closely linked to the drought indices, highlighting the significant influence of drought conditions on VCI. These results were aligned with previous studies regarding the responses of vegetation to drought indices (Zhao et al., 2018; Ji and Peters, 2003) . Also, the VCI had a stronger relationship with shorter-term drought indices (e.g., SPEI-1, SPEI-3), which could be due to the higher rate of evapotranspiration and rapid soil moisture deficits. Vicente-Serrano et al. (2013) assessed vegetation responses to multiscale drought indices and their findings indicated that vegetation conditions responded stronger to drought

indices at shorter time scales, such as SPEI-1 and SPEI-3. Notably, large areas along Vietnam's central coast and northern Myanmar exhibited non-significant or weaker correlations. Some studies suggest that local climate and geographical factors may influence these responses. For instance, in the highlands of Myanmar, the presence of fog and dew can help maintain soil moisture levels even during dry seasons or periods of low rainfall, potentially mitigating the impact of drought on vegetation ecosystems. Likewise, the central coast of Vietnam experiences high humidity and microclimate ocean variability that can influence vegetation growth. The relatively stable temperatures and precipitation in these areas can also maintain vegetation growth. Also, Fan et al. (2023) noted that agricultural practices and land use changes could enhance the resilience of vegetation to drought conditions.

5.3.3.2 Vegetation-drought response by land cover types and elevations

The influence of drought conditions on vegetation ecosystems can depend on other factors, such as land cover types and elevation characteristics. This section provides a detailed analysis of how VCI-drought relationships vary in response to different land cover types and elevation characteristics across the MSEA region. Figure 5.11 showed the responses of VCI to multifaceted drought indices across land cover types and elevation zones over the MSEA region. Overall, higher responses between the VCI and drought indices were observed in rainfed cropland, mixed forests, and deciduous forests at 100-1000 m above sea level.

Regarding the VCI-drought responses with elevations, Figure 5.11 highlighted the varied VCI-drought responses across five different elevation zones. At elevations below 1000 m, the responses of the VCI to drought indices exhibited similar patterns. However, the responses were notably lower at higher elevations (above 1000 m), particularly in irrigated cropland and mixed forest areas. For instance, the correlation coefficient between VCI and SPEI in irrigated cropland was 0.47, whereas, for the TCI, this coefficient dropped to 0.41 - the lowest observed. In mixed forest areas, the lowest correlation between VCI and TCI was only 0.33, further illustrating a weaker response of this forest type to temperature fluctuations. Notably, the TCI generally had the highest correlation with the VCI across the elevation zones. In deciduous forests, the highest correlation between the VCI and TCI was observed under 100 m elevation, while this figure was 0.56 above the 1000 m elevation zone. In comparison, higher responses of VCI to other drought indices (SPEI, SPI, and SWDI) were found in elevations from 100 to 1000 m. For instance, the highest R-values were observed at 300-500 m zones across rainfed cropland (R-value = [0.63–0.7]), mixed forest (R-value = [0.63–0.69]), and deciduous forest (R-values = [0.62–0.73). Higher responses of VCI to drought indices at lower elevations indicated that these areas are more

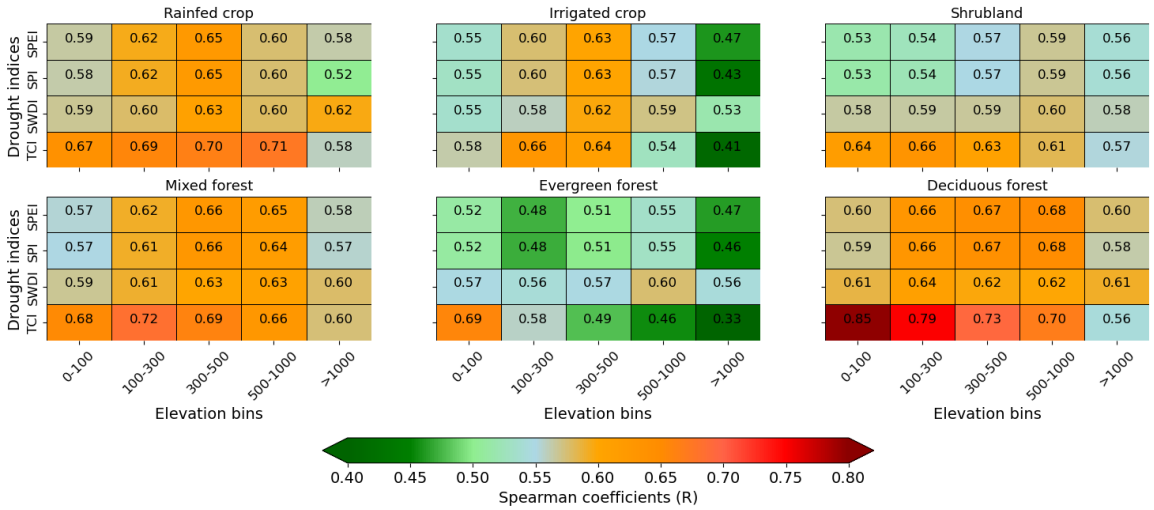

Figure 5.11: Responses of VCI to different drought indices across land cover types and elevation characteristics in the MSEA region. Dark red indicates stronger responses, while dark green represents less responsive.

vulnerable and sensitive to drought conditions. These findings are aligned with the VCI trends presented in Figure 5.4, where lower VCI trends were observed in lower elevations. Although several studies have investigated the relationship between vegetation and drought, limited research has examined this topic in tropical regions, considering elevation characteristics. Wang et al. (2021) examined the vegetation-drought responses in China and reported that higher elevations tended to have lower responses to vegetation productivity.

Regarding the VCI-drought responses concerning land cover types, the highest VCI-drought responses were observed in rainfed cropland, mixed, and deciduous forest areas. For example, the R-value between the TCI and deciduous forest VCI was around 0.73, while this number for rainfed crops was 0.67. Other vegetation types have lower responses to drought indices. In shrubland, lower responses were found with the SPEI and SPI, whereas in irrigated croplands, the lowest responses were found above 1000 m. In these elevated areas, there would be fewer irrigated croplands, and drought conditions may not significantly regulate crop growth due to the active water from mountains. Notably, the evergreen forests had the lowest responses to drought indices, especially with the SPEI and SPI. Mixed and deciduous forests are primarily found in lower elevations, where human activities have significant impacts. In comparison, evergreen forests are primarily found in higher elevations (e.g., Myanmar), where climate conditions stay relatively stable and experience less extreme heat during the dry seasons (Fan et al., 2023; Feng et al., 2020).

5.3.3.3 Impacts of drought on natural and undisturbed vegetation

This section examined the impacts of multi-temporal drought indices on the natural and undisturbed vegetation. The selection of natural vegetation in protected areas aimed to minimize human disturbance, focusing only on the impact of drought on the vegetation. We trained an RF regression using the VCI values and drought indices time series data from 2000 to 2022. The SHAP method was then applied to quantify the relative and individual contributions of each drought index to the VCI. Although the model optimization was not the primary focus of this study, the trained RF model achieved an accuracy of 94% on the training data. This performance indicated that the model is effective and reliable in generating the overall and individual contribution statistics. Here, the VCI can indicate vegetation conditions and drought conditions so that they can be used interchangeably.

Vegetation ecosystems are vulnerable to different drought conditions, including short-term and long-term droughts driven by climate and soil moisture variability. Each drought may have unique impacts on vegetation conditions with different scales. This study employed 12 different drought indices calculated at multiple timescales and grouped them into three primary drought conditions: short-term, median-term, and long-term drought. The short-term drought included six drought indices (SPI-1, SPI-3, SPEI-1, SPEI-3, SWDI, and TCI), while the median-term drought covered four drought indices (SPI-6, SPEI-6, SPI-9, and SPEI-9), and the long-term drought included two drought indices (SPI-12 and SPEI-12).

In tropical MSEA regions, short-term drought conditions have primarily driven undisturbed vegetation conditions (Figure 5.12). The SPEI-3 exhibited the highest influence on vegetation change among the examined drought indices, accounting for nearly 35% of the overall importance. The TCI ranked second, explaining nearly 20% of the observed variations, while the SWDI ranked third with 14%. SPEI-1 and SPI-1 explained about 15%, while the SWDI contributed nearly 9%. Short-term drought indices collectively explained nearly 93% of the undisturbed vegetation variations in the study region. By contrast, median-term and long-term drought indices explained only 7% of the observed variations in undisturbed vegetation conditions. For example, the SPI-9 explained less than 2% of the observed variations in the undisturbed natural vegetation, and this figure remained like other drought indices.

Figure 5.12 (b) exhibited the detailed contributions of individual observations from each drought indicator to undisturbed vegetation. Despite its smaller overall importance, the TCI has more individual variations of impact on undisturbed vegetation than the SPEI-3. For example, the wettest condition based on the TCI can increase the VCI up to 25% in some

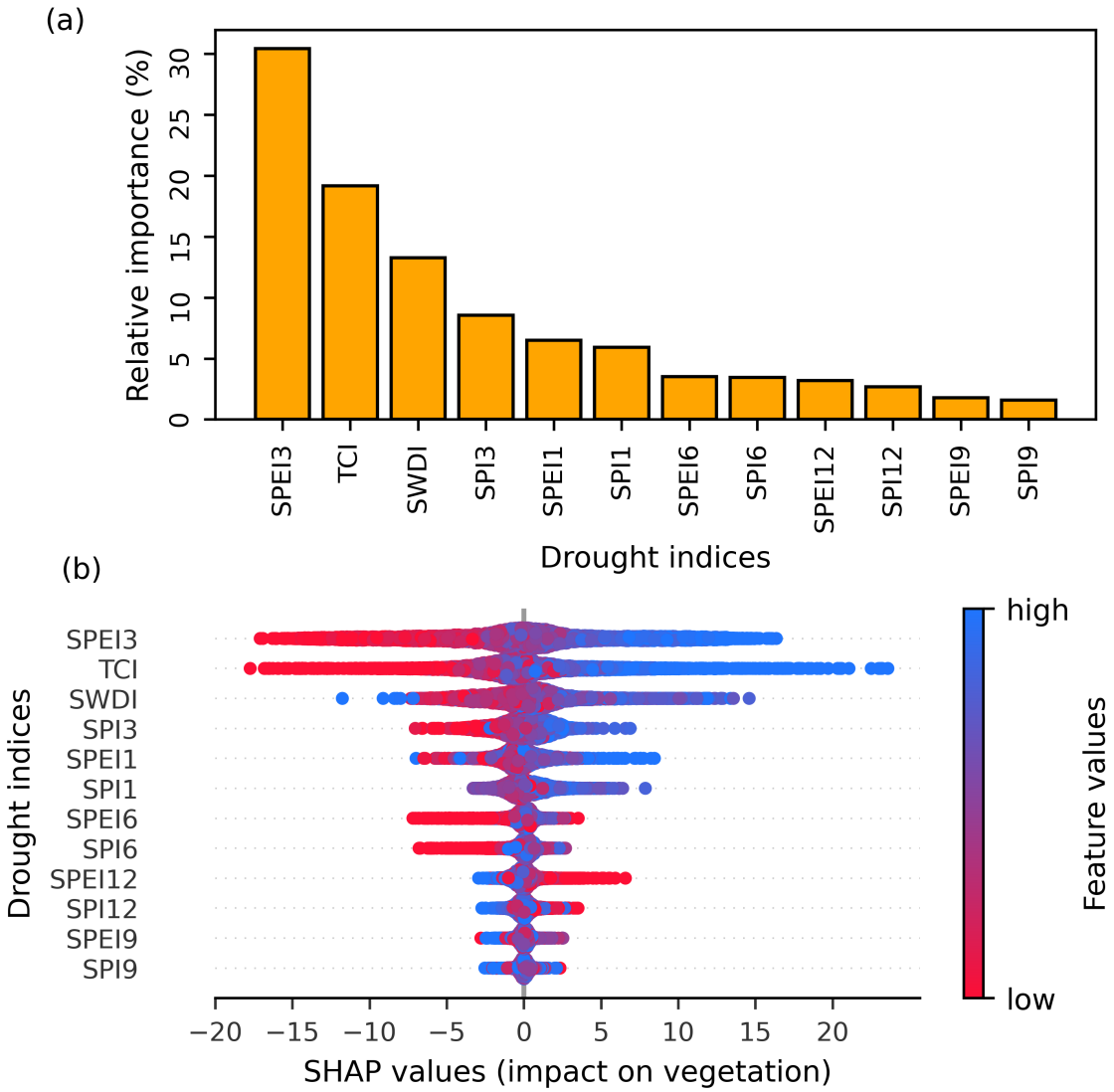

Figure 5.12: Overall and individual measures of the contribution of drought impacts on undisturbed and natural VCI across the MSEA region using the RF regression and SHAP method. The bar plot (a) indicated the relative contribution of drought indices using the SHAP method, while the bee swarm plot (b) presented the detailed contribution of individual observations to the VCI variability. Higher values in the bar plot indicated larger importance, while positive (negative) SHAP values in the bee swarm plot indicated positive (negative) contributions to increasing (declining) VCI values. The color bar represents feature observation values from low (drier conditions in red) to high (wetter conditions in blue). The combination of red and blue dots signifies a mixture of their impact on natural vegetation. Drought indices include the SWDI, SPI, TCI, and SPEI during the dry seasons from 2000 to 2022. This analysis is limited to protected areas to minimize human activities' impact on vegetation.

instances, while the driest condition can decline the VCI by 15%. The SPEI-3 can increase (decline) the VCI by 20% (15%) during the wettest (driest) conditions respectively. Soil moisture drought can increase or decrease the VCI within 10%, while this number for other short-term drought indices falls within 5-10%. The remaining drought indices did

not clearly show the influence on undisturbed VCI. These findings revealed the significant role of temperature and precipitation over the three months on undisturbed VCI. In Europe, vegetation ecosystems are more vulnerable to extreme climate conditions during the summer and spring seasons (Baumbach et al., 2017; Li et al., 2022a). In tropical regions, vegetation variability was primarily driven by extreme climate conditions (Ciemer et al., 2019; Fan et al., 2023).

Several factors may explain the different responses of undisturbed VCI to different drought indices in the tropical region. Vegetation ecosystems are typically susceptible to immediate water stress due to short-term droughts. These can cause rapid declines in soil moisture and water availability, especially during the dry seasons, making ecosystems more vulnerable to abrupt changes. For example, SPEI-3 and TCI are designed to capture short-term climate and soil moisture variability. Vicente-Serrano et al. (2010) developed the SPEI and revealed that tropical vegetation ecosystems were more sensitive to the short-term SPEI indicators. In arid and semi-arid environments, longer SPEI indices played a stronger role in vegetation variability (Zhan et al., 2022; Xu et al., 2018). These findings offer critical insights into how tropical undisturbed vegetation responds to different drought conditions across the study region. Given the ongoing climate crisis, short-term drought conditions are expected to rise and have far-reaching impacts on the natural protected ecosystems. These findings can support local authorities and conservationists in anticipating potential vegetation-induced drought areas so that proper planning and mitigation measures can be implemented to prevent potential losses or damage.

5.4 Summary

This study presented a detailed analysis of vegetation conditions' responses to climate and soil moisture drought indices across the MSEA region during the dry season. The VCI was calculated to represent vegetation conditions or vegetation-based drought, while the SPEI, SPI, SWDI, and TCI depicted the climate and soil-related drought conditions. Specifically, this study presented the spatiotemporal distribution of vegetation and climate-soil-based drought indices from 2000 to 2022. Subsequently, the response of VCI to multi-temporal and multi-type drought indices was assessed using different land use types and elevation characteristics. Lastly, this analysis investigated the influence of climate-soil drought indices on undisturbed vegetation conditions using explainable machine learning RF regression and SHAP methods. The main findings of this study are summarized as follows:

Rainfed cropland in Thailand and Cambodia frequently suffered from drought-induced stress. Higher VCI trends tended to occur in higher elevation zones. Among the vegetation

types, deciduous forests witnessed a large negative trend across elevation zones. Notable, nearly 85% of Cambodian deciduous forests suffered from decline trends under the 100 m elevation zone.

The SPEI-3 and SPI-3 shared common patterns of drought conditions but varied in severity. Higher severity was observed in the SPI-3, especially in 2005 and 2020. The SWDI revealed a relatively similar pattern across the study period, while the TCI agreed well with the SPEI-3 and SPI-3 in capturing drought variability. High positive VCI-drought responses were spatially observed across the MSEA region, primarily in Myanmar, Thailand, and Cambodia. Among the climate-soil-based drought indices, the TCI had the highest correlation with the VCI across vegetation types and elevations. Higher VCI-drought responses were observed in lower elevation zones in rainfed cropland, mixed forests, and deciduous forests. Evergreen forest and irrigated crop vegetation responded less to drought indices, especially in high-elevation zones.

Short-term drought disturbances accounted for nearly 93% of the natural and undisturbed VCI variation in the MSEA-protected areas. SPEI-3 revealed the largest influence among the examined drought indices, explaining approximately 35% of the observed vegetation dynamics, followed by the TCI ($\sim$ 20%). Based on the TCI and SPEI-3, the wettest condition can positively influence 20-25% of VCI values, while the driest conditions can decline the VCI by 15% (VCI units).

Chapter 6

Agricultural drought vulnerability in the Central Highlands of Vietnam

6.1 Research background

Drought is among the most devastating and costly natural disasters that largely impact agriculture, ecosystems, the economy, and human health. A lack of precipitation is the primary cause of drought. There are four drought types, including meteorological, hydrological, agricultural, and socioeconomic droughts. Meteorological drought originates from a precipitation deficit against the average over an extended period. Other droughts primarily stem from meteorological droughts. Agriculture is probably the most directly affected by drought among the affected sectors. Drought can cause crop failures, soil degradation, and livestock loss. Given the ongoing global warming phenomenon, droughts are projected to increase worldwide in both frequency and severity. According to the United Nations Office for Disaster Risk Reduction (UN-ODRD, 2022), drought events are projected to rise by 30% in the coming decade. This alarming trend underscores the urgent need to address drought vulnerability.

Drought vulnerability refers to the susceptibility of individuals, communities, ecosystems, or regions to drought impacts. It is a complex and multifaceted concept that arises from the interaction of various factors, such as biophysical (e.g., soil quality, climatic conditions, and water availability) and socioeconomic variables (e.g., economic resilience, infrastructure, and population density) (Serkendiz et al., 2023). These characteristics vary among regions, each with its own socioeconomic and biophysical background. Hence, understanding drought vulnerability and associated factors is key to drought mitigation and planning. A detailed drought vulnerability assessment provides local and national authorities with vital information necessary to formulate targeted plans and mitigation strategies

aimed at minimizing the potential impacts of drought (Serkendiz et al., 2023). In practice, the successful implementation of these strategies requires coordinated efforts among various organizations, stakeholders, and affected communities. Such collaboration is essential not only for addressing immediate impacts but also for developing long-term recovery strategies that enhance resilience to future droughts.

Over the past decades, several frameworks have been proposed to assess drought vulnerability across different parts of the world. Despite variations in spatiotemporal scales and input data, the vulnerability concept proposed by the Intergovernmental Panel on Climate Change (IPCC) was probably the most widely used framework for assessing geospatial drought vulnerability (Serkendiz et al., 2023; Upadhyay and Sherly, 2023; Sahana et al., 2021). For example, Serkendiz et al. (2023) assessed agricultural drought vulnerability in Turkey using the IPCC's vulnerability concept, considering vulnerability components: exposure, sensitivity, and adaptive capacity using multi-dimensional variables. Likewise, several other studies have assessed drought vulnerability using this concept (Sahana et al., 2021; Vyas et al., 2024; Swami and Parthasarathy, 2021; Upadhyay and Sherly, 2023). Other studies used satellite-based vegetation indices and machine-learning methods to assess agricultural drought vulnerability (Kafy et al., 2023; Roy et al., 2022; Kundu et al., 2024).

The Central Highlands is a key crop-producing region in Vietnam, especially coffee, pepper, and cashew. However, due to the growing population, overuse of water for agriculture, and climate crisis, this region has been increasingly vulnerable to drought and listed among the most drought-prone areas in Vietnam (Vu et al., 2015). This region also suffers from an underdeveloped irrigation system despite being the main coffee producer in Vietnam. A recent study reported that the 2015-2016 drought event in the study region caused an economic loss of nearly US$ 270 million (Byrareddy et al., 2021). This drought event damaged nearly 11 thousand hectares of industrial crops, particularly coffee and pepper (Van Quang and Thanh, 2023). Despite being one of the most drought-prone regions in Vietnam, little research has been conducted in the Central Highlands to assess the agricultural drought vulnerability. Previous studies in the region mainly focused on physical drought monitoring and characteristics (Vu et al., 2015; Phuong et al., 2022; Tran et al., 2023). As one of the first drought risk assessment studies in the region, Le et al. (2021) used vegetation, precipitation, and soil moisture to derive drought indices and assessed their risk during the drought event in 2020 across the central and southern provinces of Vietnam. They found that Vietnamese Mekong provinces suffered from the highest risk of drought. However, a significant limitation of this study was its focus solely on the year 2020, which neglected the importance of temporal information in understanding drought patterns. Also,

they considered only a limited number of socioeconomic variables and overlooked drought characteristics in their analysis.

This study conducted a detailed assessment of agricultural drought vulnerability in the Central Highlands of Vietnam, using three different drought indices and 17 socioeconomic and environmental factors considered relevant to this region. Each variable was assigned to one of the three vulnerability components: exposure, sensitivity, and adaptive capacity using the IPCC's vulnerability concept framework. The principal component analysis (PCA) was used to harmonize temporal vulnerability components, while the Shannon entropy method was used to identify weights for each vulnerability component in calculating agricultural drought vulnerability. Detailed descriptions of this study are organized into six major sections, including research background (Section 6.1), study area and materials (Section 6.2), methods (Section 6.3), results (Section 6.4), discussion (Section 6.5), and conclusion (Section 6.6). The Study area and materials provides an overview of the study area and data used in this study. The method offers a detailed framework and how data were selected and analysed to produce agricultural drought vulnerability. Next, this study presented results in the Results section before discussing these findings in the subsequent section. Finally, the conclusion summarizes the key findings of this study.

6.2 Study area and materials

6.2.1 Study area

The Central Highlands (Tây Nguyên in Vietnamese) lies in the south-central part of Vietnam, covering an area of nearly 55 thousand km^2 (Figure 6.1-a). It shares borders with Cambodia and Laos and covers five provinces: Kon Tum, Gia Lai, Dak Lak, Dak Nong, and Lam Dong. This region is primarily characterized by the inland plateau of Vietnam (elevations from 500 to above 1000 m) with the Truong Son (Annamite) Mountain range. Its central location, between the North and South, creates a transitional zone between different ecological and climatic regions.

In the Central Highlands, forests are dominated among the land cover types. Historically, this area comprised vast amounts of primary forests. While significant forest cover remains today, much of the land has been converted to agricultural use. For example, forests cover the largest proportion, accounting for nearly 76% (Li et al., 2018b). In comparison, agricultural land accounted for about 26% of the land surface, primarily observed in the Dak Lak, Kon Tum, and Gia Lai provinces (Figure 6.1-b). Notably, this region is primarily covered by fertile basaltic soils, making it highly suitable for coffee, rubber, and pepper crops. The

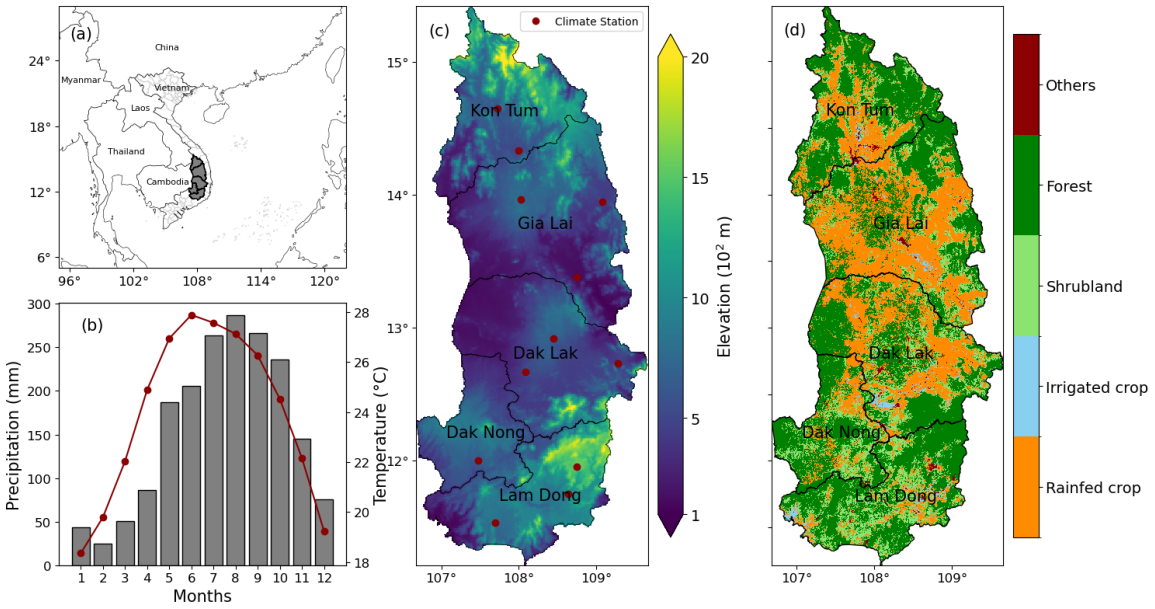

Figure 6.1: Map of the Central Highlands region (a) in Vietnam with elevations (c) and land cover (d). The bar and line plots (b) represent the station-based precipitation and temperature from 2000 to 2020. The dark red dots indicated the weather stations across the Central Highlands, while the dark gray color in the first plot (a) depicted the study area boundary.

Central Highlands produces nearly 93% of the national coffee, lifting Vietnam as the top coffee exporters worldwide (Byrareddy et al., 2021).

The climate of the Central Highlands is primarily driven by a tropical monsoonal pattern, with two distinct seasons: a wet season from May to October and a dry season from November to April. Annual temperatures in the region typically range from 21°C to 26°C, while annual precipitation rates vary between 1200 mm and 2000 mm (Quoc Lap, 2024). Rainfall is abundant during the wet season, accounting for 80% of annual precipitation (Tran, 2024), especially from August to September. In contrast, the dry season is marked by prolonged drought, making the study area particularly prone to drought hazards. Despite its agricultural importance, this area faces significant water management challenges. Irrigation systems remain underdeveloped and insufficient to meet the water demands of perennial crop farms (Quoc Lap, 2024), exacerbating the vulnerability to drought conditions.

6.2.2 Data and pre-processing

This section harnessed temporal geospatial and socio-economic data to assess the agricultural drought vulnerability in the Central Highlands of Vietnam. The geospatial data included satellite-based and reanalysis data products from 2000 to 2022, while provincial socio-economic data was collected from the Vietnam Department of Statistics. The geospatial data were collected from various sources and aggregated into annual datasets during

the dry season from 2000 to 2022. However, the socio-economic data was not consistently available over the same period due to the data availability. Socio-economic data were rasterized from provincial data using the inverse distance weighting (IDW) method (Hoque et al., 2020; Heydari Alamdarloo et al., 2020). Subsequently, geospatial and socio-economic time series were resampled at 1 km spatial resolution. The selection of data variables and how their connections to drought vulnerability are presented in Table 6.1. The following subsections describe the used data in detail.

6.2.2.1 Climate and vegetation data

This study selected the ERA5-Land reanalysis product and MODIS NDVI time series from 2000 to 2022. The ERA5-Land integrates historical observations with advanced European Centre for Medium-Range Weather Forecast simulation models (Muñoz-Sabater et al., 2021; Hersbach et al., 2020). This dataset covers global at a multi-temporal frequency (e.g., hourly, daily, and monthly) at 9 km spatial resolution. This chapter selected three main variables: daily precipitation, soil moisture, and PET (derived from air temperatures, precipitation, solar radiation, wind speed, and humidity). These variables are aggregated into monthly composites to compute drought indices. Subsequently, the PET and precipitation were used to derive the 3-month standardized precipitation evapotranspiration index (SPEI-3) and soil water deficit index (SWDI). The detailed calculation of PET and drought indices (e.g., SPEI-3 and SWDI) has been presented in Chapter 5 (Section 5.2.1 and Section 5.2.2.2).

The NDVI time series were obtained from MODIS satellites aboard Terra and Aqua sensors at 1 km spatial resolution and 16-day intervals. This dataset is an analysis-ready product derived from reflectance data that has been geometrically and atmospherically corrected to ensure high accuracy and consistency (Didan, 2021). If the MODIS 16-day composites contain cloud-related contamination, their quality band was used to identify and remove cloud and shadow pixels. Despite its high temporal resolution, the MODIS NDVI data in the MSEA region still suffers from heavy cloud and shadow contamination. The linear interpolation was applied to fill the data gap and subsequently composited into a monthly window using the median composite value method. Although the interpolation technique can fill in missing values, the monthly NDVI data may still contain noise due to sensor limitations and atmospheric interference. Hence, the monthly NDVI values are then reconstructed to maintain the reliable curve of land vegetation growth using the Savitzky-Golay method (Ha et al., 2023; Chen et al., 2021b). The NDVI was then used to calculate VCI, representing agricultural and vegetation drought conditions. The detailed calculation of this

Table 6.1: Detailed description of used variables and their rationale in assessing agricultural drought vulnerability.

Components	Variables	Rationale	Spatial resolution	Data period
Exposure	SWDI and its frequency and events	The soil moisture deficit is indicative of agricultural drought. Lower soil moisture makes crops more sensitive to drought, impacting their growth and yield.	1 km	2000 - 2022
	SPEI-3 and its frequency and events	Short-term SPEI drought indicates agricultural drought. Higher temperatures and reduced precipitation increase soil moisture deficits, intensifying drought vulnerability.	$\sim$ 10 km	2000 - 2022
	VCI and its frequency and events	VCI indicates vegetation drought. Higher soil moisture signals healthier vegetation, while lower soil moisture can cause vegetation stress, resulting in drought-induced stress.	1 km	2000 - 2022
Sensitivity	Surface water area (%)	Higher water surface reduced drought sensitivity.	30 m	2000 - 2022
	Rainfed cropland (%)	Higher rainfed crops increase drought sensitivity.	300 m	2000 - 2022
	Poverty households (%)	Higher poverty rates increase drought vulnerability	-	2010 - 2022
	Drinking water use (%)	Higher drinking water use reduces drought sensitivity	-	2010 - 2022
	Rural population (%)	A higher rural population can increase drought sensitivity	-	2000 - 2022
	Employed population (%)	A higher employed population can be more sensitive to drought.	-	2005 - 2022
	Skilled employment (%)	Higher skilled worker rates can reduce drought vulnerability.	-	2008 - 2022
	Slope (%)	Higher slopes can be more sensitive to drought due to less water retention.	90 m	-
	Elevation (m)	Higher elevation can increase drought sensitivity as it cannot keep water.	90 m	-
Adaptive capacity	Road accessibility (m)	Road accessibility is important in drought events. Faster road accessibility can better access food, water, and other resources, hence increasing adaptive capacity.	-	-
	Water accessibility (m)	Faster water accessibility to water can increase adaptive capacity.	30 m	2000 - 2022
	Average income (VND)	Higher incomes can better adapt to drought.	-	2010 - 2022
	High school graduates (%)	Higher school graduates can better adapt to drought.	-	2002 - 2017
	Social insurance (%)	Higher social insurance rates can increase drought adaptation.	-	2015 - 2022
	Unemployment insurance (%)	Higher unemployment insurance rates can reduce drought adaptation.	-	2015-2022
	Provincial GDP (VND)	Higher provincial GPD can increase drought adaptation as they have available resources to respond to drought damage.	-	2018 - 2022
	Laptop use (%)	A higher laptop use rate can increase drought adaptation. People use laptops to search for information online and better inform themselves.	-	2019 - 2022

index is referred to in the previous chapter (Section 5.2.2.1). Further information on this data is presented in Table 6.1.

6.2.2.2 Socio-economic data

Drought vulnerability is closely associated with socio-economic factors. In this study, annual socio-economic data from the Vietnam Department of Statistics (https://www.gso.gov.vn/) were collected at the provincial level. A detailed analysis of relevant literature on drought vulnerability informed the selection of eight key socio-economic variables (Serkendiz et al., 2023; Upadhyay and Sherly, 2023; Fathi-Taperasht et al., 2023; Murthy et al., 2015). These variables included skilled employment (%), rural population (%), poverty households (%), clean water use (%), employment populations (%), average income (VND), unemployment rate (%), social insurance (%), high school graduates (%), laptop use (%), unemployment insurance (%), and provincial GPD (%). Due to the availability of data, socio-economic variables can have various durations. The provincial variables were annually interpolated using the IDW method across the Central Highlands at 1 km spatial resolution with a geographic coordinate system. A detailed description of the used data and its characteristics are provided in Table 6.1.

6.2.2.3 Land cover, elevation, and water surface

Other factors, besides climate and socio-economic conditions, can influence drought vulnerability, such as land use, elevation, water surface, and road accessibility. In this analysis, the ESA CCI land cover product was used to derive agricultural land use (%) from 2000 to 2020 (Li et al., 2018b). High-resolution water surfaces were downloaded from global water surface datasets (30 m spatial resolution) from 2000 to 2022 (Pekel et al., 2016), while elevation and slope were obtained from the STRM digital elevation at 90 m (Berry et al., 2007). Road accessibility data was obtained from OpenStreetMap, which provides essential insights into the local infrastructure and its influence on drought vulnerability and adaptation. Despite their different spatial and temporal resolutions, the data were converted to a geographic coordinate system and resampled to 1 km spatial resolution.

6.3 Methodology

This section provided a detailed description of agricultural drought vulnerability assessment in the Central Highlands of Vietnam. This analysis assessed drought vulnerability based on the vulnerability framework proposed by the IPCC. A large number of relevant variables were identified for assessing drought vulnerability from exposure, sensitivity, and

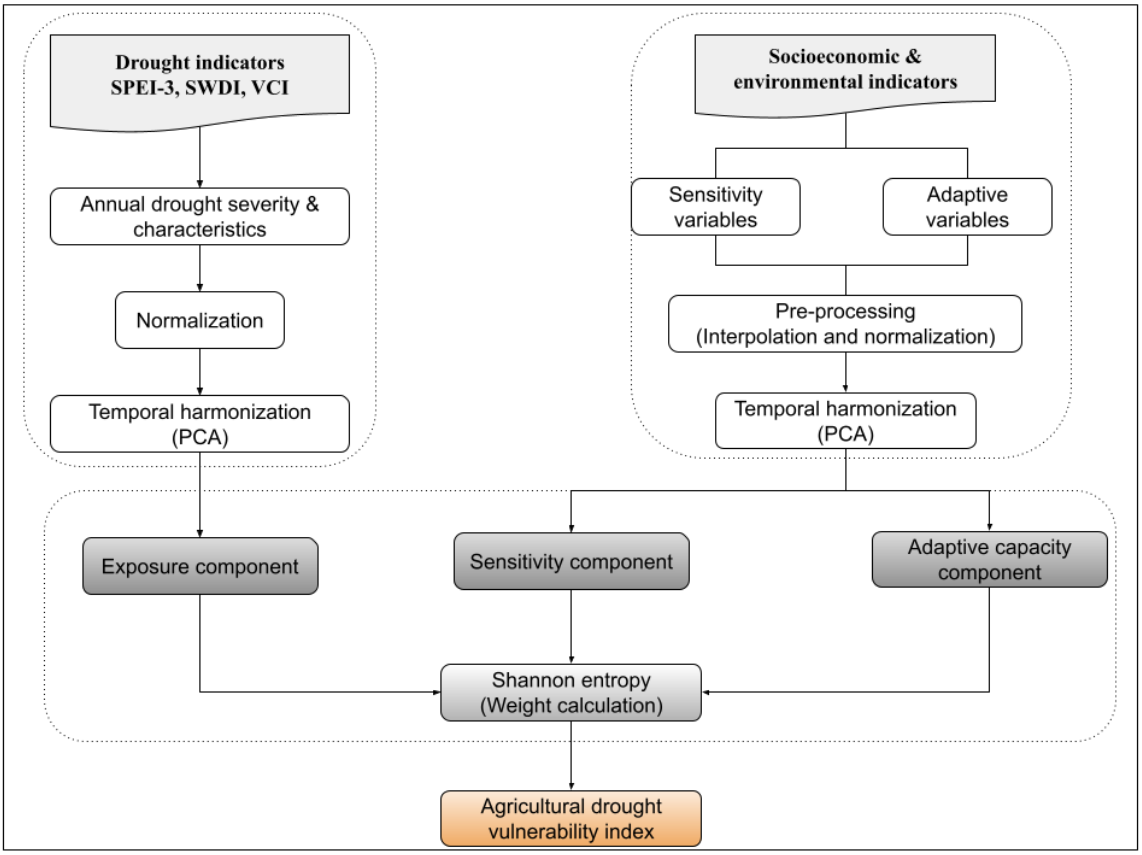

Figure 6.2: The implementation framework used in mapping and assessing agricultural drought vulnerability in the Central Highlands of Vietnam. Drought indices were calculated monthly from 2000 to 2022, while socioeconomic variables were available on an annual scale, though their availability varied over the study period.

adaptive capacity perspectives. Collected data was then normalized and transformed using principal component analysis (PCA) to derive meaningful representations of spatiotemporal framework components. Finally, a statistical method was used to derive the weightings for each component and calculate the agricultural drought vulnerability index. Figure 6.2 described the overall framework of agricultural drought vulnerability in the Central Highlands.

6.3.1 Assessment framework of drought vulnerability

Over the past decades, numerous frameworks have been proposed to assess drought vulnerability (Dhawale et al., 2024; Shah et al., 2020). These frameworks often use multidimensional analysis approaches. This means they combine different data variables (e.g., environmental, social, and economic factors) to provide a holistic view of vulnerability. Here, this study adopted the definition of vulnerability outlined by the Intergovernmental Panel on Climate Change (IPCC) to guide the development of drought vulnerability assessment frameworks. According to the IPCC, vulnerability comprises three components: ex-

posure, sensitivity, and adaptive capacity (Hinkel, 2011). Exposure identifies the locations and frequency/severity of drought, capturing the physical characteristics and recurrence of drought conditions (o'Brien et al., 2004). Sensitivity refers to the degree to which a system or population suffers once drought occurs (Serkendiz et al., 2023). Adaptive capacity indicates the ability of a system, community, or society to adjust, cope with, and recover from the impacts of drought (Füssel and Klein, 2006).

Although the IPCC's framework has been widely used in vulnerability assessment, a standardized operational method for assessing drought vulnerability has yet to be fully developed. The selection of variables for each component (exposure, sensitivity, adaptive capacity) can be complex and lack uniform guidelines. A common approach involves the use of indicator-based variables (Ionescu et al., 2009; Ahsan and Warner, 2014; Blauhut et al., 2016; Wilhelmi and Wilhite, 2002; Carrão et al., 2016; Serkendiz et al., 2023), which are classified into one of the three components. Subsequently, these indicators are aggregated through a mathematical formula to derive a drought vulnerability index. Here, the agricultural drought vulnerability is calculated using the following equation (Eq. 12) (Serkendiz et al., 2023).

$$ADVI = (E + S) - AC \tag{12}$$

Where ADVI is the agricultural drought vulnerability index, E is the exposure component, S is the sensitivity component, and AC is the adaptive capacity component.

The first part of the equation (E+S) refers to the potential impact of drought, while the second part subtracts the adaptive capacity. This means that a region with high exposure, sensitivity, and adaptive capacity will have lower vulnerability because its adaptive resources can counteract potential impacts. In contrast, a region with low adaptive capacity but high exposure and sensitivity will suffer from greater vulnerability as it lacks the means to cope effectively.

6.3.2 Identification of potential variables

Understanding and selecting appropriate variables are the first essential steps in assessing drought vulnerability. The choice of variables can directly influence the accuracy and relevance of the analysis. Thus, the selected variables ensure the analysis captures the multidimensional nature of drought vulnerability. The selection of variables should consider the geographic, environmental, and socio-economic context of the location, as well as data availability (Table 6.1). These variables should align with the conceptual ICPP framework,

representing the three core components: exposure, sensitivity, and adaptive capacity. A literature survey revealed that recent agricultural drought vulnerability studies primarily selected variables related to climatic conditions, soil quality, water resources, economic characteristics, and population indicators (Serkendiz et al., 2023; Upadhyay and Sherly, 2023; Dhawale et al., 2024). Description of each variable and its rationale are presented in

In the Central Highlands, for example, drought conditions are largely influenced by soil moisture and climate variability. In this context, drought severity and their characteristics (frequency and drought events), derived from the SPEI-3, SWDI, and VCI time series, were used to assess the potential extent and level of drought exposure. The SPEI-3 measures meteorological drought relevant to agriculture by considering both precipitation and evapotranspiration over three months (Unganai and Kogan, 1998; Vicente-Serrano et al., 2010), while the SWDI represents agricultural drought by assessing soil moisture levels (Mishra et al., 2017). The VCI reflects ecological drought by measuring the health of vegetation and crops (Kogan, 1990). In terms of the sensitivity component, this study considered nine environmental and socio-economic variables, namely surface water area (%), rainfed cropland (%), poverty households (%), drinking water use (%), rural population (%), employed population (%), skilled employment (%), slope (%), and elevation (m). For adaptive capacity, this analysis selected seven variables, including road accessibility (%), water accessibility (%), average income (VND), provincial GDP (%), high school graduates (%), laptop use (%), social insurance (%), and unemployment insurance (%).

These variables are relevant to agricultural drought vulnerability in the Central Highlands of Vietnam. For example, higher water surface areas and drinking water use can reduce drought vulnerability because these resources provide water access to people and agriculture. A lack of water resources can cause crops to fail during drought events. In rural areas, farmers are sensitive and vulnerable to drought if they lack skills and financial resources. Thus, a higher rural population and poverty rates can be more sensitive to drought. However, higher-skilled employment rates can reduce drought vulnerability by faster adapting and mitigating drought hazards. Drought vulnerability may be higher in higher slopes and elevation areas due to erosion and poor water retention. Drought vulnerability also depends on adaptive capacity or responses. For example, improved access to roads and water resources can reduce vulnerability even during drought. Higher income levels, social insurance coverage, and strong provincial GDP also contribute to better drought adaptation by ensuring that resources are available for faster recovery. Higher laptop use and high school graduate rates can enhance drought adaptation by adopting new technologies to access weather forecasts, mitigation strategies, and faster communication. Other factors, such as unemployment, can lower adaptive capacity due to a lack of economic resources.

6.3.3 Data normalization and temporal harmonization

Drought indices and socioeconomic data were collected in various units, and to ensure meaningful analysis, these data have been aggregated and normalized. A consistent method has been applied to convert the data from different units into a common scale, enabling seamless comparison and integration across datasets. Specifically, the min-max normalization method transformed each data variable into the same value range between zero and one. The following equation was applied to all data variables (Eq. 13).

$$Z_{\mathrm{i,t}} = \frac{x_{\mathrm{i,j}} - x_{\mathrm{i,t,\ min}}}{x_{\mathrm{i,t,max}} - x_{\mathrm{i,t,min}}} \tag{13}$$

Where $Z_{\mathrm{i,t}}$ and $x_{\mathrm{i,t}}$ are normalized and raw data for the i^{th} variable at year t. The $x_{\mathrm{i,t,min}}$ and $x_{\mathrm{i,t,max}}$ present the minimum and maximum values, respectively, for the i^{th} variable at year t.

Despite the uniform value range, each indicator can have positively proportional or inversely proportional impacts on drought vulnerability. For example, higher proportions of rainfed cropland typically correspond to greater vulnerability, while larger drought index values (e.g., SPEI-3) represent wetter conditions or less vulnerability. In this study, higher normalized values represented higher resilience and lower vulnerability to drought, and vice versa. For variables (e.g., SWDI and employment insurance rate) where lower values indicate greater vulnerability, they were normalized directly. However, for other indices (e.g., unemployment insurance rate, drought frequency, and road accessibility) with an inverse relationship (where higher values indicate higher vulnerability), the value was inverted by subtracting the normalized score from 1 to ensure consistency across the dataset. This approach ensures that all variables align on a common scale, facilitating accurate comparison.

Normalized drought indices and socioeconomic variables were then temporally harmonized using the PCA method into exposure, sensitivity, and adaptive capacity components. PCA is a widely used statistical technique for reducing the complexity of multi-dimensional data into more manageable components with minimum information loss (Greenacre et al., 2022). This method identifies the directions (principal components) along which the data exhibits the greatest variance and then expresses the original variables in terms of these components. Each component is a linear combination of the original variables and is ranked by its ability to explain the variance within the dataset. The first component explains the largest variance, followed by subsequent components. Generally, the first three components were found to explain nearly 98% of the total variance, meaning that most of the information from the original variables is retained within these three components. The mathematics

of PCA can be found in previous studies (Tadić et al., 2019; Uddin et al., 2019). In this study, variables within each framework component (Table 6.1) were temporally reduced into the first three PCA components, and a scikit-learn Python package was used for this task. Subsequently, we derived the exposure, sensitivity, and adaptive capacity using the first three components and their corresponding weights (Eq. 14).

$$C = \sum_{k=1}^{3} w_k p_k \tag{14}$$

Where C represents one of the three drought vulnerability components (exposure, sensitivity, adaptive capacity), while p_k indicates the first k PCA components and their corresponding weights w_k.

6.3.4 Agricultural drought vulnerability index

The agricultural drought vulnerability index was built based on three components: exposure, sensitivity, and adaptive capacity, as presented in Section 6.3.1. Instead of arbitrarily assigning equal weights to each component, this study used Shannon entropy to derive more objective and data-driven weights for these components. This approach allows for a more accurate representation of the relative importance of each component in contributing to overall drought vulnerability.

Shannon entropy, originally introduced in information theory, measures uncertainty or disorder in a dataset. It provides a way to quantify the amount of information contained in a variable by assessing the variability or randomness present. The principle of Shannon entropy is that variables with higher variability contain less reliable information. Hence, they contribute less to overall importance, and vice versa. Here, we used Shannon entropy to identify weights that reflect the influence of each component on the drought vulnerability in the Central Highlands. After retrieving the component weights, the agricultural drought vulnerability index was revised Eq. 12 as follows (Eq. 15).

$$ADVI = (w_e * E + w_s * S) - w_a * AC \tag{15}$$

The ADVI is the agricultural drought vulnerability index, E is the exposure component, S is the sensitivity component, and AC is the adaptive capacity component. The weights for each component derived from Shannon entropy corresponded to w_e (exposure weight), w_s (sensitivity weight), and w_a (adaptive capacity weight).

6.4 Results

6.4.1 Spatiotemporal variability of drought conditions

The Central Highlands experienced varying drought conditions according to different drought indices from 2000 to 2022. While distinct drought patterns were observed during specific years in the dry seasons, the severity and spatial extent of drought varied across the indices, reflecting differences in how each index captures drought intensity and impact. Figure 6.3 exhibited the spatiotemporal distribution of VCI-based drought conditions over the study period. According to this index, the Central Highlands experienced frequent drought conditions almost annually. The most severe drought occurred in 2005, when nearly 84% of the region faced severe drought conditions. Other significant drought events were observed in 2010, 2015, 2019, and 2020, though these impacted smaller areas, primarily concentrated in the central region. Notably, the southern Gia Lai and northern Dak Lak provinces experienced severe drought conditions in 2016 and 2019. In contrast, wetter conditions prevailed in 2017-2018 and 2022, with vegetation showing healthy or green states during these periods. For example, in 2022, nearly 87% of the region exhibited green vegetation. Notably, drier conditions were observed in the early 2000s in Lam Dong province, while this pattern was the opposite in recent years, reflecting greener vegetation. Notably, nearly 40% of the dry seasons across the study period experienced extensive drought, affecting more than 50% of the region, underscoring the recurrent nature of large-scale drought events.

Figure 6.4 displayed the spatiotemporal pattern of SPEI-3-based drought conditions from 2000 to 2022 during the dry seasons. SPEI-3 represents the drought conditions based on precipitation and temperature over short periods (3 months), reflecting precipitation deficits across the study region. Overall, the Central Highlands experienced frequent climate-based drought conditions with moderate and severe intensity. According to this index, the study area witnessed the most severe drought conditions in 2005. Notably, nearly 54% of the dry seasons experienced drought conditions (from light to severe drought) from 2000 to 2022. Interestingly, the drought event that occurred in 2010 was primarily detected in Lam Dong, while the VCI-based drought conditions were observed across the study region.

Figure 6.5 showed the spatiotemporal variability of SWDI-based drought conditions, reflecting soil moisture across the study area. Overall, the region experienced localized soil moisture droughts in certain areas. It is observed that soil moisture drought events were primarily detected in the central provinces of Dak Lak, Lam Dong, and Gia Lai. The largest drought event was recorded in 2005, affecting nearly 75% of the region. Notably, the study region experienced soil moisture drought almost annually throughout the study period

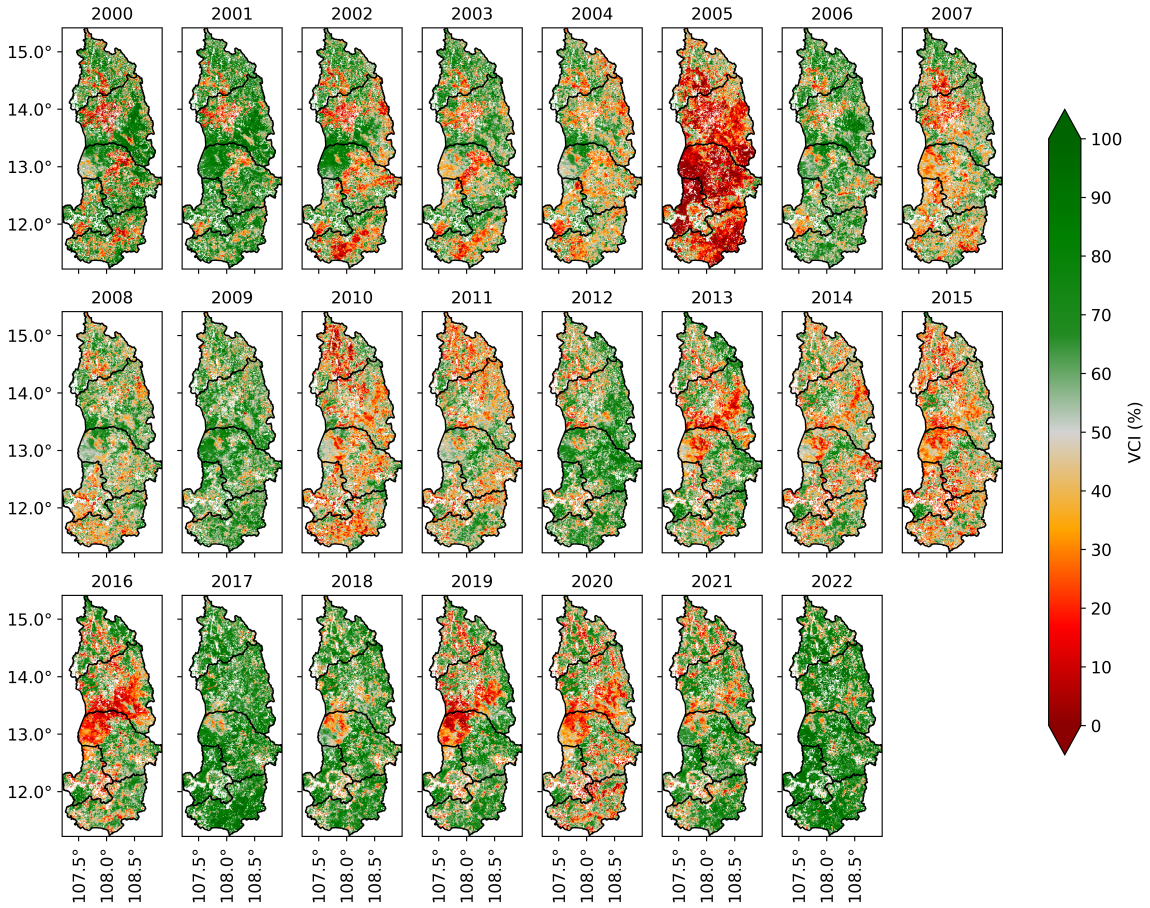

Figure 6.3: Spatiotemporal variability of VCI derived from satellite-based vegetation time series between 2000 and 2022. The dark red color represents drier (stressed vegetation) conditions, whereas the dark green color indicates wetter (greener vegetation) conditions.

(Figure 6.5). Despite drought signals in some provinces, most dry seasons experienced large-area wet conditions. For example, in 2022, nearly 97% of the region witnessed high SWDI values, reflecting non-drought soil moisture conditions.

Although drought conditions across the study region shared some temporal patterns, each indicator exhibited varying severity and spatial extents. Regardless of drought indices, the region experienced the worst drought conditions in 2005. Among the drought indices, the SPEI-3 and VCI revealed the largest drought-affected areas. According to SPEI-3, the region suffered from widespread drought during several periods (e.g., 2002-2005, 2015-2016, and 2019-2020). In comparison, the VCI ranked second in terms of detected drought areas. In contrast, the SWDI revealed consistently smaller detected drought areas over the study period. Overall, larger areas of wetting areas were detected by the SWDI, while this figure was the opposite of the VCI and SPEI-3 indices.

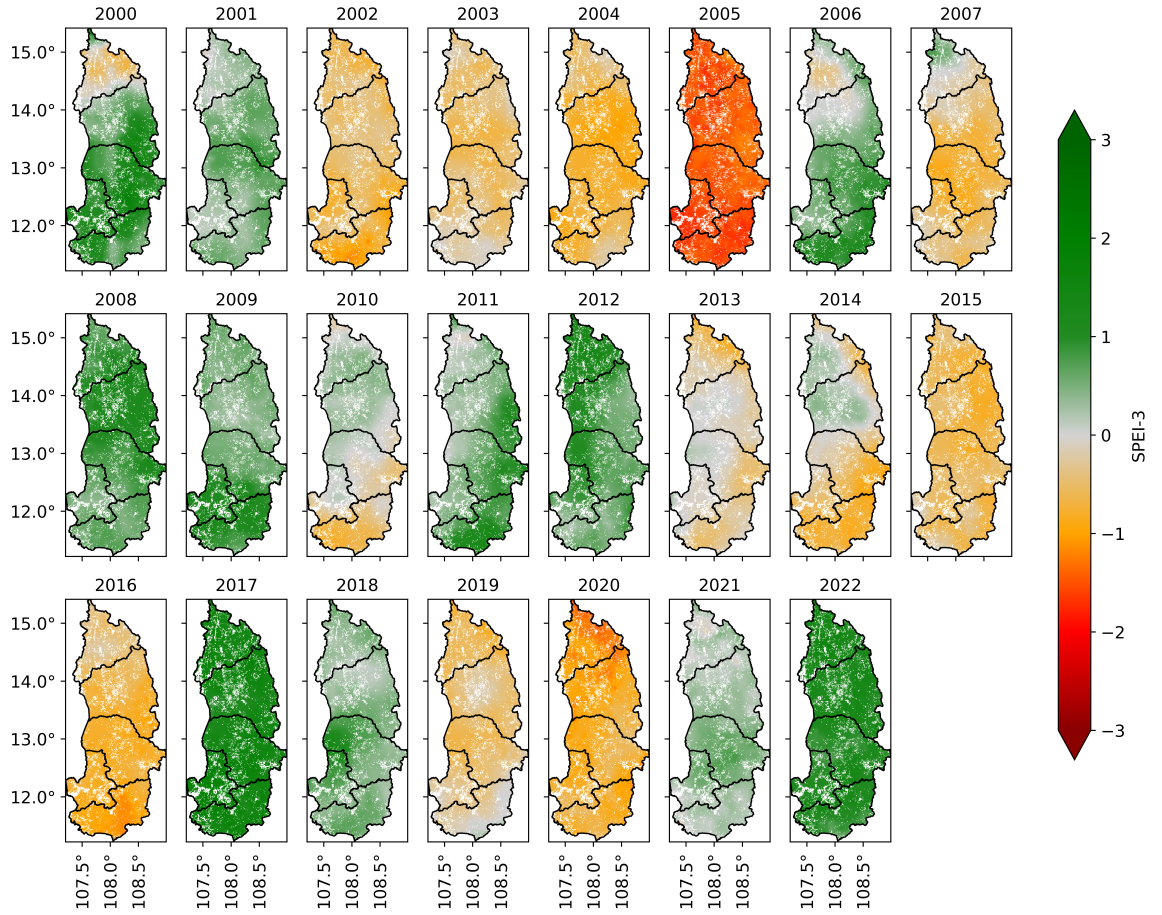

Figure 6.4: Spatiotemporal variability of SPEI-3 derived from precipitation and PET between 2000 and 2022. The dark red color represents drier conditions, whereas the dark green color indicates wetter conditions.

6.4.2 Exposure, sensitivity, and adaptive capacity

Drought vulnerability in this study consists of three components: exposure, sensitivity, and adaptive capacity. Using the PCA method, the vulnerability components were derived from climatic, environmental, and socioeconomic variables. Specifically, exposure was derived from three different drought indices and their characteristics over the study period. Sensitivity was obtained from 9 different environmental and socioeconomic factors, while the adaptive capacity component was derived from six socioeconomic factors. Figure 6.6 exhibited the spatial distribution of exposure, sensitivity, and adaptive capacity in the study area. Overall, there was a clear spatial pattern of drought exposure, sensitivity, and adaptive capacity among the provinces.

Regarding drought exposure, the Central Highlands of Vietnam experienced high exposure to drought (Figure 6.6-a). This observation was also detected in individual drought indices. Among the provinces, Kon Tum was less exposed to drought, while others were more prone to drought exposure (Figure 6.6-a). The most drought-prone regions were pri-

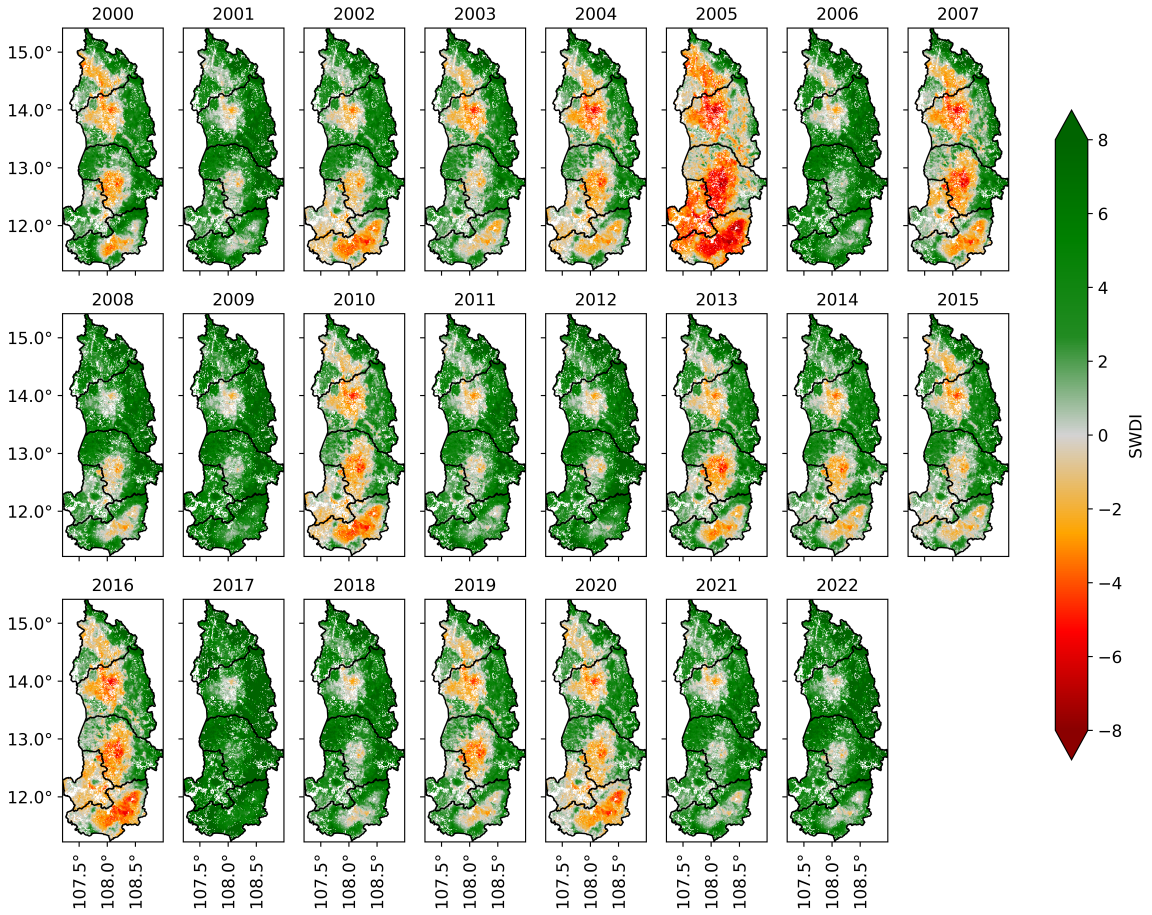

Figure 6.5: Spatiotemporal variability of soil-based SWDI drought conditions from 2000 to 2022. The dark red color represents drier conditions, whereas the dark green color indicates wetter conditions.

marily observed in the central areas of Gia Lai, Dak Lak, and Lam Dong provinces. For example, Lam Dong province suffered from the largest exposure, accounting for 51% of the province. Dak Nong was ranked second (42%), followed by Dak Lak (33%). In contrast, nearly 91% of Kon Tum province experienced non-drought exposure. Gia Lai witnessed 72% of the province without drought exposure. Notably, Dak Nong province experienced less intensive exposure despite its large exposure area.

Sensitivity is another important component of drought vulnerability. Figure 6.6-b showed that the Kon Tum and Gia Lai provinces suffered from a higher sensitivity to drought. Nearly 94% of Kon Tum province was sensitive to drought conditions, while this figure for Gia Lai province was about 80%. In contrast, other provinces demonstrated lower levels of drought sensitivity (Figure 6.6-b). For example, Lam Dong province exhibited non-sensitivity to drought events. Regarding the adaptive capacity, Figure 6.6-c revealed a distinct spatial pattern of adaptive capacity in the study region. Lam Dong and Kon Tum had higher adaptive capacity to drought vulnerability, while Gia Lai and Dak Lak experienced lower adaptive capacity. Among the provinces, Lam Dong had the highest adaptive

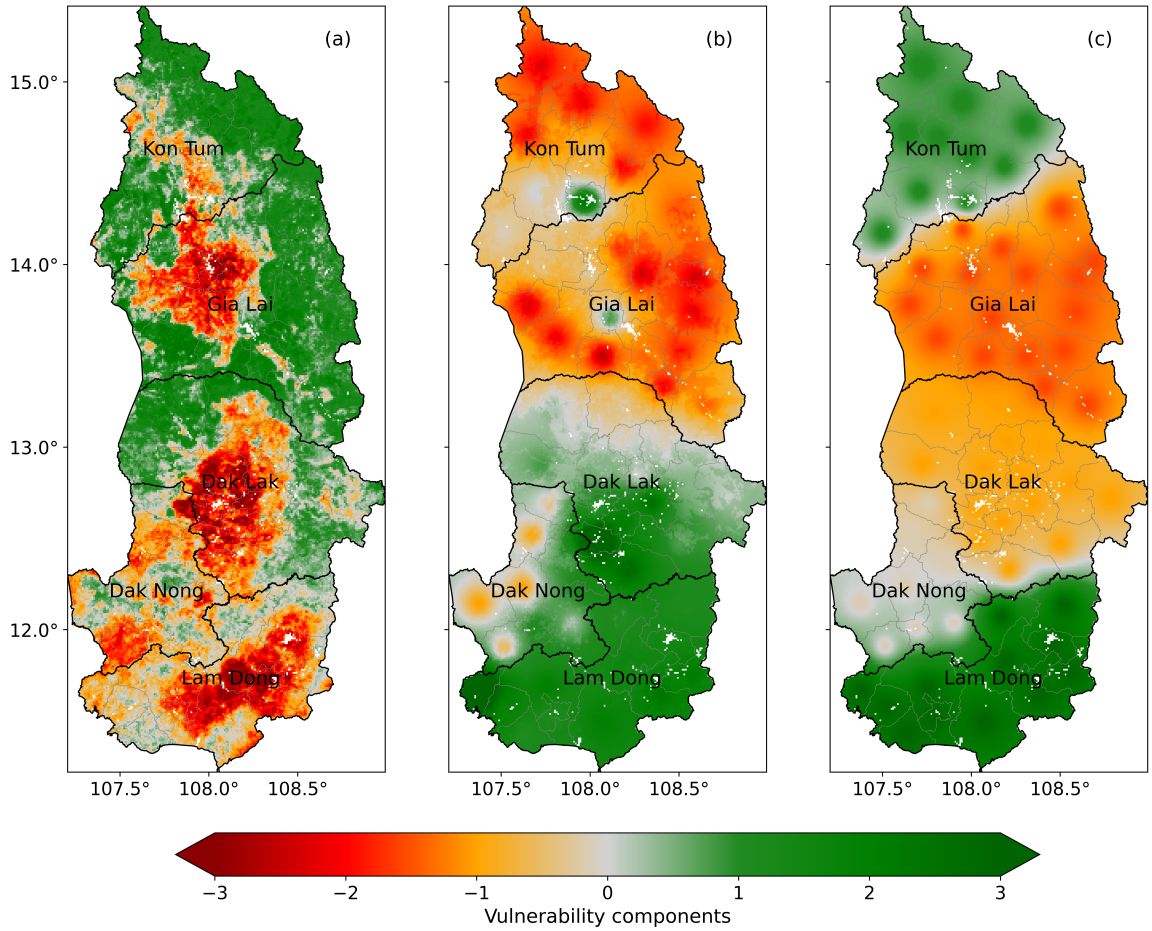

Figure 6.6: Spatial representation of three vulnerability components: (a) exposure, (b) sensitivity, and (c) adaptive capacity derived from time series variables. Dark red represents larger exposure and sensitivity or lower adaptive capacity, while dark green indicates less drought exposure and sensitivity or higher adaptive capacity.

capacity to drought impacts. By contrast, Gia Lai suffered from the lowest adaptive capacity to drought vulnerability over the study period.

6.4.3 Spatial distribution of agricultural drought vulnerability

The agricultural drought vulnerability was obtained by combining the three vulnerability components of exposure, sensitivity, and adaptive capacity factors using the Shannon entropy weighting method. The vulnerability index was then reclassified into four levels of vulnerability: very high, high, moderate, low, and very low classes using z-score classification methods. Figure 6.7 exhibited the spatial distribution of agricultural drought vulnerability and its corresponding vulnerability classification. In this analysis, the weightings assigned to each component were 0.65 for exposure, 0.27 for sensitivity, and 0.08 for adaptive capacity, reflecting the dominant influence of exposure on overall vulnerability.

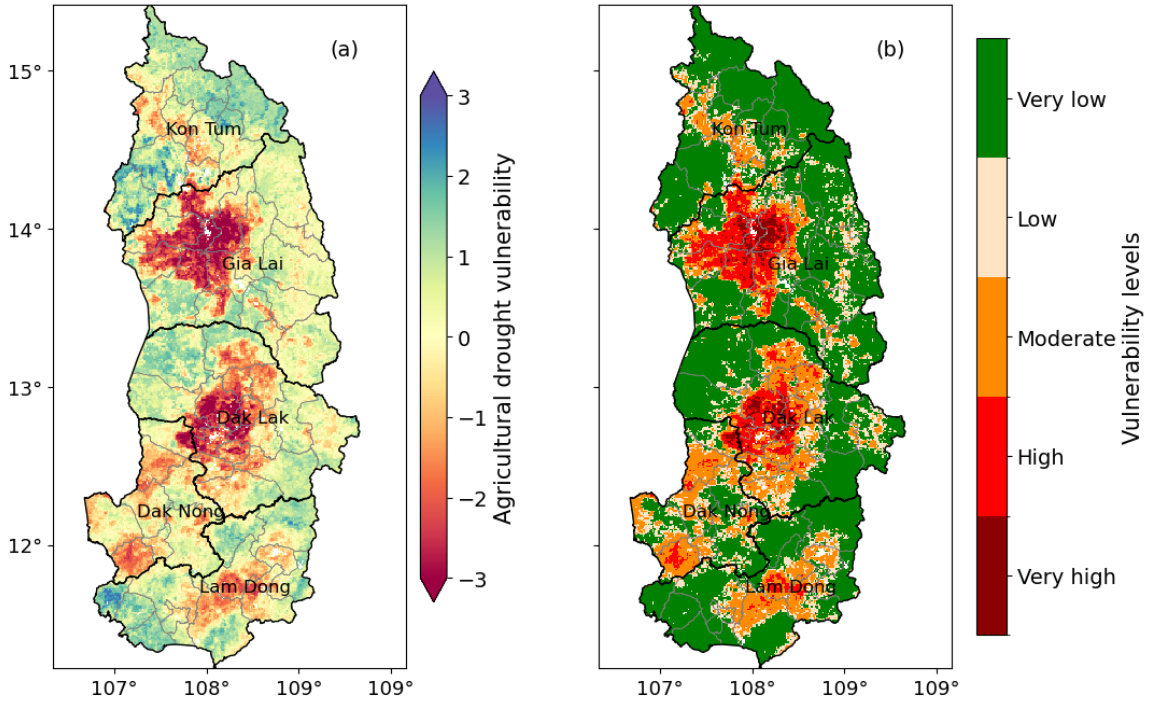

Figure 6.7: Spatial distribution of agricultural drought vulnerability (a) and corresponding vulnerability classification (b) over the Central Highlands of Vietnam based on exposure, sensitivity, and adaptive capacity components. The red in the left bar indicates more drought vulnerability, while the blue represents less vulnerability.

The study region exhibited significant variability in agricultural drought vulnerability, as indicated by ±3 ADVI values (Figure 6.7-a). Lower ADVI values indicate greater vulnerability to drought, while higher values represent lower vulnerability. Notably, the central areas of Dak Lak and Gia Lai provinces exhibited the lowest ADVI values, signaling higher drought vulnerability. Interestingly, Dak Nong province had the lowest ADVI values (-0.41) among the provinces despite its overall lower vulnerability (Figure 6.7-a). Gia Lai was ranked second (-0.28). Regarding vulnerability classification, Figure 6.7-b revealed a distinct spatial pattern of high and low vulnerability. Overall, the region experienced nearly 9% of “high to very high” vulnerability areas, while nearly 20% experienced “moderate” vulnerability. Notably, the “high and very high” drought vulnerability areas were detected in the central areas of Dak Lak and Gia Lai provinces. Nearly 17% of Gia Lai province suffered from “high and very high” vulnerability, while this number in Dak Lak was about 13%. Dak Nong province suffered from 37% of “moderate” drought vulnerability areas. Other provinces revealed a small proportion of “high” vulnerability. For example, Lam Dong province experienced nearly 3% and 18% of “high” and “moderate” drought vulnerability areas, respectively.

6.4.4 Cross-verification of drought vulnerability

Cross-verification of agricultural drought vulnerability products is crucial for effective risk management and informed agricultural planning. However, collecting on-the-ground drought vulnerability data in the study region is challenging, as such information is neither readily available nor publicly accessible. In this analysis, exposure is the major contributor to drought vulnerability, making it a key component for cross-validation. Here, exposure indicates physical drought conditions and was synthesized from the SPEI-3, SPI-3, and SWDI. Among these indices, the SWDI accounted for the largest variations in exposure. Given these insights, this analysis selected SWDI and cross-validated it with ground-based data. In the Central Highlands of Vietnam, direct soil moisture data collection remains difficult; however, because soil moisture is strongly correlated with precipitation patterns, precipitation data can serve as an effective proxy for validating drought vulnerability assessments. Thus, this analysis cross-validated SWDI using ground-based precipitation time series from 2000 to 2020.

This study calculated the ground-based SPI-3 within each province, and then the ground-based SPI-3 and SWDI were standardized before the cross-validation. Figure 6.8 exhibited the relationship between the ground-based precipitation and the SWDI. Overall, a high agreement existed between the two datasets. The temporal patterns of both datasets were closely aligned, as seen in Figure 6.8 (a1-a5). Statistical analysis revealed that most provinces had a high correlation between ground-based precipitation and SWDI. Notably, Dak Lak province showed the highest correlation, with an R-value of approximately 0.93, while Lam Dong province had the lowest R-value (R-value = 0.43). Kon Tum also displayed a strong correlation between SWDI and ground-based precipitation (R-value = 0.83). In other provinces, the correlation ranged between 0.7 and 0.8. These high R-values indicated that exposure derived from drought indices is a reliable component of drought vulnerability.

6.5 Discussion

6.5.1 Spatial discrepancies of agricultural drought vulnerability

The analysis of multiple drought indices (SWDI, SPEI-3, and VCI) in the Central Highlands of Vietnam from 2000 to 2022 revealed some temporal drought patterns across the three indices. For example, all drought indices exhibited severe drought conditions in 2005, and this finding aligned with previous findings (Vu et al., 2015; Tran et al., 2023). However, notable differences were observed in drought severity and spatial extent among the drought indices. The SPEI-3 generally showed a larger spatial extent of drought during drought

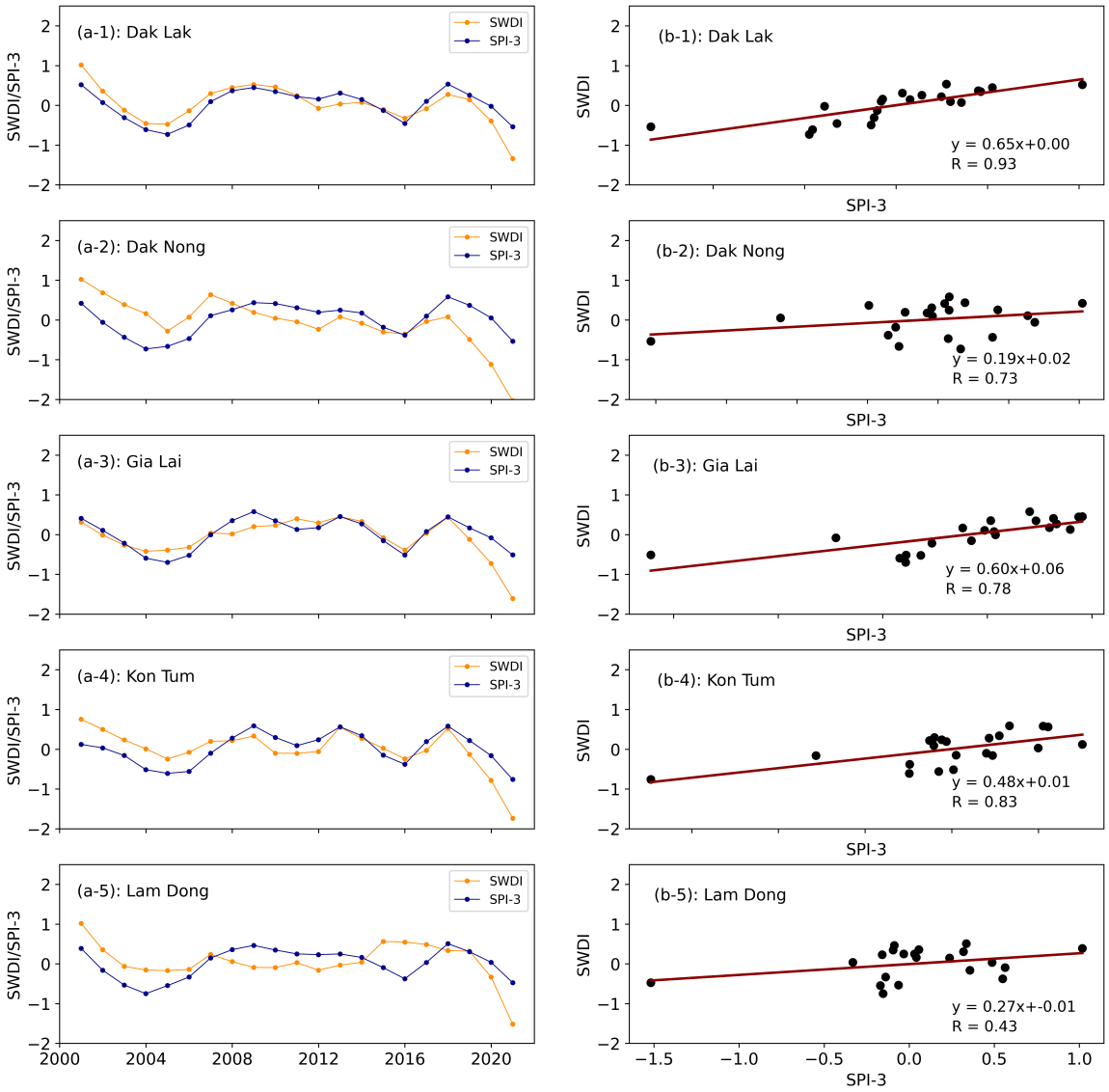

Figure 6.8: Cross-validation of SWDI and ground-based precipitation across five provinces in the Central Highlands of Vietnam from 2000 to 2020.

years over the study period. The possibility could be that the SPEI-3 captures broader climatic drought conditions over large areas during rainfall deficits and increased evaporation rates. In contrast, the SWDI detected smaller areas of drought during the same years. The soil-based indicator tended to highlight specific areas with persistent soil water deficits, reflecting local agricultural drought. The spatial consistency of the SWDI suggests that some areas are more prone to soil moisture deficits regardless of broader atmospheric conditions, possibly due to inherent soil and land cover characteristics. For example, the spatial observations of repeated drought in the central areas of Dak Lak province are closely aligned with coffee plantations (Maskell et al., 2021).

Drought vulnerability revealed significant patterns of exposure, sensitivity, and adaptive capacity across the study region. Among these factors, exposure is the main driver of

drought vulnerability, accounting for nearly 65%. Sensitivity is ranked second with 27%, followed by adaptive capacity with 8%. The Central Highlands is a drought hotspot, and several studies reported that this region has suffered from more frequent droughts than other parts of Vietnam (Nguyen-Ngoc-Bich et al., 2021; Vu et al., 2015; Tran et al., 2023). Among the three drought indices, it is observed that the SWDI contributed nearly 72% to the exposure component, indicating the dominant role of soil moisture in assessing drought vulnerability in the study region. One of the possibilities could be that industrial and rainfed crops (e.g., coffee and pepper) in this region are highly dependent on soil moisture, and climate-based indices alone are likely insufficient to explain drought variability. For the sensitivity component, it is observed that rural populations and rainfed crop areas were the main contributing factors to the sensitivity component among nine different variables. Together, these two variables accounted for nearly 60% of the observed variations in sensitivity components. Also, the poverty rate and workforce above 15 years explained 12% and 16%, respectively, the observed variations in sensitivity components. Higher rural populations and rainfed crops are more sensitive to drought, as rainfall deficits can directly affect crop production and income (Miyan, 2015; Venkatappa et al., 2021). Kon Tom and Gia Lai provinces exhibited higher sensitivity to drought because these provinces had larger rainfed areas and higher rural workforce. Notably, Gia Lai, together with Dak Lak provinces, had a lower level of adaptive capacity to drought response. Several factors could be attributed to this issue, but social insurance, unemployment insurance rates, and high school graduates mainly drive them. These three variables explained nearly 80% of the observed variations in adaptive capacity components among the six selected variables. Lower social and unemployment insurance rates in these provinces could put farmers and communities at risk when drought-induced agricultural loss occurs.

Drought vulnerability is mainly driven by exposure, accounting for nearly 65% of overall vulnerability. Large areas of agricultural drought vulnerability were detected in central areas of Dak Lak, Gia Lai, and Lam Dong provinces. These areas suffered from higher sensitivities and lower adaptive capacity, except for Lam Dong. Despite its high exposure, Lam Dong province was observed to have lower vulnerability due to lower sensitivities and higher adaptive capacity (Figure 6.6). Higher vulnerability areas were primarily detected in crop-growing areas and industrial plantations. In Dak Lak province, for example, the central area of high drought vulnerability was largely aligned with coffee plantations (Maskell et al., 2021). Although no in-situ drought vulnerability products have been reported in the study region, the detected areas of high drought vulnerability closely corresponded with the districts where the agricultural economic loss was reported (Van Quang and Thanh, 2023). This alignment demonstrated the reliability of the agricultural drought map produced in this study using multidimensional methods. Thus, the map of agricultural drought vulnerabil-

ity can support local authorities in developing drought mitigation, allocating resources to specific target interventions, and enhancing community resilience to drought.

6.5.2 Novelty and limitations

The novelty and originality of this study lie in its innovative application of the IPCC's vulnerability framework that integrates temporal climatic, environmental, and socioeconomic variables using the PCA and Shannon entropy methods. Previous research usually focused on agricultural drought vulnerability using static variables (Serkendiz et al., 2023), but this analysis proposed a novel method to harmonize temporal information from long-term drought and socioeconomic conditions. This temporal dimension enables the detection of shifts in vulnerability patterns, offering valuable insights into how drought resilience evolves in response to changing environmental and economic conditions. Also, this study used an objective weighting method to assign weights to each vulnerability component instead of equal weights. Given the specific vulnerability components and data characteristics, equal weight may not be sufficient to retrieve meaningful vulnerability assessments. This is the first detailed and multidimensional analysis of agricultural drought vulnerability in the Central Highlands of Vietnam, considering various drought indices and socioeconomic factors. The findings of this study highlighted the dominant influence of drought exposure on overall vulnerability in the region. Also, a higher adaptive capacity reduced drought vulnerability. For example, Lam Dong province had lower drought vulnerability despite higher exposure levels.

While this analysis provides valuable insights into the spatial distribution of agricultural drought vulnerability in the study region, several limitations should be acknowledged. One of the first limitations is the temporal discrepancy between the datasets. For example, drought indices in this study were monthly data from 2000 to 2022, whereas the socioeconomic data varied in duration over the study period. This mismatch may influence the overall accuracy of the drought vulnerability assessment. A more consistent time-series dataset across both dimensions would likely enhance the robustness of the findings. Another limitation is the incomplete availability of crucial variables. For example, data on irrigation practices and groundwater, a vital factor in mitigating agricultural drought impacts, was unavailable. The absence of this information restricts the comprehensiveness of the analysis. Also, there are some uncertainties in satellite-based products. For example, the land cover used in the study contains misclassification regarding its accuracy and detailed land cover types. Kuenzer et al. (2018) revealed significant differences among the global land cover products regarding their overall accuracy in the MSEA region. Given the importance of land cover in agricultural drought vulnerability assessments, any inaccuracies in rainfed

cropland can introduce errors in evaluating vulnerability. These uncertainties could, therefore, affect the accuracy of the drought vulnerability estimations in the region. A related issue is the reliability of annual water surface area in the Central Highlands. This data may represent certain periods of water surface during the year upon the availability of clear-sky collected data. The socioeconomic datasets also present challenges. These variables were spatially interpolated to ensure the spatial coverage. However, this approach may introduce variations within and between each province that do not necessarily align with ground realities. For example, it is observed that adaptive capacity component (Figure 6.6-c) exhibited a clear pattern of lower and higher ability to cope with drought along the border between Kon Tum and Gia Lai provinces. In practice, this situation may not be realistic due to their shared economic and social background. From a methodological perspective, while the PCA can effectively reduce the dimensionality of large datasets, its linear relationships between variables potentially overlook the complexity of vulnerability components. Furthermore, this study employed a data-driven approach without the participation of local stakeholders and farmers. A lack of on-the-ground surveys and localized knowledge could influence the reliability of drought vulnerability maps. Thus, future research should incorporate the local surveys and stakeholder inputs into this framework to enhance the depth of analysis and cross-validate drought vulnerability products with on-ground reports.

Last but not least, it is important to reflect on the conceptual challenges of vulnerability assessment. Vulnerability is a complex and multidimensional concept, and the choice of conceptual framework can significantly influence the outcomes. This analysis adopted the widely used IPCC concept, which defines vulnerability through three main components: exposure, sensitivity, and adaptive capacity. However, if other concepts are used, the obtained results could be slightly or substantially different. Disciplinary background could also influence the outcomes of vulnerability analysis. For instance, social scientists and hydrologists may prioritize distinct aspects of vulnerability given their experience and expertise, while economists may emphasize financial and available resources as top determinants. In our case, if a vulnerability map is undertaken by experts from other disciplinary backgrounds, they might differ from our vulnerability assessment.

6.6 Summary

This study developed a conceptual framework for agricultural drought vulnerability in the Central Highlands of Vietnam using the ICPP's vulnerability components. The PCA was used to harmonize the three components: exposure, sensitivity, and adaptive capacity from temporal drought indices and socioeconomic factors between 2000 and 2022. Agri-

cultural drought vulnerability was subsequently assessed through the proposed framework. The main findings of this study are summarized as follows:

Drought indices revealed relatively consistent temporal drought conditions but varied in severity and spatial extent. Severe droughts were detected in 2005, 2010, 2016, and 2019-2020.

The SWDI contributed nearly 72% to the exposure component among the three examined drought indices. In comparison, rural populations and rainfed crop areas were the main contributing factors to the sensitivity component among nine considered environmental and socioeconomic variables. These two variables accounted for nearly 60% of the observed variations in sensitivity components, whereas the poverty rate and workforce above 15 years explained 12% and 16%, respectively. Regarding the adaptive capacity component, social insurance, unemployment insurance rates, and high school graduates explained nearly 80% of the observed variations among the six selected variables.

Drought vulnerability in the Central Highlands of Vietnam was primarily driven by the exposure component, accounting for 65% of overall vulnerability. Higher drought exposure was found in the central areas of Dak Lak, Gia Lai, and Lam Dong provinces. Higher sensitivity was observed in Gia Lai and Kon Tum provinces, whereas higher adaptive capacity was detected in Lam Dong and Kon Tum.

The central areas of Gia Lai and Dak Nong provinces suffered from high drought vulnerability, while Lam Dong experienced primarily moderate and very low vulnerability. Other provinces witnessed low and very low vulnerability.

This study provides valuable insights into how drought vulnerability is distributed across the Central Highlands of Vietnam. This information can assist local authorities and stakeholders in mitigating potential drought impacts and planning agricultural production.

Chapter 7

Synthesis and outlook

7.1 Summary and conclusive findings

The MSEA is a major global region for agriculture and biodiversity, yet it has been increasingly vulnerable to droughts over the past decades. Drought-related hazards in the MSEA cause nearly USD 410 million in annual losses in agriculture and other economic activities (UNESCAP, 2010). These losses could threaten food security, livelihoods, and economic stability across the MSEA countries. Despite the devastating impacts of drought, there is still a lack of region-wide drought studies. Most of the drought studies in the region focus on local monitoring using limited ground-based climate data. Given the limited in-situ data and drought impacts, this dissertation aims to develop a monitoring framework for mapping drought characteristics over large areas at high spatiotemporal resolutions. Such a method enables continuous and consistent observations of drought conditions, overcoming the limitations of traditional ground-based methods. Effective drought monitoring can help optimize water resource management and reduce the negative impacts on food production, ecosystems, and regional economies. Based on satellite-based vegetation time series this dissertation presented a detailed and comprehensive analysis of drought conditions using satellite-based vegetation time series data, from a literature review to method development and drought vulnerability assessment. This section summarizes the main findings of the research, aligned with the objectives and research questions outlined in the Introduction.

Research questions 1:

- What progress has been made in monitoring drought within the study region?
- How many satellite-based drought studies have been conducted, and what are their spatiotemporal patterns?

- What types of sensors, data sources, methods, indices, and thematic applications have been employed to monitor and detect drought conditions, and how have these studies cross-validated their output drought products to ensure accuracy and reliability?
- Which research gaps exist, and how can potential remote sensing and methods address these gaps?

The first objective of this dissertation is to provide a detailed and extensive review of existing satellite-based drought literature in the Southeast Asia region, including the MSEA countries. As outlined in Chapter 3, a total of 102 satellite-based drought studies have been extracted from the Scopus and Web of Science databases over the past two decades (2000-2021). These studies were systematically analyzed to explore different dimensions, including their spatial and temporal distributions, the sensors and data used, drought indices and validation methods, thematic applications, and identifying research gaps.

The number of satellite-based drought articles in the study region significantly increased over the examined period (2000-2021), especially over the past eight years from 2 papers in 2015 to 21 papers in 2021. Vietnam and Thailand had the largest drought articles, accounting for nearly 40%. Nearly half of the articles employed optical remote sensing, while microwave remote sensing was less frequently used. Most studies focused on monitoring drought conditions using single vegetation-based or precipitation-based drought indices ($\sim$ 53%). Notably, no studies have offered spatial details of drought characteristics derived from optical sensors. Also, the application of machine learning and deep learning in drought detection to improve early warning systems and mitigation planning has received little attention. Regarding the accuracy assessment, about 22% of articles did not report cross-validation information for their drought products. While there has been a rise in time-series drought remote sensing, long-term drought measurements (e.g., $\geq$ 30 years) remain limited, highlighting the need for multi-sensor data fusion to create longer time-series observations. Also, there is a clear link between the spatial resolution of drought maps and the extent of study areas. More than half of the studies focused on local-scale drought monitoring, while nearly 64% of maps were produced at a resolution of 1 km or above. Among the drought-specific applications, agricultural and vegetative droughts received the most attention, accounting for 58% of the examined applications, whereas soil moisture and crop-specific drought monitoring remain underrepresented. Last but not least, little research has been conducted to investigate the responses of vegetation to multitemporal climate-soil drought conditions and assess drought vulnerability in the study region.

After an extensive review of existing literature, the second objective of this thesis is to develop a monitoring framework for mapping drought characteristics at a regional scale

using vegetation-based time series. Chapter 4 explored this objective in detail, and the following research questions were formulated to guide the investigation.

Research questions 2:

- What are the potentials and challenges of using satellite-based vegetation time series for monitoring and characterizing drought conditions?
- How can a drought event based on satellite-based vegetation be described using Run theory?
- What are spatiotemporal patterns of drought and their characteristics across the MSEA region from 2000 to 2022?
- Which specific years experienced severe drought, and how did drought conditions impact different land cover types during the dry and rainy seasons?
- How accurately do vegetation-based drought indicators perform compared to traditional climate-based indices?

This analysis generated a gap-free monthly VCI time series derived from MODIS-based vegetation, enabling the development of an automatic approach to identify the severe drought years and their characteristics from 2000 to 2021. Four key characteristics of drought conditions in the region have been detected, while the trend was calculated during the dry and rainy seasons. Spatiotemporal distribution of VCI-based drought conditions has been investigated at different scales and across land cover types. The key findings of this objective are summarized as follows:

Drought conditions across the MSEA region exhibited significant temporal and spatial variability. The dry season experienced more frequent and intense drought than the rainy season, especially from January to April. Rainfed crops and deciduous forests suffered the most from drought conditions. Among the MSEA countries, Vietnam has been less affected by the drought detected by the VCI in recent years, while Cambodia has faced more drought events. Rainfed crops in Laos suffered from the longest drought conditions between 2019 and 2020. Several severe drought years were identified over the study period, including 2000, 2004, 2005, 2010, 2016, 2019, and 2020.

Higher drought duration and frequency were primarily detected in Central Myanmar, Cambodia, eastern Thailand, and the Lower Mekong Delta. Central Myanmar witnessed the highest drought occurrence rate ($\sim 60\%$) from 2000 to 2021, while other countries experienced nearly 40% over the same period, except for Laos. Thailand and Vietnam experienced nearly 15 prolonged drought events over the last two decades. In recent years,

the longest drought events were primarily detected in Cambodia and Laos, whereas eastern Thailand and northern Vietnam experienced the most significant drought in the early 2000s. For example, nearly 19% of the study region suffered from long and severe drought conditions between 2019 and 2021.

Regarding the drought trends, there has been a significant increase in vegetation-based drought conditions (declining VCI) in Cambodia, parts of southern Laos, northern Myanmar, and the Vietnamese Central Highlands from 2000 to 2021. Notably, northern Vietnam and eastern Thailand experienced a wetter trend during both seasons. In contrast, Cambodia saw a significant decline in vegetation conditions, indicating its vulnerability to intense drought. Statistically, nearly 60% of Cambodia experienced a significant increase in vegetation-based drought trend over the study period. Cross-verification revealed that VCI-based drought assessments generally aligned with precipitation and temperature patterns. Stronger correlations between VCI and temperature were observed during the dry season, while precipitation deficits closely mirrored the onset of vegetation stress.

The next objective of this thesis is to assess the responses of VCI-based drought to multitemporal climate-soil drought conditions during the dry season from 2000 to 2022. This analysis also investigated the influence of climate-soil drought indices on undisturbed vegetation conditions using explainable machine learning methods. Chapter 5 was dedicated to exploring the responses of VCI to multitemporal climate-soil drought indices. The following research questions have been formulated to guide the investigation and address this objective.

Research questions 3:

- To what extent do climate and soil-based drought indicators influence vegetation-based conditions in the MSEA region, and how do these relationships vary across different land cover types and elevations?
- What are the main drivers of vegetation-based drought conditions in natural and undisturbed ecosystems in the MSEA region?

To address these research questions, this analysis calculated twelve different drought indices derived from climate-soil data between 2000 and 2022, including SPI-1, SPI-3, SPI-6, SPI-9, SPI-12, SPEI-1, SPEI-3, SPEI-6, SPEI-9, SPEI-12, SWDI, and TCI. These indices represent different drought types, including short (SPEI-1, SPI-3, SWDI, TCI), median (SPI-6, SPI-9, SPEI-6, SPEI-9), and long-term (SPI-12 and SPEI-12) drought conditions. The responses of VCI were subsequently examined using the climate-soil drought indices. Significant positive VCI-drought responses were observed across the MSEA region, primarily in Myanmar, Thailand, and Cambodia. Among the climate-soil-based drought indices,

the TCI had the highest correlation with the VCI across vegetation types and elevations (R-values = [0.56-0.85]). Considering land cover and elevations, higher VCI-drought responses were observed in lower elevation zones in rainfed cropland (R-values = [0.58-0.70]), mixed forests (R-values = [0.57-0.69]), and deciduous forests (R-values = [0.59-0.85]). Evergreen forest and irrigated crop vegetation responded less to drought indices, especially in high-elevation zones. Short-term drought disturbances accounted for nearly 93% of the observed variations in the natural and undisturbed vegetation ecosystems over the study period. SPEI-3 revealed the largest influence among the examined climate-soil drought indices, explaining approximately 35% of the observed vegetation dynamics, followed by the TCI ($\sim$ 20%). In this regard, the analysis indicated that TCI and SPEI-3 can positively impact 20-25% of VCI values under the wettest conditions. Conversely, a decline of approximately 15% in VCI units was observed during the driest conditions between 2000 and 2022.

The final objective of this dissertation is to integrate the data generated from previous chapters with socioeconomic data to assess agricultural drought vulnerability in a drought-prone region of Vietnam. This assessment used the IPCC vulnerability framework, focusing on three key components: exposure, sensitivity, and adaptive capacity. The exposure component concerns the physical conditions of drought (three drought indices and their characteristics), while sensitivity and adaptive capacity consider 16 environmental and socioeconomic factors (nine variables for sensitivity and seven for adaptive capacity). Exposure data spans from 2000 to 2022, while environmental and socioeconomic data exhibit temporal variability. The PCA was used to harmonize temporal data corresponding to each component. Subsequently, the weightings of each component were calculated using the Shannon entropy method before deriving agricultural drought vulnerability. Chapter 6 was dedicated to assessing agricultural drought vulnerability, and the following research questions have been formulated to address this objective.

Research questions 4:

- What is the vulnerability framework outlined by the Intergovernmental Panel on Climate Change (IPCC), and how is it applied in the context of agricultural drought?
- Which variables are most appropriate for assessing agricultural drought vulnerability, and how should they be assigned to each vulnerability component (exposure, sensitivity, and adaptive capacity)?
- What methods are used to harmonize temporal remote sensing data with socioeconomic time series for a detailed drought vulnerability assessment?
- To what extent does each variable contribute to the respective components of agricultural drought vulnerability?

- What are the spatial patterns of agricultural drought vulnerability, and where are the identified drought hotspots in the region?

According to the IPCC's vulnerability framework, agricultural drought vulnerability is designed to comprise exposure, sensitivity, and adaptive capacity components. In the Central Highlands of Vietnam, the SWDI contributed nearly 72% to the exposure component among the three examined drought indices (VCI, SPEI, and SWDI) from 2000 to 2022, indicating the dominant role of soil moisture in assessing drought vulnerability in the study region. In comparison, rural populations and rainfed crop areas were the main contributing factors to the sensitivity component among nine considered environmental and socioeconomic variables. These two variables accounted for nearly 60% of the observed variations in sensitivity components, whereas the poverty rate and workforce above 15 years explained 12% and 16%, respectively. Regarding the adaptive capacity component, social insurance, unemployment insurance rates, and high school graduates explained nearly 80% of the observed variations among the six selected variables.

The exposure component largely drove agricultural drought vulnerability in the Central Highlands of Vietnam, accounting for 65% of the overall vulnerability. Overall, nearly 9% of the Central Highlands suffered from high to very high drought vulnerability, while moderate vulnerability covered about 18% of the study region. Higher drought vulnerability was concentrated in the central areas of Dak Lak and Gia Lai provinces. These areas also corresponded to higher drought exposure and sensitivity. Lam Dong province experienced less drought vulnerability despite its higher exposure due to lower sensitivity and higher adaptive capacity. Other provinces in the region displayed low to very low drought vulnerability.

7.2 Outlook for future research

As global warming intensifies and human activities continue to accelerate, the frequency and severity of droughts and other extreme climate events are projected to rise across many regions worldwide, including the MSEA countries. Since agriculture is the cornerstone of the MSEA economies, drought poses significant risks to this sector. Drought usually spans vast areas and transcends political and geographical boundaries. Therefore, robust, consistent, and continuous drought monitoring and characterization are essential to inform regional drought risk management, strengthen early warning systems, and ensure agricultural resilience and food security.

Given the current monitoring framework and analysis, several aspects of future research can be further performed. The current analysis derived drought characteristics from VCI-

based indicators, but other vegetation-based indices can hold potential and accurately capture drought dynamics. Further studies are required to evaluate these indices and enhance the transferability of this framework. In addition, the responses of VCI-based conditions to multitemporal climate-soil drought indices have not yet considered other hydrological and teleconnections, such as streamflow and sea surface temperature. The inclusion of such data could enable the analysis of the influence of large-scale teleconnections and streamflow on vegetation-based drought conditions. Furthermore, human activities play a dominant role in vegetation and agricultural growth in addition to droughts. A lack of a time series of anthropogenic factors in the MSEA region makes it challenging to conduct vegetation-drought-anthropogenic analysis. This could be a potential area of future research. Another potential aspect that requires further studies is assessing the vulnerability of agricultural droughts. For example, groundwater and irrigated data should be included in the analysis to enhance reliability further. Although this assessment provides practical and more immediate impacts on agricultural planning and policies, they are often overlooked in the region. This framework could be upscaled to other drought-prone regions across the MSEA countries.

Although producing high-spatial-resolution drought data on a daily, weekly, or submonthly basis may not be achievable using a single sensor alone, integrating multiple sensor platforms offers a promising solution. This dissertation primarily used MODIS time series data from 2000 to 2022. However, drought monitoring and characterization often require a longer time series of data (e.g., $\geq$ 30 years). Integrating the MODIS data with other missions, such as AVHRR, would provide long-term historical data for robust drought understanding. Despite their less frequent data acquisition, the growing availability of Landsat and Sentinel-2 data provides high-resolution spatial observations of drought conditions. Harmonizing these products creates an excellent opportunity for high spatial and temporal resolution. Recent satellite missions, such as SMAP, also offer the potential to monitor soil moisture drought daily and weekly. Integrating these datasets will provide critical, comprehensive insights for effectively monitoring and characterizing drought.

Another aspect of further research is developing a tailored drought indicator in the MSEA region. Drought is a multifaceted phenomenon influenced by different factors, including climatic variability, soil moisture, vegetation health, water resources, and human activities. It is essential to develop a composite drought index that integrates these elements. Such an indicator also accounts for monsoonal patterns, land use practices, and topographical variations. Deep learning and machine learning has been rarely applied to monitor and forecast drought in the MSEA region, despite their potential and popularity in other fields of study. Future studies should explore this topic to better understand and forecast real-time droughts for early warning systems in the region. Last but not least, flash droughts are de-

veloping fast and causing devastating threats to agriculture and vegetation ecosystems. Due to their sudden onset and intensity, flash droughts can cause significant damage before traditional monitoring systems detect them. Therefore, future research should develop more responsive methods for real-time monitoring of flash droughts and assessing their short- and long-term impacts.

Bibliography

Abhishek, A., Das, N.N., Ines, A.V., Andreadis, K.M., Jayasinghe, S., Granger, S., Ellenburg, W.L., Dutta, R., Quyen, N.H., Markert, A.M., et al., 2021. Evaluating the impacts of drought on rice productivity over cambodia in the lower mekong basin. Journal of Hydrology 599, 126291.

Adamson, P., 2005. Drought study: analysis, forecasting, planning and management. Mekong River Commission, Vientiane, Laos .

AghaKouchak, A., Farahmand, A., Melton, F.S., Teixeira, J., Anderson, M.C., Wardlow, B.D., Hain, C.R., 2015. Remote sensing of drought: Progress, challenges and opportunities. Reviews of Geophysics 53, 452–480.

Ahsan, M.N., Warner, J., 2014. The socioeconomic vulnerability index: A pragmatic approach for assessing climate change led risks–a case study in the south-western coastal bangladesh. International Journal of Disaster Risk Reduction 8, 32–49.

Aires, F., Venot, J.P., Massuel, S., Gratiot, N., Pham-Duc, B., Prigent, C., 2020. Surface water evolution (2001–2017) at the cambodia/vietnam border in the upper mekong delta using satellite modis observations. Remote Sensing 12, 800.

Alley, W.M., 1984. The palmer drought severity index: limitations and assumptions. Journal of climate and applied meteorology , 1100–1109.

Almazroui, M., Saeed, S., Saeed, F., Islam, M.N., Ismail, M., 2020. Projections of precipitation and temperature over the south asian countries in cmip6. Earth Systems and Environment 4, 297–320.

Amalo, L.F., Hidayat, R., Sulma, S., 2017. Analysis of agricultural drought in east java using vegetation health index. AGRIVITA, Journal of Agricultural Science 40, 63–73.

Amnuaylojaroen, T., Chanvichit, P., 2019. Projection of near-future climate change and agricultural drought in mainland southeast asia under rcp8. 5. Climatic Change 155, 175–193.

Anderson, W., Taylor, C., McDermid, S., Ilboudo-Nébié, E., Seager, R., Schlenker, W., Cottier, F., De Sherbinin, A., Mendeloff, D., Markey, K., 2021. Violent conflict exacerbated drought-related food insecurity between 2009 and 2019 in sub-saharan africa. Nature Food 2, 603–615.

Arjasakusuma, S., Yamaguchi, Y., Hirano, Y., Zhou, X., 2018. Enso-and rainfall-sensitive vegetation regions in indonesia as identified from multi-sensor remote sensing data. ISPRS International Journal of Geo-Information 7, 103.

Bajgiran, P.R., Darvishsefat, A.A., Khalili, A., Makhdoum, M.F., 2008. Using avhrr-based vegetation indices for drought monitoring in the northwest of iran. Journal of Arid Environments 72, 1086–1096.

Bank, W., 2023. Thailand Poverty Brief. Technical Report. World Bank.

Bank, W., 2024. World Bank in Cambodia. Technical Report. World Bank.

Barlow, M., Zaitchik, B., Paz, S., Black, E., Evans, J., Hoell, A., 2016. A review of drought in the middle east and southwest asia. Journal of climate 29, 8547–8574.

Baumbach, L., Siegmund, J.F., Mittermeier, M., Donner, R.V., 2017. Impacts of temperature extremes on european vegetation during the growing season. Biogeosciences 14, 4891–4903.

Berhail, S., Katipoğlu, O.M., 2023. Comparison of the spi and spei as drought assessment tools in a semi-arid region: case of the wadi mekerra basin (northwest of algeria). Theoretical and Applied Climatology 154, 1373–1393.

Berry, P., Garlick, J., Smith, R., 2007. Near-global validation of the srtm dem using satellite radar altimetry. Remote Sensing of Environment 106, 17–27.

Bisquert, M., Bégué, A., Deshayes, M., Ducrot, D., 2017. Environmental evaluation of modis-derived land units. GIScience & Remote Sensing 54, 64–77.

Blauhut, V., Stahl, K., Stagge, J.H., Tallaksen, L.M., De Stefano, L., Vogt, J., 2016. Estimating drought risk across europe from reported drought impacts, drought indices, and vulnerability factors. Hydrology and Earth System Sciences 20, 2779–2800.

Bontemps, S., Defourny, P., Brockmann, C., Herold, M., Kalogirou, V., Arino, O., 2012. New global land cover mapping exercise in the framework of the esa climate change initiative, in: 2012 IEEE international geoscience and remote sensing symposium, IEEE. pp. 44–47.

Branco, E.R.F., Dos Santos, A.R., Pezzopane, J.E.M., Dos Santos, A.B., Alexandre, R.S., Bernardes, V.P., da Silva, R.G., de Souza, K.B., Moura, M.M., 2019. Space-time analysis of vegetation trends and drought occurrence in domain area of tropical forest. Journal of Environmental Management 246, 384–396.

Breiman, L., 2001. Random forests. Machine learning 45, 5–32.

Brown, P.R., Yee, N., Singleton, G.R., Kenney, A.J., Htwe, N.M., Myint, M., Aye, T., 2008. Farmers' knowledge, attitudes, and practices for rodent management in myanmar. International Journal of Pest Management 54, 69–76.

Byrareddy, V., Kouadio, L., Mushtaq, S., Kath, J., Stone, R., 2021. Coping with drought: Lessons learned from robusta coffee growers in vietnam. Climate Services 22, 100229.

Cao, R., Chen, Y., Shen, M., Chen, J., Zhou, J., Wang, C., Yang, W., 2018. A simple method to improve the quality of ndvi time-series data by integrating spatiotemporal information with the savitzky-golay filter. Remote Sensing of Environment 217, 244–257.

Cao, S., Zhang, L., He, Y., Zhang, Y., Chen, Y., Yao, S., Yang, W., Sun, Q., 2022. Effects and contributions of meteorological drought on agricultural drought under different climatic zones and vegetation types in northwest china. Science of the Total Environment 821, 153270.

Carrão, H., Naumann, G., Barbosa, P., 2016. Mapping global patterns of drought risk: An empirical framework based on sub-national estimates of hazard, exposure and vulnerability. Global Environmental Change 39, 108–124.

CCI, E.L.C., 2017. Product user guide version 2.0. UCL-Geomatics: London, UK .

Chen, A., Liu, J., Kummu, M., Varis, O., Tang, Q., Mao, G., Wang, J., Chen, D., 2021a. Multidecadal variability of the tonle sap lake flood pulse regime. Hydrological Processes 35, e14327.

Chen, C.F., Son, N.T., Chang, L.Y., Chen, C.C., 2011. Monitoring of soil moisture variability in relation to rice cropping systems in the vietnamese mekong delta using modis data. Applied Geography 31, 463–475.

Chen, J., Jönsson, P., Tamura, M., Gu, Z., Matsushita, B., Eklundh, L., 2004. A simple method for reconstructing a high-quality ndvi time-series data set based on the savitzky–golay filter. Remote sensing of Environment 91, 332–344.

Chen, S., Olofsson, P., Saphangthong, T., Woodcock, C.E., 2023. Monitoring shifting cultivation in laos with landsat time series. Remote Sensing of Environment 288, 113507.

Chen, Y., Cao, R., Chen, J., Liu, L., Matsushita, B., 2021b. A practical approach to reconstruct high-quality landsat ndvi time-series data by gap filling and the savitzky–golay filter. ISPRS Journal of Photogrammetry and Remote Sensing 180, 174–190.

Chuah, C.J., Ho, B.H., Chow, W.T., 2018. Trans-boundary variations of urban drought vulnerability and its impact on water resource management in singapore and johor, malaysia. Environmental Research Letters 13, 074011.

Ciemer, C., Boers, N., Hirota, M., Kurths, J., Müller-Hansen, F., Oliveira, R.S., Winkelmann, R., 2019. Higher resilience to climatic disturbances in tropical vegetation exposed to more variable rainfall. Nature Geoscience 12, 174–179.

Cislaghi, A., Giupponi, L., Tamburini, A., Giorgi, A., Bischetti, G.B., 2019. The effects of mountain grazing abandonment on plant community, forage value and soil properties: observations and field measurements in an alpine area. Catena 181, 104086.

Claverie, M., Ju, J., Masek, J.G., Dungan, J.L., Vermote, E.F., Roger, J.C., Skakun, S.V., Justice, C., 2018. The harmonized landsat and sentinel-2 surface reflectance data set. Remote sensing of environment 219, 145–161.

Couturier, S., Taylor, D., Siegert, F., Hoffmann, A., Bao, M., 2001. Ers sar backscatter: a potential real-time indicator of the proneness of modified rainforests to fire. Remote Sensing of Environment 76, 410–417.

Crausbay, S.D., Betancourt, J., Bradford, J., Cartwright, J., Dennison, W.C., Dunham, J., Enquist, C.A., Frazier, A.G., Hall, K.R., Littell, J.S., et al., 2020. Unfamiliar territory: Emerging themes for ecological drought research and management. One Earth 3, 337–353.

Curtis, P.G., Slay, C.M., Harris, N.L., Tyukavina, A., Hansen, M.C., 2018. Classifying drivers of global forest loss. Science 361, 1108–1111.

Dalezios, N.R., Dunkel, Z., Eslamian, S., 2017. Meteorological drought indices: definitions, in: Handbook of drought and water scarcity. CRC Press, pp. 27–44.

Damberg, L., AghaKouchak, A., 2014. Global trends and patterns of drought from space. Theoretical and applied climatology 117, 441–448.

Dandridge, C., Lakshmi, V., Bolten, J., Srinivasan, R., 2019. Evaluation of satellite-based rainfall estimates in the lower mekong river basin (southeast asia). Remote Sensing 11, 2709.

Dang, T., Yue, P., Bachofer, F., Wang, M., Zhang, M., 2020. Monitoring land surface temperature change with landsat images during dry seasons in bac binh, vietnam. Remote Sensing 12, 4067.

De Jong, W., 2010. Forest rehabilitation and its implication for forest transition theory. Biotropica 42, 3–9.

Dhawale, R., Wallace, C.S., Pietroniro, A., 2024. Assessing the multidimensional nature of flood and drought vulnerability index: A systematic review of literature. International Journal of Disaster Risk Reduction , 104764.

Didan, K., 2021. MODIS/Terra Vegetation Indices 16-Day L3 Global 1km SIN Grid V061. NASA EOSDIS Land Processes DAAC. Technical Report. Accessed 2022-07-27 from https://doi. org/10.5067/MODIS/MOD13A2. 061.

Didan, K., Munoz, A.B., Solano, R., Huete, A., et al., 2015. Modis vegetation index user's guide (mod13 series). University of Arizona: Vegetation Index and Phenology Lab 35, 2–33.

Dimyati, M., Rustanto, A., Shidiq, I.P.A., Indratmoko, S., Dimyati, R.D., Nurlambang, T., Zubair, A., Fakhruddin, A., Siddiq, A., Adhanto, D.H., et al., 2024. Spatiotemporal relation of satellite-based meteorological to agricultural drought in the downstream citarum watershed, indonesia. Environmental and Sustainability Indicators 22, 100339.

Du, T.L.T., Bui, D.D., Nguyen, M.D., Lee, H., 2018. Satellite-based, multi-indices for evaluation of agricultural droughts in a highly dynamic tropical catchment, central vietnam. Water 10, 659.

Duan, S.B., Li, Z.L., Li, H., Göttsche, F.M., Wu, H., Zhao, W., Leng, P., Zhang, X., Coll, C., 2019. Validation of collection 6 modis land surface temperature product using in situ measurements. Remote sensing of environment 225, 16–29.

Dutta, D., Kundu, A., Patel, N., Saha, S., Siddiqui, A., 2015. Assessment of agricultural drought in rajasthan (india) using remote sensing derived vegetation condition index (vci) and standardized precipitation index (spi). The Egyptian Journal of Remote Sensing and Space Science 18, 53–63.

Elkouk, A., Pokhrel, Y., Satoh, Y., Bouchaou, L., 2022. Implications of changes in climate and human development on 21st-century global drought risk. Journal of Environmental Management 317, 115378.

Erban, L.E., Gorelick, S.M., 2016. Closing the irrigation deficit in cambodia: Implications for transboundary impacts on groundwater and mekong river flow. Journal of Hydrology 535, 85–92.

ERCD-FAO, 2017. Oecd-fao agricultural outlook 2017–2026. ERCD-FAO Agricultural Outlook: Rome, Italy 2026.

Erian, W., Pulwarty, R., Vogt, J., AbuZeid, K., Bert, F., Bruntrup, M., El-Askary, H., de Estrada, M., Gaupp, F., Grundy, M., et al., 2021. GAR special report on drought 2021. United Nations Office for Disaster Risk Reduction (UNDRR).

Esfahanian, E., Nejadhashemi, A.P., Abouali, M., Adhikari, U., Zhang, Z., Daneshvar, F., Herman, M.R., 2017. Development and evaluation of a comprehensive drought index. Journal of environmental management 185, 31–43.

Fan, F., Xiao, C., Feng, Z., Yang, Y., 2023. Impact of human and climate factors on vegetation changes in mainland southeast asia and yunnan province of china. Journal of Cleaner Production 415, 137690.

Fang, B., Kansara, P., Dandridge, C., Lakshmi, V., 2021. Drought monitoring using high spatial resolution soil moisture data over australia in 2015–2019. Journal of Hydrology 594, 125960.

Fang, J., Piao, S., Zhou, L., He, J., Wei, F., Myneni, R.B., Tucker, C.J., Tan, K., 2005. Precipitation patterns alter growth of temperate vegetation. Geophysical research letters 32.

Fang, W., Huang, S., Huang, Q., Huang, G., Wang, H., Leng, G., Wang, L., Guo, Y., 2019. Probabilistic assessment of remote sensing-based terrestrial vegetation vulnerability to drought stress of the loess plateau in china. Remote Sensing of Environment 232, 111290.

Fanin, T., Van Der Werf, G.R., 2017. Precipitation–fire linkages in indonesia (1997–2015). Biogeosciences 14, 3995–4008.

Fathi-Taperasht, A., Shafizadeh-Moghadam, H., Sadian, A., Xu, T., Nikoo, M.R., 2023. Drought-induced vulnerability and resilience of different land use types using time series of modis-based indices. International Journal of Disaster Risk Reduction 91, 103703.

Feng, W., Lu, H., Yao, T., Yu, Q., 2020. Drought characteristics and its elevation dependence in the qinghai–tibet plateau during the last half-century. Scientific Reports 10, 14323.

Fensholt, R., Rasmussen, K., Nielsen, T.T., Mbow, C., 2009. Evaluation of earth observation based long term vegetation trends—intercomparing ndvi time series trend analysis consistency of sahel from avhrr gimms, terra modis and spot vgt data. Remote sensing of environment 113, 1886–1898.

Field, R.D., Van Der Werf, G.R., Shen, S.S., 2009. Human amplification of drought-induced biomass burning in indonesia since 1960. Nature Geoscience 2, 185–188.

Fok, H.S., He, Q., Chun, K.P., Zhou, Z., Chu, T., 2018. Application of enso and drought indices for water level reconstruction and prediction: A case study in the lower mekong river estuary. Water 10, 58.

Frappart, F., Biancamaria, S., Normandin, C., Blarel, F., Bourrel, L., Aumont, M., Azemar, P., Vu, P.L., Le Toan, T., Lubac, B., et al., 2018. Influence of recent climatic events on the surface water storage of the tonle sap lake. Science of the Total Environment 636, 1520–1533.

Fridell, G., 2014. Fair trade slippages and vietnam gaps: the ideological fantasies of fair trade coffee. Third World Quarterly 35, 1179–1194.

Fuller, D.O., Jessup, T.C., Salim, A., 2004. Loss of forest cover in kalimantan, indonesia, since the 1997–1998 el nino. Conservation Biology 18, 249–254.

Funk, C., Peterson, P., Landsfeld, M., Pedreros, D., Verdin, J., Shukla, S., Husak, G., Rowland, J., Harrison, L., Hoell, A., et al., 2015. The climate hazards infrared precipitation with stations—a new environmental record for monitoring extremes. Scientific data 2, 1–21.

Füssel, H.M., Klein, R.J., 2006. Climate change vulnerability assessments: an evolution of conceptual thinking. Climatic change 75, 301–329.

Gajbhiye, S., Meshram, C., Mirabbasi, R., Sharma, S., 2016. Trend analysis of rainfall time series for sindh river basin in india. Theoretical and applied climatology 125, 593–608.

Gerke, S., Evers, H.D., 2006. Globalizing local knowledge: Social science research on southeast asia, 1970-2000. SOJOURN: Journal of social issues in Southeast Asia , 1–21.

Gessner, U., Machwitz, M., Esch, T., Tillack, A., Naeimi, V., Kuenzer, C., Dech, S., 2015. Multi-sensor mapping of west african land cover using modis, asar and tandem-x/terrasar-x data. Remote Sensing of Environment 164, 282–297.

Gorelick, N., Hancher, M., Dixon, M., Ilyushchenko, S., Thau, D., Moore, R., 2017. Google earth engine: Planetary-scale geospatial analysis for everyone. Remote sensing of Environment 202, 18–27.

Goward, S.N., Markham, B., Dye, D.G., Dulaney, W., Yang, J., 1991. Normalized difference vegetation index measurements from the advanced very high resolution radiometer. Remote sensing of environment 35, 257–277.

Greenacre, M., Groenen, P.J., Hastie, T., d'Enza, A.I., Markos, A., Tuzhilina, E., 2022. Principal component analysis. Nature Reviews Methods Primers 2, 100.

Grogan, K., Pflugmacher, D., Hostert, P., Kennedy, R., Fensholt, R., 2015. Cross-border forest disturbance and the role of natural rubber in mainland southeast asia using annual landsat time series. Remote Sensing of Environment 169, 438–453.

Gu, Y., Brown, J.F., Verdin, J.P., Wardlow, B., 2007. A five-year analysis of modis ndvi and ndwi for grassland drought assessment over the central great plains of the united states. Geophysical research letters 34.

Gu, Z., Zhang, Y., Fan, H., 2021. Mapping inter-and intra-annual dynamics in water surface area of the tonle sap lake with landsat time-series and water level data. Journal of Hydrology 601, 126644.

Güçlü, Y.S., 2018. Multiple şen-innovative trend analyses and partial mann-kendall test. Journal of Hydrology 566, 685–704.

Guo, H., Bao, A., Liu, T., Ndayisaba, F., He, D., Kurban, A., De Maeyer, P., 2017. Meteorological drought analysis in the lower mekong basin using satellite-based long-term chirps product. Sustainability 9, 901.

Guo, H., Bao, A., Liu, T., Ndayisaba, F., Jiang, L., Kurban, A., De Maeyer, P., et al., 2018a. Spatial and temporal characteristics of droughts in central asia during 1966–2015. Science of the total environment 624, 1523–1538.

Guo, H., Bao, A., Ndayisaba, F., Liu, T., Jiapaer, G., El-Tantawi, A.M., De Maeyer, P., 2018b. Space-time characterization of drought events and their impacts on vegetation in central asia. Journal of Hydrology 564, 1165–1178.

Guo, P., Zhao, X., Shi, J., Huang, J., Tang, J., Zhang, R., Chen, J., Wang, Q., Zeng, J., 2021. The influence of temperature and precipitation on the vegetation dynamics of the tropical island of hainan. Theoretical and Applied Climatology 143, 429–445.

Gutman, G., Csiszar, I., Romanov, P., 2000. Using noaa/avhrr products to monitor el nino impacts: focus on indonesia in 1997–98. Bulletin of the American Meteorological Society 81, 1189–1206.

Ha, T.V., Huth, J., Bachofer, F., Kuenzer, C., 2022. A review of earth observation-based drought studies in southeast asia. Remote sensing 14, 3763.

Ha, T.V., Uereyen, S., Kuenzer, C., 2023. Agricultural drought conditions over mainland southeast asia: Spatiotemporal characteristics revealed from modis-based vegetation time-series. International Journal of Applied Earth Observation and Geoinformation 121, 103378.

Ha, T.V., Uereyen, S., Kuenzer, C., 2024. Spatiotemporal analysis of tropical vegetation ecosystems and their responses to multifaceted droughts in mainland southeast asia using satellite-based time series. GIScience & Remote Sensing 61, 2387385.

Hansen, M.C., Potapov, P.V., Moore, R., Hancher, M., Turubanova, S.A., Tyukavina, A., Thau, D., Stehman, S.V., Goetz, S.J., Loveland, T.R., et al., 2013. High-resolution global maps of 21st-century forest cover change. science 342, 850–853.

Hao, C., Zhang, J., Yao, F., 2015. Combination of multi-sensor remote sensing data for drought monitoring over southwest china. International Journal of Applied Earth Observation and Geoinformation 35, 270–283.

Hengl, T., 2018. Clay content in%(kg/kg) at 6 standard depths (0, 10, 30, 60, 100 and 200 cm) at 250 m resolution (v0. 2)[data set]. Zenodo .

Herridge, D.F., Win, M.M., Nwe, K.M.M., Kyu, K.L., Win, S.S., Shwe, T., Min, Y.Y., Denton, M.D., Cornish, P.S., 2019. The cropping systems of the central dry zone of myanmar: Productivity constraints and possible solutions. Agricultural Systems 169, 31–40.

Hersbach, H., Bell, B., Berrisford, P., Hirahara, S., Horányi, A., Muñoz-Sabater, J., Nicolas, J., Peubey, C., Radu, R., Schepers, D., et al., 2020. The era5 global reanalysis. Quarterly Journal of the Royal Meteorological Society 146, 1999–2049.

Heydari Alamdarloo, E., Khosravi, H., Nasabpour, S., Gholami, A., 2020. Assessment of drought hazard, vulnerability and risk in iran using gis techniques. j arid land 12: 984–1000.

Hidayat, H., Teuling, A.J., Vermeulen, B., Taufik, M., Kastner, K., Geertsema, T.J., Bol, D.C., Hoekman, D.H., Haryani, G.S., Van Lanen, H.A., et al., 2017. Hydrology of inland tropical lowlands: The kapuas and mahakam wetlands. Hydrology and earth system sciences 21, 2579–2594.

Hien, L.T.T., Gobin, A., Huong, P.T.T., 2019. Spatial indicators for desertification in southeast vietnam. Natural Hazards and Earth System Sciences 19, 2325–2337.

Hinkel, J., 2011. "indicators of vulnerability and adaptive capacity": towards a clarification of the science–policy interface. Global environmental change 21, 198–208.

Hoque, M.A.A., Pradhan, B., Ahmed, N., 2020. Assessing drought vulnerability using geospatial techniques in northwestern part of bangladesh. Science of the Total Environment 705, 135957.

Horion, S., Fensholt, R., Tagesson, T., Ehammer, A., 2014. Using earth observation-based dry season ndvi trends for assessment of changes in tree cover in the sahel. International Journal of Remote Sensing 35, 2493–2515.

Huang, S., Li, P., Huang, Q., Leng, G., Hou, B., Ma, L., 2017. The propagation from meteorological to hydrological drought and its potential influence factors. Journal of Hydrology 547, 184–195.

Ionescu, C., Klein, R.J., Hinkel, J., Kavi Kumar, K., Klein, R., 2009. Towards a formal framework of vulnerability to climate change. Environmental Modeling & Assessment 14, 1–16.

Jeefoo, P., 2023. Thai eastern economic corridor drought monitoring using terra/modis satellite-based data. Geographia Technica 18.

Jeganathan, C., Dash, J., Atkinson, P., 2014. Remotely sensed trends in the phenology of northern high latitude terrestrial vegetation, controlling for land cover change and vegetation type. Remote sensing of Environment 143, 154–170.

Ji, L., Peters, A.J., 2003. Assessing vegetation response to drought in the northern great plains using vegetation and drought indices. Remote sensing of Environment 87, 85–98.

Jiang, T., Su, X., Singh, V.P., Zhang, G., 2021. A novel index for ecological drought monitoring based on ecological water deficit. Ecological Indicators 129, 107804.

Jiao, W., Wang, L., McCabe, M.F., 2021. Multi-sensor remote sensing for drought characterization: current status, opportunities and a roadmap for the future. Remote Sensing of Environment 256, 112313.

Jing, W., Zhao, X., Yao, L., Jiang, H., Xu, J., Yang, J., Li, Y., 2020. Variations in terrestrial water storage in the lancang-mekong river basin from grace solutions and land surface model. Journal of Hydrology 580, 124258.

Jomsrekrayom, N., Meena, P., Laosuwan, T., 2021. Spatiotemporal analysis of vegetation drought variability in the middle of the northeast region of thailand using terra/modis satellite data. Geographia Technica 16.

de Jong, R., de Bruin, S., 2012. Linear trends in seasonal vegetation time series and the modifiable temporal unit problem. Biogeosciences 9, 71–77.

Kafy, A.A., Bakshi, A., Saha, M., Al Faisal, A., Almulhim, A.I., Rahaman, Z.A., Mohammad, P., 2023. Assessment and prediction of index based agricultural drought vulnerability using machine learning algorithms. Science of The Total Environment 867, 161394.

Kendall, M.G., 1948. Rank correlation methods. .

Khadka, D., Babel, M.S., Shrestha, S., Virdis, S.G., Collins, M., 2021. Multivariate and multi-temporal analysis of meteorological drought in the northeast of thailand. Weather and climate extremes 34, 100399.

Khadka, D., Babel, M.S., Tingsanchali, T., Penny, J., Djordjevic, S., Abatan, A.A., Giardino, A., 2024. Evaluating the impacts of climate change and land-use change on future droughts in northeast thailand. Scientific Reports 14, 9746.

Khalil, A., 2020. Drought characterization in the mae klong river basin, thailand, using standardized precipitation index. Arabian Journal of Geosciences 13, 680.

Khampeera, A., Yongchalermchai, C., Techato, K., 2018. Drought monitoring using drought indices and gis techniques in kuan kreng peat swamp, southern thailand. Walailak Journal of Science and Technology (WJST) 15, 357–370.

Knauer, K., Gessner, U., Dech, S., Kuenzer, C., 2014. Remote sensing of vegetation dynamics in west africa. International Journal of Remote Sensing 35, 6357–6396.

Kogan, F., Stark, R., Gitelson, A., Jargalsaikhan, L., Dugrajav, C., Tsooj, S., 2004. Derivation of pasture biomass in mongolia from avhrr-based vegetation health indices. International Journal of Remote Sensing 25, 2889–2896.

Kogan, F.N., 1990. Remote sensing of weather impacts on vegetation in non-homogeneous areas. International Journal of remote sensing 11, 1405–1419.

Kogan, F.N., 1995a. Application of vegetation index and brightness temperature for drought detection. Advances in space research 15, 91–100.

Kogan, F.N., 1995b. Droughts of the late 1980s in the united states as derived from noaa polar-orbiting satellite data. Bulletin of the American Meteorological Society 76, 655–668.

Kuenzer, C., Leinenkugel, P., Vollmuth, M., Dech, S., 2018. Comparing global land-cover products–implications for geoscience applications: an investigation for the trans-boundary mekong basin, in: Remote Sensing the Mekong. Routledge, pp. 6–33.

Kundu, B., Rana, N.K., Kundu, S., 2024. Enhancing drought resilience: machine learning–based vulnerability assessment in uttar pradesh, india. Environmental Science and Pollution Research , 1–18.

Kuswanto, H., Naufal, A., 2019. Evaluation of performance of drought prediction in indonesia based on trmm and merra-2 using machine learning methods. MethodsX 6, 1238–1251.

Laimighofer, J., Laaha, G., 2022. How standard are standardized drought indices? uncertainty components for the spi and spei case. Journal of Hydrology 613, 128385.

Lakshmi, V., Le, M.H., Goffin, B.D., Besnier, J., Pham, H.T., Do, H.X., Fang, B., Mohammed, I., Bolten, J.D., 2023. Regional analysis of the 2015–16 lower mekong river basin drought using nasa satellite observations. Journal of Hydrology: Regional Studies 46, 101362.

Laosuwan, T., Sangpradid, S., Gomasathit, T., Rotjanakusol, T., et al., 2016. Application of remote sensing technology for drought monitoring in mahasarakham province, thailand. International Journal of Geoinformatics 12, 17–25.

Le, M.H., Kim, H., Moon, H., Zhang, R., Lakshmi, V., Nguyen, L.B., 2020a. Assessment of drought conditions over vietnam using standardized precipitation evapotranspiration index, merra-2 re-analysis, and dynamic land cover. Journal of Hydrology: Regional Studies 32, 100767.

Le, M.H., Lakshmi, V., Bolten, J., Du Bui, D., 2020b. Adequacy of satellite-derived precipitation estimate for hydrological modeling in vietnam basins. Journal of Hydrology 586, 124820.

Le, M.H., Nguyen, B.Q., Pham, H.T., Patil, A., Do, H.X., Ramsankaran, R., Bolten, J.D., Lakshmi, V., 2022. Assimilation of smap products for improving streamflow simulations over tropical climate region—is spatial information more important than temporal information? Remote Sensing 14, 1607.

Le, P.V., Phan-Van, T., Mai, K.V., Tran, D.Q., 2019. Space–time variability of drought over vietnam. International Journal of Climatology 39, 5437–5451.

Le Huy, B., Le, H., Xuan, H.N., 2022. The harmful effect of the hydro-electric dams upstream of the mekong river: Effect on the ecosystems and livelihoods of people in mekong delta, vietnam. Water Conservation Science and Engineering , 1–20.

Lee, S.K., Dang, T.A., 2019. Spatio-temporal variations in meteorology drought over the mekong river delta of vietnam in the recent decades. Paddy and Water Environment 17, 35–44.

Li, J., Bevacqua, E., Chen, C., Wang, Z., Chen, X., Myneni, R.B., Wu, X., Xu, C.Y., Zhang, Z., Zscheischler, J., 2022a. Regional asymmetry in the response of global vegetation growth to springtime compound climate events. Communications Earth & Environment 3, 123.

Li, P., Feng, Z., Xiao, C., 2018a. Acquisition probability differences in cloud coverage of the available landsat observations over mainland southeast asia from 1986 to 2015. International Journal of Digital Earth 11, 437–450.

Li, T., Angeles, O., Radanielson, A., Marcaida, M., Manalo, E., 2015. Drought stress impacts of climate change on rainfed rice in south asia. Climatic Change 133, 709–720.

Li, W., MacBean, N., Ciais, P., Defourny, P., Lamarche, C., Bontemps, S., Houghton, R.A., Peng, S., 2018b. Gross and net land cover changes in the main plant functional types derived from the annual esa cci land cover maps (1992–2015). Earth System Science Data 10, 219–234.

Li, Y., Lu, H., Entekhabi, D., Gianotti, D.J.S., Yang, K., Luo, C., Feldman, A.F., Wang, W., Jiang, R., 2022b. Satellite-based assessment of meteorological and agricultural drought in mainland southeast asia. IEEE Journal of Selected Topics in Applied Earth Observations and Remote Sensing 15, 6180–6189.

Li, Z., Huffman, T., McConkey, B., Townley-Smith, L., 2013. Monitoring and modeling spatial and temporal patterns of grassland dynamics using time-series modis ndvi with climate and stocking data. Remote Sensing of Environment 138, 232–244.

Lindsay, J., Gaba, K., Harmon, L., Jarvis, S., 2021. Tonlé sap food security & agriculture iii: Evaluating changes in ecosystem vitality and freshwater health in the tonlé sap basin using remotely sensed data .

Liu, L., Peng, J., Li, G., Guan, J., Han, W., Ju, X., Zheng, J., 2023. Effects of drought and climate factors on vegetation dynamics in central asia from 1982 to 2020. Journal of Environmental Management 328, 116997.

Liu, W., Kogan, F., 1996. Monitoring regional drought using the vegetation condition index. International Journal of Remote Sensing 17, 2761–2782.

Liu, Y., Wang, Y., Du, Y., Zhao, M., Peng, J., 2016. The application of polynomial analyses to detect global vegetation dynamics during 1982–2012. International Journal of Remote Sensing 37, 1568–1584.

Lohberger, S., Stängel, M., Atwood, E.C., Siegert, F., 2018. Spatial evaluation of indonesia's 2015 fire-affected area and estimated carbon emissions using sentinel-1. Global change biology 24, 644–654.

Luong, N.D., Hiep, N.H., Bui, T.H., 2021. Investigating the spatio-temporal variation of soil moisture and agricultural drought towards supporting water resources management in the red river basin of vietnam. Sustainability 13, 4926.

Mandapaka, P.V., Qin, X., Lo, E.Y.M., 2017. Analysis of spatial patterns of daily precipitation and wet spell extremes in southeast asia. International Journal of Climatology .

Mann, H.B., 1945. Nonparametric tests against trend. Econometrica: Journal of the econometric society , 245–259.

Mao, D., Wang, Z., Luo, L., Ren, C., 2012. Integrating avhrr and modis data to monitor ndvi changes and their relationships with climatic parameters in northeast china. International Journal of Applied Earth Observation and Geoinformation 18, 528–536.

Markova, G., Baas, S., Conforti, P., Ahmed, S., 2018. 2017: the impact of disasters and crises on agriculture and food security. .

Maskell, G., Chemura, A., Nguyen, H., Gornott, C., Mondal, P., 2021. Integration of sentinel optical and radar data for mapping smallholder coffee production systems in vietnam. Remote Sensing of Environment 266, 112709.

McKee, T.B., Doesken, N.J., Kleist, J., et al., 1993. The relationship of drought frequency and duration to time scales, in: Proceedings of the 8th Conference on Applied Climatology, Boston. pp. 179–183.

Miettinen, J., Shi, C., Liew, S.C., 2017. Fire distribution in peninsular malaysia, sumatra and borneo in 2015 with special emphasis on peatland fires. Environmental management 60, 747–757.

Mishra, A., Vu, T., Veettil, A.V., Entekhabi, D., 2017. Drought monitoring with soil moisture active passive (smap) measurements. Journal of Hydrology 552, 620–632.

Mishra, A.K., Singh, V.P., 2010. A review of drought concepts. Journal of hydrology 391, 202–216.

Miyan, M.A., 2015. Droughts in asian least developed countries: vulnerability and sustainability. Weather and climate extremes 7, 8–23.

Mohd Razali, S., Marin Atucha, A.A., Nuruddin, A.A., Abdul Hamid, H., Mohd Shafri, H.Z., 2016. Monitoring vegetation drought using modis remote sensing indices for natural forest and plantation areas. Journal of Spatial Science 61, 157–172.

Mujiyo, M., Nurdianti, R., Komariah, K., Sutarno, S., 2023. Agricultural land dryness distribution using the normalized difference drought index (nddi) algorithm on landsat 8 imagery in eromoko, indonesia: 10.32526/ennrj/21/202200157. Environment and Natural Resources Journal 21, 127–139.

Muñoz-Sabater, J., Dutra, E., Agustí-Panareda, A., Albergel, C., Arduini, G., Balsamo, G., Boussetta, S., Choulga, M., Harrigan, S., Hersbach, H., et al., 2021. Era5-land: A state-of-the-art global reanalysis dataset for land applications. Earth system science data 13, 4349–4383.

Murthy, C., Laxman, B., Sai, M.S., 2015. Geospatial analysis of agricultural drought vulnerability using a composite index based on exposure, sensitivity and adaptive capacity. International journal of disaster risk reduction 12, 163–171.

Namkhan, M., Gale, G.A., Savini, T., Tantipisanuh, N., 2021. Loss and vulnerability of lowland forests in mainland southeast asia. Conservation Biology 35, 206–215.

Nguyen, M.D., Baez-Villanueva, O.M., Bui, D.D., Nguyen, P.T., Ribbe, L., 2020. Harmonization of landsat and sentinel 2 for crop monitoring in drought prone areas: Case studies of ninh thuan (vietnam) and bekaa (lebanon). Remote Sensing 12, 281.

Nguyen-Ngoc-Bich, P., Phan-Van, T., Ngo-Duc, T., Vu-Minh, T., Trinh-Tuan, L., Tangang, F.T., Juneng, L., Cruz, F., Santisirisomboon, J., Narisma, G., et al., 2021. Projected evolution of drought characteristics in vietnam based on cordex-sea downscaled cmip5 data. International Journal of Climatology 41, 5733–5751.

Nita, I., Putra, A.N., Fibrianingtyas, A., 2020. Analysis of drought hazards in agricultural land in pacitan regency, indonesia. SAINS TANAH-Journal of Soil Science and Agroclimatology 17, 7–15.

Noojipady, P., Morton, D.C., Schroeder, W., Carlson, K.M., Huang, C., Gibbs, H.K., Burns, D., Walker, N.F., Prince, S.D., 2017. Managing fire risk during drought: the influence of certification and el niño on fire-driven forest conversion for oil palm in southeast asia. Earth System Dynamics 8, 749–771.

o'Brien, K., Leichenko, R., Kelkar, U., Venema, H., Aandahl, G., Tompkins, H., Javed, A., Bhadwal, S., Barg, S., Nygaard, L., et al., 2004. Mapping vulnerability to multiple stressors: climate change and globalization in india. Global environmental change 14, 303–313.

Palanisamy, B., Narasimhan, B., Paul, S., Srinivasan, R., Wangpimool, W., Lim, S., Sayasane, R., 2021. Studying onset and evolution of agricultural drought in mekong river basin through hydrologic modeling. Water 13, 3622.

Pan, N., Feng, X., Fu, B., Wang, S., Ji, F., Pan, S., 2018. Increasing global vegetation browning hidden in overall vegetation greening: Insights from time-varying trends. Remote Sensing of Environment 214, 59–72.

Parameswaran, K., Nair, S.K., Rajeev, K., 2004. Impact of indonesian forest fires during the 1997 el nino on the aerosol distribution over the indian ocean. Advances in Space Research 33, 1098–1103.

Parida, B.R., Collado, W., Borah, R., Hazarika, M., Samarakoon, L., 2008. Detecting drought-prone areas of rice agriculture using a modis-derived soil moisture index. GIScience & Remote Sensing 45, 109–129.

Pauly, M., Crosse, W., Tosteson, J., 2022. High deforestation trajectories in cambodia slowly transformed through economic land concession restrictions and strategic execution of redd+ protected areas. Scientific Reports 12, 17102.

Pekel, J.F., Cottam, A., Gorelick, N., Belward, A.S., 2016. High-resolution mapping of global surface water and its long-term changes. Nature 540, 418–422.

Perez, G., Macapagal, M., Olivares, R., Macapagal, E., Comiso, J., 2016. Forecasting and monitoring agricultural drought in the philippines. The International Archives of the Photogrammetry, Remote Sensing and Spatial Information Sciences 41, 1263–1269.

Perez, G.J.P., Comiso, J.C., 2014. Seasonal and interannual variabilities of philippine vegetation as seen from space. Philippine Journal of Science 143, 147–155.

Pham-Duc, B., Papa, F., Prigent, C., Aires, F., Biancamaria, S., Frappart, F., 2019. Variations of surface and subsurface water storage in the lower mekong basin (vietnam and cambodia) from multisatellite observations. Water 11, 75.

Phan, T.N., Kappas, M., Nguyen, K.T., Tran, T.P., Tran, Q.V., Emam, A.R., 2019. Evaluation of modis land surface temperature products for daily air surface temperature estimation in northwest vietnam. International Journal of Remote Sensing 40, 5544–5562.

Phan, V.H., Dinh, V.T., Su, Z., 2020. Trends in long-term drought changes in the mekong river delta of vietnam. Remote sensing 12, 2974.

Phan-Van, T., Nguyen-Ngoc-Bich, P., Ngo-Duc, T., Vu-Minh, T., Le, P.V., Trinh-Tuan, L., Nguyen-Thi, T., Pham-Thanh, H., Tran-Quang, D., 2022. Drought over southeast asia and its association with large-scale drivers. Journal of Climate 35, 4959–4978.

Phuong, D.N.D., Hai, L.M., Dung, H.M., Loi, N.K., 2022. Temporal trend possibilities of annual rainfall and standardized precipitation index in the central highlands, vietnam. Earth Systems and Environment , 1–17.

Pokhrel, Y., Burbano, M., Roush, J., Kang, H., Sridhar, V., Hyndman, D.W., 2018. A review of the integrated effects of changing climate, land use, and dams on mekong river hydrology. Water 10, 266.

Power, K., Barnett, J., Dickinson, T., Axelsson, J., 2020. The role of el niño in driving drought conditions over the last 2000 years in thailand. Quaternary 3, 18.

Prasetyo, S.Y.J., Hartomo, K.D., Paseleng, M.C., 2021. Satellite imagery and machine learning for identification of aridity risk in central java indonesia. PeerJ Computer Science 7, e415.

Preedapirom, P., Robert, O., Onchang, R., Jeefoo, P., 2024. Drought monitoring using modis satellite-based data in kamphaeng phet province, thailand. International Journal of Geoinformatics 20.

Price, J., Warren, R., Forstenhäusler, N., Wallace, C., Jenkins, R., Osborn, T.J., Van Vuuren, D., 2022. Quantification of meteorological drought risks between 1.5 c and 4 c of global warming in six countries. Climatic Change 174, 12.

Qian, X., Qiu, B., Zhang, Y., 2019. Widespread decline in vegetation photosynthesis in southeast asia due to the prolonged drought during the 2015/2016 el niño. Remote Sensing 11, 910.

Quiring, S.M., Ganesh, S., 2010. Evaluating the utility of the vegetation condition index (vci) for monitoring meteorological drought in texas. Agricultural and forest meteorology 150, 330–339.

Quoc Lap, T., 2024. The impacts of climate change on meteorological drought in the central highlands region of vietnam. Journal of Hydroinformatics 26, 2416–2442.

Rahman, K.U., Ejaz, N., Shang, S., Balkhair, K.S., Alghamdi, K.M., Zaman, K., Khan, M.A., Hussain, A., 2024. A robust integrated agricultural drought index under climate and land use variations at the local scale in pakistan. Agricultural Water Management 295, 108748.

Raksapatcharawong, M., Veerakachen, W., 2019. Development of drought risk analysis platform using multiple satellite sensors. GEOMATE Journal 17, 62–69.

Raksapatcharawong, M., Veerakachen, W., Homma, K., Maki, M., Oki, K., 2020. Satellite-based drought impact assessment on rice yield in thailand with simriw- rs. Remote Sensing 12, 2099.

Raposo, V.d.M.B., Costa, V.A.F., Rodrigues, A.F., 2023. A review of recent developments on drought characterization, propagation, and influential factors. Science of the Total Environment , 165550.

Räsänen, T.A., Lindgren, V., Guillaume, J.H., Buckley, B.M., Kummu, M., 2016. On the spatial and temporal variability of enso precipitation and drought teleconnection in mainland southeast asia. Climate of the Past 12, 1889–1905.

Román, M.O., Justice, C., Paynter, I., Boucher, P.B., Devadiga, S., Endsley, A., Erb, A., Friedl, M., Gao, H., Giglio, L., et al., 2024. Continuity between nasa modis collection 6.1 and viirs collection 2 land products. Remote Sensing of Environment 302, 113963.

Rotjanakusol, T., Laosuwan, T., 2018. Remote sensing based drought monitoring in the middle-part of northeast region of thailand. Studia Universitatis Vasile Goldis Arad, Seria Stiintele Vietii 28, 14–21.

Rotjanakusol, T., Laosuwan, T., 2019a. Drought evaluation with ndvi-based standardized vegetation index in lower northeastern region of thailand. Geographia Technica 14.

Rotjanakusol, T., Laosuwan, T., 2019b. An investigation of drought around chi watershed during ten-year period using terra/modis data. Geographia Technica 14.

Roy, D.P., Lewis, P., Schaaf, C., Devadiga, S., Boschetti, L., 2006. The global impact of clouds on the production of modis bidirectional reflectance model-based composites for terrestrial monitoring. IEEE Geoscience and Remote Sensing Letters 3, 452–456.

Roy, P., Pal, S.C., Chakrabortty, R., Chowdhuri, I., Saha, A., Shit, M., 2022. Climate change and groundwater overdraft impacts on agricultural drought in india: Vulnerability assessment, food security measures and policy recommendation. Science of the total environment 849, 157850.

Ruefenacht, B., 2016. Comparison of three landsat tm compositing methods: A case study using modeled tree canopy cover. Photogrammetric Engineering & Remote Sensing 82, 199–211.

Rusdi, M., Budi, M., Farhan, A., et al., 2023. Agricultural droughts monitoring of aceh besar regency rice production center, aceh, indonesia–application vegetation conditions index using sentinel-2 image data. Journal of Ecological Engineering 24.

Sa-Nguansilp, C., Wijitkosum, S., Sriprachote, A., 2017. Agricultural drought risk assessment in lam ta kong watershed, thailand. International Journal of Geoinformatics 13, 37–43.

Sadiqi, S.S.J., Hong, E.M., Nam, W.H., Kim, T., 2022. An integrated framework for understanding ecological drought and drought resistance. Science of The Total Environment 846, 157477.

Sahana, V., Mondal, A., Sreekumar, P., 2021. Drought vulnerability and risk assessment in india: sensitivity analysis and comparison of aggregation techniques. Journal of Environmental Management 299, 113689.

Sangpradid, S., Uttaruk, Y., Rotjanakusol, T., Laosuwan, T., 2021. Forecasting time series change of the average enhanced vegetation index to monitoring drought condition by using terra/modis data. Agriculture & Forestry/Poljoprivreda i šumarstv 67.

Scott, M., Su-In, L., et al., 2017. A unified approach to interpreting model predictions. Advances in neural information processing systems 30, 4765–4774.

Sein, Z.M.M., Zhi, X., Ogou, F.K., Nooni, I.K., Lim Kam Sian, K.T., Gnitou, G.T., 2021. Spatio-temporal analysis of drought variability in myanmar based on the standardized precipitation evapotranspiration index (spei) and its impact on crop production. Agronomy 11, 1691.

Serkendiz, H., Tatli, H., Özcan, H., Çetin, M., Sungur, A., 2023. Multidimensional assessment of agricultural drought vulnerability based on socioeconomic and biophysical indicators. International Journal of Disaster Risk Reduction 98, 104121.

Shah, M.A.R., Renaud, F.G., Anderson, C.C., Wild, A., Domeneghetti, A., Polderman, A., Votsis, A., Pulvirenti, B., Basu, B., Thomson, C., et al., 2020. A review of hydrometeorological hazard, vulnerability, and risk assessment frameworks and indicators in the context of nature-based solutions. International journal of disaster risk reduction 50, 101728.

Shashikant, V., Mohamed Shariff, A.R., Wayayok, A., Kamal, M.R., Lee, Y.P., Takeuchi, W., 2021. Utilizing tvdi and ndwi to classify severity of agricultural drought in chuping, malaysia. Agronomy 11, 1243.

Shi, J., Cui, L., Tian, Z., 2020. Spatial and temporal distribution and trend in flood and drought disasters in east china. Environmental Research 185, 109406.

Shrestha, S., Bach, T.V., Pandey, V.P., 2016. Climate change impacts on groundwater resources in mekong delta under representative concentration pathways (rcps) scenarios. Environmental science & policy 61, 1–13.

Siegert, F., Ruecker, G., Hinrichs, A., Hoffmann, A., 2001. Increased damage from fires in logged forests during droughts caused by el nino. Nature 414, 437–440.

Skliris, N., Marsh, R., Haigh, I.D., Wood, M., Hirschi, J., Darby, S., Quynh, N.P., Hung, N.N., 2022. Drivers of rainfall trends in and around mainland southeast asia. Frontiers in Climate 4, 926568.

Sloan, S., Locatelli, B., Wooster, M.J., Gaveau, D.L., 2017. Fire activity in borneo driven by industrial land conversion and drought during el niño periods, 1982–2010. Global environmental change 47, 95–109.

Sohrabi, M.M., Ryu, J.H., Abatzoglou, J., Tracy, J., 2015. Development of soil moisture drought index to characterize droughts. Journal of Hydrologic Engineering 20, 04015025.

Son, N.T., Chen, C., Chen, C., Chang, L., Minh, V.Q., 2012. Monitoring agricultural drought in the lower mekong basin using modis ndvi and land surface temperature data. International Journal of Applied Earth Observation and Geoinformation 18, 417–427.

Son, N.T., Thanh, B.X., 2022. Remotely sensed drought evaluation over rice cultivated areas in cambodia during 2000 to 2019. Geocarto International 37, 1237–1255.

Sriwongsitanon, N., Gao, H., Savenije, H., Maekan, E., Saengsawan, S., Thianpopirug, S., 2015. The normalized difference infrared index (ndii) as a proxy for soil moisture storage in hydrological modelling. Hydrology & Earth System Sciences Discussions 12.

Stojanovic, M., Liberato, M.L., Sorí, R., Vázquez, M., Phan-Van, T., Duongvan, H., Hoang Cong, T., Nguyen, P.N., Nieto, R., Gimeno, L., 2020. Trends and extremes of drought episodes in vietnam sub-regions during 1980–2017 at different timescales. Water 12, 813.

Sun, Q., Miao, C., Duan, Q., Ashouri, H., Sorooshian, S., Hsu, K.L., 2018. A review of global precipitation data sets: Data sources, estimation, and intercomparisons. Reviews of Geophysics 56, 79–107.

Supharatid, S., Nafung, J., Aribarg, T., 2022. Projected changes in temperature and precipitation over mainland southeast asia by cmip6 models. Journal of Water and Climate Change 13, 337–356.

Svoboda, M.D., Fuchs, B.A., et al., 2016. Handbook of drought indicators and indices. volume 2. World Meteorological Organization Geneva, Switzerland.

Swami, D., Parthasarathy, D., 2021. Dynamics of exposure, sensitivity, adaptive capacity and agricultural vulnerability at district scale for maharashtra, india. Ecological Indicators 121, 107206.

Tadić, L., Bonacci, O., Brleković, T., 2019. An example of principal component analysis application on climate change assessment. Theoretical and applied climatology 138, 1049–1062.

Tan, M.L., Chua, V.P., Tan, K.C., Brindha, K., 2018. Evaluation of tmpa 3b43 and ncep-cfsr precipitation products in drought monitoring over singapore. International journal of remote sensing 39, 2089–2104.

Tan, M.L., Tan, K.C., Chua, V.P., Chan, N.W., 2017. Evaluation of trmm product for monitoring drought in the kelantan river basin, malaysia. Water 9, 57.

Tanaka, M., Sugimura, T., Tanaka, S., Tamai, N., 2003. Flood–drought cycle of tonle sap and mekong delta area observed by dmsp-ssm/i. International Journal of Remote Sensing 24, 1487–1504.

Tangang, F., Chung, J.X., Juneng, L., Supari, Salimun, E., Ngai, S.T., Jamaluddin, A.F., Mohd, M.S.F., Cruz, F., Narisma, G., et al., 2020. Projected future changes in rainfall in southeast asia based on cordex–sea multi-model simulations. Climate Dynamics 55, 1247–1267.

Tarpley, J., Schneider, S.R., Money, R., 1984. Global vegetation indices from the noaa-7 meteorological satellite. Journal of Climate and Applied Meteorology , 491–494.

Taylor, D., Saksena, P., Sanderson, P., Kucera, K., 1999. Environmental change and rain forests on the sunda shelf of southeast asia: drought, fire and the biological cooling of biodiversity hotspots. Biodiversity & Conservation 8, 1159–1177.

Thavorntam, W., Tantemsapya, N., 2013. Vegetation greenness modeling in response to climate change for northeast thailand. Journal of Geographical Sciences 23, 1052–1068.

Thavorntam, W., Tantemsapya, N., Armstrong, L., 2015. A combination of meteorological and satellite-based drought indices in a better drought assessment and forecasting in northeast thailand. Natural Hazards 77, 1453–1474.

Thavorntam, W., et al., 2022. Evaluation of drought in the north of thailand using meteorological and satellite-based drought indices. International Journal of Geoinformatics 18, 13–26.

Tian, Y., Peters-Lidard, C.D., 2010. A global map of uncertainties in satellite-based precipitation measurements. Geophysical Research Letters 37.

Tran, H.T., Campbell, J.B., Tran, T.D., Tran, H.T., 2017. Monitoring drought vulnerability using multispectral indices observed from sequential remote sensing (case study: Tuy phong, binh thuan, vietnam). GIScience & Remote Sensing 54, 167–184.

Tran, H.T., Campbell, J.B., Wynne, R.H., Shao, Y., Phan, S.V., 2019a. Drought and human impacts on land use and land cover change in a vietnamese coastal area. Remote Sensing 11, 333.

Tran, T.V., Bruce, D., Huang, C.Y., Tran, D.X., Myint, S.W., Nguyen, D.B., 2023. Decadal assessment of agricultural drought in the context of land use land cover change using modis multivariate spectral index time-series data. GIScience & Remote Sensing 60, 2163070.

Tran, T.V., Tran, D.X., Myint, S.W., Huang, C.y., Pham, H.V., Luu, T.H., Vo, T.M., 2019b. Examining spatiotemporal salinity dynamics in the mekong river delta using landsat time series imagery and a spatial regression approach. Science of the total environment 687, 1087–1097.

Tran, T.V., Tran, D.X., Myint, S.W., Latorre-Carmona, P., Ho, D.D., Tran, P.H., Dao, H.N., 2019c. Assessing spatiotemporal drought dynamics and its related environmental issues in the mekong river delta. Remote Sensing 11, 2742.

Tun, K.K., Shrestha, R.P., Datta, A., 2015. Assessment of land degradation and its impact on crop production in the dry zone of myanmar. International Journal of Sustainable Development & World Ecology 22, 533–544.

Uddin, M.N., Islam, A.S., Bala, S.K., Islam, G.T., Adhikary, S., Saha, D., Haque, S., Fahad, M.G.R., Akter, R., 2019. Mapping of climate vulnerability of the coastal region of bangladesh using principal component analysis. Applied geography 102, 47–57.

Udelhoven, T., Stellmes, M., del Barrio, G., Hill, J., 2009. Assessment of rainfall and ndvi anomalies in spain (1989–1999) using distributed lag models. International Journal of Remote Sensing 30, 1961–1976.

UN-ODRD, 2022. Global assessment report on disaster risk reduction 2022: Our world at risk: Transforming governance for a resilient future. UN.

Unganai, L.S., Kogan, F.N., 1998. Drought monitoring and corn yield estimation in southern africa from avhrr data. Remote sensing of environment 63, 219–232.

Upadhyay, M., Sherly, M.A., 2023. Multivariate framework for integrated drought vulnerability assessment–an application to india. International Journal of Disaster Risk Reduction 85, 103515.

Uttaruk, Y., Laosuwan, T., 2017. Drought detection by application of remote sensing technology and vegetation phenology. Journal of ecological engineering 18, 115–121.

Uttaruk, Y., Laosuwan, T., 2019. Drought analysis using satellite-based data and spectral index in upper northeastern thailand. Polish Journal of Environmental Studies 28.

Vadrevu, K.P., Lasko, K., Giglio, L., Schroeder, W., Biswas, S., Justice, C., 2019. Trends in vegetation fires in south and southeast asian countries. Scientific reports 9, 7422.

Vaiphasa, C., 2006. Consideration of smoothing techniques for hyperspectral remote sensing. ISPRS journal of photogrammetry and remote sensing 60, 91–99.

Van Quang, N., Thanh, N.H., 2023. Local government response capacity to natural disasters in the central highlands provinces, vietnam. Humanities and Social Sciences Communications 10, 1–16.

Venkatappa, M., Sasaki, N., Han, P., Abe, I., 2021. Impacts of droughts and floods on croplands and crop production in southeast asia–an application of google earth engine. Science of the Total Environment 795, 148829.

Venturas, M.D., MacKinnon, E.D., Dario, H.L., Jacobsen, A.L., Pratt, R.B., Davis, S.D., 2016. Chaparral shrub hydraulic traits, size, and life history types relate to species mortality during california's historic drought of 2014. PloS one 11, e0159145.

VGSD, 2023. Vietnam socioeconomic report. Technical Report. Vietnam General Statistics Department.

Vicente-Serrano, S.M., Beguería, S., López-Moreno, J.I., 2010. A multiscalar drought index sensitive to global warming: the standardized precipitation evapotranspiration index. Journal of climate 23, 1696–1718.

Vicente-Serrano, S.M., Gouveia, C., Camarero, J.J., Beguería, S., Trigo, R., López-Moreno, J.I., Azorín-Molina, C., Pasho, E., Lorenzo-Lacruz, J., Revuelto, J., et al., 2013. Response of vegetation to drought time-scales across global land biomes. Proceedings of the National Academy of Sciences 110, 52–57.

van Vliet, J., 2019. Direct and indirect loss of natural area from urban expansion. Nature Sustainability 2, 755–763.

Vremec, M., Collenteur, R.A., Birk, S., 2023. Improved handling of potential evapotranspiration in hydrological studies with pyet. Hydrology and Earth System Sciences Discussions 2023, 1–23.

Vu, M.T., Raghavan, S.V., Pham, D.M., Liong, S.Y., 2015. Investigating drought over the central highland, vietnam, using regional climate models. Journal of Hydrology 526, 265–273.

Vu, T.M., Raghavan, S.V., Liong, S.Y., Mishra, A.K., 2018. Uncertainties of gridded precipitation observations in characterizing spatio-temporal drought and wetness over vietnam. International Journal of Climatology 38, 2067–2081.

Vyas, S., Barua, A., Mallikarjuna, C., Baghel, T., 2024. An integrated approach for managing drought risks in the eastern himalayan region of india. International Journal of Disaster Risk Reduction 112, 104789.

Wan, Z., 2008. New refinements and validation of the modis land-surface temperature/emissivity products. Remote sensing of Environment 112, 59–74.

Wan, Z., Hook, S., Hully, 2021a. Modis/terra land surface temperature/emissivity daily l3 global 1km sin grid v061. .

Wan, Z., Hook, S., Hully, G., 2021b. Modis/terra land surface temperature/emissivity daily l3 global 1km sin grid v061. nasa eosdis land processes daa.

Wanders, N., Wada, Y., 2015. Human and climate impacts on the 21st century hydrological drought. Journal of Hydrology 526, 208–220.

Wang, L., Huang, G., Chen, W., Wang, T., Chotamonsak, C., Limsakul, A., 2022. Decadal background for active extreme drought episodes in the decade of 2010–19 over southeastern mainland asia. Journal of Climate 35, 2785–2803.

Wang, Y., Fu, B., Liu, Y., Li, Y., Feng, X., Wang, S., 2021. Response of vegetation to drought in the tibetan plateau: Elevation differentiation and the dominant factors. Agricultural and Forest Meteorology 306, 108468.

Wei, X., Huang, S., Huang, Q., Liu, D., Leng, G., Yang, H., Duan, W., Li, J., Bai, Q., Peng, J., 2022. Analysis of vegetation vulnerability dynamics and driving forces to multiple drought stresses in a changing environment. Remote Sensing 14, 4231.

Wessels, K.J., Van Den Bergh, F., Scholes, R., 2012. Limits to detectability of land degradation by trend analysis of vegetation index data. Remote sensing of Environment 125, 10–22.

West, H., Quinn, N., Horswell, M., 2019. Remote sensing for drought monitoring & impact assessment: Progress, past challenges and future opportunities. Remote Sensing of Environment 232, 111291.

Wilhelmi, O.V., Wilhite, D.A., 2002. Assessing vulnerability to agricultural drought: a nebraska case study. Natural Hazards 25, 37–58.

Wilhite, D.A., Glantz, M.H., 1985. Understanding: the drought phenomenon: the role of definitions. Water international 10, 111–120.

Wooster, M., Perry, G., Zoumas, A., 2012. Fire, drought and el niño relationships on borneo (southeast asia) in the pre-modis era (1980–2000). Biogeosciences 9, 317–340.

Wulder, M.A., Roy, D.P., Radeloff, V.C., Loveland, T.R., Anderson, M.C., Johnson, D.M., Healey, S., Zhu, Z., Scambos, T.A., Pahlevan, N., et al., 2022. Fifty years of landsat science and impacts. Remote Sensing of Environment 280, 113195.

Xiao, C., Li, P., Feng, Z., 2023. Agricultural expansion and forest retreat in mainland southeast asia since the late 1980s. Land Degradation & Development 34, 5606–5621.

Xie, F., Fan, H., 2021. Deriving drought indices from modis vegetation indices (ndvi/evi) and land surface temperature (lst): Is data reconstruction necessary? International Journal of applied earth observation and geoinformation 101, 102352.

Xu, H.j., Wang, X.p., Zhao, C.y., Yang, X.m., 2018. Diverse responses of vegetation growth to meteorological drought across climate zones and land biomes in northern china from 1981 to 2014. Agricultural and Forest Meteorology 262, 1–13.

Xu, Z., Cao, L., Zhong, S., Liu, G., Yang, Y., Zhu, S., Luo, X., Di, L., 2020. Trends in global vegetative drought from long-term satellite remote sensing data. IEEE Journal of Selected Topics in Applied Earth Observations and Remote Sensing 13, 815–826.

Yevjevich, V.M., et al., 1967. An objective approach to definitions and investigations of continental hydrologic droughts. volume 23. Colorado State University Fort Collins, CO, USA.

Yilmaz, M., 2023. Accuracy assessment of temperature trends from era5 and era5-land. Science of the Total Environment 856, 159182.

Yin, G., He, W., Liu, X., Xia, Y., Zhang, H., 2024. Wetting or greening? probing the global trends in vegetation condition index (vci). International Journal of Applied Earth Observation and Geoinformation 129, 103822.

Yuan, S., Stuart, A.M., Laborte, A.G., Rattalino Edreira, J.I., Dobermann, A., Kien, L.V.N., Thuy, L.T., Paothong, K., Traesang, P., Tint, K.M., et al., 2022a. Southeast asia must narrow down the yield gap to continue to be a major rice bowl. Nature Food 3, 217–226.

Yuan, Y., Bao, A., Jiang, P., Hamdi, R., Termonia, P., De Maeyer, P., Guo, H., Zheng, G., Yu, T., Prishchepov, A.V., 2022b. Probabilistic assessment of vegetation vulnerability to drought stress in central asia. Journal of Environmental Management 310, 114504.

Zeng, Z., Estes, L., Ziegler, A.D., Chen, A., Searchinger, T., Hua, F., Guan, K., Jintrawet, A., F. Wood, E., 2018. Highland cropland expansion and forest loss in southeast asia in the twenty-first century. Nature Geoscience 11, 556–562.

Zhan, C., Liang, C., Zhao, L., Jiang, S., Niu, K., Zhang, Y., 2022. Drought-related cumulative and time-lag effects on vegetation dynamics across the yellow river basin, china. Ecological Indicators 143, 109409.

Zhang, B., Cao, J., Bai, Y., Zhou, X., Ning, Z., Yang, S., Hu, L., 2013. Effects of rainfall amount and frequency on vegetation growth in a tibetan alpine meadow. Climatic Change 118, 197–212.

Zhang, B., Zhang, L., Guo, H., Leinenkugel, P., Zhou, Y., Li, L., Shen, Q., 2014. Drought impact on vegetation productivity in the lower mekong basin. International Journal of Remote Sensing 35, 2835–2856.

Zhang, L., Zhou, T., 2015. Drought over east asia: a review. Journal of Climate 28, 3375–3399.

Zhang, Y., Zhu, Z., Liu, Z., Zeng, Z., Ciais, P., Huang, M., Liu, Y., Piao, S., 2016. Seasonal and interannual changes in vegetation activity of tropical forests in southeast asia. Agricultural and Forest Meteorology 224, 1–10.

Zhao, A., Zhang, A., Cao, S., Liu, X., Liu, J., Cheng, D., 2018. Responses of vegetation productivity to multi-scale drought in loess plateau, china. Catena 163, 165–171.

Zhao, B., Yang, D., Yang, S., Santisirisomboon, J., 2022. Spatiotemporal characteristics of droughts and their propagation during the past 67 years in northern thailand. Atmosphere 13, 277.

Zhao, M., Zhou, Y., Li, X., Cheng, W., Zhou, C., Ma, T., Li, M., Huang, K., 2020. Mapping urban dynamics (1992–2018) in southeast asia using consistent nighttime light data from dmsp and viirs. Remote Sensing of Environment 248, 111980.

Zhu, Y., Liu, Y., Wang, W., Singh, V.P., Ren, L., 2021. A global perspective on the probability of propagation of drought: From meteorological to soil moisture. Journal of Hydrology 603, 126907.

Zoungrana, B.J., Conrad, C., Thiel, M., Amekudzi, L.K., Da, E.D., 2018. Modis ndvi trends and fractional land cover change for improved assessments of vegetation degradation in burkina faso, west africa. Journal of Arid Environments 153, 66–75.

Eidesstattliche Erklärung

Versicherung an Eides Statt

Ich, Ha Van Tuyen, versichere an Eides Statt durch meine Unterschrift, dass ich die Dissertation "Spatiotemporal Characterization and Analysis of Droughts in Mainland Southeast Asia – Unlocking the Potential of Long Earth Observation Time Series" selbständig und ohne fremde Hilfe angefertigt, alle Stellen, die ich wörtlich oder dem Sinne nach aus Veröffentlichungen entnommen habe, als solche kenntlich gemacht und ich auch keine anderen als die von mir angegebenen Quellen und Hilfsmittel benutzt habe. Ich versichere an Eides Statt durch meine Unterschrift, dass ich die Regeln der Universität Würzburg über gute wissenschaftliche Praxis eingehalten habe, insbesondere, dass ich die Gelegenheit zum Promotionsvorhaben nicht kommerziell vermittelt bekommen und insbesondere nicht eine Person oder Organisation eingeschaltet habe, die gegen Entgelt Betreuer bzw. Betreuerinnen für die Anfertigung von Dissertationen sucht.

Ich versichere an Eides Statt, dass ich die vorgenannten Angaben nach bestem Wissen und Gewissen gemacht habe und dass die Angaben der Wahrheit entsprechen und ich nichts verschwiegen habe. Die Strafbarkeit einer falschen eidesstattlichen Versicherung ist mir bekannt, namentlich die Strafandrohung gemäß § 156 StGB bis zu drei Jahren Freiheitsstrafe oder Geldstrafe bei vorsätzlicher Begehung der Tat bzw. gemäß § 161 Abs.1 StGB bis zu einem Jahr Freiheitsstrafe oder Geldstrafe bei fahrlässiger Begehung.

München, 20.11.2024

Unterschrift

Tuyen Ha Van

Deutsches Zentrum für Luft- und Raumfahrt (DLR)
Abteilung für Landoberfläche Dynamik, Erdbeobachtung Zentrum, Münchener Str. 20, 82234 Weßling, Deutschland

FORSCHUNGSINTERESSEN

- Dürregefahren
- Fernerkundung
- Dürre in der Landwirtschaft
- Geodaten Wissenschaft
- Zeitreihenanalyse
- Maschinelles Lernen

AUSBILDING

2018	Master-Abschluss in Umweltmanagement. Massey University, Neuseeland
2014	Bachelor in Landmanagement. Thai Nguyen Universität für Land- und Forstwirtschaft, Vietnam

ERFAHRUNG

2021–Jetzt	Doktorand bei Land Surface Dynamics, DLR
2018–2021	Dozent, Fakultät für Naturressourcenmanagement, Thai Nguyen Universität für Land- und Forstwirtschaft, Vietnam

PUBLIKATIONEN

Begutachtete Artikel

2024 **Ha, T. V**., Uereyen, S., & Kuenzer, C. (2024). Spatiotemporal analysis of tropical vegetation ecosystems and their responses to multifaceted droughts in Mainland Southeast Asia using satellite-based time series. *GIScience & Remote Sensing*, *61*(1), 2387385. https://doi.org/10.1080/15481603.2024.2387385

2023 **Ha, T. V**., Uereyen, S., & Kuenzer, C. (2023). Agricultural drought conditions over mainland Southeast Asia: Spatiotemporal characteristics revealed from MODIS-based vegetation time-series. *International Journal of Applied Earth Observation and Geoinformation*, 121, 103378. https://doi.org/10.1016/j.jag.2023.103378

Thi, N. Q., Govind, A., Le, M.-H., Linh, N. T., Anh, T. T. M., Hai, N. K., & **Ha, T. V**. (2023). Spatiotemporal characterization of droughts and vegetation response in Northwest Africa from 1981 to 2020. *The Egyptian Journal of Remote Sensing and Space Science*, 26(3), 393-401. https://doi.org/10.1016/j.ejrs.2023.05.006

2022 **Ha, T. V**., Huth, J., Bachofer, F., & Kuenzer, C. (2022). A review of earth observation-based drought studies in Southeast Asia. *Journal Remote Sensing*, 14(15), 3763. https://doi.org/10.3390/rs14153763

KONFERENZEN

2024 **Ha, T. V**., Uereyen, S., & Kuenzer, C. (2024). Space-time variability of vegetation and their multi-faceted drought impacts in the tropical and subtropical regions. *EGU24*. Viena, Austria. April 15-19, 2024. (**Oral**)

2023 **Ha, T. V**., Uereyen, S., Juliane, H., & Kuenzer, C. (2023). Spatiotemporal characteristics of drought and their impacts on cropland in the Lower Mekong Basin from 2000 to 2022. *The 42nd EARSel Symposium*. Bucharest, Romania. July 3-7, 2023. (**Oral**)

Ha, T. V., Uereyen, S., Juliane, H., & Kuenzer, C. (2023). Drought remote sensing and application in Mainland Southeast Asia. *International Symposium on Remote Sensing of Environment (ISRSE-39)*. Antalya, Turkey. April 24-28, 2023. (**Poster**)

2022 **Ha, T. V**., Juliane, H., & Kuenzer, C. (2022). Characterizing drought conditions using satellite-based precipitation time series in Mainland Southeast Asia, *DLR Symposium*. Wessling, Germany. April 20, 2022. (**Poster**)

KURSE UND SOMMERSCHULEN

2024 Teilnahme an den Online Kursen **"Statistics and Geodata Analysis Using Python",** Freie University Berlin.

2023 Teilnahme an den Online Kursen **"Geo-Python and Automating GIS Processes",** University of Helsinki, Finland.

Teilnahme an den Online Kursen **"Geographic Software Design Using Python",** University of Tennessee, USA.

2022-2023 Teilnahme an den Kursen **Deutsch für Ausländer,** DLR.

Unterschrift

Tuyen Ha Van